Final Technical Report

for Grant No. NGR22-009-839

APPLICATIONS TO EARTH PHYSICS: VERY-LONG-BASELINE INTERFEROMETRY AND DATA ANALYSIS

from the National Aeronautics and Space Administration

Goddard Space Flight Center

Greenbelt, Maryland 20771

for the period

April 1, 1974 - March 15, 1982

submitted by the

Department of Earth and Planetary Sciences

Massachusetts Institute of Technology

Cambridge, MA 02139

Principal Investigators:

Charles C. Counselman III

Irwin I. Shapiro

Date: April 1982

Table of Contents

Introduction

The contents of this report cover a range of very-long-baseline-interferometry experiments applied to Earth physics. The research for these articles was conducted between 1974 and 1982, in part under the auspices of NASA Grant No. NGR 22-009-839.

3-6

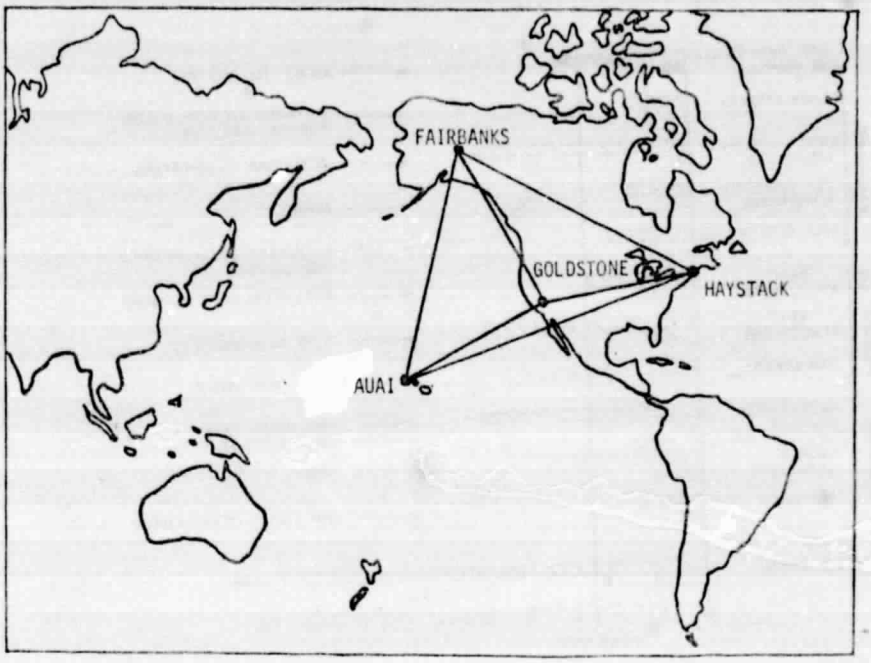

Fig. 3. PPME station configuration.

The error budget for determination of baselines for the PPME is shown on Fig. 5. The cross-hatched bars indicate the error budget for the 1972—1973 series of four measurements described earlier in the paper. The open bars represent the error budget for the new VLBI system for PPME.

Note that we are showing a current error budget of 25 cm even though the experimental data shown on Fig. 2 has a formal error of about half that value. We have purposely been conservative in the error budget in order to

MEASUREMENT ACCURACY GOALS

FOR 24 HOUR VLBI OBSERVATION

EQUATORIAL BASELINE COMPONENTS	5 cm
POLAR BASELINE COMPONENTS	8 cm
POLAR MOTION	10 cm
VARIATIONS IN UT.1	0.15 ms

Fig. 4. PPME measurement accuracy goals.

14

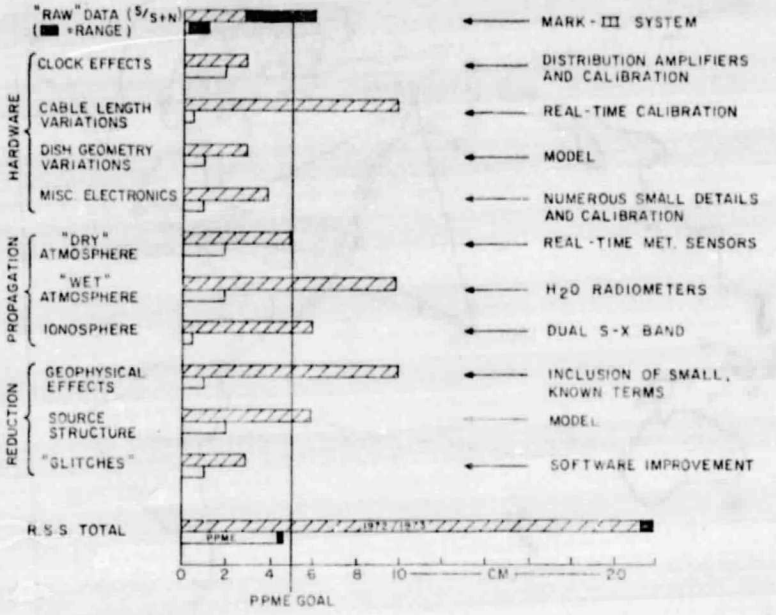

Fig. 5. PPME error budget.

cover the possibility of small systematic biases which may not be apparent when viewing the data output.

The changes required in the VLBI system in order to achieve the 5-cm PPME goal are shown at the right hand of Fig. 5. An improvement in the signal/noise ratio of the VLBI system of a factor of 20 will be achieved by a new wideband recording system entitled 'Mark III'. The present 'Mark I' system records at a data rate of 720 kB/sec, while the new 'Mark III' system will record at a data rate of about 112 MB/sec.

The addition of real-time calibration of all of the cable lengths will produce a significant reduction in the system error. When the system is used to measure at centimeter accuracies, great care must be taken to accurately monitor the length of the cables going up to the antenna which can vary in length as the antenna moves across the sky.

Significant corrections are required to account for the propagation through the atmosphere and the ionosphere. At the present time these parameters are modeled. However when one desires centimeter level accuracy, the generalized models are not accurate enough for determining the propagation correction for the wet atmosphere and the ionosphere. More direct measurements are required. Recent work at the Goddard Space Flight Center has demonstrated that the dry atmosphere can be accurately modeled such that one can determine that correction very accurately utilizing real-time sensors for temperature and pressure at the antenna. The wet atmosphere is a

different question. We plan to mount a microwave radiometer on the VLBI antenna boresighted with the VLBI antenna. This microwave radiometer will operate at frequencies on and off the 22-GHz water vapor line in order to directly measure the water vapor content along the path to the radio source. Field tests of microwave radiometers have shown that it is feasible to determine the correction for the wet atmosphere to within 2 cm. The PPME VLBI system will operate simultaneously at 2300 MHz and 8400 MHz in order to measure the difference in path length at the two frequencies caused by the ionosphere. By utilizing the known frequency dependence of path length in the ionosphere, it will be possible to compute the ionospheric correction to an accuracy of less than a centimeter..

The geophysical effects listed are such items as diurnal polar motion, UT.1, earth tides, and ocean loading. These are parameters that are solved for in the VLBI determination of baselines. Improvements in this area come from improvements in the modeling of these various parameters and the experimental determination of their characteristics to greater precision.

Another scientific output of this VLBI program will be a better determination of source structure. Although the quasars used for sources in VLBI are extremely small, they still have a finite angular size and a source structure. This must be taken into consideration in the sophisticated processing for centimeter level accuracies. The arrangement of these stations for PPME provides a radio astronomy array which will have very high resolving power for determinations of the source structure.

A block diagram of the new PPME VLBI station is shown on Fig. 6. The key features are as follows. There are two receivers, simultaneously receiving signals at the S-band (2300 MHz) and X-band (8400 MHz) for the determination of ionospheric propagation. These two receiver outputs go to the 'Mark III' backend system where each IF channel is converted to 14 video channels, each 2 MHz wide, and spanning a total RF bandwidth of 100 MHz. With the two receivers there is a total of 28 such video channels. Each video channel is digitized at a 4 MB/sec rate and recorded on a 28 track tape recorder. The 'Mark III' system is computer-controlled for reliable automated operation. The computer also operates the calibration system which measures the lengths of cables going up to the receiver and also provides the phase calibration signals at the input of the receiver. As mentioned earlier, each station has a microwave radiometer system for measuring the water vapor content. Likewise they have a meteorological recording system. The frequency standard for the station will be a hydrogen maser frequency standard that was developed by Harry Peters at Goddard.

Figure 7 is a diagram of the PPME data flow after the data are recorded at the station and sent back to a central processing facility. A key feature of this system is that the correlator will be able to process tapes from as many as four different stations simultaneously. This simultaneous fringe processing permits closure solutions to be determined around the various triangles formed by the baselines. This high capability correlator will be implemented

16

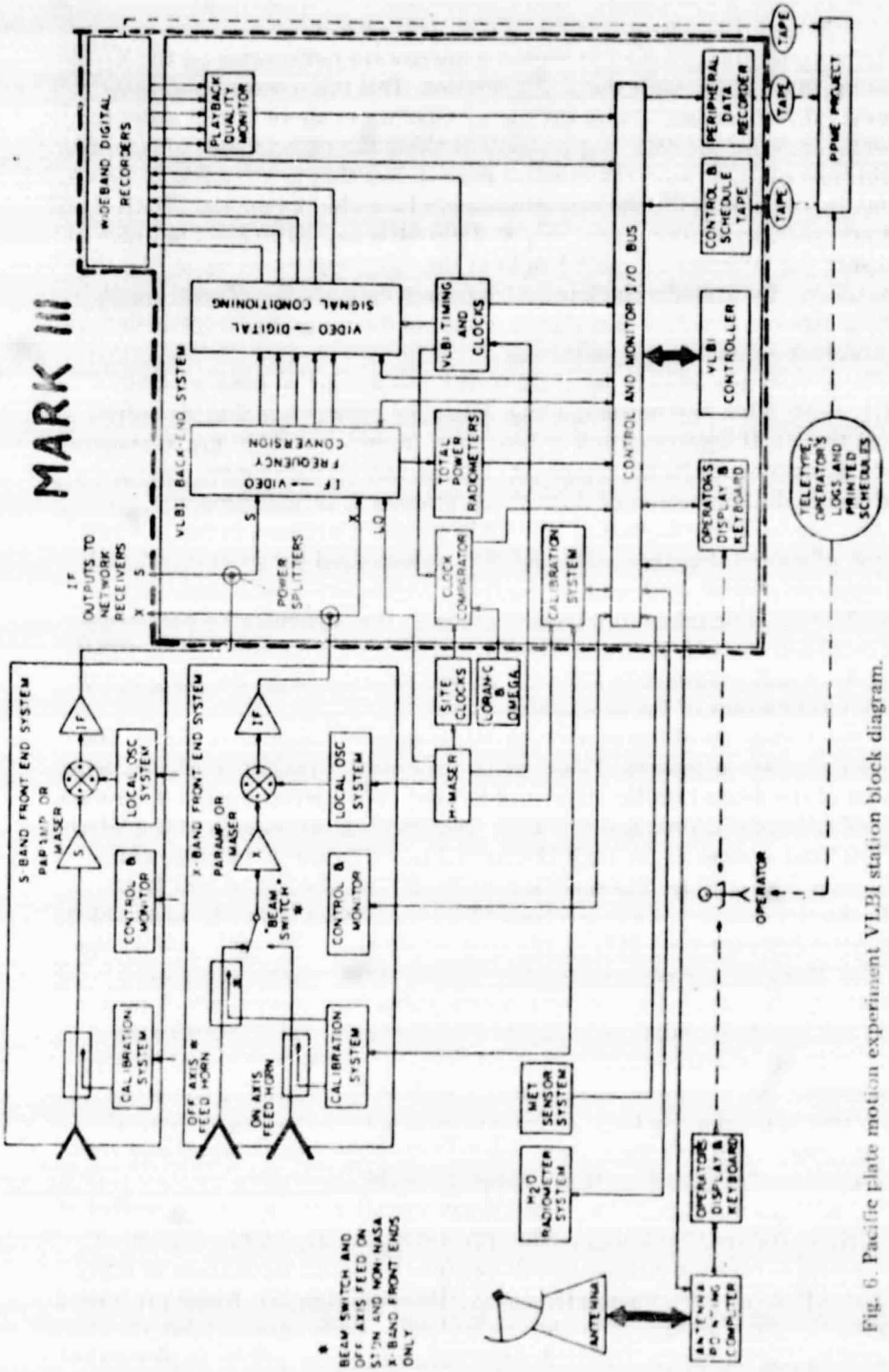

Fig. 6. Pacific plate motion experiment VLBI station block diagram.

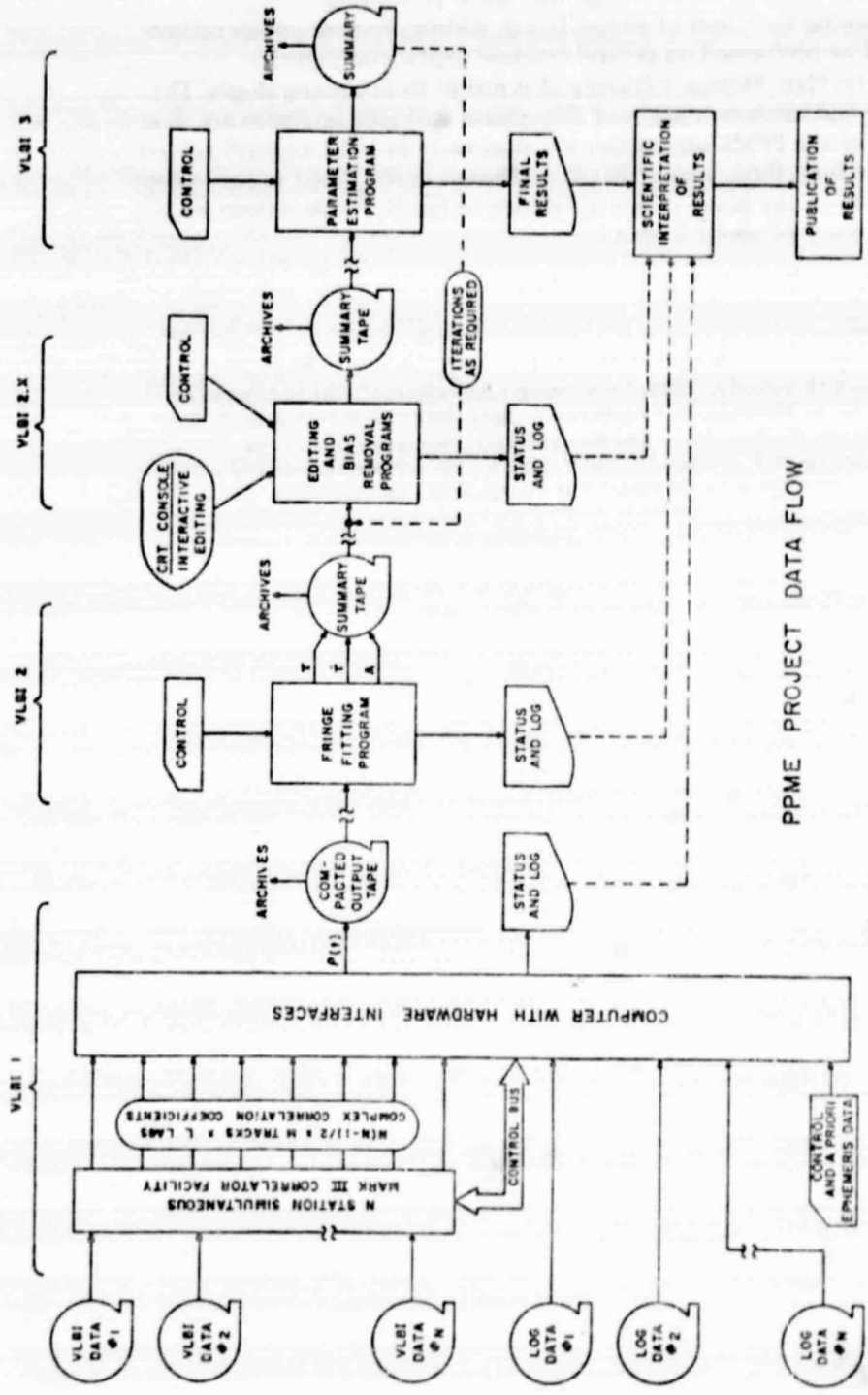

Fig. 7. PPME data flow diagram.

in hardware in order to achieve very high speed processing.

The following functions of fringe fitting, editing, and parameter estimation will all be performed on general purpose digital computers.

The Pacific Plate Motion Experiment is just in its beginning stages. The engineering and implementation of this system will take several years. It is expected that the PPME operations will start early in 1978 and will be continued for at least three years. This should result in the direct measurement of the motion of the island of Kauai relative to the North American Plate with an accuracy of about 2 cm/yr.

REFERENCES

Knight, C.A. and Shapiro, I.I., 1970. Geophysical implications of long baseline interferometry. In: L. Mansinha, D. Smylie and A. Beck (Editors), Earthquake Displacement Fields and the Rotation of the Earth. Reidel, Dordrecht.

Minster, J.B., Jordan, T.H., Molnar, P. and Haines, E., 1974. Numerical modelling of instantaneous plate tectonics. Geophys. J. R. Astron. Soc., 36: 541–576.

THE ASTROPHYSICAL JOURNAL, 196:13–39, 1975 February 15

FINE STRUCTURE OF 25 EXTRAGALACTIC RADIO SOURCES

J. J. WITTELS, C. A. KNIGHT, AND I. I. SHAPIRO
Massachusetts Institute of Technology

H. F. HINTEREGGER, A. E. E. ROGERS, AND A. R. WHITNEY
Northeast Radio Observatory Corporation

T. A. CLARK, L. K. HUTTON, AND G. E. MARANDINO
Goddard Space Flight Center and University of Maryland

A. E. NIELL*
Jet Propulsion Laboratory

B. O. RÖNNÄNG AND O. E. H. RYDBECK
Onsala Space Observatory and Chalmers University of Technology

AND

W. K. KLEMPERER AND W. W. WARNOCK
National Oceanic and Atmospheric Administration
Received 1974 January 21; revised 1974 July 1

ABSTRACT

Between 1972 April and 1973 May, 25 extragalactic radio sources were observed interferometrically at 7.8 GHz ($\lambda \simeq 3.8$ cm) with five pairings of antennas. These sources exhibit a broad variety of fine structures from very simple to complex. Although the structure and the total power of some of these sources have remained unchanged within the sensitivity of our measurements during the year of observations, both the total flux and the correlated flux of others have undergone large changes in a few weeks.

Subject heading: quasi-stellar sources or objects

I. INTRODUCTION

The small-scale structure of extragalactic radio sources, particularly QSOs, provides an important clue for the understanding of the physical processes occurring in these objects and their origin and evolution. With very-long-baseline interferometry (VLBI), we have probed such sources down to a scale of tenths of a milliarcsecond and discovered a wide variety of behavior: the structure may vary on a time scale of days or months or virtually not at all; the correlated flux data may be compatible with simple models, such as those composed of one or two components, or may exhibit very complicated patterns.

In this paper we present, for 25 sources, data obtained from VLBI observations carried out between 1972 April and 1973 May. Section II contains a brief description of the observations, some aspects of the data processing, and a discussion of errors. Section III is devoted to an explanation of the figures. Individual sources are discussed in § IV.

II. OBSERVATIONS

The four radio antennas used in these observations and their locations and diameters are: Haystack, Massachusetts 120-foot (36.6 m); Goldstone, California 210-foot (64 m); Onsala, Sweden 84-foot (25.6 m); and Fairbanks, Alaska 85-foot (26 m).[1] Table 1 shows which antennas were used on each observation day. All observations reported here were made near 7.8 GHz with left-circular polarization (I.E.E.E. convention). A wide-band synthesis technique (Rogers 1970; Hinteregger *et al.* 1972) was employed on all observation days except 1972 July 3 and 1973

[1] Hereafter H = Haystack, G = Goldstone, O = Onsala, and F = Fairbanks.

TABLE 1

LIST OF EXPERIMENTS

Symbol	Date	Antennas
□	1972 April 14, 15	H, G
○	1972 May 9, 10	H, G, F
△	1972 May 29, 30	H, G, F
	1972 June 3	H, F
	1972 June 6, 7	H, G, F
+	1972 June 27, 28	H, G
	1972 July 3, 4	H, G
X	1972 August 29, 30	H, G
Y	1972 November 7	H, G
✦	1973 February 4, 5	H, G
⊼	1973 March 30, 31	H, G
Z	1973 May 17, 18	H, G, O
	1973 May 18, 19	H, O
	1973 May 22, 23	H, O

NOTE.—H = Haystack, G = Goldstone, F = Fairbanks, O = Onsala.

* NASA-NRC Resident Research Associate.

TABLE 2

CONTRIBUTIONS OF INTERFEROMETER HARDWARE AND SOFTWARE TO ERRORS IN FRINGE-AMPLITUDE DETERMINATIONS

Source of Error	Effect on Amplitude	Method of Determination
Antenna pointing	Variable—conceivably up to 100 percent	When source temperature is measured, pointing error is determined from radiometry data and removed in normalization. When source temperature is not measured, pointing error cannot be estimated reliably but can only decrease fringe amplitude.
Difference in polarization between antennas	< 1 percent (cross-polarization down by more than 20 dB)	Engineering data on feeds.
Difference in dispersion (nonlinear phase versus frequency response) between feed systems	< 0.01 percent (< 25° MHz^{-2})	Theoretical estimate.
Difference in dispersion between low-noise amplifiers	< 0.01 percent (< 25° MHz^{-2})	Theoretical estimate.
Local-oscillator phase noise	< 0.2 percent ($\Delta\phi_{rms}$ < 10°)	Phase noise measured using phase-calibration signal.
Difference in intermediate frequency dispersion	< 0.01 percent (< 25° MHz^{-2})	Manufacturer's specifications.
Partial nonoverlap of bandpass at high fringe rates	< 3 percent (< 10 kHz in 360 kHz)	Theoretical estimate.
Difference in dispersion between frequency converters; recording and processing	< 6 percent in toto	Measurements made with artificial noise sources injected into frequency converters (see text).
Bias in fringe amplitude due to estimation of amplitude rather than intensity (Whitney 1974)	Only important when the amplitude is near zero. Worst case in this paper has the estimate of the amplitude too high by about 0.2 fu (see note to table 3).	Theoretical estimate.

May 17–18. Hydrogen-maser frequency standards were used at all sites on all dates except for 1973 May 17–18, when a rubidium standard had to be used at Goldstone.

The Mark I system was used to record the data on magnetic tape. The accuracy of this system and of our data-processing programs was recently checked (Rogers 1973) by simultaneously recording two tapes at Haystack using separate video converters. The input to each converter consisted of an independent noise source plus a fraction of the same noise source. This fraction of correlated signal was measured with square-law detectors that were attached to each converter output, and the results were compared with the output of the processing programs for a set of fringe rates in the range from 0.5 to 20,000 Hz, which encompassed the observed fringe rates. The fraction of correlated noise was also varied to range between 0.03 and 0.28. The comparison showed that the difference varied but was always within 6 percent—about 3 times the uncertainty of the square-law detector measurements.

The separate instrumental and data-processor contributions to the degradation of the fringe amplitude, including those measured in the above test, are listed in table 2. The effect of the atmosphere on the fringe amplitude is negligible except at low elevation angles where it is still expected to be less than a few percent.

The unnormalized fringe amplitude from each pair of tapes was normalized by use of ON-source (T_{ON}) and OFF-source (T_{OFF}) system temperatures for each antenna site:

$$\text{N.A.} = \text{U.A.}\left[\left(\frac{T_{ON}}{T_{ON} - T_{OFF}}\right)_{\text{site 1}}\left(\frac{T_{ON}}{T_{ON} - T_{OFF}}\right)_{\text{site 2}}\right]^{1/2},$$

where N.A. denotes the normalized fringe amplitude and U.A. the unnormalized amplitude. The U.A. is approximately equal to twice the fraction of correlated bits minus 1, which formulation takes into account the effects of system noise. For a large signal-to-noise ratio, the standard deviation of the estimate of each U.A. is proportional to the inverse square root of the product of the bandwidth and the integration time; for Mark I this standard deviation[2] is 2.4×10^{-4}. In most experiments the values of U.A. were based on data obtained in a set of channels 360 kHz wide centered at frequencies 1–50 MHz from the central channel at 7850 MHz. In some cases the data from one or more of the separate frequency channels were not used; in these cases the standard deviation was increased by the square root of the ratio of the total number of channels to the number actually used.

The uncertainties in the estimates of U.A., for the observations reported here, were negligible compared with the radiometry errors (i.e., compared with the errors in the estimates of T_{ON} and T_{OFF}), except for

[2] All errors quoted in this paper are estimates of 1 σ.

TABLE 3

TOTAL FLUX MEASUREMENTS (fu)*

	1972 April 14, 15	1972 May 9, 10	1972 May 29, 30	1972 June 3, 6, 7	1972 June 27, 28	1972 July 3, 4†	1972 August 29, 30	1972 November 7	1973 February 4, 5	1973 March 30, 31	1973 May 17, 18	1973 May 18, 19	1973 May 22, 23
3C 84	...	51.0 ± 5.0	49.2 ± 2.6	...	...	45.0 ± 5.0	...	...	...	...	55.8 ± 2.8	55.8 ± 2.8	55.8 ± 2.8
NRAO 140	...	2.7 ± 0.3	...	...	...	...	...	2.6 ± 0.1	...	...	...	...	...
CTA 26	...	...	...	...	...	...	...	3.8 ± 0.2	...	...	...	...	...
NRAO 150	...	8.8 ± 0.8	...	...	...	8.3 ± 0.9	...	...	...	...	...	10.4 ± 1.2	...
3C 120	...	...	...	9.4 ± 0.6	...	...	13.4 ± 0.7	15.8 ± 1.2	14.4 ± 0.7	16.5 ± 0.8	14.7 ± 0.7	14.7 ± 0.7	...
OJ 287	6.2 ± 0.4	5.9 ± 0.6	5.8 ± 0.4	5.0 ± 0.4	...	4.8 ± 0.6	5.5 ± 0.4	7.0 ± 0.6	8.0 ± 0.4	7.3 ± 0.4	7.1 ± 0.4	...	...
4C 39.25	11.8 ± 0.8	...	11.6 ± 0.6	...	9.0 ± 0.5	9.8 ± 1.1	11.2 ± 0.5	...	12.0 ± 0.6	12.0 ± 0.6	...	10.9 ± 0.8	10.9 ± 0.8
OK 290	...	2.0 ± 0.3	...	...	...	1.7 ± 0.2	...	2.0 ± 0.1	...	...	...	...	...
1055+01	...	3.7 ± 0.4	...	...	...	...	...	...	...	...	...	...	...
1116+12	...	1.5 ± 0.2	...	...	...	...	...	...	...	...	...	...	...
1127−14	...	5.7 ± 0.5	...	...	...	...	...	...	...	...	...	...	...
1148−00	...	1.4 ± 0.2	...	...	...	...	...	...	...	...	...	...	...
3C 274	...	49.1 ± 2.0‡	...	49.1 ± 2.0‡	...	...	...	49.1 ± 2.0‡	...	49.1 ± 2.0‡	49.1 ± 2.0‡	49.1 ± 2.0‡	49.1 ± 2.0‡
OQ 208	...	...	...	...	...	2.3 ± 0.2	2.3 ± 0.3	2.4 ± 0.2	2.9 ± 0.2	2.9 ± 0.2	...	...	...
OR 103	...	...	...	...	...	2.3 ± 0.3	...	...	...	...	...	...	...
CTD 93	...	...	...	...	...	1.3 ± 0.2	...	...	...	...	...	...	...
NRAO 512	...	2.0 ± 0.3	...	...	...	1.5 ± 0.2	...	...	...	...	...	...	...
3C 345	...	10.9 ± 0.9	9.6 ± 1.0	...	8.8 ± 0.5	8.3 ± 1.1	10.0 ± 0.6	...	11.8 ± 0.6	11.4 ± 0.6	...	12.4 ± 1.2	12.4 ± 1.2
OV 080	...	...	...	...	...	1.1 ± 0.2	...	...	...	...	...	...	...
3C 418	...	...	...	...	...	...	...	3.7 ± 0.2	3.9 ± 0.2	3.8 ± 0.2	3.9 ± 0.2	3.9 ± 0.2	3.9 ± 0.2
PKS 2134+00	12.6 ± 0.2§	...	12.3 ± 0.3§	...	12.1 ± 0.3§	...	12.0 ± 0.2§	12.0 ± 0.3§	12.2 ± 0.3§	12.3 ± 0.6	...	12.4 ± 1.1	12.4 ± 1.1
OX 161	...	...	...	...	...	1.2 ± 0.2	...	...	...	...	...	...	...
VRO 42.22.01	8.4 ± 0.7	...	8.0 ± 0.4	8.3 ± 0.6	8.3 ± 0.5	...	8.2 ± 0.5	5.9 ± 0.4	5.6 ± 0.3	5.6 ± 0.3	7.9 ± 0.4	7.9 ± 0.4	7.9 ± 0.4
CTA 102	...	...	...	3.0 ± 0.3	...	...	...	...	...	...	...	...	...
3C 454.3	15.1 ± 1.1	...	13.9 ± 1.1	...	13.0 ± 0.7	...	13.4 ± 0.3	13.2 ± 0.7	11.9 ± 0.6	11.7 ± 0.6	...	11.9 ± 1.5	11.9 ± 1.5
DR 21	...	...	...	...	...	...	...	...	...	21.7 ± 0.7‖	21.7 ± 0.7‖	...	...

* Each column gives the total flux and the associated standard error, both in flux units; 1 fu = 10^{-26} W m^{-2} Hz^{-1}.

† There were no good calibration sources observed on 1972 July 3, 4; scale was fixed by calibration on 1972 June 27, 28.

‡ Calibration source. The total flux is from Baars and Hartsuijker (1972). A correction factor of 1.04 was applied for partial resolution by the 2'.2 beam at G. The flux of this source was assumed to be time independent.

§ Calibration source. The total fluxes were obtained from the data of Dent (private communication) by interpolation.

‖ Calibration source. The total flux is from Dent (1972*b*). A correction factor of 1.024 was applied for partial resolution by the 2'.2 beam at G. The flux of this source was assumed to be time independent.

sources with correlated fluxes less than 3 fu. These measurements of T_{ON} and T_{OFF} were always wide-band measurements encompassing the entire synthesized bandwidth. No attempt was made to measure the variation of system gain over the individual frequency channels (see table 2).

The methods of measurement of T_{ON} and T_{OFF} varied: Initially a chart recording, and later a noise-adding radiometer, was used at G; at H and O a calibrated noise tube and a chart recording were used. As will be explained below, no usable radiometry data were obtained at F.

At O, the system temperature, $(T_{OFF})_O$, of about 60° K, the antenna efficiency of about 12 percent, and the radiometer bandwidth of 2 MHz yielded a system sensitivity insufficient to determine source temperature reliably. Therefore, source temperatures $(T_{ON} - T_{OFF})_O$ were always estimated by using those measured during the same experiment at another site and multiplying by the ratio of the effective areas (A_e) of the antennas. For example,

$$(T_{ON} - T_{OFF})_O = \frac{(A_e)_O}{(A_e)_G} (T_{ON} - T_{OFF})_G ,$$

and

$$(T_{ON})_O = (T_{ON} - T_{OFF})_O + (T_{OFF})_O .$$

The values used for $(A_e)_G$ and $(T_{ON} - T_{OFF})_G$ were those for the elevation angle corresponding to the maximum effective area; the effective areas of all other antennas were assumed not to vary with elevation angle.

At F, a system temperature of 300° K, previously measured, was used. No sources could be seen above this background so that here also source temperatures were calculated as above.

Each T_{ON}, T_{OFF}, or $(T_{ON} - T_{OFF})$ that was based on direct measurements was taken as the mean of the values obtained during, or immediately before or after, each observation. Since the statistical sample was always small, the standard error for each such temperature estimate was assigned the value $[(T_M - T_m)/2]$, where T_M and T_m were the maximum and minimum of the relevant measured values, respectively.

When the source temperature was calculated, the error was taken as the square root of the summed squares of the errors in the quantities used in the calculation. These errors do not include uncertainties due to the assumption that A_e is independent of elevation. In addition, they do not include two other sources of systematic uncertainty: (1) an elevation-dependent error due to atmospheric absorption that, at low elevation angles, is larger than the uncertainty due to the variation of A_e; (2) an antenna pointing error due to the inability to detect the sources in total power at F and O. Both of these effects, when uncorrected, cause the fringe amplitude to be underestimated. Some of these problems were so severe at F that data are presented here only for 3C 84, the strongest source; for other sources, even the ratios of the fringe amplitudes for the two independent baselines involving F were unusable.

The resultant error in N.A. was taken as the square root of the summed squares of the relevant errors, including that for U.A. The largest contribution to this error came from the measurement of the source temperature, $(T_{ON} - T_{OFF})$.

The correlated flux was obtained from the N.A. by multiplying the latter by the total flux of the source.[3] Total flux (T.F.) was calculated from the same radiometry data used in the normalization:

$$\text{T.F.} = (T_{ON} - T_{OFF}) \left[\frac{\text{Flux of Calibrator}}{(T_{ON} - T_{OFF})_{\text{Calibrator}}} \right] ,$$

where $(T_{ON} - T_{OFF})$ was the maximum value obtained for the source during the given day of observation. The error in total flux was estimated by taking the square root of the summed squares of the errors in $(T_{ON} - T_{OFF})$ of the source and the calibrator, and the error in the estimate of the flux of the calibrator.

Whenever possible, the data from the G site, where the system temperature was lowest and the effective antenna area largest, were used to obtain $(T_{ON} - T_{OFF})$. Either PKS 2134+00 (Dent 1974), 3C 274 (Baars and Hartsuijker 1972), DR 21 (Dent 1972*b*), or some combination of these sources was used for calibration. The total flux for each source on each day is given in table 3, with the calibrator sources for each day being marked.

Table 4 contains estimates of the individual contributions to the errors in the correlated flux, as well as a decomposition of these errors into systematic and random components.

On 1973 May 17–18 the measurements had an added source of error: the phase noise introduced by the rubidium standard used at G. This phase noise usually had a negligible effect on the correlated flux, but at times reduced it by as much as 30–40 percent; for these times we reduced the effect of these phase fluctuations by processing coherently over segments of data shorter than the 180-second tape, and then averaging the segments incoherently.

III. FIGURES

Results from these observations are presented in figures 1–32, along with the *u-v* track traced out by each source from rise to set on each interferometer baseline for which data are plotted. Note that data were not always taken during the entire period of mutual visibility shown by the track. Results for sources observed fewer than about 10 times on a given baseline are listed in table 5. Figures 15, 16, and 22 are somewhat unconventional as they show correlated flux as a function of u and v. These plots are useful for visualizing the variations of correlated flux with changes in baseline projection.

[3] In this paper the term "flux" refers to the power incident per unit area per unit frequency interval (i.e., the modifier "density" is consistently omitted).

TABLE 4

A. CONTRIBUTIONS TO ERRORS IN CORRELATED-FLUX DETERMINATIONS

Source of Error	Effect on Correlated Flux (CF)
Unnormalized fringe-amplitude estimates (R)* . . .	Fractional error depends on the unnormalized amplitude, the number of short records, and the number of usable frequency channels; however, typically:

CF (fu)	HG	HO	GO	HF	GF
10.0	$\ll 1\%$	$< 1\%$	$< 1\%$	1%	. . .
4.0	< 1	2	1	3	. . .
2.0	1	3	2	5	3%
1.0	2	5	3	. . .	5
0.5	3	8	4	. . .	7

System-temperature measurements.	G and H, $\leqslant 1\%$ (R) O, $\leqslant 5\%$ (R) F, $\leqslant 10\%$ (R and S)
Source-temperature measurements (R).	Depends on total flux (TF). We consider four categories:

TF:	0–4 fu	4–12 fu	12–20 fu	> 20 fu
G:	10–20%	$\sim 5\%$	$\sim 3\%$	$\sim 1\%$
H:	(not measured)	5–10%	$\sim 5\%$	$\leqslant 3\%$

Antenna efficiencies used to calculate source temperatures (S).	H $\approx 3\%$, G $\approx 2\%$, O $\approx 5\%$; F $\approx 5\%$†
Total-flux measurements (S).	See table 3

* R indicates error contribution is random; S indicates error contribution is systematic.

† These errors do not include any systematic effects due to possible variation of efficiency with antenna orientation—not a problem at H and O but may be a problem at F where it was not measured—or due to atmospheric effects at low elevation.

B. SEPARATION INTO SYSTEMATIC AND RANDOM CONTRIBUTIONS TO THE ERROR IN CORRELATED-FLUX DETERMINATIONS

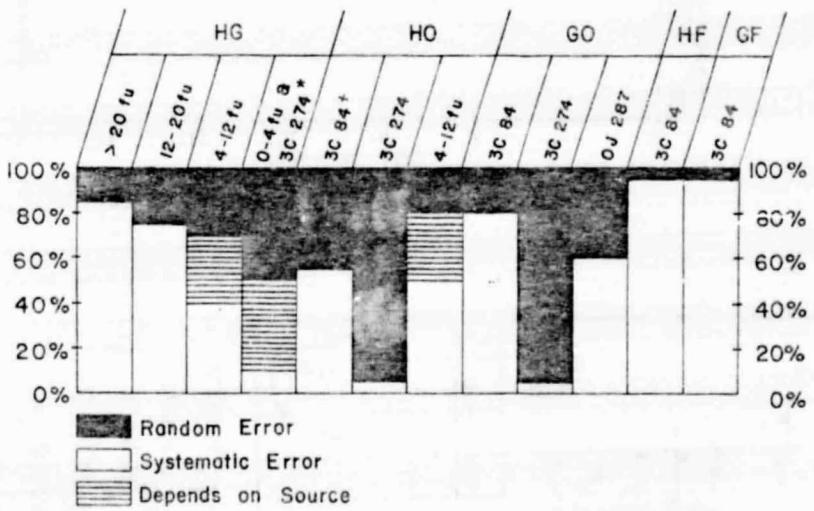

* 3C 274 is included with sources between 0 and 4 fu because its compact component contains only 2–3 fu.

† When there is only one source in a category, only the source name is listed.

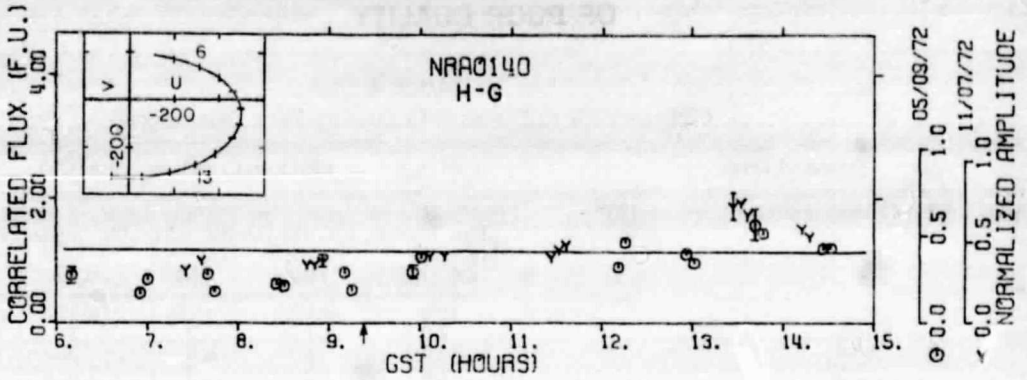

FIG. 1.—Correlated flux versus GST for the QSO NRAO 140, measured with the H-G interferometer. The line through the data points is a sketch only, and has no theoretical basis. The inset shows the $u - v$ track from rise to set for the H-G baseline. Tick marks are on the (GST) hour. The u and v axes have units of fringes per arcsecond, and are defined as follows: u is measured positive in the direction of increasing right ascension, and v is measured positive toward north. The arrow on the GST scale marks the time when the interferometer hour angle is zero.

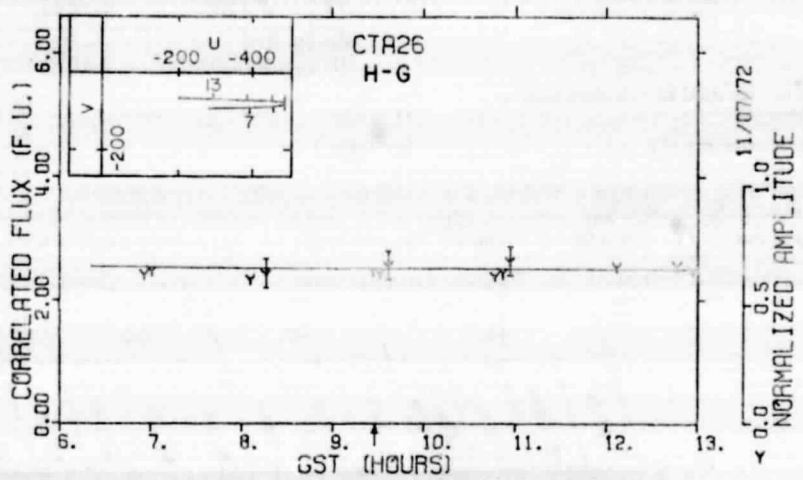

FIG. 2.—As in fig. 1, but for the QSO CTA 26

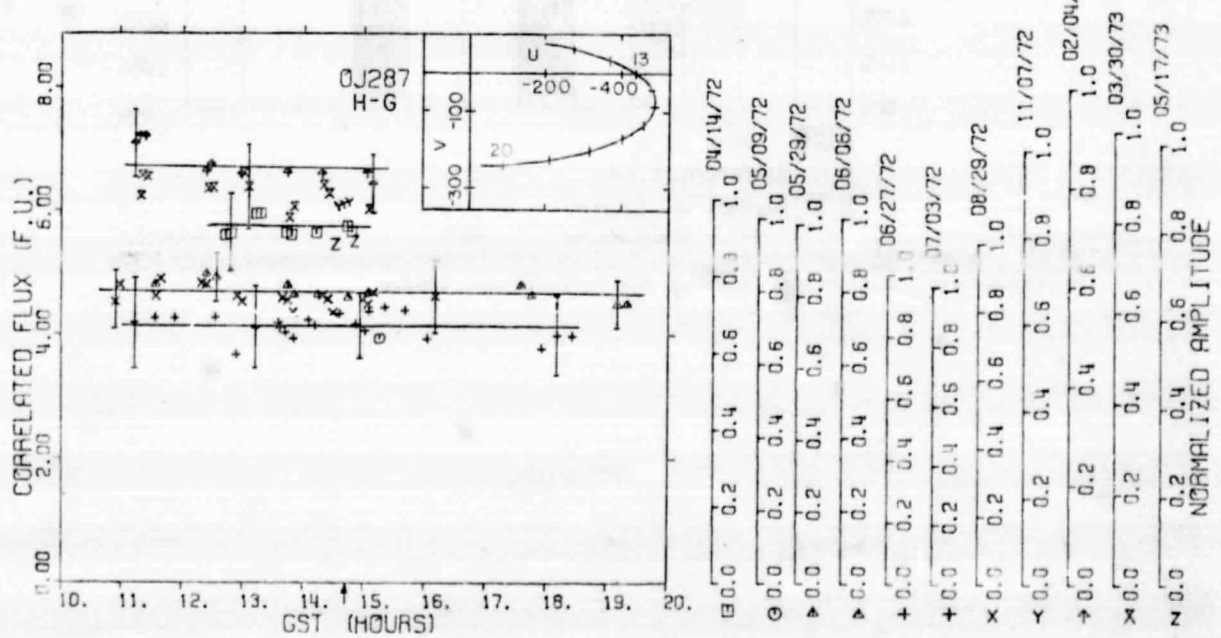

FIG. 3.—As in fig. 1, but for the BSO OJ 287

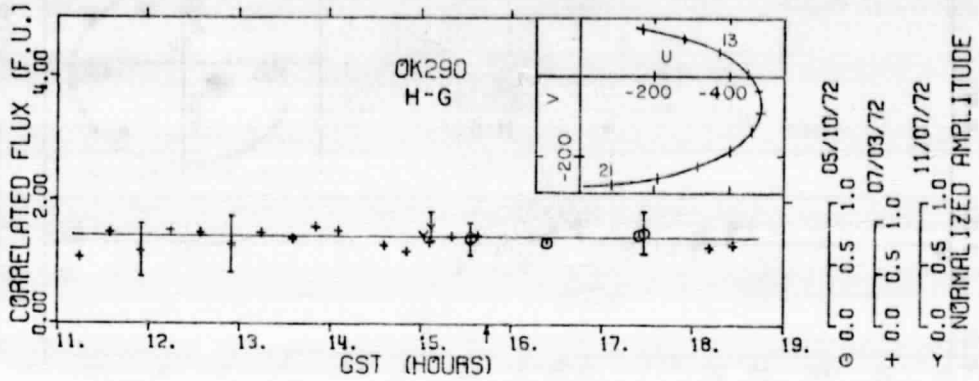

FIG. 4.—As in fig. 1, but for the BSO OK 290

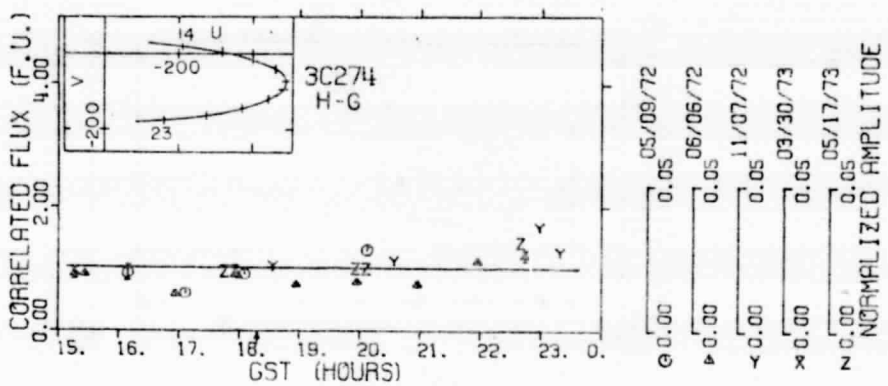

FIG. 5.—As in fig. 1, but for the elliptical galaxy 3C 274

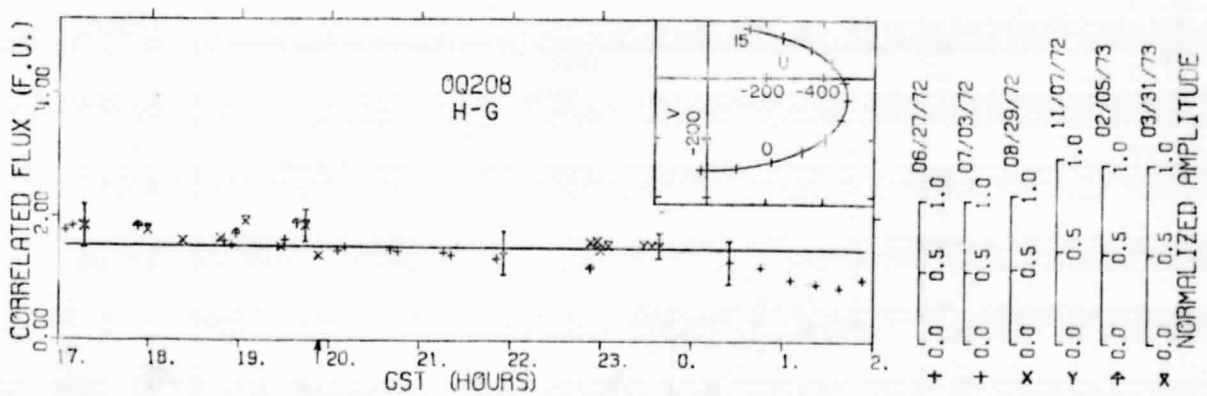

FIG. 6.—As in fig. 1, but for the Seyfert galaxy OQ 208

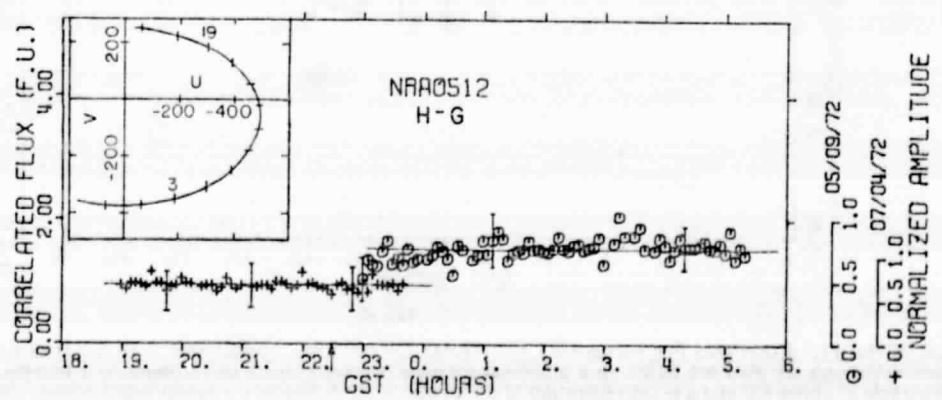

FIG. 7.—As in fig. 1, but for the unidentified object NRAO 512

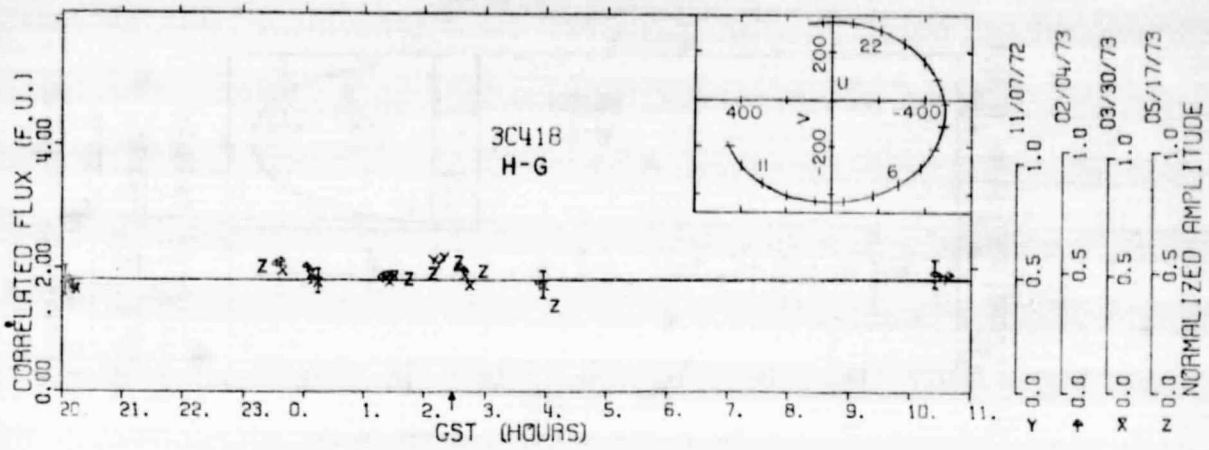

FIG. 8.—As in fig. 1, but for the unidentified object 3C 418

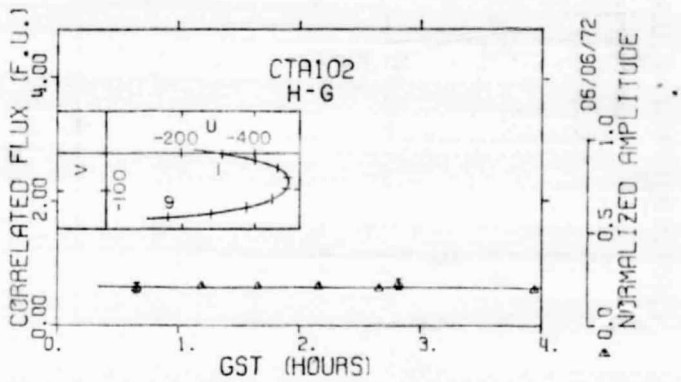

FIG. 9.—As in fig. 1, but for the QSO CTA 102

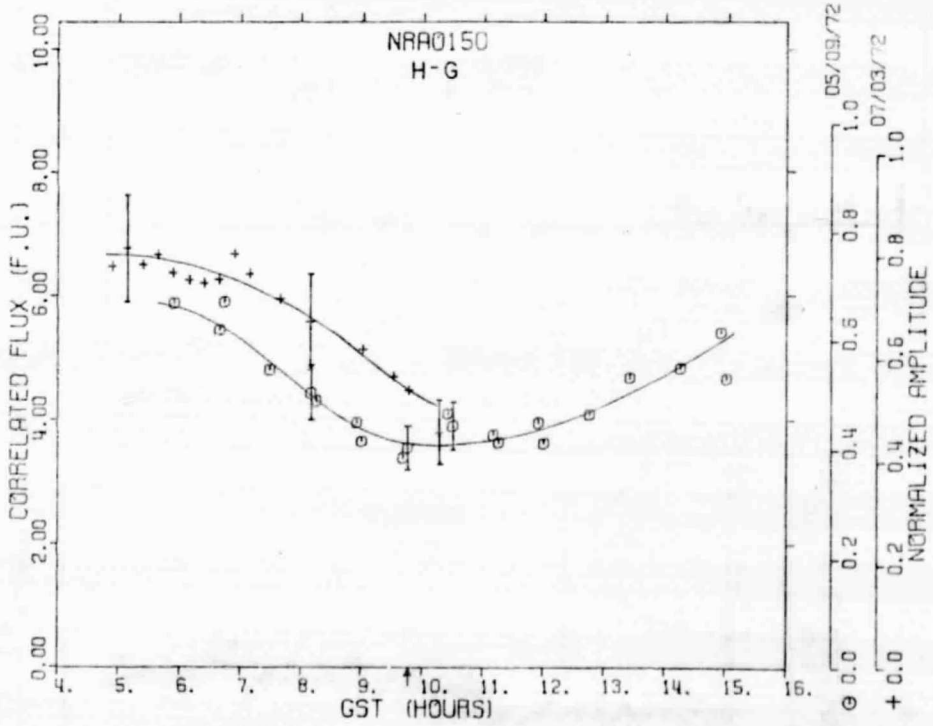

FIG. 10

FIGS. 10 and 11.—Correlated flux versus GST for NRAO 150 observed, respectively, with the H-G and H-O interferometers. The curves through the data are based on a graphical solution (see text) which corresponds to a two-point-source model with a position angle of about 65° and a point separation of about 0.8×10^{-9}. The arrow marks interferometer hour angle equal to zero.

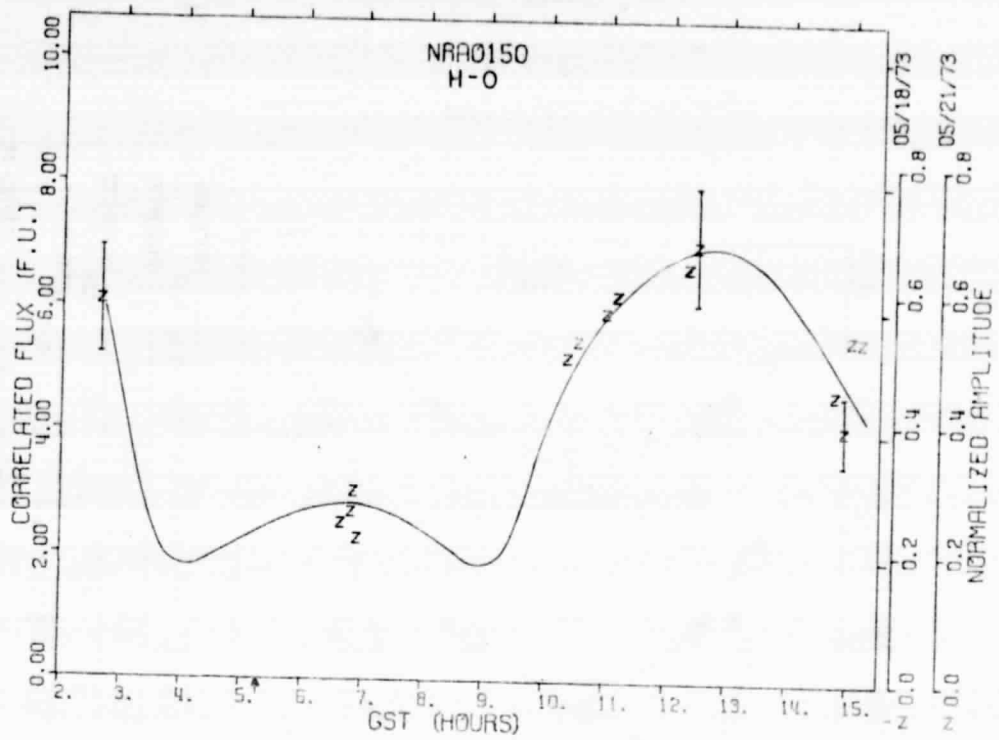

FIG. 11

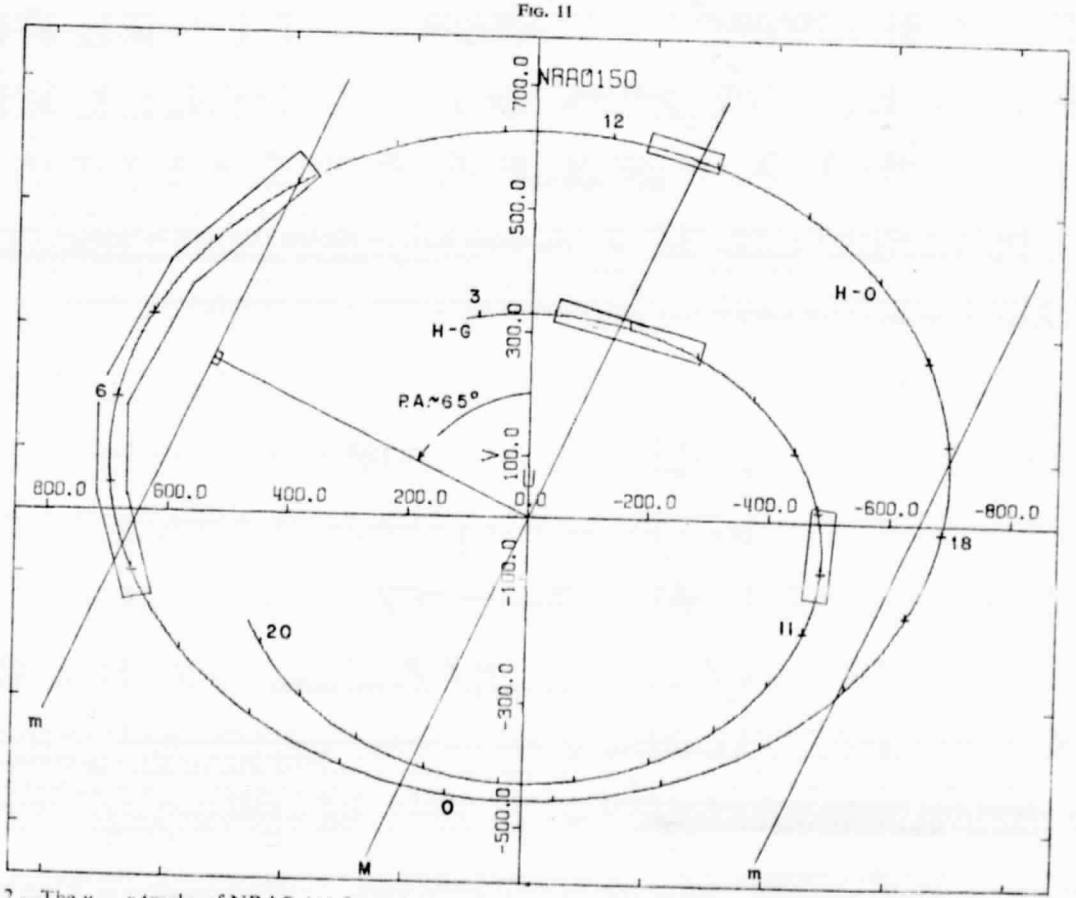

FIG. 12.—The $u - v$ tracks of NRAO 150 from rise to set for the H-G and H-O baselines. The principal maximum and the first minimum, labeled *M* and *m*, respectively, correspond to the model described in the caption of figs. 10 and 11. The boxes enclose regions of the $u - v$ curves where maxima or minima are permitted by the available data. The u and v axes have units of fringes per arcsecond. Tick marks are on the (GST) hour.

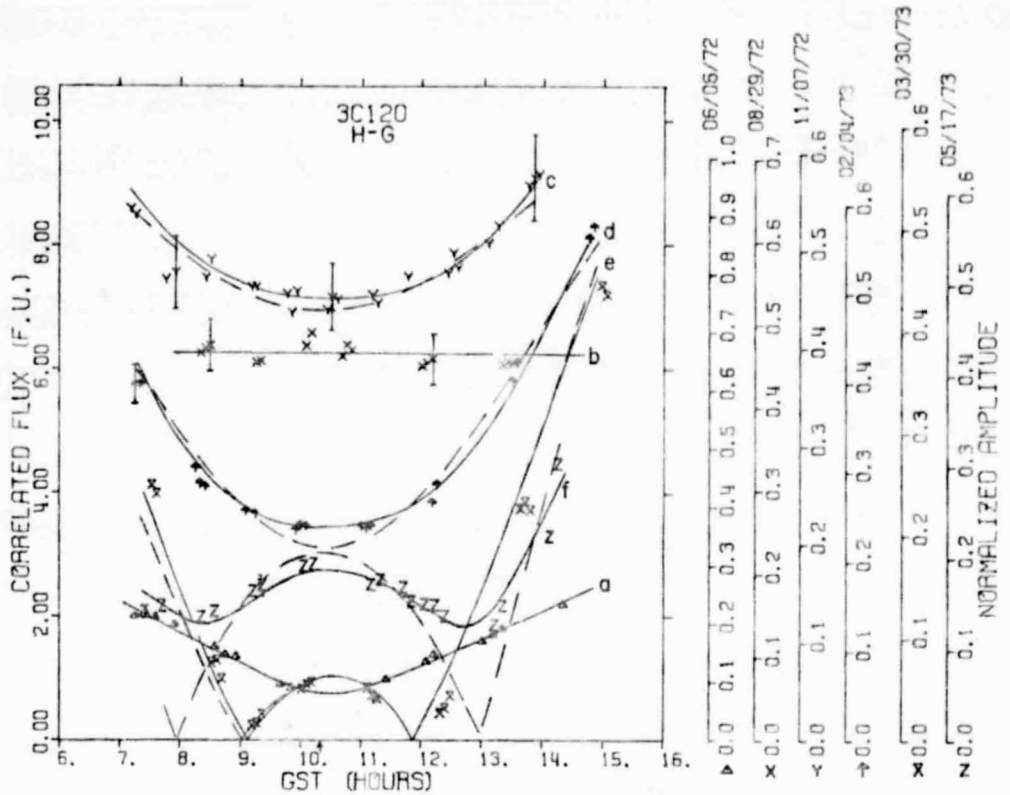

FIG. 13.—Correlated flux versus GST for the Seyfert galaxy 3C 120 observed with the H-G interferometer. The labels a, b, c, d, e, and f each refer to a given day's data and to the curve(s) shown for that day. The solid curve for 1972 June, labeled a, is a sketch only and has no theoretical basis. The solid line for 1972 August, labeled b, represents a single point source. For c, d, e, and f, 1972 November and 1973 February, March, and May, respectively, the solid curves represent a time-variable two-point-source model and the dashed lines a ring-source model. The arrow marks interferometer hour angle equal to zero.

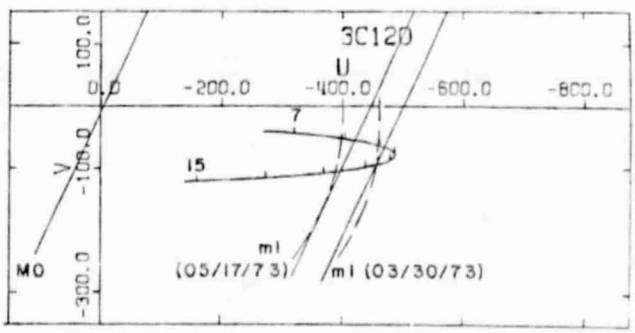

FIG. 14.—As in the inset of fig. 1, but for 3C 120. The solid lines represent the principal maximum and the first minimum, on the two dates indicated, for the time-variable two-point-source model. The dashed circular arcs represent the first minimum, on the same two dates, for the ring-source model.

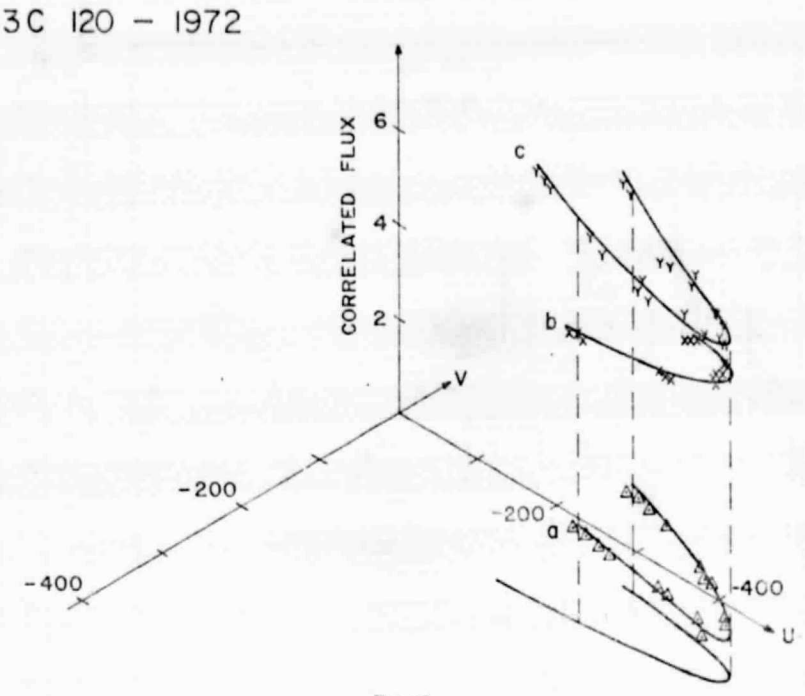

FIG. 15

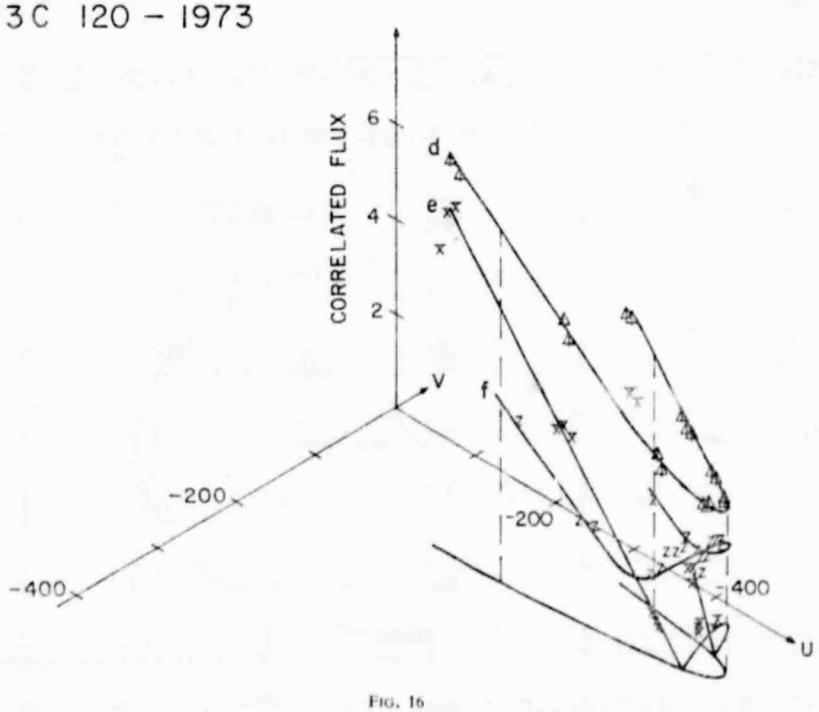

FIG. 16

FIGS. 15 and 16.—Correlated flux as a function of u and v for 3C 120, observed with the H-G interferometer in 1972 and 1973, respectively. The $u - v$ track extends from the first to the last point. Curves a, b, c, d, e, and f are sketches through the data points and have no theoretical basis. The u and v axes have units of fringes per arcsecond. The symbols are the same as in fig. 13.

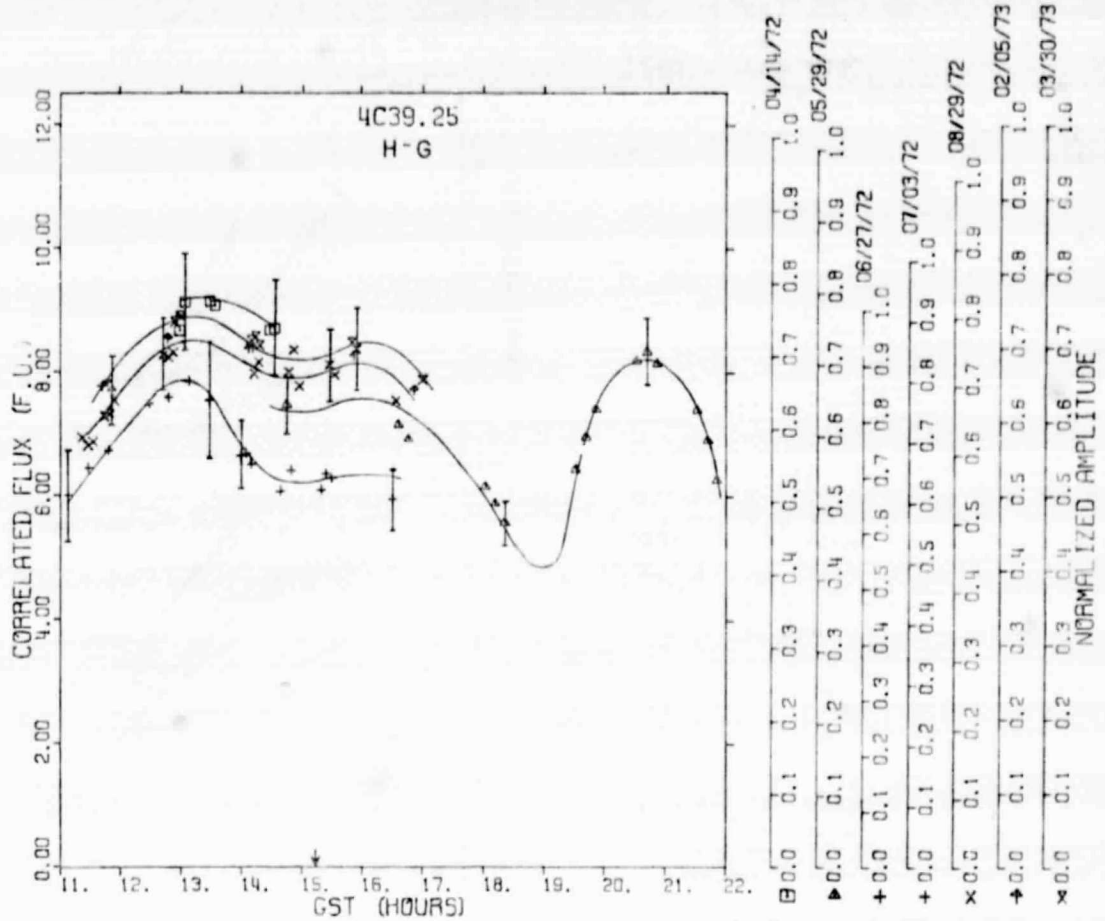

FIG. 17.—As in fig. 1, but for the QSO 4C 39.25

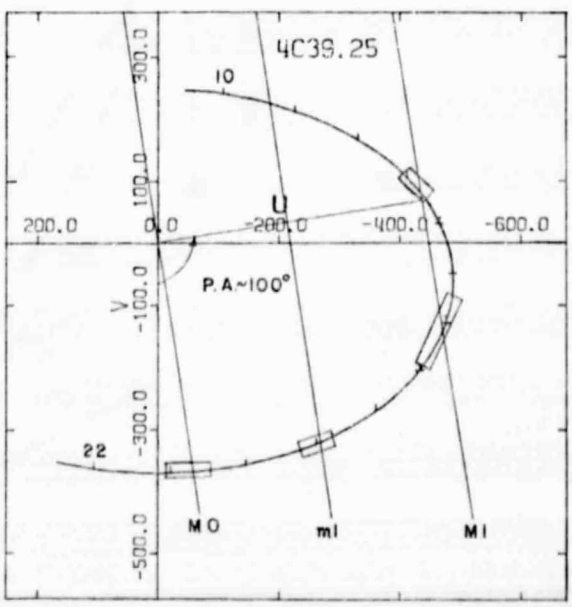

FIG. 18.—As in the inset of fig. 1, but for 4C 39.25. The maxima and minima, labeled *M* and *m*, respectively, with number indicating the order, are for a two-point-source model with a position angle of about 100° and a point separation of about 2.3 × 10^{-3}.

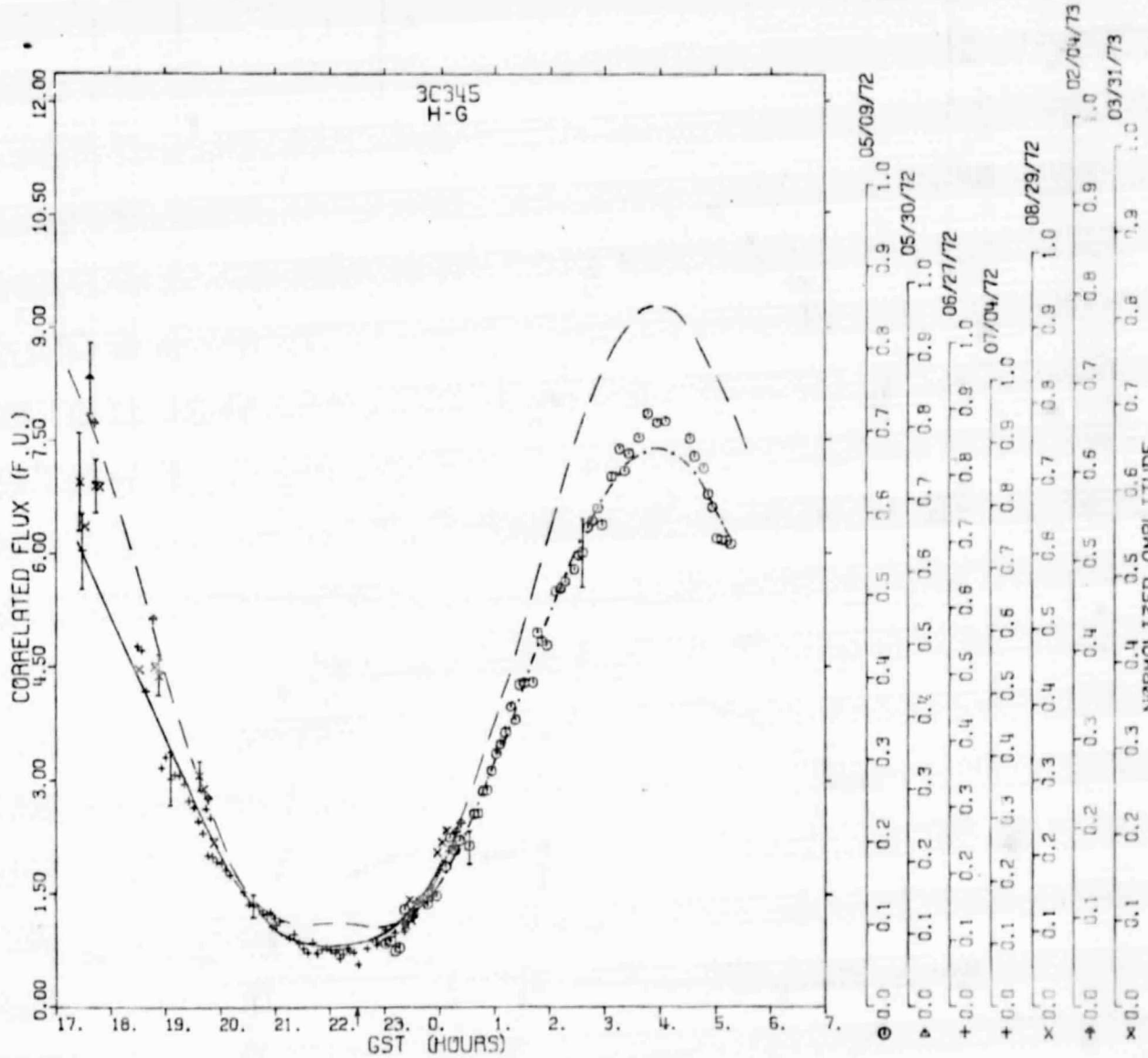

FIG. 19

FIGS. 19 and 20.—Correlated flux versus GST for the QSO 3C 345 observed, respectively, with the H-G and H-O interferometers. The curves through the data are for a two-point-source model with a position angle of 100°, a point separation of about 1705×10^{-3}", and a total strength of 7.4 (*dot-dashed curve*), 7.0 (*solid curve*), and 9.3 fu (*dashed curve*), respectively, for the three groups of data discussed in the text. The arrow marks interferometer hour angle equal to zero.

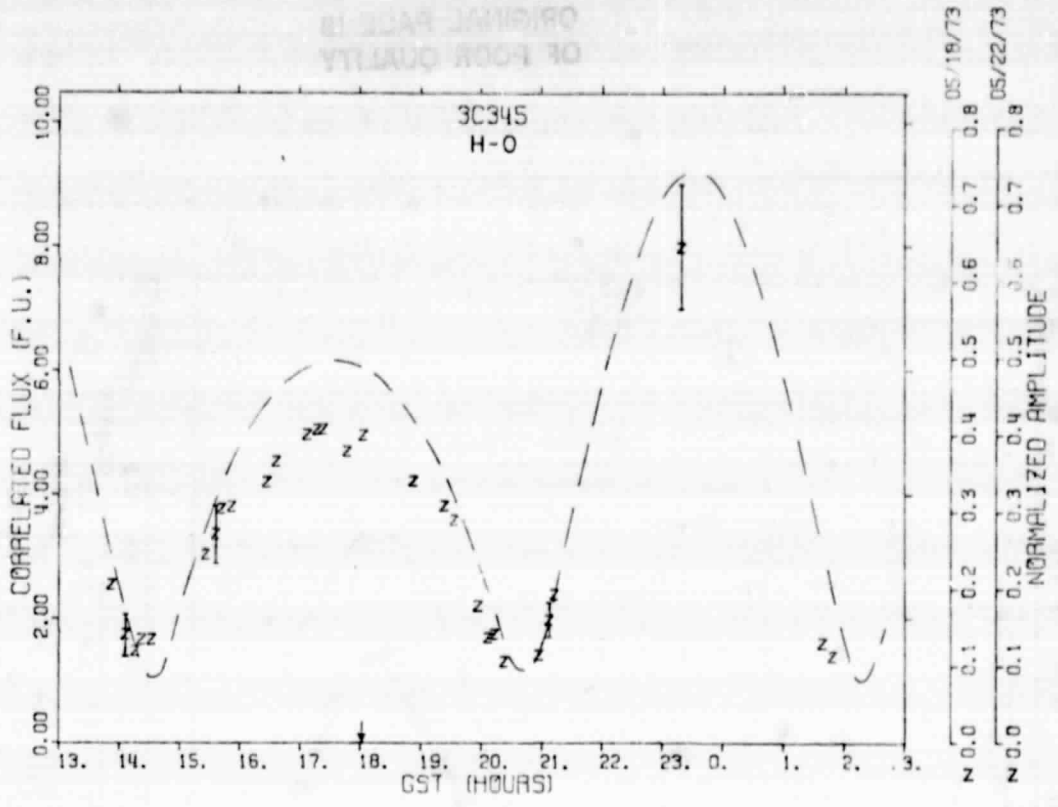

FIG. 20

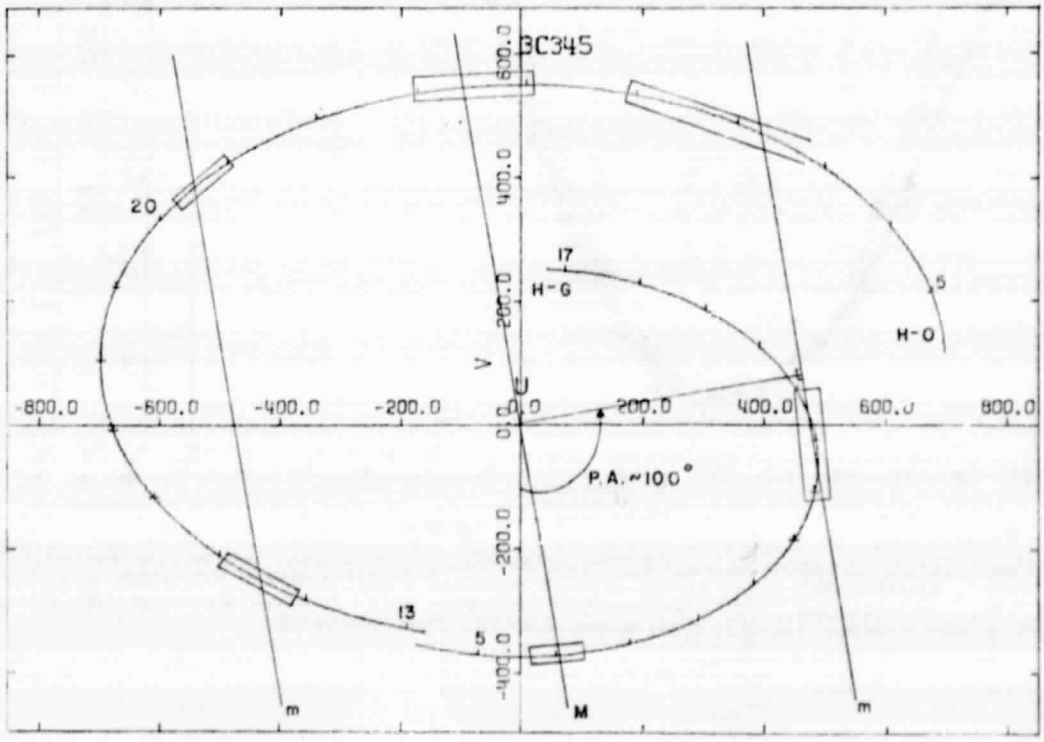

FIG. 21.—The $u - v$ tracks for 3C 345 from rise to set for the H-G and H-O baselines. Tick marks are on the (GST) hour. The lines of maxima and minima, labeled M and m, respectively, correspond to the two-point-source model described in figs. 19 and 20. The boxes enclose those regions of the $u - v$ curves where the data permit maxima and minima to be located. The u and v axes have units of fringes per arcsecond.

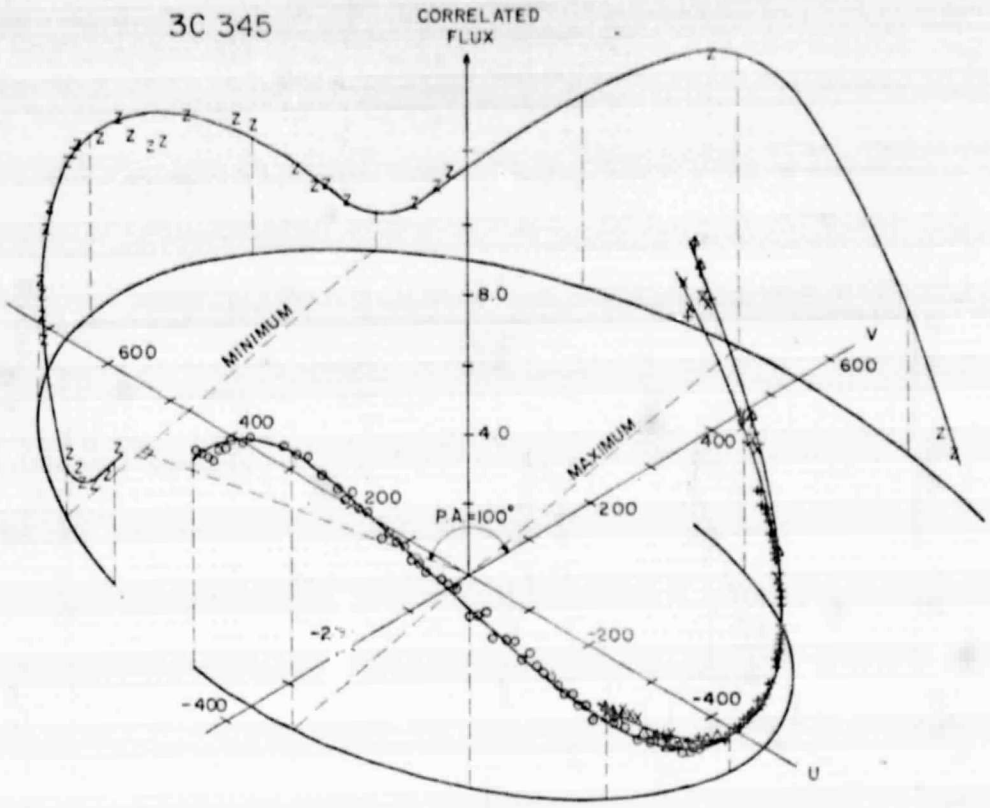

FIG. 22.—Correlated flux as a function of u and v for 3C 345 observed with the H-G and H-O interferometers. The $u - v$ tracks extend from the first to the last data point on each baseline. The locations of the maxima and minima correspond to the two-point-source model described in figs. 19 and 20, but the curves through the data are sketches and have no theoretical basis. The symbols are the same as used in fig. 19. The u and v axes have units of fringes per arcsecond.

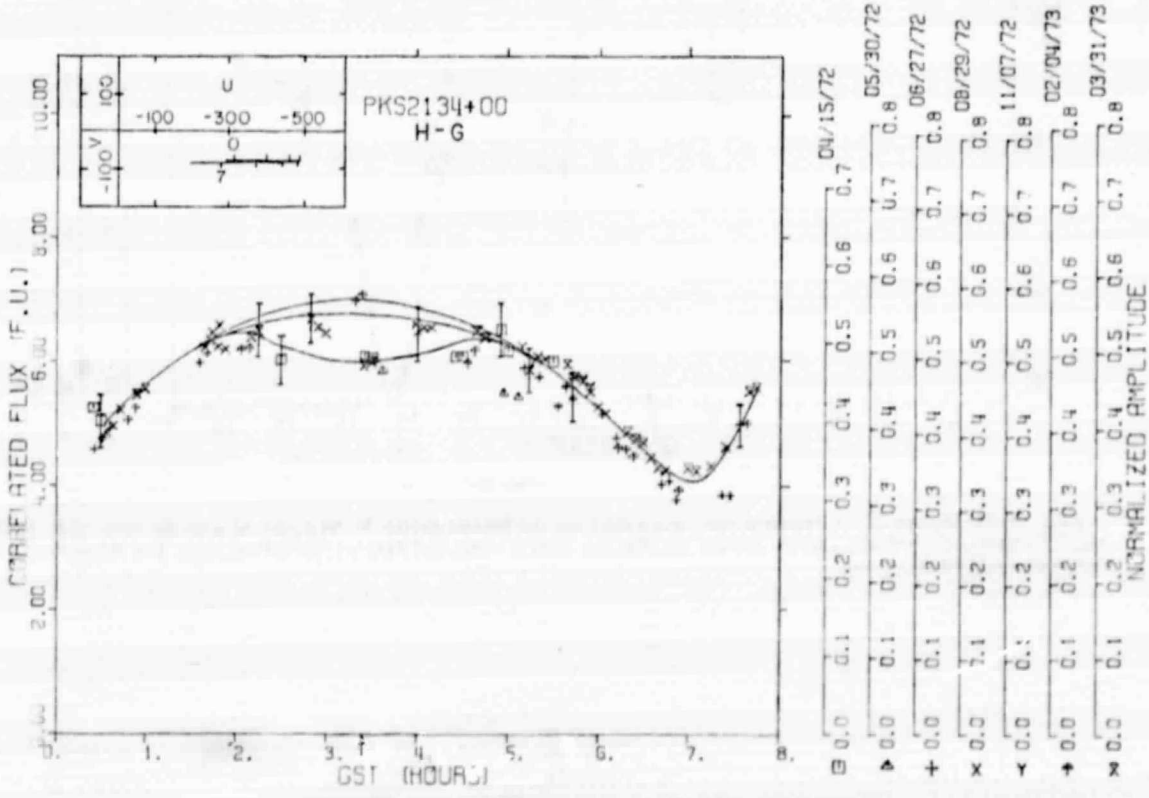

FIG. 23.—As in fig. 1, but for the QSO PKS 2134+00

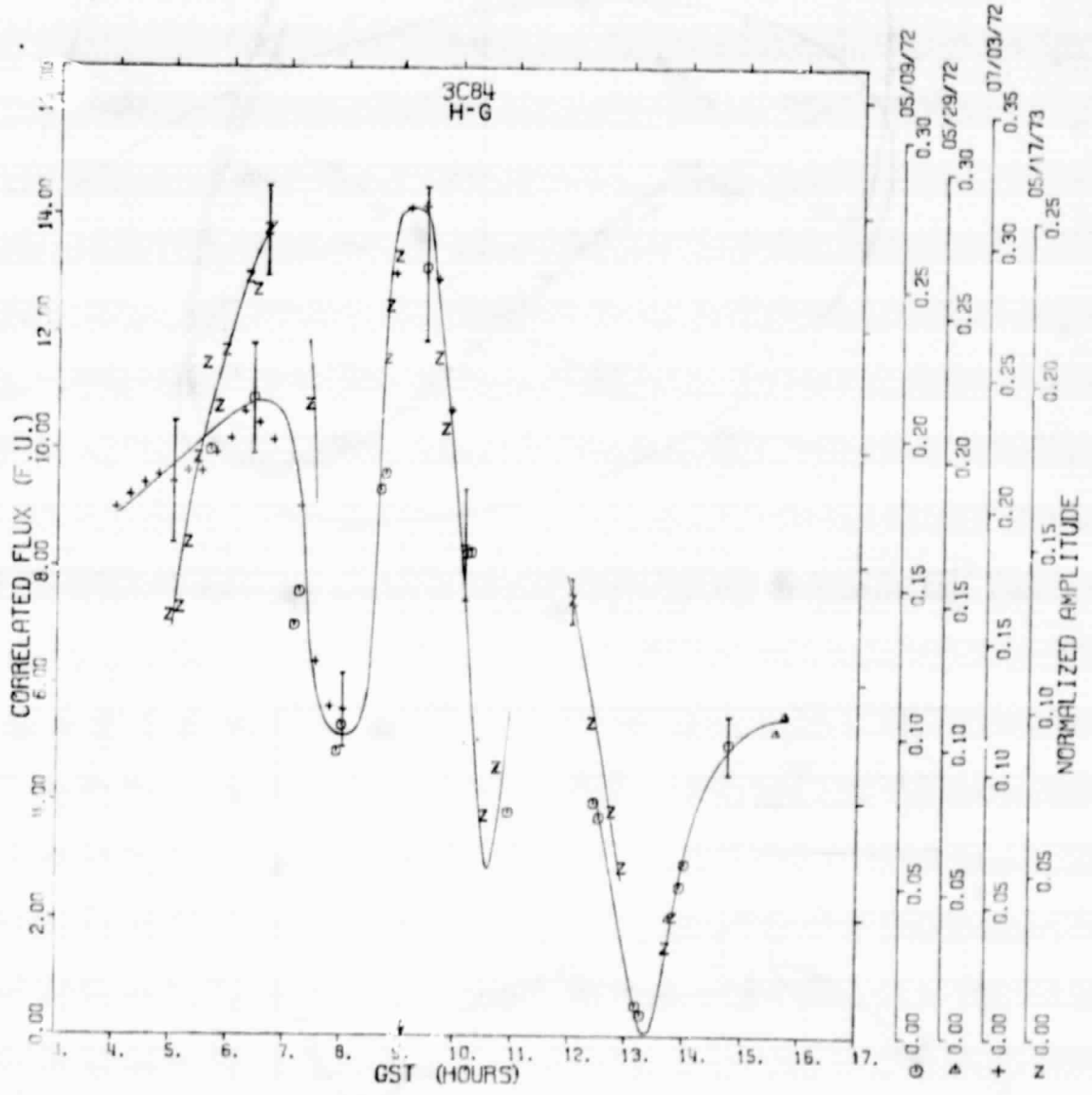

FIG. 24

FIGS. 24, 25, 26, and 27.—Correlated flux versus GST for the Seyfert galaxy 3C 84 observed with the H-G, H-F, H-O, and G-O interferometers, respectively. Curves through the data are sketches only and have no theoretical basis. The arrow marks interferometer hour angle equal to zero.

ORIGINAL PAGE IS
OF POOR QUALITY

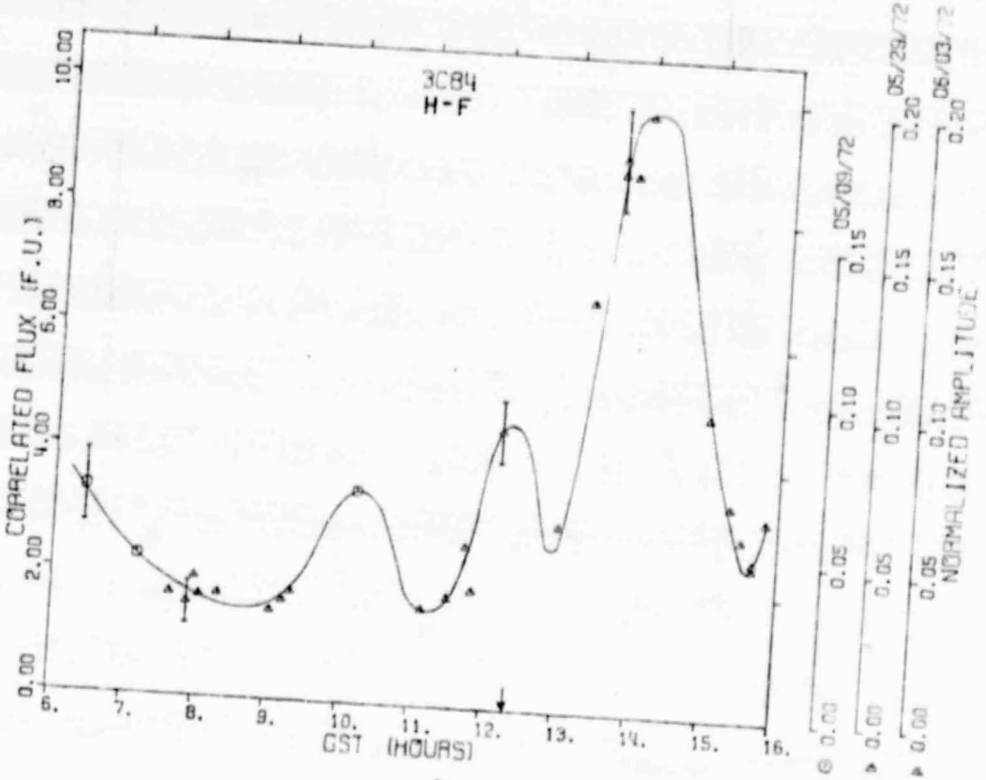

FIG. 25

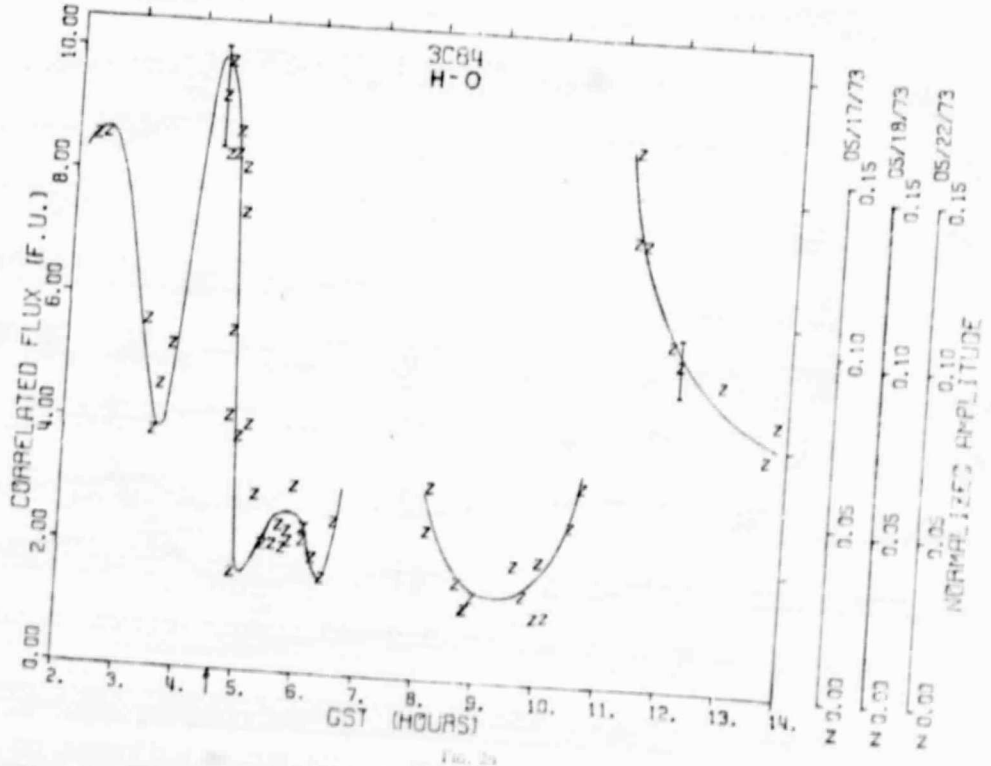

FIG. 26

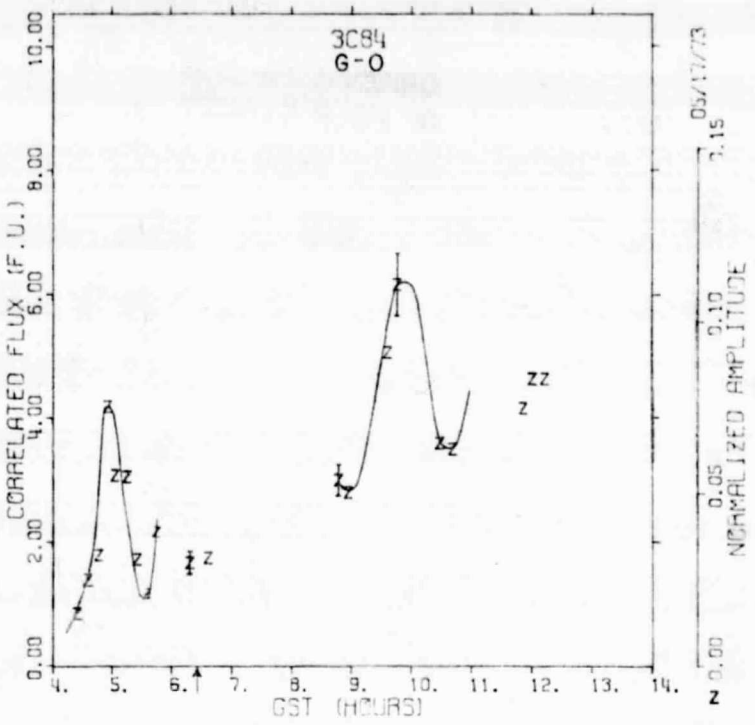

FIG. 27

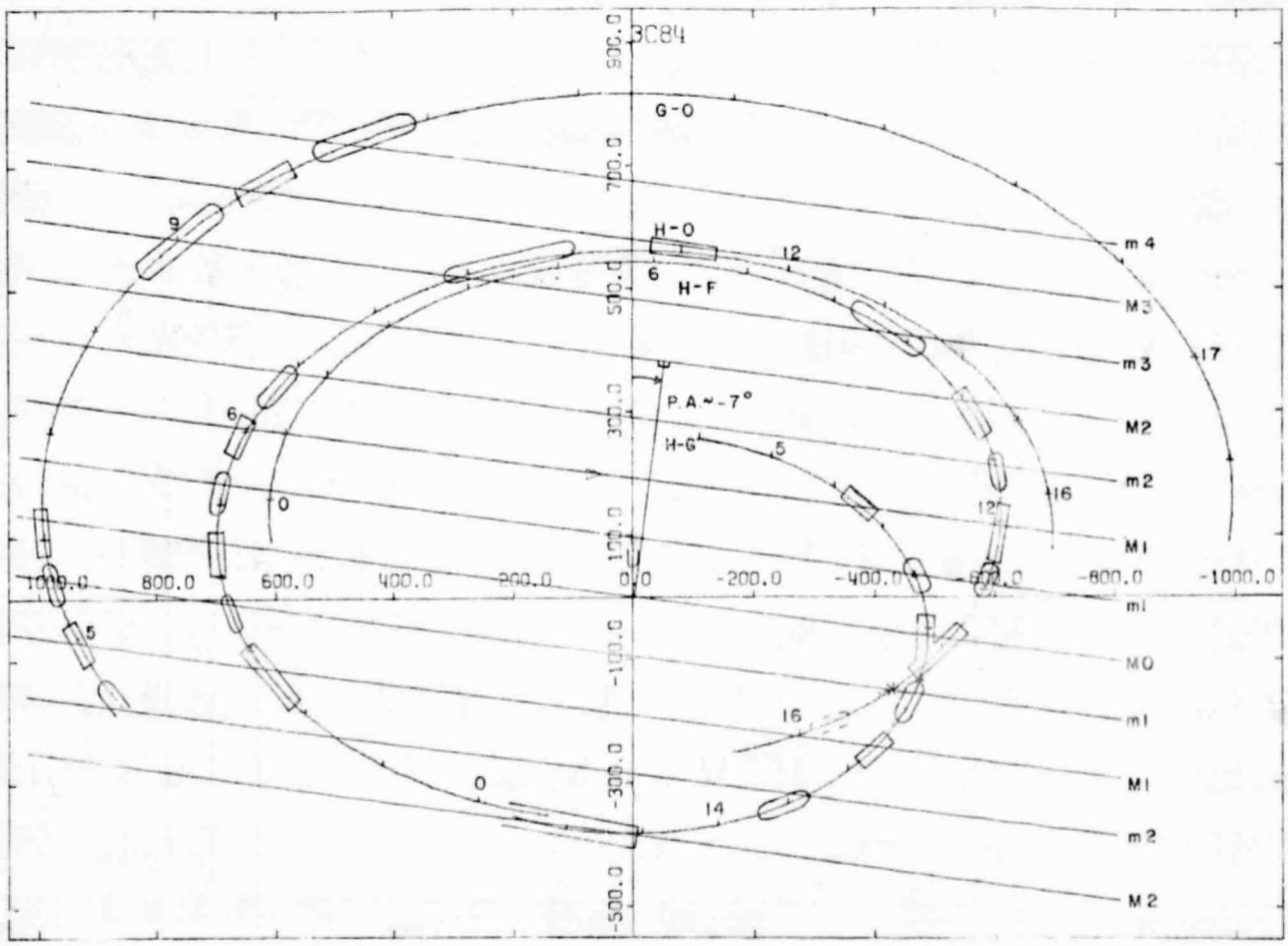

FIG. 28.—The $u - v$ tracks of 3C 84 from rise to set for the H-G, H-F, H-O, and G-O baselines. Tick marks are on the (GST) hour. Lines of maxima and minima, labeled M and m, respectively, and numbered by order, correspond to the two most widely separated points in the linear model (see text) with a position angle of $-7°$ and a point separation of $5° \times 10^{-9}$. Boxes and circles enclose regions of the $u - v$ track in which the data permit maxima and minima, respectively. The dashed circle on the H-F track indicates that the minimum in the data did not appear to fall at the expected position. The u and v axes have units of fringes per arcsecond.

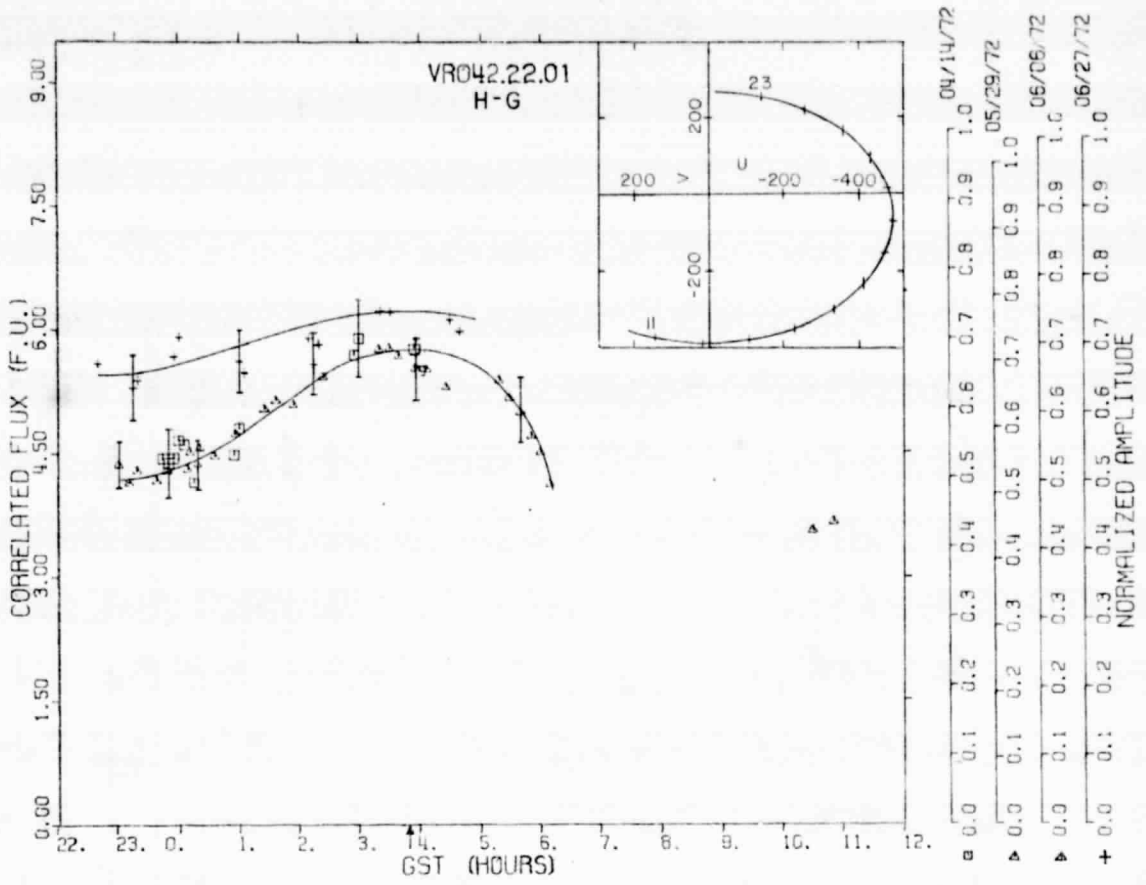

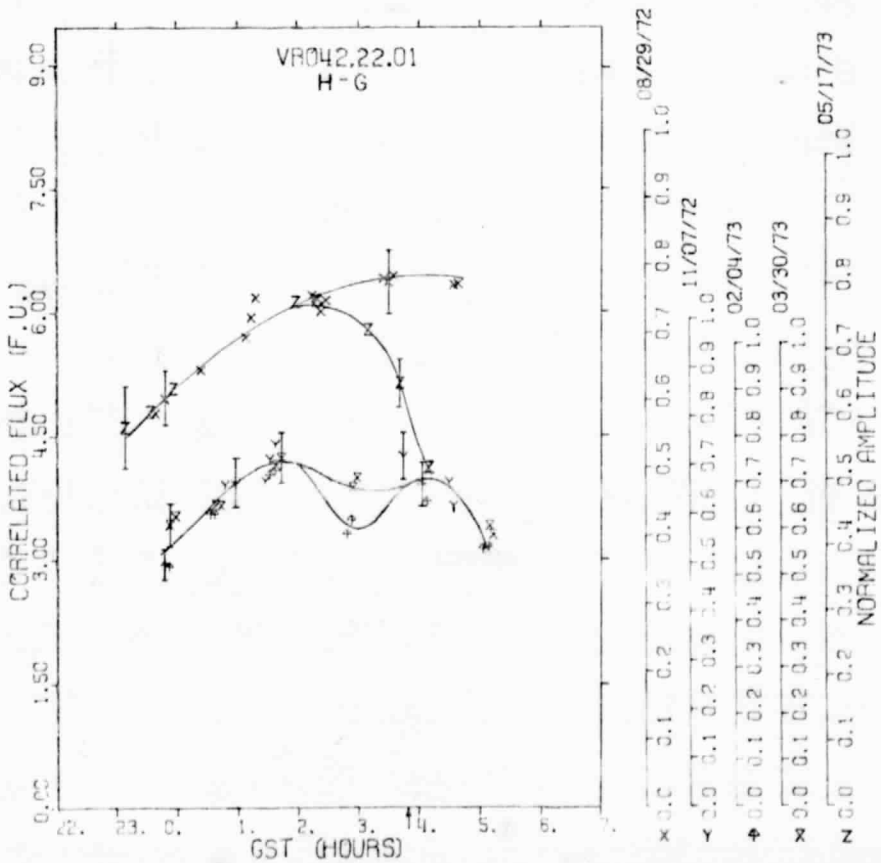

FIGS. 29 (*top*) and 30 (*bottom*).—As in fig. 1, but for the center of an elliptical galaxy, VRO 42.22.01

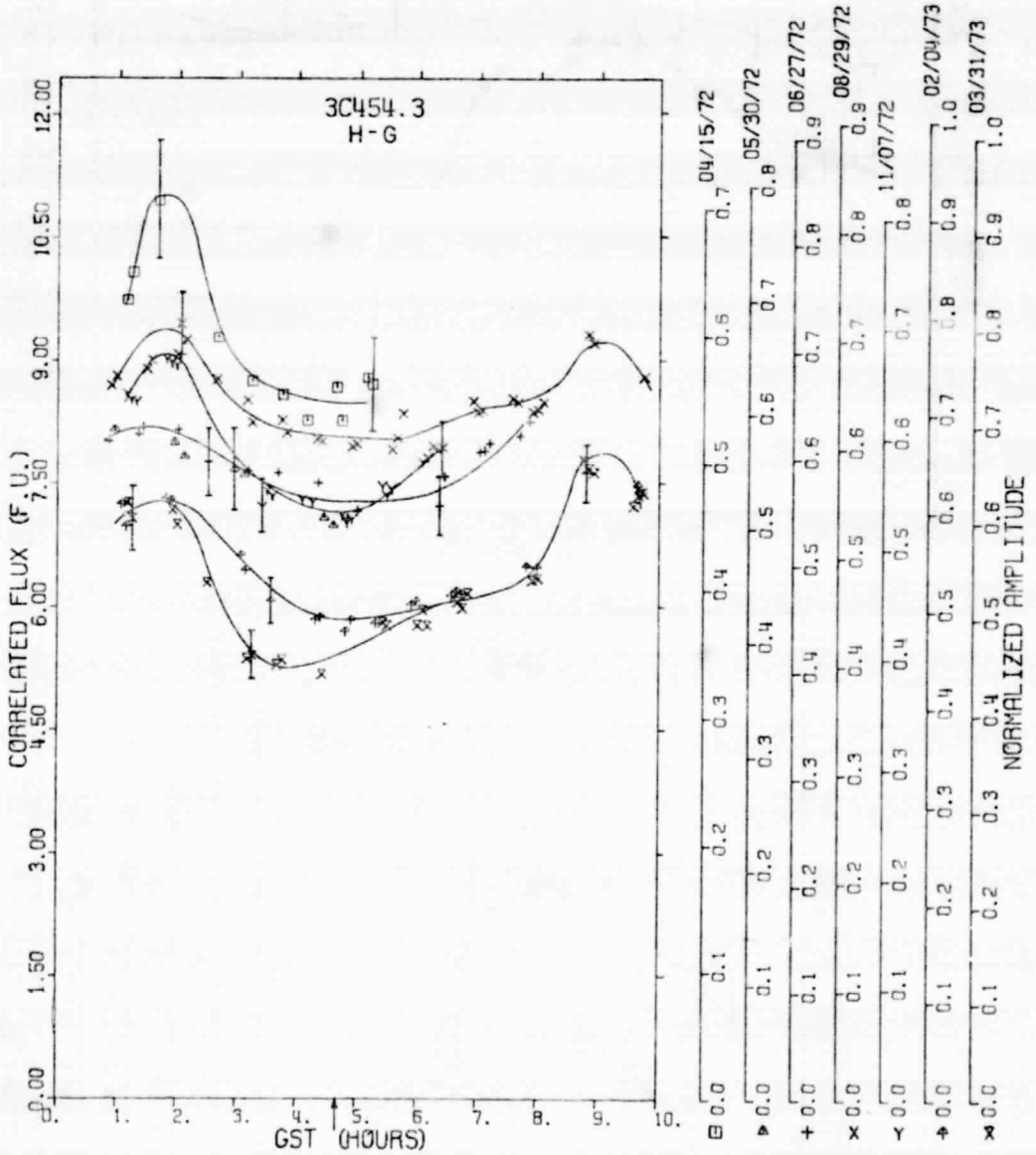

FIG. 31.—As in fig. 1, but for the QSO 3C 454.3

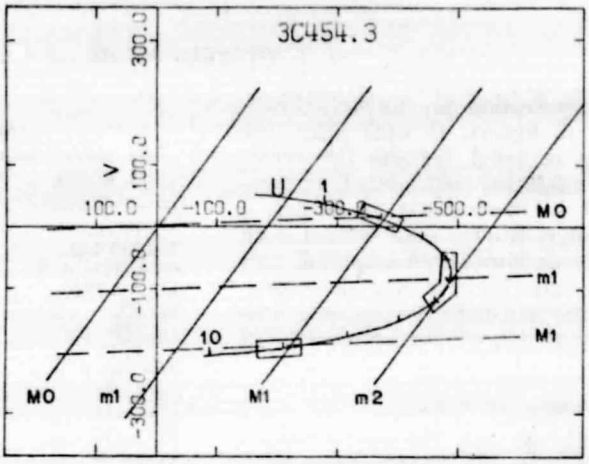

FIG. 32.—As in the inset of fig. 1, but for 3C 454.3. The solid lines of maxima and minima, labeled M and m, respectively, and numbered by order, correspond to a two-point-source model with a position angle of 53° and a point separation of $3\overset{''}{.}5 \times 10^{-3}$; the dashed lines correspond to a two-point-source model with a position angle of about 3° and a point separation of $5'' \times 10^{-3}$. Boxes enclose regions of the $u - v$ track where the data permit maxima and minima.

TABLE 5

CORRELATED FLUXES FROM SHORT SERIES OF OBSERVATIONS

Source	Date	GST	Normalized Amplitude	Correlated Flux (fu)	Baseline	u (fringes per arcsecond)	v
			Data for Sources Not Shown in Figures				
1055+01.....	1972 May 9, 10	$17^h33^m56^s$	0.433 ± 0.044	1.62 ± 0.23	H-G	−478.2	− 81.7
		17 36 56	0.448 ± 0.045	1.68 ± 0.23		−476.8	− 81.9
		18 34 06	0.218 ± 0.028	0.82 ± 0.13		−435.5	− 85.3
		19 34 16	0.481 ± 0.050	1.80 ± 0.25		−363.0	− 88.4
		20 32 26	0.050 ± 0.019	0.19 ± 0.07		−269.3	− 90.8
1116+12.....	1972 May 9, 10	16 14 43	0.114 ± 0.046	0.17 ± 0.07	H-G	−476.3	− 52.6
		18 15 03	0.362 ± 0.098	0.54 ± 0.16		−467.1	−108.4
1127−14.....	1972 May 9, 10	15 40 38	0.167 ± 0.017	0.95 ± 0.13	H-G	−445.5	−127.1
		16 41 48	0.135 ± 0.015	0.77 ± 0.11		−482.8	− 95.5
		16 45 49	0.150 ± 0.015	0.86 ± 0.12		−484.0	− 93.3
		17 41 58	0.142 ± 0.015	0.81 ± 0.11		−486.1	− 63.1
		18 42 08	0.218 ± 0.017	1.24 ± 0.15		−456.1	− 31.6
		19 42 17	0.392 ± 0.028	2.23 ± 0.26		−394.8	− 3.1
1148−00.....	1972 May 9, 10	17 18 54	0.099 ± 0.048	0.14 ± 0.07	H-G	−487.0	− 78.9
		19 15 13	0.238 ± 0.080	0.33 ± 0.12		−445.8	− 77.8
OR 103.....	1972 July 3, 4	00 15 22	0.661 ± 0.164	1.52 ± 0.43	H-G	−308.9	−147.0
		00 35 25	0.673 ± 0.167	1.55 ± 0.43		−274.6	−151.7
		00 55 29	0.636 ± 0.168	1.46 ± 0.43		−238.2	−155.9
		01 15 32	0.674 ± 0.178	1.55 ± 0.46		−200.0	−159.4
		01 30 35	0.623 ± 0.164	1.43 ± 0.42		−170.3	−161.6
CTD 93.....	1972 July 3, 4	02 35 45	0.197 ± 0.096	0.26 ± 0.13	H-G	−170.0	−276.6
		02 40 46	0.134 ± 0.064	0.17 ± 0.09		−159.9	−278.2
OV 080	1972 July 3, 4	02 55 48	0.347 ± 0.185	0.38 ± 0.21	H-G	−460.8	−100.7
		03 00 49	0.425 ± 0.226	0.47 ± 0.26		−457.1	−102.1
OX 161	1972 July 3, 4	03 15 52	0.333 ± 0.144	0.40 ± 0.18	H-G	−488.2	− 70.5
		03 20 53	0.398 ± 0.171	0.48 ± 0.22		−488.6	− 73.2
			Additional Data for Sources Shown in Figures				
3C 84..	1972 May 9, 10	06 25 07	0.030 ± 0.004	1.54 ± 0.23	G-F	+283.7	+389.0
		07 10 14	0.019 ± 0.003	0.99 ± 0.19		+221.8	+422.0
		10 10 44	0.016 ± 0.004	0.80 ± 0.19		− 83.4	+460.0
		12 26 06	0.045 ± 0.005	2.28 ± 0.33		−289.9	+384.9
		13 56 21	0.054 ± 0.005	2.75 ± 0.36		−376.1	+297.0
	1972 May 29, 30	13 39 56	0.014 ± 0.003	0.68 ± 0.15	G-F	−364.4	+314.6
		13 49 57	0.012 ± 0.003	0.61 ± 0.15		−371.8	+303.9
OJ 287.....	1973 May 17, 18	14 37 59	0.893 ± 0.110	6.34 ± 0.86	H-O	+281.8	+346.1
		14 37 59	0.754 ± 0.069	5.35 ± 0.59	G-O	+770.5	+416.7
		14 48 00	0.708 ± 0.069	5.03 ± 0.59		+742.2	+428.1
3C 274.....	1973 May 17, 18	17 45 29	0.014 ± 0.005	0.67 ± 0.24	H-O	+359.4	+260.4
		17 55 31	0.022 ± 0.004	1.03 ± 0.21		+332.8	+263.6
		17 45 29	0.011 ± 0.002	0.53 ± 0.11	G-O	+843.1	+321.9
		17 55 31	0.010 ± 0.002	0.49 ± 0.10		+819.2	+329.8

Data from a given observation day are plotted with the same symbol in all figures; in each figure the symbol for each day is listed beneath the corresponding normalized amplitude axis, and all the symbols are listed in table 1. Observations spaced only a few days apart are plotted with the same symbol, even though there is a separate normalized-amplitude axis on the right side of the figure for each observation day. Note that 1.0 on the normalized-amplitude axis corresponds to the total flux on the correlated-flux axis.

IV. DISCUSSION OF RESULTS

In this paper we discuss only the milliarcsecond structure of the sources as our measurements have little sensitivity to any larger-scale components. The sources are divided into groups according to the minimum number of point components apparently required for a model to yield results compatible with all the data herein presented. More complex models, including extended components, are always possible to construct, but our arrangement is designed to point out a minimum possible level of complexity. Within each group, sources are listed in order of increasing right ascension; the type of object is given in parentheses after the radio name, as is the redshift when available. Table 6 gives the right ascension and declination of each of the sources observed for convenience.

For the sources listed in table 5, but not shown in figures, there are insufficient data to classify them by number of components. However, it should be noted that 1055+01, 1116+12, 1127−14, and 1148−00 seem to show variations in the correlated flux with baseline projection, whereas OR 103 does not.

a) Sources with a Minimum of One Point Component

Sources considered to contain a single, point component have correlated fluxes independent of projected baseline (i.e., "flat," horizontal curves). This group includes NRAO 140 (QSO, $z = 1.258$), figure 1; CTA 26 (QSO, $z = 0.852$), figure 2; OJ 287 (BSO), figure 3; OK 290 (BSO), figure 4; 3C 274 (elliptical galaxy, $z = 0.004$), figure 5; OQ 208 (Seyfert galaxy, $z = 0.077$), figure 6; NRAO 512 (unidentified), figure 7; 3C 418 (no optical object identified), figure 8; and CTA 102 (QSO, $z = 1.037$), figure 9. For most of these sources, our measurements lack the sensitivity to determine whether or not the curves of correlated flux have significant structure. For OJ 287, however, we can conclude that its correlated-flux curve is flat within about 10 percent, about twice the uncertainty of each data point. For NRAO 140, the deviations from horizontal may be significant. The measurements of correlated flux presented by Cohen *et al.* (1971) agree well with our corresponding measurements obtained at about 9:15 and 13:30 GST, thus tending to confirm the significance of the difference in the values of correlated fluxes we obtained for these times. For OQ 208, the slightly negative slope of the correlated flux in figure 6 may also be significant. It should also be noted that the total flux of OQ 208 changed significantly between late 1972 and early 1973.

TABLE 6

SOURCE POSITIONS (1950.0)

Source	Right Ascension	Declination
3C 84	3h16m29s5	+41°19′52″
NRAO 140	3 33 22.4	+32 08 37
CTA 26	3 36 59.2	−01 56 19
NRAO 150	3 55 47.4	+50 49 38
3C 120	4 30 31.6	+05 14 59
OJ 287	8 51 57.2	+20 17 59
4C 39.25	9 23 55.3	+39 15 24
OK 290	9 53 59.4	+25 29 40
1055+01	10 55 55.3	+01 50 03
1116+12	11 16 20.6	+12 51 07
1127−14	11 27 35.7	−14 32 55
1148−00	11 48 10.2	−00 07 13
3C 274	12 28 18.0	+12 39 43
OQ 208	14 04 45.6	+28 41 29
OR 103	15 01 52.5	+10 41 19
CTD 93	16 07 08.9	+26 49 13
NRAO 512	16 38 48.1	+39 52 31
3C 345	16 41 17.6	+39 54 11
OV 080	19 47 39.2	+07 59 16
3C 418	20 37 07.4	+51 08 36
DR 21	20 37 14.3	+42 08 56
PKS 2134+00	21 34 05.2	+00 28 25
OX 161	21 36 36.0	+14 10 00
VRO 42.22.01	22 00 39.4	+42 02 08
CTA 102	22 30 07.8	+11 28 23
3C 454.3	22 51 29.5	+15 52 54

For each of the sources considered in this section the point component does not contain all of the flux since the normalized amplitudes are all less than unity. In addition, some of the sources show time variability in their N.A.'s. For OJ 287, for example, the normalized amplitude ranges between 0.75 and 0.95; the flux in the point component is time-variable as well, as indicated in figure 3 by the change in the correlated flux from one date to another. For NRAO 512 (see fig. 7) the significant change in correlated flux between the two observing days may be due to a decrease in the flux from the point component, since the normalized amplitude remained about constant. The possibility that the change in correlated flux may be due to a systematic difference in the calibration for these two days may be discounted since 3C 345, observed concurrently, showed the same correlated flux on the two days: it is unlikely that any systematic effect that made NRAO 512 appear to change would have had exactly the right sign and magnitude to make 3C 345 appear not to change.

Finally, we note that for 3C 274 at least 95 percent of the flux is resolved on all baselines used in our experiments, with the remaining 5 percent ($\leqslant 2.5$ fu) being contained in a small unresolved component (fig. 5 and table 5). As with the weak sources discussed above, our measurements lack the sensitivity to determine conclusively whether or not this small component is partially resolved with our interferometers. By contrast, Cohen *et al.* (1971) and Kellermann *et al.* (1973*a*) interpret their data as showing this compact component to be just resolved with the H-G interferometer.

b) Sources with a Minimum of Two Point Components

Sources in this category are those for which a two-point model was the simplest one consistent with the measured correlated fluxes. In the following discussion errors are quoted only for those model parameters calculated by a least-squares fitting procedure, and not for those determined by graphical means.

i) *NRAO 150* (no optical object identified)

We have very few data for NRAO 150 (see figs. 10 and 11), and the observation days are widely spaced. Unfortunately we cannot test the significance of the change in level of the correlated-flux data by comparison with another source since the only source observed simultaneously on both observation days, 3C 120, is itself highly variable. The large error bars and the large gaps in the u-v plane coverage for NRAO 150, especially for the H–O baseline, make the determination of the locations of the maxima and minima for each day's data uncertain. Nevertheless, the curves indicate that a time-independent two-component model may provide a reasonable description and allow an estimate of a maximum size for the source to be made. We do this by ignoring the differences in correlated-flux level between 1972 July and May, combining all of the data, and assuming a pair of minima occur as close to the maxima as the data will allow (see fig. 11). This assumption corresponds to minimizing the spacing in the u-v plane between the principal maximum and the first minimum, corresponding to the largest possible source spacing. Then from a graphical solution (see fig. 12) we find that the line joining the (assumed) two components has a position angle of about 65° and that the components can have a maximum separation of about $0\overset{''}{.}8 \times 10^{-3}$. This graphical solution does not yield a useful result for the relative strengths of the components since the minimum value of the correlated flux is very uncertain.

ii) *3C 120* (Seyfert galaxy, $z = 0.033$)

The 1972 data for 3C 120 have been discussed previously by Shapiro *et al.* (1973) and Kellermann *et al.* (1973*b*); these data were consistent with a model with either two separating components, one or two stationary but time-variable components, or a single spherically or circularly symmetric expanding component. The 1973 data from February, March, and May are consistent with the first possibility, but may not be consistent with the other two (see figs. 13, 14, 15, and 16). We will now outline the analysis which leads to this conclusion.

All of the correlated-flux data for 3C 120 obtained between 1972 November and 1973 May can be fitted well with a two-point component model characterized by four variable parameters: separation of the point components, the position angle of the line connecting the two point components, the total correlated flux $(S_1 + S_2)$, and the fractional difference in strengths, $(S_1 - S_2)/(S_1 + S_2)$, where S_1 and S_2 are the contributions to the correlated flux from the individual point components. Solving for all four parameters from each set of data separately, using the weighted least-squares, or maximum-likelihood, estimator, we find that the 1973 March data yield the smallest uncertainty in position angle (10 percent). We therefore fixed the position angle at 65°, as given by the March data, and re-solved for the three remaining parameters from each set of data separately. The results, with the accompanying standard errors, are given in table 7 and the corresponding curves for the model are plotted as solid lines c, d, e, and f in figure 13. The point separation given by this model remains at about $0\overset{''}{.}99 \times 10^{-3}$ between 1972 November and 1973 February and thereafter increases nearly linearly to $1\overset{''}{.}2 \times 10^{-3}$ by 1973 May. This rate corresponds to an apparent velocity of diameter expansion of 1.5–2 c by 1973 May, if we take $z = 0.033$, $H = 75$ km s^{-1} Mpc^{-1}, and $q_0 = 1$.

If the separation and relative orientation of the point components in this model are held fixed at the 1972 November values (table 7), but the fluxes of the components are allowed to vary, we find that to match the remaining data the flux from one component must increase and the other decrease until by 1973 March the two are almost equal. As could be inferred from the results for the three-parameter models above, this stationary-point model does not agree well with the 1973 May data because between March and May the minima in the correlated-flux curves move toward the origin in the u-v plane. To circumvent this problem one could postulate that an additional outburst began

TABLE 7

3C 120 MODEL PARAMETERS

Date of Observations	Two-Point Model (Position Angle = 65°) $(S_1 + S_2)$* (fu)	$(S_1 - S_2)/(S_1 + S_2)$	Separation (units $0\overset{''}{.}001$)	Ring Model S† (fu)	Diameter (units $0\overset{''}{.}001$)
1972 November...	11.97 ± 0.68‡	0.594 ± 0.024	0.988 ± 0.010	10.06 ± 0.19	0.740 ± 0.024
1973 February....	10.42 ± 0.19	0.326 ± 0.008	1.004 ± 0.003	9.39 ± 0.19	1.166 ± 0.014
1973 March.....	10.22 ± 0.14	0.017 ± 0.008	1.112 ± 0.002	10.87 ± 0.19	1.648 ± 0.007
1973 May.....	7.78 ± 0.43	0.239 ± 0.012	1.230 ± 0.002	11.73 ± 0.65	1.926 ± 0.010

* S_1 and S_2 are the correlated fluxes for the individual components.

† S is the correlated flux of the ring.

‡ Formal standard error for the weighted rms of the postfit residuals = 1.

between 1973 March and May. However the presence of this outburst should have become apparent in the total flux of the source within a few months; our total-flux measurements for 1973 August (12.1 ± 0.6 fu) and October (11.0 ± 0.6) indicate that if there were such an outburst, it would have had to have been just large enough to cause the correlated flux to change, but not large enough to affect the total flux significantly. We have not yet tried to determine, however, whether an additional outburst, under this restriction, can adequately model the 1973 May data.

We also compared the data with a uniform expanding-ring model; the estimates for the two parameters, source size and strength, from each separate set of data are given in table 7, with the corresponding curves for this model being plotted in figure 13 as the dashed lines c, d, e, and f (see also fig. 14). The experiments conducted between 1972 August and 1973 March each show good agreement between data and model, but for 1973 May the model is in poor agreement with the data. Thus, on balance, the ring model does not represent the data nearly as well as the three-parameter model discussed above. Part of the difficulty is caused by the 1973 May data having smooth, nonzero minima in contrast to the null present in March. By increasing the complexity of the uniform ring, or disk, model and postulating non-uniform distributions, this difficulty can be alleviated. Greater complexity must be incorporated into this model for it to be consistent as well with the increases and decreases observed in the total flux of the source. Phase-closure data from 1973 May, to be published separately, also indicate that a uniform circular distribution of radiation is too simple a model to describe 3C 120 adequately. Finally, we note that the implied expansion velocities for the ring model (see table 7) are quite different from those for the two-point model, and that the estimated correlated flux is especially different for 1973 May.

iii) *4C 39.25* (QSO, $z = 0.699$)

Although the total flux of 4C 39.25 and the level of the correlated flux have both undergone large fractional changes, the shape of the correlated-flux curve did not change substantially with time (see fig. 17). A two-point-source model with a position angle of about 100° and a point separation of about $2\overset{''}{.}3 \times 10^{-3}$ (see fig. 18) is consistent with the main features of the correlated-flux curve. The major discrepancy is that in the 1972 June and July data there does not appear to be a broad maximum between 13–17 hours GST, as required by this model. As with NRAO 150 we cannot determine a useful value for the relative source strength with the simple graphical technique employed here.

iv) *3C 345* (QSO, $z = 0.595$)

Since the total flux of 3C 345 varied substantially during these observations, three groups of H-G data with the total flux nearly constant in each group—1972 May 9/10, 1972 June 27/28 and July 3/4, and 1973 February 4/5 and March 31—were each modeled separately by a two-point-component model of the same form as that described in the discussion of 3C 120. In the three cases, the two points were found to have a separation of $(1\overset{''}{.}05 \pm 0\overset{''}{.}05) \times 10^{-3}$ and a position angle of 100° ± 1° (figs. 19, 20, 21, and 22). Figure 19 shows the curves for this model obtained from each of these groups of data.

The only significant difference among the three sets of parameters was in the total correlated flux for the two components, which was $(S_1 + S_2) = 7.4 \pm 0.1$, 7.0 ± 0.1, and 9.3 ± 0.3 fu, respectively, for the three groups of data, reflecting the changes in total flux for the source. The fractional difference in strengths of the points remained at about $(S_1 - S_2)/(S_1 + S_2) = 0.72 \pm 0.02$; one might not expect independent components to change in a coordinated manner, but mechanisms consistent with such an observation are easy to fabricate.

It should be noted that when Cohen *et al.* (1971) observed 3C 345 with the H-G interferometer in 1971 February, the data also exhibited the same minimum and maximum but the entire correlated flux curve was about 3 fu higher than in 1972 and 1973. This difference cannot be explained by an overall scaling difference because the ratios of maximum to minimum correlated flux were not the same for the two sets of data.

In 1973 May, 3C 345 was also observed with the H-O interferometer (figs. 20 and 22). The minima and maxima of the correlated-flux curve confirm the separation and position angle deduced from the H-G data. However, the overall level of the correlated flux curve for the model based on the 1973 H-G data, and shown as a dashed line in figure 20, is too high, especially since the total flux rose slightly between March and May. The fact that the model curve agrees better at low than high correlated flux indicates that the discrepancy may be at least partially due to an overall scale error, such as could result if the efficiency of the Onsala antenna had been lower than assumed, since all source temperatures were calculated for Onsala using this efficiency. This possibility could not be tested since there were no other sources observed simultaneously on both baselines for which useful comparisons could easily be made.

v) *PKS 2134+00* (QSO, $z = 1.936$)

The total flux of this source remained essentially constant at about 12 fu between 1972 April and 1973 March (Dent 1972*a*). The correlated flux, however, appears to have undergone minor changes, just larger than the measurement uncertainty. For example, as seen in figure 23, at the maximum resolution of the interferometer (03:25 GST), the correlated flux seems to oscillate with time between about 6 and 7 fu. Further, the location of the minimum at about 7 hours GST may have moved slightly from one observation day to the next, but the spacing between data points on any given day is too large to define accurately the location of the minimum.

The 1971 data of Cohen *et al.* (1971) show the same general trends as the data presented here; however, the overall level of the former set is higher by about a factor of 1.5. Since the ratio of the maximum to

minimum measured correlated flux is about 1.4 for their data and 1.5 for our early 1972 data, the higher level of the Cohen *et al.* correlated fluxes may well be due mainly to a scale difference of about a factor of 1.5 in normalization.

We have not attempted detailed model fitting with PKS 2134+00 because the sensitivities of the measurements to position angle and separation for a two-point-component model are very poor due to the near constancy of the v component of the u-v track for any single baseline. Data taken by us in 1973 August and October on six independent baselines simultaneously, which are still being analyzed, should reduce this "declination" problem and help to determine whether there are small variations with time of the correlated flux for this source.

c) *Sources with a Minimum of Three Point Components*

Attempts to develop useful models with more than two points are hampered by the rapid increase in the number of free parameters. Therefore, sources that are more complex than two components cannot yet be modeled adequately, unless their structure is linear. Such linearity may be present in the cases of some of the sources discussed below.

i) *3C 84* (Seyfert galaxy, $z = 0.017$)

The correlated flux of 3C 84 varies faster with changing baseline orientation than that of any other source yet observed. It is also clear from figure 24 that the correlated flux of this source is time variable. This conclusion is supported by the 1971 February data of Cohen *et al.* (1971), which show the maximum at 06 hours GST higher than the maximum at 09 hours GST; locations of maxima and minima are compatible with figure 24.

It is evident from figure 24 that no two-point model can be consistent with this rapidly varying curve. If one sketches the locations of the maxima and minima for all four baselines (see figs. 24–27) on the u-v tracks (see fig. 28), it is possible to draw a set of lines corresponding to the two most widely spaced components of the source, which fall at a position angle between $-6°$ and $-8°$ and are separated by about $5'' \times 10^{-3}$. [Note that only the minimum near 16 hours GST (see fig. 28) of the H-F baseline, coming from by far the most unreliable data and based on only a few points, does not seem to fall close to the "proper" position.]

Phase-closure data from the H-G-O three-site interferometer (Rogers *et al.* 1974) for 1973 May are consistent with a linear model for the source that contains at least three components oriented at a position angle between $-8°$ and $-10°$ with the widest spacing between components being just under $5''.0 \times 10^{-3}$. Legg *et al.* (1973) interpreted their interferometry data as suggesting a model consisting of four aligned components with a position angle of about $-6°$ and a maximum separation between components of about $6''.5 \times 10^{-3}$, which is greater than we obtained either by graphical methods (see fig. 28) or by use of phase-closure data (Rogers *et al.* 1974). We did not, however, make a detailed comparison between this model and our data.

ii) *VRO 42.22.01* (BL Lacertae—center of a giant elliptical galaxy, $z = 0.07$, Oke and Gunn 1974)

The emissions from this source have been observed at a variety of frequencies (Epstein *et al.* 1972); fluctuations at each have been observed at a variety of time scales. As can be seen from figures 29 and 30, the small-scale radio structure exhibited at 7.8 GHz changes considerably over a period of about 2 months, the time between days of observation.

The data of Cohen *et al.* (1971) show the same general trends as our data from late May and early June of 1972. In particular, the ratio of the maximum flux to that at about 4 hours before the maximum is about the same for both sets of data, whereas the level of the Cohen *et al.* data is higher by a factor of about 1.5 than that of our data from early 1972. This ratio is virtually identical to the corresponding ratio found for PKS 2134+00 thus lending support to the possibility of a normalization difference between the data sets.

Clark *et al.* (1973) suggest that, although VRO 42.22.01 is highly variable, it maintains an elongation at a position angle of 180°, and Andrew (1973) has attempted to explain their data in terms of a double-outburst model. The u-v plane coverage of our measurements does not permit us either to confirm or contradict this position angle. However, data taken by us in late 1973 on six independent baselines should provide a better test for both the elongation and the model.

iii) *3C 454.3* (QSO, $z = 0.859$)

Although the characteristic shape of the correlated-flux versus GST curve for 3C 454.3 (i.e., peaks at the ends and a valley in the middle) has been present throughout these observations, there are secondary features of the curve, which are also time-variable, that may indicate the presence of at least one more component. Such features are responsible for our placing the source in this category. We may obtain some information about the two main components of the source by studying the gross features of the correlated flux curve.

If we assume that the two peaks of figure 31 both lie on the first subsidiary maximum (the solid line M1 in fig. 32), then the solid lines of maxima and minima in this figure would correspond to two point components oriented at a position angle of about 53° and separated by about $3''.5 \times 10^{-3}$. A least-squares fit—based on the two-component model described in the discussion of 3C 120—to the 1973 February data, which shows both peaks, gives a position angle of $52° \pm 2°$ and a point separation of $(3''.58 \pm 0''.02) \times 10^{-3}$. It is also possible that the first peak may lie on the principal maximum with the second peak lying on

the first subsidiary maximum. This possibility corresponds to two point components separated by about $5'' \times 10^{-3}$ and oriented at an angle of about 3° as shown by the dashed lines in figure 32. For both models, the fractional difference in strengths of the components, $(S_1 - S_2)/(S_1 + S_2)$, can be estimated graphically. This ratio was about 0.77 in 1972 April, rose to between 0.85 and 0.90 by 1972 May, and decreased back down again to about 0.7 by 1973 March. The second model is much less likely to be valid than the first, since the angles of intersection between the lines of extrema and the *u-v* track require that the maxima be very broad and the minimum narrow (see fig. 32). The data in figure 31 show the opposite trend and thus agree better with the first model.

The 1971 data of Cohen *et al.* (1971) show trends very different from our 1972 data but reasonably similar to those for our data from early 1973, thus indicating that 3C 454.3 has undergone large variations in correlated flux during these 2 years.

The above discussion represents only a minimal attempt to fabricate models consistent with the data. Many interesting questions such as "Are sources with more than two components linear?" "Do sources exhibit symmetry of any kind?" "Does this symmetry change with time?" "Does the tendency of sources to have milliarcsecond structure, independent of redshift, signify more than a baseline-resolution effect?" have yet to be explored; new techniques for analyzing the data are required to obtain meaningful answers for some. Comparison of the *u-v* plane coverage of the existing data with that possible on the baselines used suggests that future experiments should be carefully scheduled to fill in gaps. Use of more than one baseline simultaneously is necessary to remove ambiguities in models for sources at low declination and to allow use of the phase-closure technique. Clearly, much remains to be done with VLBI in the exploration of the fine structure of extragalactic radio sources.

We thank the Radio Astronomy Experiment Selection (RAES) Panel, then chaired by J. Greenstein and formed by the National Aeronautics and Space Administration and the Jet Propulsion Laboratory (JPL), for establishment of the "Quasar Patrol" under which some of the observations reported here were made. We are indebted to the staffs of the Haystack Observatory, the Goldstone tracking station, the Onsala Space Observatory, and the National Oceanic and Atmospheric Administration's satellite tracking station near Fairbanks, Alaska, for their support. We give special thanks to G. Catuna of Haystack, C. Menyuk of M.I.T., and D. J. Spitzmesser and L. Skjerve of JPL for their assistance. We also thank D. Kaufmann for his invaluable aid in making available Goddard Space Flight Center hydrogen-maser frequency standards at both Fairbanks and Onsala, and M. H. Cohen for useful discussions on source structure. These data represent one phase of research carried out at the Jet Propulsion Laboratory, California Institute of Technology, under contract NAS 7-100, sponsored by the National Aeronautics and Space Administration. Radio astronomy programs at Haystack Observatory are conducted with support from the National Science Foundation, grant GP-25865. Participation of the M.I.T. experimenters is supported in part by the National Science Foundation, grant GA-36283X. The VLBI program at the Onsala Space Observatory is supported in part by the Swedish Natural Science Research Council and the Swedish Board for Technical Development.

REFERENCES

Andrews, B. H. 1973, *Ap. J. (Letters)*, **186**, L3.
Baars, J. W. M., and Hartsuijker, A. P. 1972, *Astr. and Ap.*, **17**, 172.
Clark, B. G., Kellermann, K. I., Cohen, M. H., Shaffer, D. B., Broderick, J. J., Jauncey, D. L., Matveyenko, L. I., and Moiseev, I. G. 1973, *Ap. J. (Letters)*, **182**, L57.
Cohen, M. H., Cannon, W., Purcell, G. H., Shaffer, D. B., Broderick, J. J., Kellermann, K. I., and Jauncey, D. L. 1971, *Ap. J.*, **170**, 207.
Dent, W. A. 1972*a*, *Ap. J. (Letters)*, **175**, L55.
———. 1972*b*, *Ap. J.*, **177**, 93.
———. 1974, *ibid.*, in press.
Epstein, E. E., *et al.* 1972, *Ap. J. (Letters)*, **178**, L51.
Hinteregger, H. F., Shapiro, I. I., Robertson, D. S., Knight, C. A., Whitney, A. R., Rogers, A. E. E., Moran, J. M., Clark, T. A., and Burke, B. F. 1972, *Science*, **178**, 396.
Kellermann, K. I., Clark, B. G., Cohen, M. H., Shaffer, D. B., Broderick, J. J., and Jauncey, D. L. 1973*a*, *Ap. J. (Letters)*, **179**, L141.
Kellermann, K. I., Clark, B. G., Jauncey, D. L., Broderick, J. J., Shaffer, D. B., Cohen, M. H., and Niell, A. E. 1973*b*, *Ap. J. (Letters)*, **183**, L51.
Legg, T. H., Broten, N. W., Fort, D. N., Yen, J. L., Bolt, E. V., Barber, P. C., and Quigley, M. J. S. 1973, *Nature*, **244**, 18.
Oke, J. B., and Gunn, J. E. 1974, *Ap. J. (Letters)*, **189**, L5.
Rogers, A. E. E. 1970, *Radio Science*, **5**, 1239.
———. 1973, private communication.
Rogers, A. E. E., Hinteregger, H. F., Whitney, A. R., Counselman, C. C., Shapiro, I. I., Wittels, J. J., Klemperer, W. K., Warnock, W. W., Clark, T. A., Hutton, L. K., Marandino, G. E., Rönnäng, B. O., Rydbeck, O. E. H., and Niell, A. E. 1974, *Ap. J.*, in press.
Shapiro, I. I., Hinteregger, H. F., Knight, C. A., Punsky, J. J., Robertson, D. S., Rogers, A. E. E., Whitney, A. R., Clark, T. A., Marandino, G. E., Goldstein, R. M., and Spitzmesser, D. J. 1973, *Ap. J. (Letters)*, **183**, L47.
Whitney, A. R. 1974, Ph.D. Thesis, Massachusetts Institute of Technology.

C. A. KNIGHT, I. I. SHAPIRO, and J. J. WITTELS: Department of Earth and Planetary Sciences and Department of Physics, Massachusetts Institute of Technology, Cambridge, MA 02139

H. F. HINTEREGGER, A. E. E. ROGERS, and A. R. WHITNEY: Northeast Radio Observatory Corporation, Haystack Observatory, Westford, MA 01886

T. A. CLARK, L. K. HUTTON, and G. E. MARANDINO: Goddard Space Flight Center and University of Maryland, Greenbelt, MD 20771

A. E. NIELL: Jet Propulsion Laboratory, Pasadena, CA 91103

B. O. RÖNNÄNG and O. E. H. RYDBECK: Onsala Space Observatory, Research Laboratory of Electronics, Chalmers University of Technology, Gothenburg, Sweden

W. K. KLEMPERER: National Oceanic and Atmospheric Administration, Boulder, CO 80302

W. W. WARNOCK: Martin-Marietta Corporation, Denver, CO 80201

Radio Science, Volume 11, Number 5, pages 421–432, May 1976

A very-long-baseline interferometer system for geodetic applications

A. R. Whitney, A. E. E. Rogers, H. F. Hinteregger, C. A. Knight, J. I. Levine, and S. Lippincott

Northeast Radio Observatory Corporation, Haystack Observatory, Westford, Massachusetts 01886

T. A. Clark

Goddard Space Flight Center, Greenbelt, Maryland 20771

I. I. Shapiro and D. S. Robertson

Department of Earth and Planetary Sciences and Department of Physics, Massachusetts Institute of Technology, Cambridge, Massachusetts 02139

(Received September 16, 1975.)

A very-long-baseline interferometer system was designed and built for geodetic applications. Each interferometer terminal records a 360-kHz spectral band of noise from a compact extragalactic radio source. The center frequency of the spectral band can be selected to sample sequentially bands covering a much wider frequency range to obtain subnanosecond accuracy in group-delay measurements. A tunnel-diode pulse generator is used to calibrate the delays in the receiver. The necessary sets of algorithms and computer programs have been developed to analyze the data and have allowed the system to be employed to make accurate determinations of vector baselines, radio-source positions, polar motion, and universal time.

1. INTRODUCTION

In early 1967, three groups of radio astronomers, two in the United States [*Bare et al.*, 1967; *Moran et al.*, 1967] and one in Canada [*Broten et al.*, 1967], demonstrated that radio interferometric observations of compact extragalactic radio sources could be made with widely separated antennas, utilizing an atomic clock at each site to control the heterodyning and recording of the signals. Initially, this technique of very-long-baseline interferometry (VLBI) was used to study only the structure of radio sources. Our group undertook a program of instrumentation improvement primarily to allow accurate measurement of group delays to make possible precise determinations of vector baselines [*Hinteregger et al.*, 1972], radio-source positions [*Rogers et al.*, 1973], polar motion, universal time, and earth tides [*Shapiro et al.*, 1974]. In order to measure the group delays with an accuracy greatly exceeding the inverse of the recorded bandwidth, a method of bandwidth synthesis was developed [*Rogers*, 1970; *Hinteregger et al.*, 1972] in which the receiver passband is switched to sample signals over a wide band. More recently, the bandwidth-synthesis method has been adapted by a group at the Jet Propulsion Laboratory [*Thomas et al.*, 1974; *Ong et al.*, 1975].

In this paper we describe our geodetic VLBI system in some detail. In section 2 we discuss the design philosophy that underlies the system and describe the major subunits of the equipment. Section 3 contains a description of the special device designed to calibrate the delays suffered by the radio signals in passing through the receiver system. Section 4 is devoted to a brief outline of the dependence of the primary "observables" on the geodetic quantities of interest, whereas section 5 is concerned with the extraction of estimates of these observables from the recorded signals, and section 6 with the errors associated with these estimates. Finally, in section 7 we present some typical results from observations made with this system and discuss the prospects for future improvements.

2. DESCRIPTION OF THE INTERFEROMETER TERMINAL

The major goal of the geodetic VLBI system is the measurement of the difference in the time

of arrival of radio signals at each pair of stations of an interferometric array. Unfortunately, in practice, this difference in arrival times cannot be extracted from measurements of the fringe phase because of the "2π-ambiguity" problem, as discussed in section 4. To circumvent this difficulty, we designed the VLBI system to measure the difference in the group delays of the signals as distinct from the difference in the phase delays which is ambiguously related to the fringe phase. The difference in group delays (hereinafter "group delay") is, by definition, the derivative of fringe phase with respect to frequency; this relation is, in principle, free from ambiguity problems. However, the accuracy with which the group delay can be extracted from the measurements is directly proportional to the bandwidth of the recorded signal. The available recording equipment places a severe constraint on this bandwidth and therefore we developed a bandwidth-synthesis system in which the receiver passband is switched, cyclically, over a set of up to sixteen different frequencies encompassing a band up to several hundred times wider than that of the 360-kHz recorded signal. (This wider band is limited fundamentally by the bandwidth of the feed and front-end receiver.) Because the wider band is sampled so sparsely, the increased resolution in group-delay measurements is, in practice, accompanied by ambiguities. These group-delay ambiguities can easily be resolved as they are far more widely spaced than are the 2π ambiguities in the corresponding phase-delay measurements. This technique of bandwidth synthesis in frequency space for the determination of accurate group delays is closely analogous to the more familiar use of antenna arrays to synthesize beam patterns with high angular resolution [*Rogers*, 1970].

The need for accurate measurements of group delay to determine parameters of geodetic interest also imposes other requirements on a VLBI system. Thus a very stable time and frequency standard is required at each site as is a correspondingly stable, or well calibrated, local-oscillator system. For the former we have employed primarily hydrogen-maser standards.

The choice of a center frequency (for the observations) is dictated largely by the desire to minimize ionospheric effects. If two sets of measurements at very widely separated center frequencies (say, a ratio of three to four between them) could be made simultaneously with equivalent accuracy, then these plasma influences could be eliminated. However, the construction of such dual-band equipment was not economically feasible and, instead, we chose a relatively high center frequency, near 8 GHz, for which the ionospheric effects would be small and for which both the necessary instrumentation and the radio sources to observe would be available.

We now describe the particular instrumentation developed for use in geodetic VLBI experiments. Each antenna site (Table 1) participating in such an experiment is equipped with a receiving terminal to amplify, format, and record the radio-source signals for later processing. The receiving terminal

TABLE 1. Antenna system parameters.

	Haystack	Goldstone	Fairbanks	Onsala
Location	Westford, Mass.	Goldstone, Calif.	Gilmore Creek, Alaska	Onsala, Sweden
Organization	Northeast Radio Observatory Corp.	Jet Propulsion Laboratory	National Oceanic & Atmospheric Admin.	Chalmers Univ. of Technology
Antenna diameter	120′	210′	85′	84′
Approx. antenna efficiency at *X*-band ($\lambda \sim 3.8$ cm)	40%	50%	20%	12%
First-stage low-noise radio frequency amplifier	Cooled paramp	Maser	Uncooled paramp	Maser
Approx. receiver bandwidth	200 MHz	40 MHz	150 MHz	25 MHz
Approx. system temperature	70 K	30 K	300 K	50 K

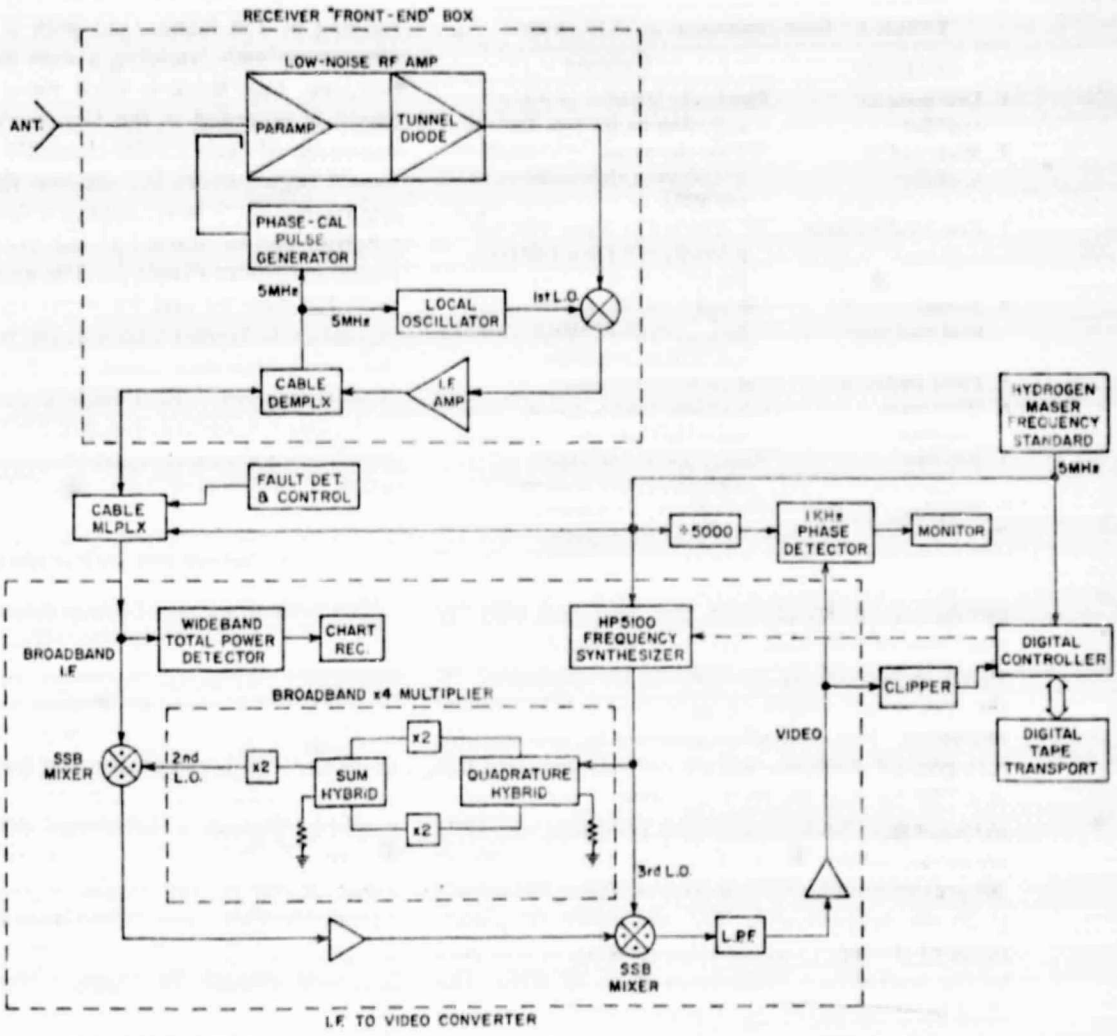

Fig. 1. Block diagram of a VLBI terminal.

(Figure 1) consists of the basic units listed in Table 2. Items 1 through 6 are located in the "front end" box on the antenna whereas the remaining equipment is located at ground level. The frequency standard provides a 5-MHz reference signal which controls the clock, the phase-calibration pulses, the sample pulses, and the frequencies of the local-oscillator signals. The second and third local-oscillator signals, generated with the aid of a frequency synthesizer (Figure 1), are digitally controlled to select various pre-programmed received-frequency bands, or "channels." (It would also have been possible to switch the first local oscillator [*Hinteregger et al.*, 1972], but this option was avoided to simplify the instrumentation. No loss in spanned bandwidth was entailed, because the bandwidth of the intermediate-frequency equipment was greater than that of the receiver.)

The selection of channels is altered in a cyclic fashion synchronously at all stations. Typically, five of the sixteen possible frequency channels are used and sampled every second with each being sampled for 0.2 sec. For each frequency in the sequence, the second and third local-oscillator signals always return to the same phases that they would have had if not interrupted, provided that none of the frequency dividers in the synthesizer is interrupted. This condition is met on the Hewlett-Packard 5100A

TABLE 2. Basic components of VLBI terminal.

Component	Comment
1. Low-noise RF amplifier	Parametric amplifier or maser, depending on site (see Table 1)
2. Mixer and IF amplifiers	*X*-band conversion to a broadband IF (spanning approximately 100 to 250 MHz)
3. First local oscillator	Phase-locked oscillator with lock points from 7.3 to 8.3 GHz in 200-MHz steps
4. Second and third local oscillators	Derived from digitally-controlled Hewlett-Packard 5100A frequency synthesizer (see section 2)
5. Phase calibrator	See section 3 for details
6. IF-to-video converter	Conversion from broadband IF to video (360 kHz video bandwidth)
7. Recorder	Ampex TM-16 with digital controller [*Bare et al.*, 1967]
8. Frequency standard	Hydrogen maser (stability = 1 in 10^{13} over 10^3 seconds)

synthesizer if frequencies are switched only by multiples of 100 kHz. The second local-oscillator signal is derived by multiplying the frequency of the synthesizer output signal by four in a broadband multiplier. This multiplier consists of two quadrature-phased doublers whose outputs are summed in a 180° hybrid; the hybrid output is then doubled in frequency. Such a quadrupler produces very little harmonic output lower than the fourth (>40 db suppression) and good rejection of higher harmonics (>20 db suppression). The allowable frequency range of the input signal to the quadrupler is limited by the hybrid to a range from 10 to 50 MHz. The third local-oscillator signal is derived directly from the synthesizer.

A single coaxial cable carries the 5-MHz reference signal for the local oscillator, the phase calibrator, and the control signals. This same cable is used to return the intermediate-frequency (IF) signal and the system-monitoring information to the ground level equipment. The IF signal is converted to a 360-kHz bandwidth signal at video through two stages of image-rejection mixing. The final image-rejection mixer uses a wideband video hybrid [*Rogers*, 1971] followed by a 360-kHz low-pass filter.

After amplification, the video signal is clipped and sampled, quantized to one bit (see section 5), and recorded on digital magnetic tape. The data recording system is similar to that employed in the first VLBI experiments [*Bare et al.*, 1967; *Moran et al.*, 1967], and uses a 7-track digital recorder running at 150 inches/sec with a density of 800 characters/inch, yielding a data rate of 720 kilobits/sec. One track is used for a parity bit; the epoch is recorded in the first 8 characters at the beginning of each 23,000-character record. A new record begins every 0.2 sec and there is a gap of approximately 5 msec between records. The tape recorder can be started at any preset time by the digital controller (Table 2). The epoch for the first recorded data bit and for every data bit recorded thereafter is known unless there is a bad spot on the tape which may cause the data to go "out of synchronization." Since each record is individually time-tagged, however, synchronization will be reacquired as soon as a recognizable time tag is encountered.

3. PHASE-DELAY CALIBRATION

The measurements of group delay are, of course, influenced by any dispersive effects of the instrumentation. Primarily to reduce such effects, we incorporated a phase-calibration system into each VLBI terminal. Thus, the phase-delay variations in the receiver for each sampled frequency channel are calibrated by injecting pulses into the low-noise amplifier through a directional coupler as shown in Figure 2. These pulses are generated by a tunnel diode driven by the 5-MHz signal from the frequency standard. The pulses from the tunnel diode are gated so that only every fifth positive pulse is passed through the coupler. The gating process serves to eliminate negative pulses and to reduce the pulse repetition rate to 1 pulse/μsec. This pulse train produces one calibration spectral line every MHz, which determines the minimum possible spacing for the calibrated frequency channels. The frequency of the total local-oscillator signal is chosen to be 1 kHz lower than the nearest integral MHz so that the calibration signal emerges at 1 kHz in the video band. The phase-calibration signal is present continuously and is extracted from each data record through multiplication of the signal by the quadrature components of a 1-kHz sine wave. The calibration phase can be determined to within 3 deg rms for each record even when the power in the calibration signal is as low as 1% of the video power. The phase calibrator has a temperature coefficient of 5 psec/°C and no known sensitivity to other environmental conditions. A system to correct for the cable-delay changes in the calibrator

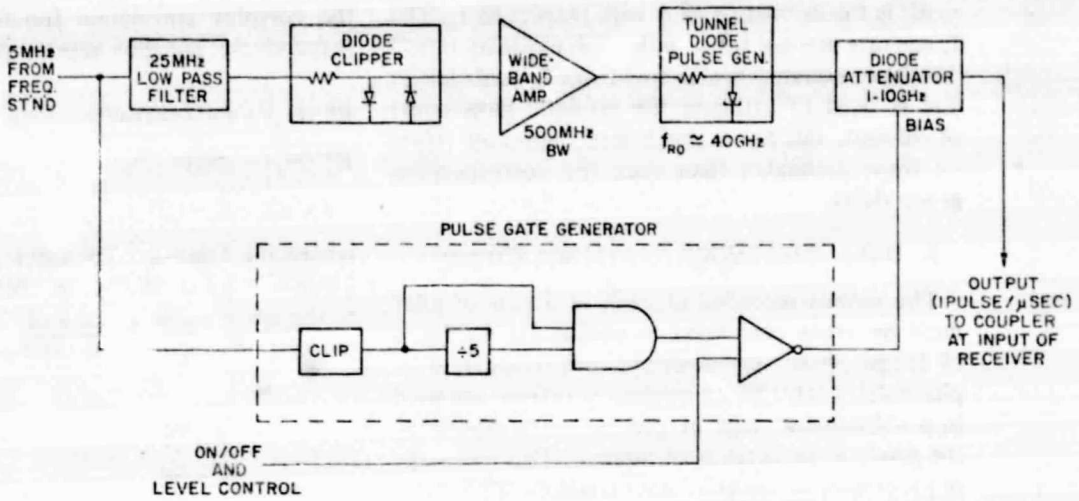

Fig. 2. Block diagram of the phase-calibration system.

has recently been completed but not yet used in a VLBI experiment.

4. VLBI OBSERVABLES

The interferometer can be used to determine, as a function of time and frequency, the fringe phase and the fringe amplitude of the signals from compact extragalactic radio sources. For geodetic applications, the fringe phase is of primary interest: its derivative with respect to (angular) frequency yields the group delay. In the absence of noise, and after instrumental calibration, the fringe phase, ϕ, for observations with circularly polarized feeds, may be expressed as

$$\phi(t_x) \simeq \omega_k[(1 - R_y)\tau_g + (E_x - E_y) + R_x(t_x + E_x) - R_y(t_y + E_y)] \pm (\psi_x - \psi_y) + \Phi_{px} - \Phi_{py} + \theta_{xy} + 2\pi q \quad (1)$$

where the subscripts x and y refer to the reference and remote sites, respectively; t_x and t_y are the times as given on the reference and remote site clocks, respectively; τ_g is the difference in the delays of a signal propagating in vacuum from the source to the two sites (hereinafter "geometric delay"); ω_k is the angular frequency of the algebraic sum of the frequencies of the local-oscillator signals; E_x and E_y are the epoch errors and R_x and R_y the drift-rate errors of the reference and remote clocks, respectively; ψ_x and ψ_y are the corresponding position angles of the antenna feeds (positive sign for left-hand circular polarization—IEEE definition); Φ_{px} and Φ_{py} are the propagation-medium phase shifts due to the atmosphere and ionosphere over the reference and remote sites, respectively; θ_{xy} is the phase of the so-called source visibility function and represents, in effect, the modification of the fringe phase due to the source being partially resolved by the interferometer; and q is an integer that indicates the ambiguity, discussed earlier, in the relation of fringe phase to τ_g.

The approximate expression for τ_g is

$$\tau_g = -(1/c)\,\vec{B} \cdot \hat{e} \quad (2)$$

where c is the speed of light, $\hat{e}$ is a unit vector in the direction of the radio source, and $\vec{B}$ is the baseline vector that extends from the reference site at the time of arrival of a wavefront to the remote site at the time of arrival there of the same wavefront, on the assumption that the propagation is in vacuum.

The group delay, τ, being the derivative of the fringe phase with respect to the angular frequency ω_k, is given by

$$\tau(t_x) \simeq (1 - R_y)\tau_g + (E_x - E_y) + R_x(t_x + E_x) - R_y(t_y + E_y) + \tau_{pxy} + \theta'_{xy} \quad (3)$$

where τ_{pxy} is the propagation-medium contribution to the group delay and θ'_{xy} denotes the contribution of the source visibility function to τ. The "fringe

rate" is the derivative of ϕ with respect to t_x. The fringe rate divided by ω_k is the "phase-delay rate." The latter quantity is also free from 2π ambiguities and is used to estimate the geodetic parameters of interest, but has a much less important effect on these estimates than does the corresponding group delay.

5. DATA CORRELATION AND FRINGE ROTATION

The signals recorded at each of a pair of sites must be cross correlated to obtain the estimates of fringe phase, group delay, and fringe rate or phase-delay rate. These estimates, in turn, are used in a subsequent stage of processing to determine the geodetic parameters of interest. This last stage of processing involves a rather standard application of least-squares parameter estimation and is not described here in detail. The first stage of processing, on the other hand, being both novel and crucial to the interferometer system, is described in some detail.

The video signal, $V(t)$, at each site is infinitely clipped and sampled so that the sample value, $V(n)$, is given by

$$V(n) = \begin{cases} +1, & \text{if } V(t) \geq 0 \\ -1, & \text{if } V(t) < 0 \end{cases} \tag{4}$$

where n represents the sample number corresponding to the time t. The recorded data tapes containing these samples are processed on a general purpose computer (CDC 3300) with the aid of a peripheral processor interfaced to the computer via direct memory access. The peripheral processor "rotates the fringes" (i.e., corrects for the difference in the Doppler shift of the signal at the two sites) and cross correlates the data streams. The correlation, along with the fringe rotation, is performed on a record-by-record basis. For each record, the *a priori* value assumed for the group delay, quantized in units of the sample period, is held constant. This value is termed the "bit offset" between the two data streams. The rate of fringe rotation, i.e., the fringe rate, is also held constant for each record. The bit offset can be as large as 20 msec, but even for the highest possible fringe rate (≈20 kHz at our X-band radio frequency), the change in offset during one record would be less than 0.5 μsec which is about one third of the interval between samples. The quantities calculated for the rth record, the so-called cosine and sine parts of the complex correlation function, $R_c^{(r)}$ and $R_s^{(r)}$, respectively, are thus approximated by

$$\begin{aligned} R_c^{(r)}(l\tau_s) &= \sin[(\pi/2)\rho_c^{(r)}] \\ R_s^{(r)}(l\tau_s) &= \sin[(\pi/2)\rho_s^{(r)}]; \\ l &= -3, -2, -1, 0, 1, 2, 3 \end{aligned} \tag{5}$$

where the familiar Van Vleck clipping correction [*Van Vleck and Middleton*, 1966] has been applied to the corresponding parts of the "clipped signal" correlation functions, $\rho_c^{(r)}$ and $\rho_s^{(r)}$, which are given by

$$\begin{aligned} \rho_c^{(r)}(l\tau_s) &= \frac{\beta}{N^{(r)}} \sum_{n=1}^{N^{(r)}} V_x(n)\, C[(n-1)\Omega^{(r)}\tau_s] \\ &\quad \cdot V_y(n+m-l) \\ \rho_s^{(r)}(l\tau_s) &= \frac{\beta}{N^{(r)}} \sum_{n=1}^{N^{(r)}} V_x(n)\, S[(n-1)\Omega^{(r)}\tau_s] \\ &\quad \cdot V_y(n+m-l) \end{aligned} \tag{6}$$

where τ_s is the (constant) time interval between samples; $\Omega^{(r)}$ is the *a priori* value assumed for the fringe rate; V_x and V_y are the video samples (see (4)) at the reference and remote sites, respectively; n is the sample index, or bit number, within the rth record; $N^{(r)}$ is the number of samples, or bits, on the rth record in each stream which may be correlated with those in the other; m is the bit offset, i.e., the integer nearest the (in general nonintegral) number of bits that corresponds to the *a priori* value assumed for τ; and l is the integer index for the offsets in the evaluation of the correlation function. The number of bits in one record is thus equal to $N^{(r)} + m$. The functions $S(n\Omega^{(r)}\tau_s)$ and $C(n\Omega^{(r)}\tau_s)$ are three-level approximations to sine and cosine functions. For the interval $(-\pi, \pi)$, we use

$$C(x) = \begin{cases} +1, & 0 \leq |x| \leq 3\pi/8 \\ 0, & 3\pi/8 < |x| \leq 5\pi/8 \\ -1, & 5\pi/8 < |x| \leq \pi \end{cases} \quad ; \quad x \equiv n\Omega^{(r)}\tau_s \tag{7}$$

with the sine function approximation being identical except for a 90° phase shift. The factor β in (6) accounts for the average reduction in the correlation caused by the differences between $S(n\Omega^{(r)}\tau_s)$ and $C(n\Omega^{(r)}\tau_s)$ and the true sine and cosine functions; it is easily shown that

$$\beta = \pi/[4\cos(\pi/8)] \approx 1.18 \quad (8)$$

This three-level representation is especially efficient to use since multiplication by minus one is accomplished by forming the (binary) complement of the data sample and multiplication by zero is accomplished by omitting the term in the summation process.

After the correlation and rotation are performed for each record, the sine and cosine parts of the complex correlation function are transformed to the (video) frequency domain. In addition, the phases of the complex correlation functions formed from $R_c^{(r)}(l\tau_s)$ and $R_s^{(r)}(l\tau_s)$ are rotated to counteract the operations of (6) that cause each record to be started with zero phase. The resultant expression for the one-record complex correlation function in the frequency domain is therefore:

$$S^{(r)}(\omega_v) = \exp(-i\omega^{(r)}\tau^{(r)}) \sum_{l=-3}^{3} [R_c^{(r)}(l\tau_s) - iR_s^{(r)}(l\tau_s)] \cdot \exp(-il\tau_s\omega_v);\ v = 1, 2, \ldots, 7 \quad (9)$$

where r, as before, is the record index; ω_v is an (angular) video frequency with $\tau_s\omega_v = 2\pi v/16$; $\omega^{(r)}$ is the (angular) radio frequency translated to zero frequency for the rth record ($\omega^{(r)}$ takes on for successive records the different values included in the frequency-switching sequence; see section 2); and $\tau^{(r)}$ is the *a priori* value assumed for the group delay for the epoch of the first bit correlated ($n = 1$) on the rth record. A simple correction for the "fractional-bit delay" is now applied to each value of $S^{(r)}(\omega_v)$, followed by summation over the video band for seven different trial delays separated by τ_s, yielding

$$R^{(r)}(l\tau_s) = \sum_{v=1}^{7} S^{(r)}(\omega_v)\exp(il\tau_s\omega_v) \cdot \exp[-i\omega_v(\tau^{(r)} - m\tau_s)];\ l = -3, -2, \ldots, 2, 3 \quad (10)$$

where the last factor represents the phase correction for the difference between the bit offset and the value of $\tau^{(r)}$. Equations (9) and (10) apply for upper sideband frequency conversion. For lower sideband conversion, the sign of ω_v should be changed in both (9) and (10).

Finally, a delay/delay-rate resolution function, $D(\Delta\tau, \Delta\dot{\tau})$, is defined as a two-dimensional transform of the complex correlation function, summed over all records:

$$D(\Delta\tau, \Delta\dot{\tau}) = \sum_r R^{(r)}\exp[-i\omega^{(r)}(\Delta\tau + \Delta\dot{\tau}t_x^{(r)})] \quad (11)$$

where, as shown previously [*Rogers*, 1970], the values of $\Delta\tau$ and $\Delta\dot{\tau}$ for which $|D(\Delta\tau, \Delta\dot{\tau})|$ is a maximum are the maximum-likelihood estimates of the residual group delay and phase-delay rate, respectively. Here "residual" refers to the difference between the true value and the *a priori* value assumed in the data processing. In (11), the values of $\Delta\tau$ and $\Delta\dot{\tau}$ are appropriate for the start of the three-minute observation with $t_x^{(r)}$ being the time elapsed from this epoch to the start of the rth record as measured on the clock at the reference site. There has been no need to consider higher-order terms in the expansion of the difference between the true and the *a priori* value for the group delay. Further, it is acceptable to use as the argument of $R^{(r)}$ that value of $l\tau_s$ (l an integer) which is closest to $\Delta\tau$, even though this argument changes discontinuously.

To achieve computational efficiency with adequate accuracy, the maximization of $|D(\Delta\tau, \Delta\dot{\tau})|$ is carried out in successive stages. First, we obtain the values of $\Delta\tau$ and $\Delta\dot{\tau}$ which maximize the sum of the magnitudes of the "single channel" (coarse) delay/delay-rate resolution functions:

$$\sum_{k=1}^{K} |D_k(\Delta\tau, \Delta\dot{\tau})| \quad (12)$$

where $D_k(\Delta\tau, \Delta\dot{\tau})$ is defined as is $D(\Delta\tau, \Delta\dot{\tau})$ in (11) except that only the records corresponding to the kth frequency channel contribute to D_k. The approximate maximization of expression (12) is carried out by evaluating it for each point in a two-dimensional array of 7 trial values for $\Delta\tau$, spaced by the sampling interval τ_s (≈1.4 μsec), and 256 trial values for $\Delta\dot{\tau}$, spaced by approximately 0.4 psec/sec for a radio frequency of about 8 GHz. Both sets of trial values are centered on zero, corresponding to the *a priori* estimates of $\Delta\tau$ and $\Delta\dot{\tau}$. Next, a two-dimensional Fourier transform is utilized for the maximization of (11) with the grid containing 256 delay values, spaced by 1/256 of the inverse of the smallest separation in frequency between any two of the K channels (usually about 2 nsec), and 5 delay-rate values, spaced by approximately 0.1 psec/sec. These trial values are centered on the "coarse" estimates obtained above in the approximate maximization of expression (12). In the vicinity of the "fine" estimates obtained from

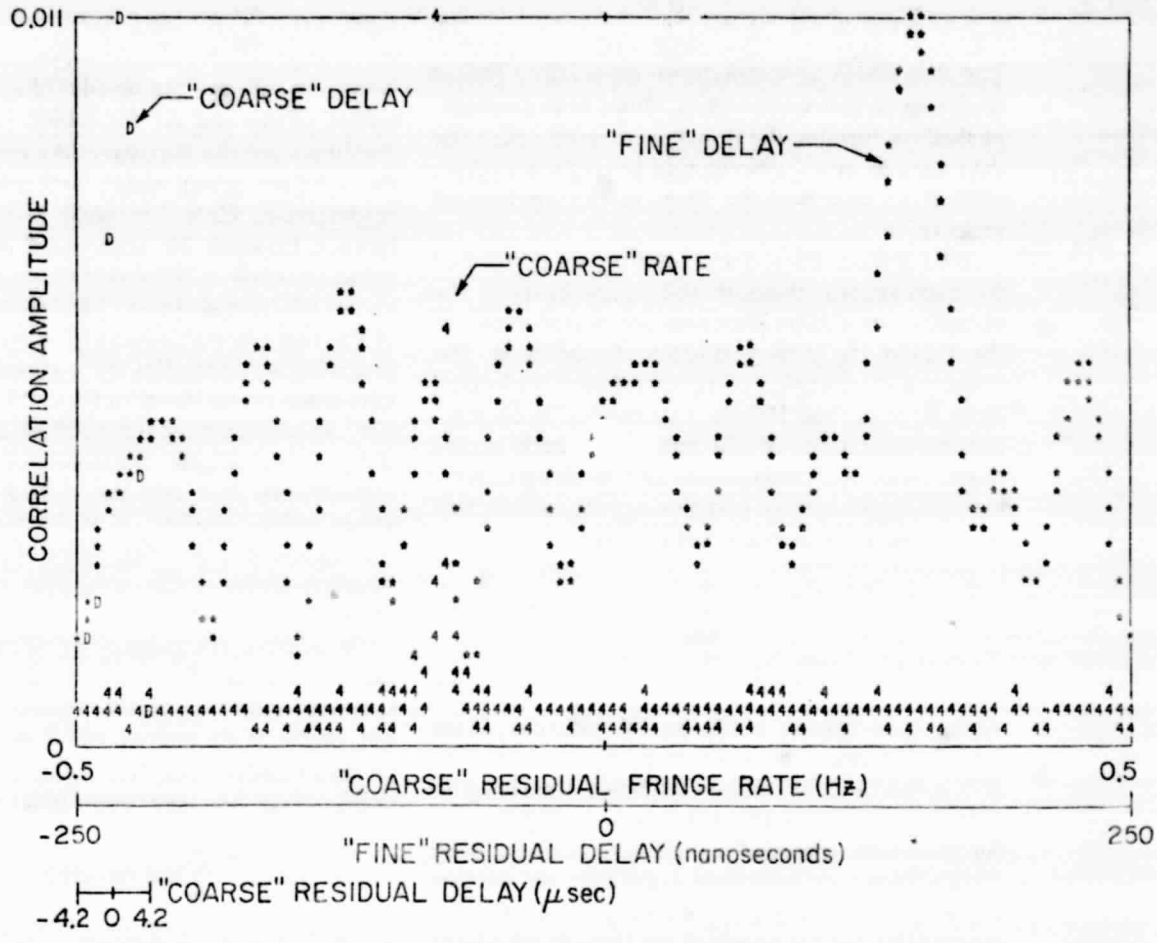

Fig. 3. Delay/delay-rate resolution function from a three-minute observation of the extragalactic radio source VRO 42.22.01 started at 13:48 UT on 6 March 1974 with the Goldstone-Haystack interferometer. The letters *D* show, on an arbitrary linear scale, the coarse, single-channel delay-resolution function. The numerals 4 display the coarse fringe-rate spectrum, and the stars display the fine, multichannel delay-resolution function. See text for further explanation.

the second maximization procedure, a further factor of four decrease in the grid spacing in delay is utilized before a two-dimensional (nonquantized) parabolic interpolation is performed to determine the final estimates of the residual group delay and phase-delay rate.

Figure 3 shows a sample output from the fringe processor for an observation involving five frequency channels ($K = 5$). The relative separations were 0, 14, 16, 22, and 26 MHz, yielding a set of pairwise differences of 1, 2, 3, 4, 5, 6, 7, 8, 11, and 13 in units of 2 MHz, the minimum frequency separation. This approximate maximization of the number of differences with a minimization of the redundancy of differences tends to minimize the magnitudes of the "sidelobes" in $|D(\Delta\tau, \Delta\dot{\tau})|$ as illustrated in the figure and described further below. The letters *D* display expression (12) as a function of $\Delta\tau$ for seven values spaced by τ_s; the common value of $\Delta\dot{\tau}$ is the one that yielded the maximum in the first maximization procedure. The numerals 4 display the coarse "fringe-rate spectrum," i.e., expression (12) plotted as a function of $\Delta\dot{\tau}$, converted to residual fringe rate, for that value of $\Delta\tau$ which yielded the maximum. The spacing of the $\Delta\dot{\tau}$ values, approximately 0.5 psec/sec, corresponds to an incremental fringe rate of about 4 mHz at the *X*-band frequencies used. Because of computer "overplot-

ting," not all points are shown.

The stars in Figure 3 depict $|D(\Delta\tau,\Delta\dot{\tau})|$ as a function of $\Delta\tau$ with the common value of $\Delta\dot{\tau}$ being the final estimate of the residual phase-delay rate. The function is evaluated at 256 points, spaced at intervals of approximately 2 nsec, to cover the full 500-nsec range that constitutes the basic periodicity of $|D(\Delta\tau,\Delta\dot{\tau})|$, viewed as a function of $\Delta\tau$. Apart from the effects of errors, this "fine" delay-resolution function is invariant under reflection about that value of $\Delta\tau$ for which the function is a maximum. (We ignore here the "envelope" effect of the nonzero (360 kHz) width of each frequency channel which serves to alter slightly the values of $|D(\Delta\tau,\Delta\dot{\tau})|$ for neighboring "periods" of its argument.)

Figure 4 shows the fringe amplitudes (letters A) and phases (numerals) for each frequency channel in the sequence of five; these values correspond to the amplitudes and phases of the coherent averages of the appropriate sets of values of $R^{(i)}$, after removal of the effects of the estimated residual group delay and phase-delay rate. Both ordinate scales are linear and the abscissa scale depicts time from 0 to 3 min, separately for each channel. The points shown are spaced 10 sec apart in time and represent these averages over ten records for each of the five frequency channels. The same systematic trend that can be seen in the phases for each channel probably results from some combination of atmospheric-induced and frequency-standard phase fluctuations. The segment of Figure 4 farthest to the right shows the phase calibrator phases for the reference station, with the numerals 1 through 5 denoting the frequency channel, and for the remote station, with the letters A through E denoting the frequency channel. These points are spaced 20 sec apart in time with each representing a coherent average over that period. (Quantization in the computer-produced graphs is responsible for the discontinuous appearance of all of the curves. For the same reason, there are missing E's and a missing D which coincide, respectively, with the appropriate 4's and B.)

6. ERROR ANALYSIS

It is of obvious importance to determine the uncertainties in the estimates of the group delays and the phase-delay rates. These uncertainties can be derived in a straightforward manner [*Rogers*,

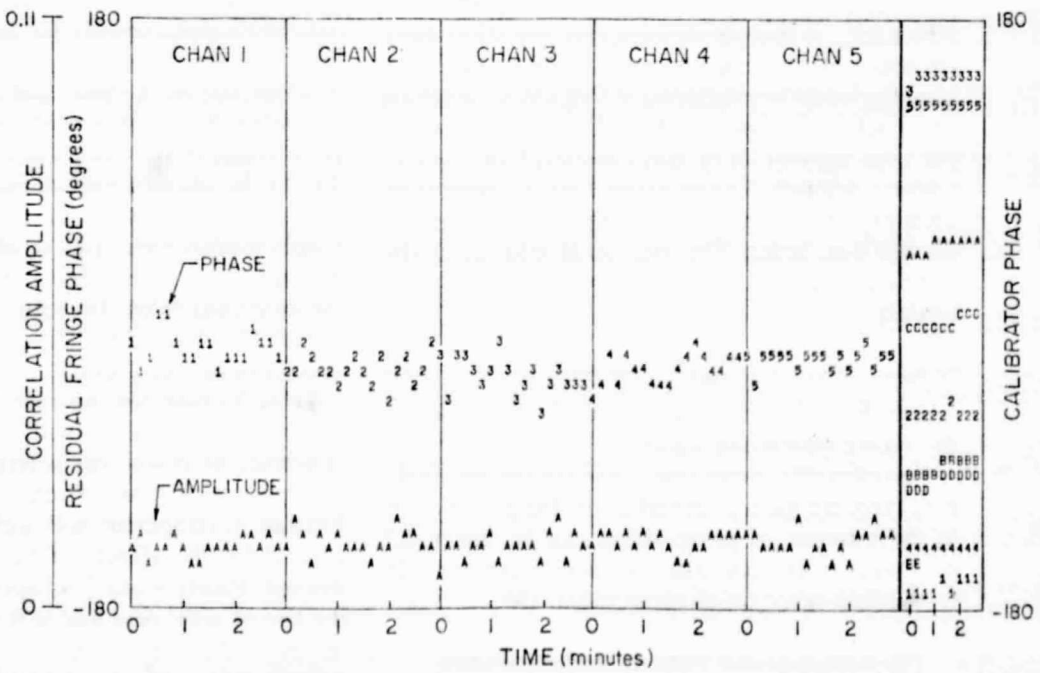

Fig. 4. Fringe phases (numerals) and fringe amplitudes (letters A) displayed for each frequency channel separately for the observation described in Figure 3. Shown at the right are the calibrator phases. See text for further details.

1970; *Moran*, 1973] in terms of the system characteristics, and only the results are given here.

The standard deviation, $\sigma(\phi)$, in the estimate of the fringe phase for a single frequency channel is given by

$$\sigma(\phi) \simeq \frac{\pi}{2}\left[\frac{T_s T_s' + T_a T_s' + T_a' T_s}{T_a T_a' N^{(ch)}}\right]^{1/2} \text{ radians} \qquad (13)$$

where T_s and T_s' are the system temperatures at the two sites; T_a and T_a' are the corresponding contributions of the correlated portions of the flux to the antenna temperatures; and $N^{(ch)}$ is the number of bits correlated for the given frequency channel (the sum of $N^{(r)}$ over all records r that correspond to this channel on the data tape). The standard deviation, $\sigma(\dot{\tau})$, in the estimate of the phase-delay rate for a single frequency channel is

$$\sigma(\dot{\tau}) \simeq [12^{1/2}\sigma(\phi)]/\omega_k t_I \quad \text{sec/sec} \qquad (14)$$

where t_I is the total time of integration and ω_k is defined in section 4. The corresponding standard deviation for the estimate of the fringe rate is $\omega_k \sigma(\dot{\tau})$. The standard deviation, $\sigma(\tau)$, in the estimate of the group delay is

$$\sigma(\tau) \simeq \sigma(\phi)/(2\pi\Delta f_{rms}) \quad \text{sec} \qquad (15)$$

where Δf_{rms} is the root-mean-square deviation about the mean of the frequencies of the local-oscillator signals used in the programmed frequency-switching sequence, and where now $\sigma(\phi)$ is computed using the total number N of bits correlated for all frequency channels for the entire time of integration (sum of $N^{(r)}$ over all records r that were correlated on the data tape). The rms error $\sigma(\phi_{cal})$ in the estimate of each of the calibration phases is approximately

$$\sigma(\phi_{cal}) \simeq (\pi P/2N^{(ch)}P_{cal})^{1/2} \quad \text{radians} \qquad (16)$$

where P_{cal}/P is the fraction of the total power due to the calibration signal.

Equation (15) shows that, even for the relatively small rms frequency spread of 10 MHz, the error in the estimate of group delay can be under 0.2 nsec when $\sigma(\phi)$ is less than 0.01, which corresponds to signal-to-noise ratios greater than 100.

7. RESULTS AND FUTURE IMPROVEMENTS

Measurement errors have, in fact, been well under 1 nsec for group delays determined from observations of strong sources when sufficiently sensitive interferometer systems have been used. This accuracy is illustrated in Figure 5 by the sample of postfit residuals from the Goldstone-Haystack VLBI experiment of 29–30 August 1972. These residuals represent the observed delays minus the theoretical delays with the latter being based on the weighted-least-squares analysis of the total of 196 observations. By this analysis, estimates were obtained simultaneously for the radio-source positions, the three components of the interferometer baseline, the clock epoch and rate differences, and the parameters that describe the excess electrical path length in the zenith direction over each site due to the atmosphere. A modified cosecant law was used to represent the atmospheric delay and simple models were used to attempt to correct for the small ($\lesssim$1 nsec) effects of the ionosphere and the solid-earth tides. The rms of the postfit residuals for all 196 observations from this experiment was slightly under 0.25 nsec.

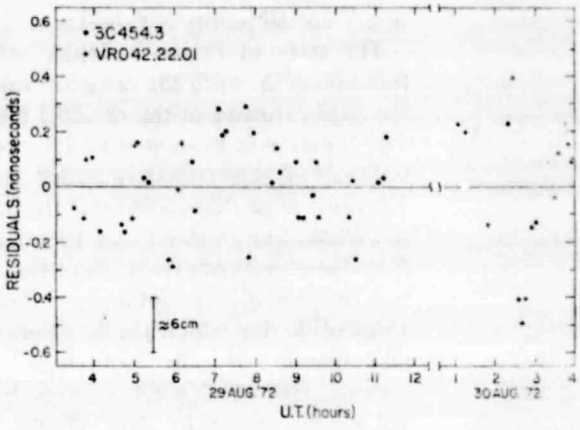

Fig. 5. Postfit residuals from observations of the extragalactic radio sources VRO 42.22.01 and 3C 454.3. See text for discussion.

Table 3 compares the current level of expected measurement accuracy with the accuracy actually achieved, as estimated, where possible, from the consistency of results from separate experiments. Further development will include radiometers to correct for the effects of the neutral atmosphere through observations [*Schaper et al.*, 1970] along the line of sight near and at the 22-GHz frequency of the water-vapor spectral-line emission. Ionospheric delays can be corrected more accurately by observing simultaneously at two widely-separated frequency bands, as mentioned earlier, and we

TABLE 3. Measurement accuracies.

Measured quantity	Theoretical standard deviation[1]	Typical rms error	Comments
Fringe phase	0.5 deg	—	Very difficult quantity to use except in differential experiments[2]
Phase-delay rate	0.1 psec/sec	0.2 psec/sec	Typical errors based on postfit residuals[3]
Group delay	0.2 nsec	0.3 nsec	Typical errors based on postfit residuals[3]
Source positions	—	0.05 arcsec	rms spread in 4 separate experiments [*Rogers et al.*, 1973]
Baseline length	—	20 cm	rms spread in 9 separate experiments [*Shapiro et al.*, 1974]
Polar motion	—	50 cm	formal standard error [*Shapiro et al.*, 1974]
Universal time (UT.1)	—	1 msec	formal standard error [*Shapiro et al.*, 1974]
Clock synchronization	—	1 nsec	formal standard error

[1] Based on 180-second coherent integration and signal-to-noise ratio of 100, approximately that achieved on the Haystack-Goldstone baseline with an unresolved source with flux density about 5×10^{-26} wm^{-2} Hz^{-1}. Estimate of phase-delay rate standard deviation also includes effects of instability of the frequency standard (see Table 2).

[2] Differential VLBI [*Counselman et al.*, 1972] experiments have made use of fringe phase by reducing the effect of ambiguity through maintenance of continuous phase tracking.

[3] The rms residuals are larger than the theoretical uncertainty owing to systematic effects not adequately included in the model, such as variations in the atmosphere and ionosphere.

hope to add an *S*-band receiver to our *X*-band system for this purpose. Since the phase calibrator is a broadband device, its signal can be split to calibrate both receivers simultaneously. Major reductions in group-delay measurement errors can be achieved through use of substantially wider bandwidth receivers and/or VLBI recording systems; both are technically feasible, the former now being available commercially and the latter being under development by our group.

Acknowledgments. We would like to thank W. Rutkowski for designing and building an improved device for frequency-switching a synthesizer, and the staff of the Haystack Observatory for help in the hardware construction. We also thank R. A. Ballew and C. F. Martin of the Defense Mapping Agency whose support and encouragement have done much to promote the development of VLBI for geodetic applications. This development was supported by the Advanced Research Projects Agency (contract F23601-71-C-0092). Radio astronomy programs at Haystack are supported by the National Science Foundation, grant MPS 71-02109 A07. The work at the Massachusetts Institute of Technology was supported in part by the National Science Foundation, grant DES 74-22712.

REFERENCES

Bare, C. C., B. G. Clark, K. I. Kellermann, M. H. Cohen, and D. L. Jauncey (1967), Interferometer experiments with independent local oscillators, *Science*, *157*, 189–191.

Broten, N. W., T. H. Legg, J. L. Locke, C. C. McLeish, R. S. Richards, R. M. Chisholm, H. P. Gush, J. L. Yen, and J. A. Galt (1967), Long baseline interferometry: A new technique, *Science*, *156*, 1592–1593.

Counselman, C. C., III, H. F. Hinteregger, and I. I. Shapiro (1972), Astronomical applications of differential interferometry, *Science*, *178*, 607–608.

Hinteregger, H. F., I. I. Shapiro, D. S. Robertson, C. A. Knight, R. A. Ergas, A. R. Whitney, A. E. E. Rogers, J. M. Moran, T. A. Clark, and B. F. Burke (1972), Precision geodesy via radio interferometry, *Science*, *178*, 396–398.

Moran, J. M. (1973), Spectral-line analysis of very-long-baseline interferometric data, *Proc. IEEE*, *61*, 1236–1242.

Moran, J. M., P. O. Crowther, B. F. Burke, A. H. Barrett, A. E. E. Rogers, J. A. Ball, J. C. Carter, and C. C. Bare (1967), Spectral line interferometry with independent time standards at stations separated by 845 km, *Science*, *157*, 676–677.

Ong, K. M., P. F. MacDoran, J. B. Thomas, H. F. Fliegel, L. J. Skjerve, D. J. Spitzmesser, P. D. Batelaan, S. T. Paine, and M. G. Newsted (1975), A demonstration of radio interferometric surveying using DSS 14 and the Project Aries transportable antenna, *Deep Space Net. Prog. Rep. 42-26*, pp. 41–53, Jet Propulsion Laboratory, Pasadena, CA.

Rogers, A. E. E. (1970), Very-long-baseline interferometry with large effective bandwidth for phase-delay measurements, *Radio Sci.*, *5*, 1239–1248.

Rogers, A. E. E. (1971), Broadband passive 90° RC hybrid with low component sensitivity for use in the video range of frequencies, *Proc. IEEE*, *59*, 1617–1618.

Rogers, A. E. E., C. C. Counselman III, H. F. Hinteregger,

C. A. Knight, D. S. Robertson, I. I. Shapiro, A. R. Whitney, and T. A. Clark (1973), Extragalactic radio sources: Accurate positions from very-long-baseline observations, *Astrophys. J.*, *186*, 801-806.

Schaper, L. W., D. H. Staelin, and J. W. Waters (1970), The estimation of tropospheric electrical path length by microwave radiometry, *Proc. IEEE*, *58*, 272-273.

Shapiro, I. I., D. S. Robertson, C. A. Knight, C. C. Counselman III, A. E. E. Rogers, H. F. Hinteregger, S. Lippincott, A. R. Whitney, T. A. Clark, A. E. Niell, and D. J. Spitzmesser (1974), Transcontinental baselines and the rotation of the earth measured by radio interferometry, *Science*, *186*, 920-922; *191*, 451.

Thomas, J. B., J. L. Fanselow, P. F. MacDoran, D. J. Spitzmesser, and L. J. Skjerve (1974), Radio interferometry measurements of a 16-km baseline with 4-cm precision, *Tech. Rep. 32-1526, Vol. XIX*, pp. 1-15, Jet Propulsion Laboratory, Pasadena, CA.

Van Vleck, J. H., and D. Middleton (1966), The spectrum of clipped noise, *Proc. IEEE*, *54*, 2-19.

Reprinted from:
METHODS OF EXPERIMENTAL PHYSICS, VOL. 12
ASTROPHYSICS, PART C
Radio Observations

ACADEMIC PRESS, INC.
New York San Francisco London

5.6. Estimation of Astrometric and Geodetic Parameters*

5.6.1. Introduction

The technique of very long baseline interferometry (VLBI) has enormous potential for important applications in astrometry and geodesy. Considerable progress has already been made in the exploitation of this technique for these applications, but the ultimate accuracy inherent in the method has not even been approached: VLBI is in a stage of rapid improvement and probably will not achieve a mature status for some years to come. In this chapter, we confine discussion to the information content of the VLBI observables and to the deduction of the relevant astrometric and geodetic quantities from this content. References to results already obtained are included.

5.6.2. VLBI Observables

Interferometric observations of a point source of continuum radio radiation can yield fringe phase and fringe amplitude as functions of time and frequency. Because the observations, for practical reasons, are usually broken up into relatively short time intervals and relatively narrow frequency intervals, it is convenient to consider two additional ("derived") quantities: the time derivative of the fringe phase, the so-called fringe rate, and the angular frequency derivative of the fringe phase, the so-called differenced group delays or, simply, group delay. In similar language, the fringe phase and the fringe rate, after division by the angular frequency, are the differenced phase delays and the differenced phase delay rates, respectively. Despite the obvious lack of parallelism, we adopt the currently used terms: fringe amplitude, fringe phase, fringe rate, and group delay.

The manner in which the fringe phase ϕ, the fringe rate $\dot{\phi}$, and the group delay τ are determined from the true observables—the recorded signals—is discussed elsewhere in this volume, as are the expressions for the uncertainties in these determinations (see Chapter 5.5). A discussion of the problems associated with the extraction of fringe amplitude from the recorded signals can also be found in Chapter 5.5 and elsewhere.[1,2] Since our principal

[1] A. R. Whitney, Ph.D. Thesis, Dept. Elec. Eng., Massachusetts Inst. of Technol. (1974).
[2] J. J. Wittels *et al.*, *Astrophys. J.* **196**, 13 (1975).

* Chapter 5.6 is by Irwin I. Shapiro

concern here is with geodetic and astrometric measurements, we shall concentrate mainly on ϕ, $\dot{\phi}$, and τ. We may express these "second-generation" observables theoretically. To do so, we choose a coordinate system with origin at the solar-system barycenter, and we assume the validity of general relativity. The reason for this seemingly bizarre choice for a system to describe quantities inferred from earth-based observations is simple: In order to combine in a comprehensive analysis diverse astronomical observations, such as of interplanetary time delays and of pulsar signals, and to determine quantities which are each sensitive to more than one of the observables, it is far easier to do all the computations in one coordinate system than to do each in a system convenient for one particular observable and then to convert each to a common system. The opportunities for error in the latter procedure are plentiful because of the importance of relativistic effects in modern observations.

In terms of the so-called isotropic Schwarzschild coordinates, one can show that for two elements i and j of an interferometer array:

$$\phi_{ij}(t) \simeq \omega\tau_{ij}(t) - 2\omega\tau_{ij}^{p} + 2\pi n, \tag{5.6.1}$$

$$\frac{d\phi_{ij}(t)}{dT_i} \simeq \omega\frac{d\,\Delta t}{dt} - \frac{\omega}{c^2}[\dot{\mathbf{R}}\cdot(\dot{\mathbf{r}}_j - \dot{\mathbf{r}}_i) + \ddot{\mathbf{R}}\cdot(\mathbf{r}_j - \mathbf{r}_i)] + \omega(\dot{\tau}_{ij}^{c} + \dot{\tau}_{ij}^{a} - \dot{\tau}_{ij}^{p}), \tag{5.6.2}$$

$$\tau_{ij}(t) \simeq \Delta t - \frac{1}{c^2}[\dot{\mathbf{R}}\cdot(\mathbf{r}_i - \mathbf{r}_i)] - \frac{1}{c^2}[\ddot{\mathbf{R}}\cdot\mathbf{r}_j + \dot{\mathbf{R}}\cdot\dot{\mathbf{r}}_j]\,\Delta t + \tau_{ij}^{c} + \tau_{ij}^{a} + \tau_{ij}^{p}, \tag{5.6.3}$$

where

$$T_i(t) = t + \mathrm{UTC} - \mathrm{A1} - 32.15 - \frac{1}{c^2}\dot{\mathbf{R}}\cdot\mathbf{r}_i + \mathrm{LPT} + \sum_{k=0}^{K}\alpha_{ik}(t - t_0)^k \quad [\mathrm{sec}], \tag{5.6.4}$$

$$\Delta t(t) \simeq \frac{1}{c}(\mathbf{r}_i - \mathbf{r}_j)\cdot\hat{\mathbf{e}}_s - \left[\frac{1}{c}(\dot{\mathbf{R}} + \dot{\mathbf{r}}_j)\cdot\hat{\mathbf{e}}_s\right]\left[\frac{1}{c}(\mathbf{r}_i - \mathbf{r}_j)\cdot\hat{\mathbf{e}}_s\right] \times\left[1 - \frac{1}{c}(\dot{\mathbf{R}} + \dot{\mathbf{r}}_j)\cdot\hat{\mathbf{e}}_s\right], \tag{5.6.5}$$

$$\tau_{ij}^{c} \simeq \sum_{k=0}^{K}\{\alpha_{ik}(t - t_0)^k - \alpha_{jk}(t - t_0 - \Delta t)^k\}, \tag{5.6.6}$$

and where t is coordinate time, T_i the clock reading at site i, ω the angular (radio) frequency to which the fringe phase is referred, n an integer indicating the ambiguity in fringe phase, c the speed of light, $\mathbf{r}_i(t)$ the geocentric position of the interferometer element i at coordinate time t, $\mathbf{R}(t)$ the barycentric

position of the center of mass of the earth at coordinate time t, $\hat{\mathbf{e}}_s$ the unit vector in the direction of the observed (point) source of the radio radiation (we ignore here possible parallax effects), τ^c_{ij} the difference in the deviations of the clocks at sites i and j from "true" atomic time at the respective sites, τ^a_{ij} the delay introduced by the neutral atmosphere, and τ^p_{ij} the delay caused by the difference in the integrated charged particle content along the paths from the source to the two sites. This last delay has an effect on ϕ_{ij} and $\omega\tau_{ij}$ of nearly equal magnitude but opposite sign in our weak-magnetic-field, dilute-plasma case. The main contribution to τ^p_{ij} comes from the earth's ionosphere (Chapter 2.1) since nearer the source, presumably, the charged-particle contents along the two paths are very nearly equal. In the expression for the coordinate-time dependence of the time, T_i, kept at site i, we note that UTC denotes coordinated universal time which the site attempts to maintain. A1 denotes atomic time as kept by the United States Naval Observatory, LPT represents the long-period ($\gg 1$ day) terms in the expression for atomic time in terms of coordinate time, 32.15 sec represents the epoch offset of A1 and coordinate time chosen for convenience in other astronomical applications, and the Kth order polynomial is a simple model representing the deviation of the actual clock performance from the desired, referenced to t_0 which may be the midpoint of a short ($\simeq 1$ day) series of interferometric observations. The quantity Δt represents the coordinate-time interval between the arrival of the signal at the two sites.

A superposed dot in the equations signifies differentiation with respect to coordinate time. The i-j asymmetry in the equations is introduced because (i) the delay is measured with respect to time as kept at site i, and (ii) the fringe rate is defined in terms of the derivative of the fringe phase with respect to time as kept at site i. For a clear, elementary discussion of these observables, see Chapters 5.1 and 5.5.

From the point of view of this chapter, the terms τ^p_{ij} and τ^a_{ij} are sources of noise. The effect of the former can be virtually eliminated through exploitation of the frequency dependence of the index of refraction of a plasma (see Chapter 2.1). If the VLBI measurements are made simultaneously in two frequency bands centered at f_1 and f_2 ($f_2 > f_1$), then the standard deviation $\sigma(\tau_f)$ in the determination of τ freed from charged particle effects is related to the standard deviations $\sigma(\tau_k)$ of the group delays measured at the frequency bands f_k ($k = 1, 2$) by the expression

$$\sigma(\tau_f) \simeq (f_2^2 - f_1^2)^{-1}\{f_1^4\sigma^2(\tau_1) + f_2^4\sigma^2(\tau_2)\}^{1/2}. \tag{5.6.7}$$

For $f_2 \simeq 4f_1$ and $\sigma(\tau_2) \simeq \sigma(\tau_1)$, we find $\sigma(\tau_f) \simeq 1.07\sigma(\tau_k)$. Thus, the degradation in the measurement accuracy caused by the charged particles will be about 7% when this procedure is used. A further improvement, by an order of magnitude or more, would be possible if the fringe phase could be deter-

mined unambiguously, for example by sufficient accuracy in the measurements of τ at the two frequency bands. For such a circumstance, we find

$$\sigma(\tau_f) \simeq [2\pi(f_2^2 - f_1^2)]^{-1}\{f_1^2\sigma^2(\phi_1) + f_2^2\sigma^2(\phi_2)\}^{1/2}, \quad (5.6.8)$$

where $\sigma(\phi_k)$, $k = 1, 2$, is the standard deviation of the measurement of fringe phase in the kth frequency band. When converted to comparable units, $\sigma(\phi_k)/\sigma(\tau_k)$ is approximately equal to B_k/f_k, where B_k is the rms about the mean of the synthesized bands used to determine the group delay (see Section 5.5.5). Since B_k/f_k is usually small, use of fringe phase, if possible, is advantageous in the determination of τ_f.

The calibration of the electrical path length of the neutral atmosphere (Section 2.5.4) presents the main limitation on the accuracy achievable with VLBI in astrometric and geodetic applications. A new method, not yet tried in a VLBI experiment, shows the most promise for this path length calibration. This method[3] involves monitoring the brightness temperature of the atmosphere at and near the 22 GHz water-vapor spectral line along the line-of-sight from each interferometer antenna to the source. The measured brightness temperatures at each site are used to infer the electrical path length by means of an empirical, linear algorithm. The algorithm, in turn, is based on a statistical analysis of large sets of actual radiosonde data from which both the implied electrical path lengths and the brightness temperatures at the various frequencies were calculated. The linear relationships deduced led to errors in the determinations of zenith electrical path lengths of about 1 cm rms in winter and 1.4 cm rms in summer, both for the Northeastern United States.

5.6.3. Information Content of Observables

The VLBI observables are affected not only by the propagation medium and the relative behavior of the clocks at the two sites, as indicated explicitly above, but also by the source's structure and motion, the solid-earth tides, the crustal motions, polar motion, speed of rotation, nutation, and precession of the earth, and other small physical effects. These effects due to the source and to the earth (see Section 5.6.4) primarily affect Eqs. (5.6.1)–(5.6.3) through the time dependences of $\hat{\mathbf{e}}_s$ and $\mathbf{r}_i$, respectively. Given suitable parametrizations for all of these influences, useful estimates of the parameters can be obtained from analysis of the VLBI observations, provided the data are of sufficient accuracy, span a sufficiently long interval of time, and are of such a character as to eliminate degeneracy—the complete masking of the effects of one parameter by those of a combination of other parameters.

To reproduce the explicit parametrizations employed for each of these

[3] L. W. Schaper, D. H. Staelin, and J. W. Waters, *Proc. IEEE* 58, 272 (1970).

effects on the VLBI observables would be to proceed well beyond the scope of this chapter. Instead, we will consider an oversimplified situation which is nonetheless amenable to a presentation of the most important ideas. Thus, we consider the earth to be a rigid body rotating with a constant and known angular velocity vector, and each source to be at infinite distance, of infinitesimal extent, and with an unvarying output of radio radiation that travels in vacuum between source and site. If, further, the clocks at the two sites differ only in their epoch setting and in their rate ($\alpha_{ik} \neq \alpha_{jk}$, $k = 0, 1$), we can conclude that for group-delay measurements, for example, the time dependence will be a diurnal sinusoid superimposed on a linear term that, in general, neither intercepts the origin nor has zero slope. The constant, or intercept of the linear term, represents the additive effects of the clock-epoch offset and the product of the polar, or axial, components of the baseline vector and the source-position unit vector [see Eq. (5.5.1)]. The slope of the linear term represents, of course, the clock-rate offset. The amplitude of the sinusoid measures the product of the equatorial component of the baseline and of the source-position unit vector, as also illustrated in Eq. (5.5.1); the phase of the sinusoid is a measure of the "tilt" of the baseline with respect to the plane normal to $\hat{\mathbf{e}}_s$. In this model, then, any number of group-delay observations of a single source can provide no more than four quantities: the intercept and slope of the straight line, and the phase and amplitude of the superposed sinusoid. These four quantities constitute the information content of the group-delay observable. The situation for the fringe-phase observable is similar. For the fringe-rate observable, three quantities provide the total information content; all sensitivity to the time-independent terms in ϕ vanish upon differentiation.

Considering the information content of these observables, how may we determine the three baseline components, the two source position components, and the two clock difference characteristics? The unknowns seem to combine to seven and the knowns to only four for even the group-delay observable—clearly an untenable situation. Actually, the unknowns total one less since we are free to choose our origin of right ascension. The origin of declination is provided by the plane normal to the (given) angular velocity vector. To play a "winning game," we try the strategy of observing additional sources: Each new source for which we obtain group-delay observations can provide up to three new quantities, since the slope of the linear term is the only one independent of the source. But each new source adds only two new unknowns. Observations of a minimum of three sources are thus required to solve for all relevant parameters.[4] Two caveats must be mentioned:

(i) With fringe phase instead of group delay used as the observable, the

[4] I. I. Shapiro and C. A. Knight, *in* "Earthquake Displacement Fields and the Rotation of the Earth" (A. Beck, ed.), p. 284. Reidel Publ., Dordrecht, 1970.

game can not be won completely if an unknown constant phase is introduced with each source. In such an event, the number of unknowns added for each new source just equals the number of knowns. Further, unless the fringe phases observed for a source can be followed through a substantial fraction of the diurnal cycle without introduction of 2π ambiguities, little useful information can be deduced about baseline components or source positions.

(ii) With fringe rate alone used as the observable, it is not possible, in principle, to determine either the clock offset, as mentioned, the polar component of the baseline, or the declination of all sources. The declination of one source—a near equatorial one is the best single choice—may be fixed in accord with, say, optical observations, or an overall constraint may be applied to insure that, for example, the weighted mean of the source declinations equals a preset constant determined from optical data.

Although omitted here for brevity, it can be shown that for the necessary number of group-delay observations of three sources, the relations in terms of the unknowns can, in fact, be inverted to yield solutions for all of the relevant quantities; there are no degeneracies if the observations of each source span a reasonable fraction of the diurnal cycle.

Analyses similar to those given above are easily carried out for combinations of observables and for interferometer arrays with three or more elements. In brief, these show that, to be able to solve for all relevant parameters, at least two sources must be observed no matter how many elements in the array.

5.6.4. Astrometric and Geodetic Parameters

Using the principles described in the previous sections, and extensions thereof, we can utilize VLBI observations to deduce the positions and structures of extragalactic sources, to test the predictions of general relativity, to determine satellite orbits, to estimate the relative positions of radio transmitters placed on the moon by the Apollo astronauts, and to determine various other quantities of geophysical and astronomical interest. Here we describe some of these methods and give references to the major results so far obtained.

5.6.4.1. Source Position. Fringe rates and group delays have been used successfully to determine positions of sources of compact continuum radiation since 1969.[1,5–7] The accuracy achieved has so far progressed from uncertainties of several arc seconds down to uncertainties of about one-tenth of a.r. arc second. In the most recent such determinations,[8] the authors

[5] M. H. Cohen and D. B. Shaffer, *Astron. J.* **76**, 91 (1971).
[6] H. F. Hinteregger *et al.*, *Science* **173**, 396 (1972).
[7] M. H. Cohen, *Astrophys. Lett.* **12**, 81 (1972).
[8] A. E. E. Rogers *et al.*, *Astrophys. J.* **186**, 806 (1973).

made use of a weighted-least-squares estimator to find the source positions from sets of redundant data obtained at a radio frequency near 7850 MHz ($\lambda \simeq 3.8$ cm) with a 3900-km-baseline interferometer—the so-called "Goldstack" interferometer formed by the 64-m-diameter antenna of the Jet Propulsion Laboratory in Goldstone, California and the 36.6-m-diameter antenna of the Haystack Observatory in Westford, Massachusetts.

Fringe phases were first utilized to obtain estimates of the relative positions of closely spaced, discrete water-vapor masers ($\lambda \simeq 1.3$ cm) in our galaxy. These emission regions all were visible in the antenna beam of each element of the interferometer employed. Even though the separate, 3-min VLBI observations were spaced $\frac{1}{2}$ h apart, it was possible to determine accurate relative positions of the distinct regions from the fringe phases. We may outline the method briefly as follows. The relative fringe phase, $\Delta\phi(t)$, between a pair of the discrete sources, measured at time t, may be expressed as

$$\Delta\phi(t) = \Phi(\Delta\alpha, \Delta\delta; t) + \varepsilon + 2\pi n \tag{5.6.9}$$

in the strong signal case, where ε ($\ll 2\pi$) is the Gaussianly distributed error in the (ambiguous) phase determination, n is an integer, and Φ represents the theoretical value of the relative phase given as a function of the differences, $\Delta\alpha$ and $\Delta\delta$, in the right ascension and declination coordinates, respectively, of the pair of sources (other dependences have been omitted for brevity). The conditional probability density for $\Delta\alpha$ and $\Delta\delta$, given the set of independent relative fringe-phase estimates $\Delta\phi(t_{ij})$ and the assumption that all values of n are equally probable, can be written as

$$p(\Delta\alpha, \Delta\delta \mid \Delta\phi) \propto p_0(\Delta\alpha, \Delta\delta) \times \prod_{i=1}^{I} \prod_{j=1}^{J_i} \sum_{n=-\infty}^{\infty} \frac{1}{\sigma_{ij}} \times \exp\{-[\Delta\phi(t_{ij}) - 2\pi n - \Phi(\Delta\alpha, \Delta\delta; t_{ij})]^2/2\sigma_{ij}^2\}, \tag{5.6.10}$$

where σ_{ij} is the standard deviation of the relative fringe phase from the jth of J_i observations on the ith of I independent baselines, and where $p_0(\Delta\alpha, \Delta\delta)$ represents the joint *a priori* probability density of $\Delta\alpha$ and $\Delta\delta$ determined from the unambiguous fringe rate data as described in Chapter 5.5. The relative position is then taken to be that set $(\Delta\alpha, \Delta\delta)$ for which the right side of Eq. (5.6.10) is a maximum. In practice, this estimate is easily obtained by a systematic evaluation of p over successively finer grids in the $\Delta\alpha\,\Delta\delta$-plane. Because of its relatively slow variation with $\Delta\alpha$ and $\Delta\delta$, p_0 serves mainly to delimit the area of search for the maximum of p. Further details are given by Reisz *et al.*[9] who determined the separation of two components 0.3 arc sec apart in the radio source W3 (OH), with an error ellipse whose

[9] A. C. Reisz *et al.*, *Astrophys. J.* **186**, 537 (1973).

ORIGINAL PAGE
BLACK AND WHITE PHOTOGRAPH

major and minor axes were 0.0003 and 0.0001 arc sec, respectively. A three-element interferometer with maximum antenna spacing of 845 km was used in this 1971 experiment: Haystack, the National Radio Astronomy Observatory's 42.7-m-diameter antenna in Green Bank, West Virginia, and the Naval Research Laboratory's 25.9-m-diameter antenna at Maryland Point, Maryland.

For a pair of sources whose angular separation in the sky is not too great, a two-element interferometer can be used to monitor the fringe phase for each source, without the introduction of any 2π ambiguities, by switching rapidly back and forth from observations of one to observations of the other. Aside from the obvious conditions on mutual visibility, the limitation on angular separation is set primarily by the slew rates of the antennas forming the interferometer. By subtraction of the fringe phase functions for the two sources the resultant differenced fringe phase is essentially freed from the effects of any clock wandering and, for neighboring sources, from almost all of the effects of the propagation medium. Analysis of this differenced phase observable can therefore yield a very high accuracy in the estimate of the relative source positions, approaching that achieved for the discrete water-vapor maser regions. The difference observable, $\Delta\phi$, may be written as

$$\Delta\phi(t) \simeq (\omega B/c)\{\Delta\alpha \cos D \cos\delta \sin(A_0 + \Omega t - \alpha) - \Delta\delta \cos D \sin\delta \cos(A_0 + \Omega t - \alpha) + \Delta\delta \sin D \cos\delta\}, \tag{5.6.11}$$

where $B \equiv |\mathbf{r}_2 - \mathbf{r}_1|$, α and δ are the coordinates of the reference source, A_0 and D, respectively, the right ascension, or hour angle, at epoch and the declination of the baseline, and Ω the angular velocity of the earth. We have omitted terms of higher order in $\Delta\alpha$ and $\Delta\delta$, as well as others indicated in Eq. (5.6.1).

For some pairs of sources we find, for example, that $\Delta\delta = O(\Delta\alpha^2)$; in such cases Eq. (5.6.11) for the differenced fringe phase, accurate to $O(\Delta\alpha)$, must be augmented by the term $-\frac{1}{2}\Delta\alpha^2 \cos D \cos\delta \cos(A_0 + \Omega t - \alpha)$ inside the braces. A similar modification is required for $\Delta\alpha = O(\Delta\delta^2)$. As a simple illustration, consider the effects on the estimates of $\Delta\alpha$ and $\Delta\delta$ of an error in baseline direction for the case in which $\Delta\delta = O(\Delta\alpha^2)$:

$$\delta\,\Delta\alpha \simeq \Delta\alpha\,\delta D \tan D, \tag{5.6.12}$$

$$\delta\,\Delta\delta \simeq \Delta\alpha\,\delta A \cot\delta, \tag{5.6.13}$$

where δA and δD are the baseline direction uncertainties. Thus, for baselines nearly East–West (small D) and high declination sources, the estimates of $\Delta\alpha$ and $\Delta\delta$ are both insensitive to baseline direction errors and to equivalent errors in the length of the day and polar motion, discussed in Section 5.6.4.5.

The pair of compact continuum radio sources 3C345 and NRAO 512 are separated in the sky by only about 10^{-2} rad, with the separation in declination being only 5×10^{-4} rad; therefore $\Delta\delta \approx O(\Delta\alpha^2)$. Four separate sets of observations that utilized this switching technique with the Goldstack interferometer ($\lambda \simeq 3.8$ cm) were carried out on this source pair between 1971 and 1974, and yielded differences in position with an rms scatter about the mean of under 1.5 and 2.0 milliarc sec in right ascension and declination, respectively. These results obtained by the VLBI Group of the Goddard Space Flight Center, the Haystack Observatory, and the Massachusetts Institute of Technology, can be used to set an upper limit of about 0.0005 arc sec/yr on the relative proper motion of this pair and, approximately, on the "absolute" proper motion of either source, since it is highly improbable that their individual proper motions could be coordinated. Continuation of such measurements, with improvements in accuracy, could lead in the relatively near future to bounds on, or measurements of, proper motion of u[illegible] in the determination of the distance scale for extragalactic objects.

If two or more antennas are available at each site of an interferometer array, then the switching described above can be avoided, and any two or more sources that are mutually visible from every site can be monitored continuously and the difference fringe phases freed from clock effects if the same clock, or frequency standard, is used at a given site to govern the local-oscillator signals for each of the antennas at that site. The only combination of this type so far utilized successfully for precision astrometry has been a four-antenna combination: two antennas at each end of the 845-km baseline formed by the Haystack Observatory and the National Radio Astronomy Observatory in Green Bank, West Virginia. These observations, carried out in 1972 at a radio frequency of 8105 MHz ($\lambda \simeq 3.7$ cm) by the above-mentioned VLBI Group, yielded postfit residuals for the difference fringe phases of about 20 psec rms ($\sigma_\phi \simeq 50°$); because of systematic effects not yet completely understood, the uncertainty of the relative source positions is at the level of a few hundredths of an arcsecond. Using such data in conjunction with an a priori covariance matrix, based on other observations, allows the baselines to be estimated as well as the source positions.

This "four-antenna" technique can also be applied to the detection of changes in relative positions of source pairs due to the changing deflection of radio waves by the sun's gravitational field as the line of sight to one or the other of the sources of a given pair passes near the sun. Such a test was performed in September–October 1972 with the Haystack–NRAO configuration discussed above[10]; observations of the pair of extragalactic continuum sources 3C273B and 3C279 yielded nearly the predicted change in relative

[10] C. C. Counselman, III *et al.*, *Phys. Rev. Lett.* **33**, 1621 (1974).

position for the period surrounding the occultation of the latter by the sun on October 8. In particular, this change was found to be 0.99 ± 0.03 times that deduced from the theory of general relativity; a significant limitation was provided by the fluctuations in the solar corona which occasionally wreaked havoc on the fringe phases for observations made with 3C279 within a few degrees of the sun.

5.6.4.2. Source Structure. Almost all of the compact extragalactic radio sources observed with the VLBI technique have exhibited fine structure; for many, this structure changes very rapidly with time.[11–13] One of the main astrometric challenges posed by these sources is the mapping of their fine structure and internal kinematics so as to provide a solid base for the theoretical understanding of their behavior. For radio continuum observations, this mapping, in principle, encompasses the determination of only the brightness distribution of a source and its changes with time. The brightness distribution for a very distant source whose radiation is spatially incoherent is related to the interferometer fringe amplitude and phase through the well-known Fourier transform relation (see Sections 5.1.2 and 5.5.5)

$$V(u, v) = \iint B(x, y) e^{i(ux+vy)}\, dx\, dy, \tag{5.6.14}$$

where V is the so-called visibility function whose amplitude and phase are the fringe amplitude and fringe phase, respectively. The parameters u and v represent the resolution, say in fringes per arcsecond, of the interferometer in the East–West and North–South directions, respectively (Section 5.1.1). The parameters x and y, defined along corresponding directions in the sky, represent the Cartesian coordinates of the source on the plane of the sky with respect to some defined origin near the center of the source (Section 5.5.5). Since the source is always confined to a small region of the sky, the above relation can be inverted to infer uniquely the brightness distribution, provided $V(u, v)$ is sampled in accord with the requirements of the two-dimensional analog of the Nyquist theorem. For any given two-element interferometer, only an ellipse, or arc thereof, in the uv-plane can be sampled. Further, only the amplitude of $V(u, v)$ can be determined usefully at these sample points; uncorrelated fluctuations in the propagation paths through the atmosphere over the two sites makes the fringe phase virtually worthless for the determination of source structure. For an interferometer array with three or more elements, however, the sum of the fringe phases around a closed "loop" of baselines in the array is virtually freed from propagation

[11] C. A. Knight *et al.*, *Science* **172**, 52 (1971).
[12] A. R. Whitney *et al.*, *Science* **173**, 225 (1971).
[13] M. H. Cohen *et al.*, *Astrophys. J.* **170**, 207 (1971).

effects and clock errors. This "closure" phase ϕ_c, which contains information only on source structure, can be written for three baselines as[14]

$$\phi_c \simeq \phi_{12}(t_1) - \phi_{13}(t_1) + \phi_{23}(t_2), \tag{5.6.15}$$

where $\phi_{ij}(t_i)$ signifies the fringe phase measured on the ij baseline referred to the time of arrival t_i of the signal at site i.

No VLBI array yet available is able, through the earth's rotation, to sample the required parts of the uv-plane to produce a unique brightness distribution for any source. With the limited available fringe-amplitude and closure-phase data, one usually resorts to parametrized models of the brightness distribution using the data to estimate the parameters via a suitable algorithm such as the maximum-likelihood estimator. The models may consist of the characteristics of two or more point sources of radiation, Gaussianly distributed sources of radiation, truncated one- or two-dimensional series representations of the brightness distribution, etc.—the limit is set only by the imaginations of the model makers and the capabilities of the computer! One may also parametrize the visibility function itself and, after estimation of the parameters through comparison with the available data, invert Eq. (5.6.14) to obtain the brightness distribution.[14] The difficulty with these types of approaches is that the results can be no better than the models, and may, in fact, bear little resemblance to the actual brightness distributions. In the future, larger, better arranged arrays will come into use, and the modeling problems will be much alleviated.

5.6.4.3. Satellite Orbits. The VLBI technique can also be used to determine accurately the orbits of earth satellites if they emit radio radiation. For satellites at synchronous altitude, even effective radiated powers as low as a milliwatt, spread over a 10-MHz bandwidth, yield signals comparable in strength to those received from extragalactic radio sources.

The reduction of the recorded VLBI signals to produce the observables (see Section 5.6.2) is more complicated for satellites than for natural sources. The motion of the satellite during the recording must be accounted for explicitly and with reasonable accuracy to avoid "washing out" of the fringes: In the cross correlation of the signals (see Chapter 5.5), the a priori model must include a preliminary orbit of the satellite.

The final processing of the observables also requires modification. One must account in the equations of Section 5.6.2 for the changing parallax of the source introduced by its orbit. Although it appears that, for this application, a geocentric frame would be more appropriate, the reference frame we have chosen produces no particular difficulties since the vectors can

[14] A. E. E. Rogers *et al.*, *Astrophys. J.* **193**, 293 (1974).

be expanded in such a manner that the appropriate common parts cancel. The parameters to be estimated must be augmented to allow for the six independent orbital elements; the basic estimator may remain unchanged. If the a priori orbit was not of sufficient accuracy, the cross correlation and final processing can be repeated with the original a priori orbit replaced by the orbit obtained from the first iteration.

This application of VLBI was first tried in 1969. From only 7 hr of observations of the TACSAT I communications satellite which was in a synchronous, nearly equatorial orbit, an extremely accurate orbit was produced: six-place accuracy in both semimajor axis and eccentricity, as judged by the consistency of the results obtained from the group-delay and fringe-rate data, separately.[15] The observations were made from three sites (Haystack, Green Bank, and the Owens Valley Radio Observatory, Big Pine, California (longest baseline 3500 km)) over a 10 MHz bandwidth centered at about 7.3 GHz.

The VLBI technique for satellite-orbit determination can be compared with conventional radio tracking methods and with laser ranging.[15] Here, we shall only intercompare the utility for geodetic applications of VLBI observations of satellites and extragalactic radio sources. The celestial sources have one essential advantage. They have negligibly small proper motions, and hence provide an excellent approximation to an inertial reference frame. Having the radiation sources on the satellite allows the baselines to be located with respect to the center of mass of the earth. Ties to this center degrade with the decrease in parallax accompanying an increase in the altitude of the satellite relative to the length of the baseline; observations of extragalactic sources are completely insensitive to any parallel displacement of the baseline. Similarly, observations of satellites provide sensitivity to the earth's gravitational potential. This sensitivity, however, is a double-edged sword since, for the determination of baselines, deficiencies in the theoretical model of the potential are a hindrance.

The most promising approach may be to make use simultaneously of both natural and artificial sources. The satellites can then be located accurately with respect to a stellar frame; relative errors might be kept as low as a milliarcsecond if the satellite passes close to, and slowly by, one of the natural sources that constitute the inertial frame. One can even envision a hierarchy of ground terminals for geodetic use: The most sensitive installations can be used to observe both satellites and natural sources, while small, transportable terminals observe only the stronger signals from satellites. With the orbits determined precisely, relative to the inertial frames, by the large installations, the VLBI observations by the portable ones can be used

[15] R. A. Preston *et al.*, *Science* **178**, 407 (1972).

to determine geodetic ties directly. For this latter purpose, the satellites might be equipped with corner reflectors so as to be suitable targets for laser observations as well. An important role in the geodetic applications might also be played here by radio emissions from spacecraft in interplanetary flight and in orbit about, or emplaced on, other planets.

5.6.4.4. Lunar Applications. The Apollo astronauts left a number of transmitters on the lunar surface. Five are still operating and may continue to do so for many years. They provide the opportunity, through differential interferometry,[16] to set up a selenodetic reference system, to measure accurately the moon's libration, and to relate the moon's orbital position to the inertial reference frame formed by the extragalactic radio sources.

The signals from these so-called ALSEP transmitters are characterized by a carrier and narrow-band modulation, with the former containing a small fraction of the power. The presence of a carrier allows a significant simplification in the VLBI apparatus: Instead of recording the signals themselves, one can compare at each site the received signals from any pair of ALSEPs and record only the cycle count of the suitably multiplied difference frequency. Voice communication or teletype between sites can then be used to establish immediately whether all systems are operating properly.

Since the ALSEP transmissions are at S-band frequencies ($\lambda \simeq 13$ cm), the ionosphere affects noticeably even the difference fringe phases. The transmissions from the different ALSEPs span an interval of 4 MHz, and these separations can be exploited to reduce the sensitivity of the results to the ionosphere when, for example, all five ALSEPs are observed simultaneously.

Analysis of the potential of such differential VLBI observations of the ALSEP transmitters for the establishment of a set of selenodetic reference points indicates that the uncertainties in the determinations of the vectors between the ALSEPs should be reducible to about one meter. At the present level of development of the technique, only dekameter accuracy has been obtained.[17] The uncertainties in the determinations of the moon's position with respect to the extragalactic radio sources might be reducible to the milliarcsecond level, but no results have yet been obtained. The parameters describing the moon's libration have also not yet been deduced from the VLBI observations, but should, when the technique is developed, yield values perhaps comparable in accuracy to those obtainable from laser observations of the retroreflectors emplaced on the lunar surface by the astronauts.

5.6.4.5. Geophysical Applications. The various motions of the earth's crust can be separated and measured with great accuracy via VLBI. We dis-

[16] C. C. Counselman, III, H. F. Hinteregger, and I. I. Shapiro, *Science* **178**, 607 (1972).

[17] C. C. Counselman, III, H. F. Hinteregger, R. W. King, and I. I. Shapiro, *Science* **181**, 772 (1973).

cuss briefly these motions, the methods of measurement, and the levels of accuracy so far attained.

The precession and nutation of the earth, due primarily to the solar and lunar torques exerted on the earth's equatorial bulge, are manifested by a movement of the earth's axis of rotation in an inertial frame. The coordinates of the sources (but not the lengths of the arcs between them!) will therefore appear to change if the equator of date is always used to define the origin of declination. From the pattern of change, the parameters characterizing the precession and nutation can be estimated. In actual practice, this parametrization is added to the theoretical model of the observable, and values for all relevant parameters are determined simultaneously. The period of the precession is about 26,000 yr, whereas that of the principal nutation is about 18.7 yr; thus, a number of years of observation are required for an adequate separation of the contributions of each to the observed pattern. Similar statements apply to the other periodicities present in the usual series expansion of the nutation. Except for the relative insensitivity of the VLBI measurements to the instantaneous orientation of the ecliptic, the VLBI determination of the precession would surpass the optical in a few years, despite the far longer span of the optical observations. VLBI can also be used to determine the orientation of the ecliptic (the earth's orbital plane) with respect to the frame formed by the extragalactic sources. The method requires point sources of radiation on or near other planets such as could be provided by the radio transponders on spacecraft landers or orbiters. Sets of differential VLBI observations of such spacecraft and extragalactic sources that at times lie nearly along the same line of sight can be used to infer the orientations of the orbital planes of the earth and the other planets. Observations of pulsars can, in addition, be used to determine the orientation of the ecliptic with respect to the earth's equator.[18]

There are a number of geophysical effects, most as yet poorly understood, that cause variations in the length of the day and in the orientation of the earth's crust with respect to its axis of rotation. These two types of changes are usually referred to as variations in universal time (UT1) and polar motion. Measurements of UT1 and polar motion can be made with VLBI because of their effects on the baseline vector: The direction (but not the length!) of this vector will be changed. This effect of UT1 and polar motion on the baseline contrasts with the effect of precession and nutation which cause an apparent change in the direction of the sources. Since the direction of a vector can be described by only two parameters, it is not possible to determine variations in UT1 and both components of polar motion using only a single two-element interferometer.

Variations in UT1 and in one component of polar motion have been

[18] I. I. Shapiro, *Trans. Amer. Geophys. Un.* **51**, 266 (1970).

determined with VLBI from a series of observations with the two-element Goldstack interferometer.[19] Since this interferometer has a very small North–South component, the changes in UT1 affected mainly the right ascension, or hour angle, of the baseline, and the changes in polar motion affected mainly the declination. The accuracies achieved seem to have surpassed those attained via conventional optical techniques.

The tidal bulges raised on the earth by the moon and sun also affect the baseline, both directly and indirectly, through changes in the earth's orientation caused, for example, by the effect of torques exerted on the bulge. The largest effect is due to the semidiurnal tidal component which can introduce a maximum offset in the baseline of an amplitude of several tens of centimeters. This component has apparently already been detected from analysis of VLBI observations[19] but the measurements are not yet accurate enough to deduce a useful value for the relevant Love numbers. The effects of lateral inhomogeneities in the earth, and of ocean loading on the solid-earth tides, should both be accessible for study with suitable placement of the interferometer elements and with increased accuracy in the measurements and in the calibration of the propagation medium.

The vector baselines have been determined by the VLBI technique for sites separated by distances of from 845 up to 8000 km,[1,6,19] and also for sites separated by distances of 16 km[20] and less. Three-site "closure" experiments were also performed over transcontinental distances.[1] The accuracies achieved on the short baselines, on the order of 5 cm in length, are nearly sufficient for monitoring accurately crustal motions across faults. The baseline accuracies achieved over the transcontinental and intercontinental distances were 20 cm or worse, depending on the signal-to-noise ratio available for the different interferometers used. The lower limit was actually set by systematic errors that can be, but have not yet been, sharply reduced by the use of appropriate calibration techniques (see Section 5.6.2).

To make important contributions to the measurement of crustal distortions, or plate tectonics, one must reduce the errors in baseline determination to the centimeter level through calibration and increases in signal-to-noise ratios. The calibration of the propagation medium is only a problem in regard to the neutral atmosphere; all other but the clock effects on the VLBI measurements can be considered as "signal" for the purposes of this chapter. Increases in signal-to-noise ratios seem most readily obtainable by the use of wideband instrumentation recorders,[21] which could provide a 50 MHz or greater bandwidth compared with the 360 kHz or less used in the

[19] I. I. Shapiro *et al.*, *Science* **186**, 920 (1974).

[20] J. B. Thomas, J. L. Fanselow, P. F. MacDoran, D. J. Spitzmesser, and L. Skjerve, Jet Propulsion Lab. Tech. Rep. **32-1526**, p. 36 (1974).

[21] H. F. Hinteregger, Ph.D. Thesis, Dept. of Phys., Massachusetts Inst. of Technol. (1972).

experiments described above. When such improved systems come into use, a new era could begin in our understanding of the fine structure of the earth's crustal motions and in elucidating, for example, the possible relations of strain accumulation in the crust and polar motion to earthquakes and earthquake prediction.

Reprinted from:

THE ASTRONOMICAL JOURNAL VOLUME 81, NUMBER 8 AUGUST 1976

Radio source positions from very-long-baseline interferometry observations

T. A. Clark, L. K. Hutton, and G. E. Marandino

Goddard Space Flight Center, Greenbelt, Maryland 20771

University of Maryland, College Park, Maryland 20742

C. C. Counselman, D. S. Robertson, I. I. Shapiro, and J. J. Wittels

Department of Earth and Planetary Sciences and Department of Physics, Massachusetts Institute of Technology, Cambridge, Massachusetts 02139

H. F. Hinteregger, C. A. Knight, A. E. E. Rogers, and A. R. Whitney

Northeast Radio Observatory Corporation, Haystack Observatory, Westford, Massachusetts 01886

A. E. Niell

Jet Propulsion Laboratory, Pasadena, California 91103

B. O. Rönnäng and O. E. H. Rydbeck

Chalmers University of Technology, Onsala Space Observatory, Onsala, Sweden

(Received 20 February 1976)

Accurate positions of compact radio sources have been determined from very-long-baseline interferometry (VLBI) observations based on the bandwidth-synthesis technique. The coordinates for 18 extragalactic sources were obtained from sets of observations spread over the period from April 1972 to January 1975; the scatter among the independent determinations of the source coordinates from the separate sets of observations is about 0".05, except for the declinations of near-equatorial sources where the scatter is about 0".15. Comparison of our positions with those determined with the Cambridge 5-km radio interferometer shows the rms scatter about the mean difference to be about 0".04 in each coordinate (no sources of low declination were in common). A similar comparison of our results with those obtained by the Jet Propulsion Laboratory from separate VLBI observations yields a slightly larger rms scatter, after exclusion of the declinations of the near-equatorial sources. We also obtained a position for the Galactic object, β Persei (Algol), which agrees well with the position given in the FK 4 catalogue: $\Delta\alpha(\text{VLBI}-\text{FK4}) = -0^s.001 \pm 0^s.007$ and $\Delta\delta = -0".12 \pm 0".09$.

INTRODUCTION

OBSERVATION of compact extragalactic radio sources via the technique of very-long-baseline interferometry (VLBI) offers the possibility to form an excellent approximation to an inertial frame through precise determination of the relative positions of such sources. VLBI holds the potential for the reduction of the uncertainty in these determinations to the milliseconds-of-arc level. But the results published to date (see, e.g., Cohen and Shaffer 1971; Hinteregger *et al.* 1972; Cohen 1972; Rogers *et al.* 1973), although showing steady improvement down to an uncertainty level of a tenth of a second of arc, clearly fall well short of this goal.

Here we report results from an extended series of VLBI observations that yielded an additional twofold improvement: The coordinates of 18 compact extragalactic radio sources were determined with an uncertainty in each coordinate of about 0".05, except for the declination of near-equatorial sources for which the uncertainty is about threefold greater.

A unique aspect of the present work is the determination from VLBI observations of the coordinates of the Galactic source β Persei (Algol), a fundamental star in the FK4 catalogue (Fricke and Kopff 1963). This result allows the VLBI positions to be related directly to the stellar reference system.

I. OBSERVATIONS AND DATA REDUCTION

Source positions were determined from 18 separate sets of observations distributed between April 1972 and January 1975. Each set spanned one to four days and involved two, three, or four of the following five antenna systems: the 37-m-diameter antenna at the Haystack Observatory in Westford, Massachusetts; the 64-m-diameter antenna of the Jet Propulsion Laboratory in Goldstone, California; the 43-m-diameter antenna of the National Radio Astronomy Observatory in Green Bank, West Virginia; the 26-m-diameter antenna of the National Oceanic and Atmospheric Agency in Gilmore Creek, Alaska; and the 26-m-diameter antenna of the Chalmers University of Technology in Onsala, Sweden.

All observations were made at radio frequencies near 7850 MHz ($\lambda \simeq 3.8$ cm) with left-circular polarization (IEEE definition), and were recorded using the Mark I system (Clark *et al.* 1968). The duration of an individual observation was 3 min. A hydrogen-maser frequency standard was used at each site for each set of observations with only a few exceptions. The band-

TABLE I. Positions of extragalactic radio sources from VLBI observations.

Source	Right ascension (1950.0)	Elliptic aberration[a]	Declination (1950.0)	Elliptic aberration[a]	Number of solutions[b]
3C 84	$3^h16^m29^s550\pm0^s002$[c]	0s019	41 19′51″.69±0″.07[c]	0″.16	12
NRAO 140	3 33 22.386±0.002	0.018	32 08 36.44±0.07	0.11	2
CTA 26	3 36 58.937±0.002	0.016	−01 56 16.79±0.20	−0.04	1
NRAO 150	3 55 45.235±0.004	0.027	50 49 20.11±0.04	0.16	8
3C 120	4 30 31.586±0.003	0.019	05 14 59.49±0.19	−0.01	14
OI 287	8 51 57.231±0.003	0.021	20 17 58.45±0.07	−0.09	13
4C 39.25	9 23 55.297±0.004	0.023	39 15 23.73±0.03	−0.16	16
3C 273B	12 26 33.246[d]	0.002	02 19 43.31±0.13	−0.04	18
3C 279	12 53 35.834±0.002	−0.001	−05 31 07.99±0.14	0.00	17
OQ 208	14 04 45.625±0.001	−0.009	28 41 29.41±0.05	−0.18	6
OQ 172	14 42 50.496±0.020	−0.011	10 11 12.53±1.36	−0.08	1
NRAO 512	16 38 48.199±0.001	−0.025	39 52 30.23±0.01	−0.14	4
3C 345	16 41 17.635±0.002	−0.025	39 54 10.96±0.04	−0.13	15
3C 418	20 37 07.490±0.006	−0.032	51 08 35.66±0.03	0.11	6
PKS 2134+00	21 34 05.226±0.003	−0.017	00 28 25.03±0.23	−0.03	14
VRO 42.22.01	22 00 39.385±0.005	−0.020	42 02 08.40±0.04	0.15	16
CTA 102	22 30 07.827±0.006	−0.013	11 28 22.49±0.57	0.03	1
3C 454.3	22 51 29.533±0.003	−0.011	15 52 54.24±0.05	0.05	14

[a] The addition to our results of these contributions of elliptic aberration allows direct comparison with positions given in accord with conventional practice in optical astrometry.

[b] Each solution was based on the data from a single experiment of duration 1–4 days.

[c] The uncertainties given represent the root-weighted-mean-square (rms) spread of the individual solutions about the weighted mean, except when only one solution was available. In these latter cases, the uncertainties represent twice the formal standard errors which in turn are based on scaling the rms of the postfit residuals to unity.

[d] This value defines the origin of right ascension and is based on the result for the right ascension of 3C 273B obtained by Hazard *et al.* (1971).

width-synthesis technique, as in our prior work (Hinteregger *et al.* 1972; Rogers *et al.* 1973), was used throughout. The precise dates of the observations and detailed information on the equipment used are given by Robertson (1975).

The data-reduction procedures used to obtain the group delay and the fringe rate from each pair of Mark I recordings were as outlined by Rogers *et al.* (1973) and further described by Whitney *et al.* (1976). The algorithms and computer programs used in the estimation of the source positions from the group delays and fringe rates are given in Robertson (1975). Typically, for each set of data, we used a weighted-least-squares estimator to determine the values for the three components of each independent baseline, the clock epoch- and rate-offset parameters for each day for each baseline, the zenith electrical path length of the atmosphere for each site for each day, and the coordinates of the relevant sources. Although both the group delays and the fringe rates were utilized in the analysis to determine source positions, the fringe rates have, in all but one instance, only an insignificant effect on our results. The rate data will therefore be largely ignored in subsequent discussion.

II. RESULTS AND DISCUSSION

In the first part of this section, we discuss, in turn, the positions we obtained for extragalactic sources, the estimated uncertainties in these determinations, and the comparisons between our positions and those determined independently with different radio interferometric techniques. In the second part, we present our result for the position of Algol and compare it with the FK4 position.

Our estimates of the positions of the 18 observed extragalactic sources are gathered in Table I. Declinations were determined with respect to the equator of date, whereas right ascensions were determined with respect to an origin defined by the value given in Table I for 3C 273B. The source coordinates, with the effects of elliptic aberration removed, were referred back to the mean equator and equinox of 1950.0 via the standard formulas for precession and nutation.

The values shown in Table I for the source coordinates, with the exceptions to be discussed below, each represent the weighted mean of the estimates determined separately from the independent sets of observations. The number N of such independent estimates is given for each source in the last column of Table I. For $N > 1$, each uncertainty shown in Table I is the root-weighted-mean-square (rms) scatter about the weighted mean of the estimates from the independent sets of observations. Thus, the uncertainty given is not the standard error of the weighted mean which would be smaller by the factor $(N-1)^{-1/2}$. Because of the dominance of systematic errors in the individual results, as discussed below, the quoted uncertainties are more reliable indicators of the "true" 70% confidence limits on our coordinate determinations.

The rms scatter estimates of uncertainty given in the table can be contrasted with corresponding ones based on the postfit residuals or on the signal-to-noise ratios achieved in individual observations. An rms scatter result was typically found to be about twice the formal standard error that corresponded to a value of unity for the weighted postfit residuals of the group delays from a single experiment. The achievement of this value of unity, on the other hand, typically required a doubling

of the uncertainties expected on the basis of the signal-to-noise ratios for individual measurements of group delays.

Trends often present in the postfit residuals (Robertson 1975) for a given source are also indicative of the influence of systematic errors and lend further support to our choice of the rms scatter uncertainty over either the twofold smaller formal standard error or the fourfold smaller one based on the signal-to-noise ratios from the measurements. The causes of such systematic errors are presumably combinations of the effects of the instabilities of the frequency standards employed, the variations in the propagation medium, and the drifts in the phase responses of the receiver systems. It was not possible to pinpoint the contributions from each cause for each set of observations. However, in some of the sets of observations, the effects of long-term (on the order of hours) clock "wander" were unmistakable. In analyzing data from sites so affected, we therefore made use of a differencing technique (Shapiro *et al.* 1974; Robertson 1975) in which the group delays from neighboring observations were subtracted to form new observables that were effectively freed from the long-term components of the clock drifts.

For the sources observed in only one set of observations ($N = 1$), the rms-scatter approach to the estimate of the errors in the coordinates is clearly inappropriate. In order to place the uncertainties in the estimates of the coordinates for these sources on a basis comparable to the uncertainties given for the coordinates of the other sources, we multiplied the formal standard errors by 2 (see above). We also note that for the single source for which $N = 2$, the rms scatter was, respectively, somewhat less and somewhat greater than twice the average formal standard error in right ascension and declination.

Overall, we note that for 11 of the 17 sources the uncertainties in the right-ascension coordinates are under 0.005, and in only one case was 0.01 reached or exceeded; for that source, OQ 172, only a single 3-min observation had been made. (Thus, in this case, and only in this case, the fringe rate played an important role.) With regard to the declinations, eight of the 18 uncertainties are less than or equal to 0.05; of the other ten uncertainties, three are 0.07 and five are two- or threefold higher due primarily to the declinations being 5° or under in absolute value. The remaining two larger uncertainties are for OQ 172, observed only once, and for CTA 102 which was observed in only one set of observations and has a declination of only 11°.

The accuracy of these determinations of relative positions does not seem to have been degraded by errors in the standard expressions for precession and nutation. Arclengths between the positions of pairs of sources remain invariant under rotations of the coordinate system and these arclengths, for the selected cases investigated, showed rms scatters consistent with those exhibited by the individual coordinates. Errors in precession and nutation would in any event affect our results only insofar as the errors in the precession and nutation changed during the approximately 3-yr period covered by our observations. Errors involved in the transformation to 1950.0 coordinates can be removed simply by transforming back to the corresponding coordinate system for an epoch, say, at the midpoint of our observation period. Of course, at any time when more accurate expressions for the precession and nutation become available, the data can be reprocessed and all effects of such errors thereby removed. Any inadequacies in our models for polar motion and UT.1 are unimportant for the determination of source positions since we solved independently for the baseline coordinates from each set of observations. Only the very small changes in the errors in our models for polar motion and UT.1 over the course of a single set of observations affect our results for source positions.

TABLE II. Comparison of VLBI and Cambridge 5-km interferometer[a] positions for extragalactic radio sources.

Source	$\Delta\alpha$(VLBI − Cambridge) (0.001)	$\Delta\delta$(VLBI − Cambridge) (0.01)
3C 84	7	−8
NRAO 140	2	−8
OJ 287	3	−25[b]
4C 39.25	6	−1
OQ 208	−1	−4
NRAO512	6	0
3C 345	8	1
VRO 42.22.01	5	−5
CTA 102	21[b]	8
3C 454.3	12	6

[a] Elsmore and Ryle (1975).
[b] See text for discussion.

Comparison of the coordinates shown in Table I with those we reported previously for 12 of the same extragalactic sources (Rogers *et al.* 1973) shows the agreement to be very good. The differences were less than, or comparable to, the root sum square (rss) of the quoted uncertainties in all cases but that of the declination of 3C 120, for which the difference was about 1.4 times the rss of the uncertainties. Of course, in drawing conclusions from this good agreement, one must bear in mind that the two sets of determinations were not independent. The second includes most of the data from the first.

The most accurate published values for the positions of extragalactic radio sources, other than ours, are probably those of Elsmore and Ryle (1975). We therefore compared our positions with theirs for the ten sources that were in common in the two sets. This comparison is displayed in Table II. The agreement is good in almost all cases. The disagreement between the declinations obtained for OJ 287 is surprisingly large, about threefold larger than the rss of the uncertainties given for each. Furthermore, in not one of our 13 independent determinations did the declination even reach within 0.05 of the Cambridge value. One might suspect that this difference is due to a genuine difference between the centers of brightness of the unresolved components of the

source as viewed by interferometers of resolving powers differing by a factor of order 1000. However, militating against such a possibility is our result (Wittels *et al.* 1975) that OJ 287 is almost completely unresolved, yielding typically a normalized fringe amplitude of about 0.9 with our interferometers. Conceivably, the difference might be due instead, or in part, to the difference in radio frequencies employed: the Cambridge group observed at a frequency of about 5 GHz as compared with our 8 GHz. Perhaps most likely, the uncertainty assigned by at least one of the two groups has been underestimated.

The only other coordinate value represented in Table II differing by as much as three times the rss of the uncertainties is the right ascension of CTA 102, but here any conclusion must be constrained by the fact that we have only one independent VLBI determination.

Omitting from consideration the declination of OJ 287 and the right ascension of CTA 102, we computed the weighted mean of the differences between the VLBI and the Cambridge coordinates and obtained

$$\overline{\Delta\alpha}(\text{VLBI} - \text{Cambridge}) \simeq 0^{s}.006 \simeq 0''.08,$$

$$\overline{\Delta\delta}(\text{VLBI} - \text{Cambridge}) \simeq -0''.02.$$

The bias between the right ascension values may be due, at least in part, to different definitions of origin. Elsmore and Ryle (1975) used the right ascension of Algol to define the origin in their system. The uncertainty of about $0''.09$ in our single determination of Algol's right ascension, given below, is consistent with this interpretation of the bias. The bias between the declination values is clearly insignificant for the present level of accuracy and sample size.

With the right ascension bias removed, and still omitting α_{CTA102} and δ_{OJ287}, we find that the root-weighted-mean-square differences in $\Delta\alpha \cos\delta$ and $\Delta\delta$ are

$$\sigma(\Delta\alpha \cos\delta) \simeq 0^{s}.003 \simeq 0''.04,$$

$$\sigma(\Delta\delta) \simeq 0''.04,$$

in accord with the uncertainties given for the individual estimates.

Another comparison was made with the results (Fanselow 1973) obtained independently at the Jet Propulsion Laboratory from VLBI observations made at a radio frequency of about 2.3 GHz. These observations, however, involved only fringe-rate data which are very insensitive to declinations for near-equatorial sources; we therefore restricted our comparison of the declinations to those exceeding 10°. For the nine sources in common, and the seven declinations exceeding 10°, we obtained

$$\overline{\Delta\alpha}(8\text{ GHz} - 2.3\text{ GHz}) \simeq 0^{s}.002 \simeq 0''.02,$$

$$\overline{\Delta\delta}(8\text{ GHz} - 2.3\text{ GHz}) \simeq 0''.01,$$

and

TABLE III. Position of Galactic radio source β Persei (Algol) from VLBI observations.

	Coordinate in 1950.0 system	Elliptic aberration[a]	Proper motion[b]
Right ascension	$03^{h}04^{m}54^{s}.338 \pm 0^{s}.006$	$0^{s}.017$	$0^{s}.008$
Declination	$40°\ 45'\ 52''.19 \pm 0''.08$	$0''.16$	$0''.06$

[a] The addition of the elliptic aberration to our results yields values compatible with the conventional practice in optical astrometry.

[b] The subtraction of these values of proper motion were used in the conversion of our 1975.04 position for Algol to the 1950.0 position given in the table.

$$\sigma(\Delta\alpha \cos\delta) \simeq 0^{s}.004 \simeq 0''.06,$$

$$\sigma(\Delta\delta) \simeq 0''.05,$$

where these quantities were calculated as for the comparison of our results with those of Elsmore and Ryle. We note that the Jet Propulsion Laboratory solution for the source coordinates incorporated, as *a priori* constraints, the corresponding optical positions and their uncertainties, thus yielding an origin for the right ascension coordinate different in principle from ours. The small average difference obtained in the comparison may therefore be somewhat fortuitous. Similarly, the mean difference in the declination values is smaller than could be expected on the basis of the uncertainties in our individual determinations. The rms scatter for the comparison of right ascensions is also smaller than the value expected from the uncertainties accompanying the Jet Propulsion Laboratory's individual estimates. On the other hand, the rms scatter for the comparison of declinations is close to the value expected.

In addition to the determination of the positions of extragalactic sources, we also obtained a result for the Galactic radio source β Persei (Algol). This source, which flares from time to time (Hjellming 1972), was detectable during our scheduled observations in mid-January 1975 and allowed us to make useful VLBI observations over a period of about 8 h (Clark *et al.* 1976). The values we obtained for the right ascension and declination are given in Table III with the basis for the quoted uncertainties being as described above for $N = 1$. Comparison with the FK4 catalogue position (Fricke and Kopff 1963) for Algol yields

$$\Delta\alpha(\text{VLBI} - \text{FK4}) = -0^{s}.001 \pm 0^{s}.007,$$

$$\Delta\delta(\text{VLBI} - \text{FK4}) = -0''.12 \pm 0''.09,$$

where the quoted uncertainties include contributions from the random errors in the FK4 catalogue position as given by Fricke and Kopff (1963). Since the more distant companion, Algol C, was separated by only $0''.06$ from the close binary pair, Algol AB, during our observations (Bachmann and Hershey 1975), we could not determine the origin of the radio flare within the Algol system. However, Ryle and Elsmore (1973) concluded from four separate determinations of the position of Algol that the close pair AB was the source of the radio emission.

Our results for the position of Algol therefore indicate that, at least to within 0.″1, our choice of origin for the right ascension coordinate is consistent with that of the FK4 catalogue.

ACKNOWLEDGMENTS

We are indebted to the staffs of the participating observatories for their important aid. Some of the observations reported here were made as part of the Quasar Patrol sponsored by the National Aeronautics and Space Administration and the Jet Propulsion Laboratory. The experimenters at the Massachusetts Institute of Technology were supported in part by the National Science Foundation, Grant DES74-22712, and in part by the National Aeronautics and Space Administration, Grant NAS 5-22843. Radio astronomy programs at the Haystack Observatory are conducted with support from the National Science Foundation, Grant MPS 71-02109 A07. This work also represents one phase of research carried out at the Jet Propulsion Laboratory, California Institute of Technology, under Contract NAS 7-100, sponsored by the National Aeronautics and Space Administration. The National Radio Astronomy Observatory is operated by Associated Universities, Inc., under contract with the National Science Foundation. The VLBI program at the Onsala Space Observatory is supported in part by the Swedish Natural Science Research Council and the Swedish Board for Technical Development. The successful use of the National Oceanic and Atmospheric Agency's facility in Gilmore Creek, Alaska, was accomplished with the invaluable aid of W. K. Klemperer and W. W. Warnock.

REFERENCES

Bachmann, P. J., and Hershey, J. L. (1975). Astron. J. **80,** 836.
Clark, B. G., Kellermann, K. I., Bare, C. C., Cohen, M. H., and Jauncey, D. L. (1968). Astrophys. J. **153,** 705.
Clark, T. A., Hutton, L. K., Ma, C., Shapiro, I. I., Wittels, J. J., Robertson, D. S., Hinteregger, H. F., Knight, C. A., Rogers, A. E. E., Whitney, A. R., Niell, A. E., Resch, G. M., and Webster, W. J. (1976). Astrophys. J. Lett. **206,** L107.
Cohen, M. H., and Shaffer, D. B. (1971). Astron. J. **76,** 91.
Cohen, M. H. (1972). Astrophys. Lett. **12,** 81.
Elsmore, B., and Ryle, M. (1976). Mon. Not. R. Astron. Soc. **174,** 411.
Fanselow, J. L. (1973). Private communication.
Fricke, W., and Kopff, A. (1963). *Fourth Fundamental Catalogue (FK4)* (Braun, Karlsruhe), pp. 24–25.
Hazard, C., Sutton, J., Argue, A. N., Kenworthy, C. M., Morrison, L. V., and Murray, C. A. (1971). Nat. Phys. Sci. **233,** 89.
Hinteregger, H. F., Shapiro, I. I., Robertson, D. S., Knight, C. A., Ergas, R. A., Whitney, A. R., Rogers, A. E. E., Moran, J. M., Clark, T. A., and Burke, B. F. (1972). Science **178,** 396.
Hjellming, R. M. (1972). Nat. Phys. Sci. **238,** 52.
Robertson, D. S. (1975). Ph.D. thesis, Mass. Inst. Tech.
Rogers, A. E. E., Counselman, C. C., III, Hinteregger, H. F., Knight, C. A., Robertson, D. S., Shapiro, I. I., Whitney, A. R., and Clark, T. A. (1973). Astrophys. J. **186,** 801.
Ryle, M., and Elsmore, B. (1973). Mon. Not. R. Astron. Soc. **164,** 223.
Shapiro, I. I., Robertson, D. S., Knight, C. A., Counselman, C. C., III, Rogers, A. E. E., Hinteregger, H. F., Lippincott, S., Whitney, A. R., Clark, T. A., Niell, A. E., and Spitzmesser, D. J. (1974). Science **186,** 920.
Whitney, A. R., Rogers, A. E. E., Hinteregger, H. F., Knight, C. A., Levine, J. I., Lippincott, S., Clark, T. A., Shapiro, I. I., and Robertson, D. S. (1976). Radio Sci. **11,** 421.
Wittels, J. J., Knight, C. A., Shapiro, I. I., Hinteregger, H. F., Rogers, A. E. E., Whitney, A. R., Clark, T. A., Hutton, L. K., Marandino, G. E., Niell, A. E., Rönnäng, B. O., Rydbeck, O. E. H., Klemperer, W. K., and Warnock, W. W. (1975). Astrophys. J. **196,** 13.

1622 PROCEEDINGS OF THE IEEE, VOL. 65, NO. 11, NOVEMBER 1977

VLBI Clock Synchronization

C. C. COUNSELMAN, III, I. I. SHAPIRO, A. E. E. ROGERS, H. F. HINTEREGGER, C. A. KNIGHT, A. R. WHITNEY, AND T. A. CLARK

***Abstract*—Atomic clocks at widely separated sites can be synchronized to within several nanoseconds from a few minutes of very-long-baseline interferometry (VLBI) observations, and to within one nanosecond from several hours of such observations.**

Introduction

The use of satellites for the accurate synchronization of remote clocks has been reviewed recently by Easton *et al.* [1]. We wish to call attention to a ground-based passive radio technique—very-long-baseline interferometry (VLBI)—capable of at least equal accuracy.

Technique

Time and frequency comparisons between widely-separated sites can be accomplished by VLBI through simultaneous observations at these sites of compact extragalactic radio sources. The signals received

Manuscript received May 26, 1977. The experiments described in this paper were supported by the National Science Foundation under Grant EAR76-22615, the Advanced Research Projects Agency under Contract 23601-71-0092 Mod 2, the United States Geological Survey under Contract 14-08-001-14148, and the National Aeronautics and Space Administration under Contract NAS5-22843 and Grant NGR22-009-839. The Haystack Observatory is partially supported by the National Science Foundation under Grant GP-25865.

C. C. Counselman, III, and I. I. Shapiro are with Massachusetts Institute of Technology, Cambridge, MA 02139.

A. E. E. Rogers, H. F. Hinteregger, C. A. Knight, and A. R. Whitney are with the Haystack Observatory, Westford, MA 01886.

T. A. Clark is with the Goddard Space Flight Center, Greenbelt, MD 20771.

are converted at each site to low frequencies, sampled, and, in present systems, recorded on magnetic tape, with the frequency-conversion and the sampling being governed by an atomic clock [2].

The tapes are brought together and each pair, from the observations of a given source, is cross-correlated to estimate the difference, and its rate of change, between the times indicated by the clocks at the two sites at the instants the same signal was received. A set of these delay and delay-rate estimates from observations of several sources is analyzed to determine the relative positions of the receiving antennas, the directions to the sources, the rotation of the earth, and the epoch and rate differences between the clocks.

The results for epoch differences obtained from our many transcontinental and intercontinental VLBI experiments have been only nominal because we never measured the approximately constant delays suffered by the signals in passing through the antennas, receivers, and recording systems. Differences between these delays at any two sites were thus indistinguishable from clock epoch differences and were lumped in with these in the analyses. (The "absolute" accuracy of our results for rate differences, on the other hand, has been limited primarily by the instabilities of the atomic clocks.) Recently we developed a system for measuring directly and continuously, and to within a few picoseconds, the delay between the output of the antenna's feed and the site clock [2]. The remainder of the system delay, associated with the antenna feed and reflector geometry, is stable and can be either measured or calculated with subnanosecond accuracy. Alternatively, with a transportable antenna and receiver system, one could perform a separate short-baseline experiment at each site to determine once and for all the differences between the antenna and feed delays at the various sites [3]. With these system delays calibrated, VLBI can be used to synchronize clocks.

If several-nanosecond accuracy is desired, then a few minutes of VLBI observations, and an equal length of time for analysis, are sufficient provided antenna positions and source directions have been determined previously. Tape transportation requirements delay the result for up to several days; however, in an operational system, results could be obtained almost immediately by the use of telecommunications links to relay the necessary data–about 10^8 bits. To obtain subnanosecond accuracy in synchronization by VLBI, a few hours of observation are needed, primarily because the variations in the earth's rotation must then be estimated simultaneously with the clock-synchronization parameters [4].

Experiments

The potential accuracy of VLBI for clock epoch and rate comparisons is demonstrated by results from long- and short-baseline experiments. To show the accuracy obtainable from a few minutes of observations on a long baseline, we considered the set of nearly 200 delay estimates, each obtained from a single pair of 3-min tape recordings that we made simultaneously at the Haystack antenna in Massachusetts and the Goldstone antenna in California during 24 h on the 29th and 30th of August, 1972 [4]. These estimates were compared with predictions based solely on our other knowledge of antenna positions, source directions, etc. The differences scattered by 2 ns (rms) about a straight line; the intercept and slope correspond, respectively, to the epoch and average rate differences between the hydrogen-maser clocks that were used at these sites. This rms scatter indicates the accuracy in epoch synchronization achievable with only a few minutes of data.

To show the improved accuracy obtainable with a few hours of data, we divided the data from this experiment into two, disjoint, 12-h sets. From each set separately we estimated two earth-rotation parameters, the clock epoch difference at the "boundary" time, and the average clock rate difference over the respective 12-h period. The epoch estimates differed by 0.7 ± 0.8 ns, and the rate estimates by $(1.1 \pm 0.3) \times 10^{-13}$. The latter result is about at the level of stability then achieved by the hydrogen masers. The uncertainties quoted in both cases are formal standard deviations.

The epoch offset results from these long baseline experiments are only relative due to the lack of system delay calibration, discussed above. To demonstrate *absolute* epoch synchronization we conducted an experiment in February 1977 between two Haystack Observatory antennas 1.24 km apart. Here we measured the delay between the output of each antenna's feed and the hydrogen maser clock and calculated from the physical dimensions the additional delay associated with each antenna's feed and reflectors. For epoch comparison, three observations were made of the radio source 3C 273B, with the direction to this source and the relative positions of the antennas having been determined in previous experiments [3]. A portable rubidium clock, carried three times between the sites, provided an independent external determination of the epoch offset. The difference between the means of the VLBI and the traveling-clock results was 9 ± 11 ns, about 10 ns of the estimated uncertainty being associated with the rubidium clock. A more definitive test of epoch synchronization capability, with a portable clock of much better stability, is obviously desired. Nevertheless, the result of this experiment, coupled with our transcontinental-baseline results, indicates that VLBI can be used to synchronize clocks over distances of several thousand kilometers with errors at the nanosecond level. Further, we know of no reason why the uncertainty could not be reduced to the tenth-nanosecond level [5]. Two points should be emphasized: (i) The clocks need not be hydrogen masers, although, of course, the accuracy of the synchronization will be limited by the stability of the standards used; and (ii) The clocks need not be nearly synchronized *ab initio*; the VLBI method can be used with the clocks many seconds from synchronization with the only penalty being a small increase in the data-processing time.

References

[1] R. L. Easton *et al.*, "Dissemination of time and frequency by satellite," *Proc. IEEE*, vol. 64, pp. 1482–1493, 1976.
[2] A. R. Whitney *et al.*, "A very-long-baseline interferometer system for geodetic applications," *Radio Science*, vol. 11, pp. 431–432, 1976.
[3] A. E. E. Rogers *et al.*, "Geodesy by radio interferometry: determination of a 1.24-km baseline vector with ~5-mm repeatability," *J. Geophys. Res.*, 1977, in press.
[4] I. I. Shapiro *et al.*, "Transcontinental baselines and the rotation of the earth measured by radio interferometry," *Science*, vol. 186, pp. 920–922, 1974; and vol. 191, p. 451, 1976.
[5] C. C. Counselman, III, "Radio astrometry," *Ann. Rev. Astron. Astrophys.*, vol. 14, pp. 197–214, 1976.

VOL. 83, NO. B1 JOURNAL OF GEOPHYSICAL RESEARCH JANUARY 10, 1978

Geodesy by Radio Interferometry: Determination of a 1.24-km Base Line Vector With ~5-mm Repeatability

A. E. E. ROGERS, C. A. KNIGHT, H. F. HINTEREGGER, AND A. R. WHITNEY

Northeast Radio Observatory Corporation, Haystack Observatory, Westford, Massachusetts 01886

C. C. COUNSELMAN III, I. I. SHAPIRO,[1] AND S. A. GOUREVITCH

Department of Earth and Planetary Sciences, Massachusetts Institute of Technology Cambridge, Massachusetts 02139

T. A. CLARK

Goddard Space Flight Center, Greenbelt, Maryland 20771

The 1.24-km base line vector between the two antennas of the Haystack Observatory was determined from X band radio interferometric observations of extragalactic sources via a new method that utilizes the precision inherent in fringe phase measurements. This method was employed in 11 separate experiments distributed between October 1974 and January 1976, each being between about 5 and 20 hours in duration. The rms scatters about the means for the vertical and the two horizontal components of the base line obtained from the 11 independent determinations were 7, 5, and 3 mm, respectively. The corresponding scatter for the base line length was 3 mm; the mean differed from the result obtained in a conventional survey by 8 mm, well within the 20-mm uncertainty of the survey. (The determination of the direction from the survey was too crude to be useful.) Another external check on our data was possible, since the azimuth and elevation axes of one of the antennas do not intersect but are separated by 318 mm. We estimated this horizontal offset from the radio interferometry data and found a difference of 10 ± 9 mm from the directly measured value, the relatively large rms scatter being due to the ~0.96 correlation between the estimate of this offset and that of the vertical component of the base line. Use of a newly completed calibration system in future experiments should allow the scatter to be reduced to the millimeter level in all coordinates for short base lines. For long base lines, such repeatability should be degraded only to about the centimeter level if calibrated observations with sufficient sensitivity are made simultaneously at two frequency bands. An assessment of the accuracy of either our present or future base line results awaits the availability of an accepted, more accurate, standard for comparison. Nonetheless, base line changes can be determined reliably at any established level of repeatability.

1. INTRODUCTION

The technique of very long base line interferometry (VLBI) has been under development for several years to enable vector base lines to be determined between arbitrary points on the earth's crust from observations of extragalactic radio sources [*Shapiro and Knight*, 1970; *Hinteregger et al.*, 1971, 1972; *Shapiro et al.*, 1974; *Thomas et al.*, 1976; *Ong et al.*, 1976]. A major goal of this continuing effort is to reduce the uncertainty in such determinations to the millimeter level for short base lines and to the centimeter level for intercontinental base lines, the observations extending over about 8 hours or somewhat less in each case. We have recently used radio interferometry to determine, in 11 separate experiments, the rather short 1.24-km base line between the Haystack and Westford antennas of the Haystack Observatory in Westford, Massachusetts. Our purpose was twofold: (1) to demonstrate the effectiveness of a new method that we developed to use measurements of group delays (see, for example, *Shapiro* [1976]) to eliminate the '2π' ambiguities in the far more precise measurements of phase delays, so that the latter could be employed for the determination of the base line and (2) to separate, to a high degree, the purely instrumental contributions to the errors in the base line estimates from all other contributions, such as those caused by inadequacies in our model of the propagation medium.

2. DESCRIPTION OF EXPERIMENTS

In Table 1 we show the relevant parameters of the antennas and receivers used. The remainder of the interferometer system was the same as is described by *Whitney et al.* [1976]. At Haystack the X band ($f \simeq 7850$ MHz) signals received from the extragalactic radio sources were converted to base band (0–360 kHz), clipped, sampled, and recorded digitally on magnetic tape. The same procedure was followed at Westford except that the intermediate frequency signals were carried by a sufficiently stable cable to Haystack, where, solely for convenience, the final operations on the signals were performed. The local oscillators used in the frequency conversions were switched over about a 100-MHz range in order to obtain adequate group delay resolution. The group and the phase delays through each receiving system were monitored continuously by injecting a low-level calibration signal, derived directly from the local frequency standard, into the receiver 'front end.' Unfortunately, cable measurement systems to monitor the variations in the delays of the calibration signals incurred between the frequency standards on the ground and the receiver front ends on the antennas were not available for these experiments. These variations were due to a combination of flexure and temperature effects. Although each type of effect can introduce variations of about 1 cm in electrical path length, the cables on the antennas often suffer rapid flexure

[1] Also at the Department of Physics, Massachusetts Institute of Technology, Cambridge, Massachusetts 02139.

Paper number 7B0850.
0148-0227/78/017B-0850$03.00

TABLE 1. Antenna and Receiver Characteristics

Antenna	Diameter, m	Effective Aperture, m²	Mount	Receiver System Noise Temperature, °K
Haystack	37	500	intersecting azimuth and elevation axes	≈75
Westford	18	125	elevation axis offset from azimuth axis	≈200

effects, associated with changes in pointing, whereas the remaining, longer cables undergo slower changes in electrical length due primarily to temperature variations.

The frequency standard used at Haystack was the NASA Goddard Space Flight Center NP-3 hydrogen maser; at Westford the Smithsonian Astrophysical Observatory VLG-10-P2 hydrogen maser standard was used. The sensitivities of these differently designed standards to pressure, temperature, and magnetic field variations were measured in separate experiments [*Whitney et al.*, 1975]. Under the conditions of our experiments and for the relevant time intervals of about 10^3 to 3×10^4 s (see below) the relative frequency stabilities of the two standards were typically of the order of 1 part in 10^{13}. Of the total of 11 Haystack-Westford interferometry experiments performed, 5 utilized these two independent frequency standards. Unfortunately, owing to an equipment limitation, which has since been removed, it was not possible to compare directly the relative behavior of the two standards in a useful manner during these experiments. In six of the last seven experiments the local oscillator signals for the receiver systems at both sites were derived from a single hydrogen maser standard, in part to provide a comparison and in part because only one standard was available for the last few experiments. These six experiments in some ways resemble conventional radio interferometric experiments. However, the cables used in conventional interferometry to convey the signals from the single standard to the interferometer elements are usually substantially better stabilized than was possible for our experiments. In our case the variations in the electrical path length of the cables served, in effect, to reduce the relative stability of the 'standards' at the two sites to the order of 1 part in 10^{14} over the relevant time intervals, which were always less than 1 day. In this sense then, all 11 experiments were performed with independent standards, the relative frequency stability, however, being about an order of magnitude greater for the experiments that involved only a single hydrogen maser. The relative frequency stability achieved in the latter experiments—about 1 part in 10^{14}—is, of course, the level of performance to be expected from the use of separate state-of-the-art hydrogen maser standards under controlled environmental conditions; we expect that such performance will indeed be obtained with the use of separate standards in future VLBI experiments.

In the present interferometry experiments, observations, each of 3-min duration, were made alternately of a number of extragalactic radio sources (Table 2). Different, but not disjoint, sets of sources were observed in the different experiments, and the schedules of the observations for the common sources differed from one experiment to the next. In each experiment the spacing between observations varied from 10 to 15 min. The signals received at the two antennas were recorded at Haystack on separate magnetic tapes, which were then immediately cross-correlated to determine the group delay, the (ambiguous) phase delay, and the phase delay rate. The processing for each observation was thus completed before the next observation began, and the performance of the interferometer was monitored in 'real time,' the required number of magnetic tapes being reduced to two. A description of the processing algorithms employed is given by *Whitney* [1974] and *Whitney et al.* [1976].

3. Data Analysis

The analysis of the group and phase delays and of the phase delay rates was carried out in two stages: preliminary and final. The preliminary stage was designed to enable the 2π ambiguity in each phase delay measurement to be removed. This goal was itself reached in two steps. In the first step the

TABLE 2. Coordinates of Observed Extragalactic Radio Sources

Source	Right Ascension (1950.0)			Declination (1950.0)			Experiment*
	Hours	Minutes	Seconds	Degrees	Minutes	Seconds	
3C 84	3	16	29.55	41	19	51.6	all
NRAO 150	3	55	45.23	50	49	20.0	all but 5
3C 120	4	30	31.59	5	14	59.5	all but 4 and 5
OJ 287	8	51	57.23	20	17	58.4	1
4C 39.25	9	23	55.30	39	15	23.7	all but 5, 6, and 10
3C 273B	12	26	33.25	2	19	43.3	all but 1, 5, 6, and 10
3C 345	16	41	17.63	39	54	11.0	all
PKS 2134+00	21	34	5.23	0	28	25.0	1, 2, 5, 8, 9, and 10
VRO 42.22.01	22	0	39.39	42	2	8.4	1, 2, and 8
3C 454.3	22	51	29.53	15	52	54.2	all but 3 and 4

See *Rogers et al.* [1973] and *Clark et al.* [1976].

*The entries in this column give the numbers of the experiments, ordered chronologically (see Table 3), in which the source in the corresponding row was observed. 'All' signifies that the source was observed in all experiments; 'all but *n* and *m*' indicates that the source was observed in every experiment except the *n*th and *m*th.

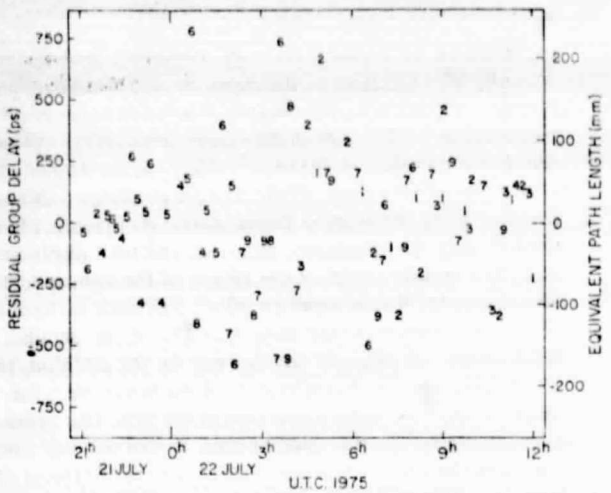

Fig. 1. Postfit residuals from the analysis of the (crude) group delay measurements from a typical experiment. The numbers refer to the observed sources in order of increasing right ascension (see Table 2).

group delays and the (less important) phase delay rates were analyzed by weighted least squares to obtain estimates of five relevant parameters for each experiment: the three components of the base line vector and the two coefficients representing the differences in the epoch and rate settings of the independent frequency standards that also served as clocks, or time standards, at the two sites. For the experiments that utilized a single frequency standard, epoch and rate parameters were still utilized because of the unknown differences and variations in the electrical path lengths from the standard to the two antennas, as was discussed in section 2. We will therefore refer hereafter to differences in clock behavior even for those experiments in which only a single frequency standard was involved.

The uncertainties in the measured group delays ranged from about 0.1 to 0.6 ns, primarily because of the limited signal-to-noise ratios available with this system. For the stronger of the extragalactic radio sources observed, there was also a substantial fractional contribution to the error from instrumental effects, due principally to the aforementioned lack of measurement of the variations in the electrical path lengths of the cables. Postfit group delay residuals from a typical experiment are shown in Figure 1.

The theoretical values for the group delays, based on the parameter estimates obtained in the weighted least squares analysis of the measured group delays for each experiment, had smaller uncertainties as a result of averaging. These uncertainties were of the order of 0.15 ns ($\simeq$ 4.5 cm), equivalent to a phase uncertainty of somewhat more than 2π radians for the 3.8-cm wavelength of the radio observations. (Recall that phase delay is related to phase via multiplication of the former by the (angular) radio frequency of the observations.) The difference between the group delay and the phase delay, due to the dispersive nature of the ionosphere and other plasma between source and antenna, appears to be negligible (see section 5) for these Haystack-Westford interferometric measurements because only the very small differences between the integrated plasma densities along the lines of sight from the source to the two antennas contribute to the two delay observables.

Despite the relative crudity of the group delay solutions it proved possible to use them, in the second step of the preliminary stage of the analysis, to eliminate the 2π ambiguities in the phase delays for each experiment separately. We describe the procedure used, first qualitatively and then quantitatively (see also *Reisz et al.* [1973]). We defined a suitable, albeit ad hoc, function of the inherently ambiguous phase measurements and of their theoretical values determined from the group delay solution. We then varied the estimate of the base line vector, upon which the theoretical values of the phases depend, until a maximum of this function was attained. (However, we did not vary the 'clock' parameters about the values obtained from the group delay solution because the function was insensitive to these parameters, as is explained below.) The value of the base line vector that yielded the maximum of the ad hoc function was then used in a straightforward manner to add to the measured phases the appropriate integer multiples of 2π so as to remove the ambiguities present in the original phase observables; the conversion to phase delays followed trivially. We note that this procedure does not necessarily remove an overall constant delay that would be the same for all observations in a given experiment; however, such a constant is wholly absorbed in the estimate of the epoch offset and has no effect on base line determination.

The specific function that we maximized was

$$f(\mathbf{B}) \equiv \sum_{i=2}^{N-1} w_i \cos(\rho_i - \mu_i) \tag{1}$$

the weighted sum of the cosines of the differences between the residual phases ρ_i, defined below, and the corresponding 'mean' values μ_i, obtained by linear interpolation in time between the phasors corresponding to the residual phases for the immediately preceding and following observations. In particular, we have

$$\rho_i \equiv \phi_i^{\text{obs}} - \phi_i^{\text{theor}} \tag{2}$$

$$\mu_i \equiv \tan^{-1}\left[\frac{(t_{i+1} - t_i)\sin\rho_{i-1} + (t_i - t_{i-1})\sin\rho_{i+1}}{(t_{i+1} - t_i)\cos\rho_{i-1} + (t_i - t_{i-1})\cos\rho_{i+1}}\right] \tag{3}$$

where ϕ_i^{obs} is the ith of the N values of phase observed in the experiment (the first and last values contribute to f only through μ, not directly through ρ), where

$$\phi_i^{\text{theor}} = (\omega/c)\mathbf{B}_i \cdot \hat{s}_i + \phi_i^{\text{osc}} \tag{4}$$

and where ω is the (angular) radio frequency to which the observations of phase referred; c is the speed of light; $\mathbf{B}_i$ is the base line vector appropriate for the reference time t_i of the ith measurement; $\hat{s}_i$ is the unit vector in the direction toward the source observed at t_i; and ϕ_i^{osc} ($\equiv \phi^{\text{osc}}(t_i)$) is the difference between the phases of the local oscillators of the receivers at the two sites, calculated from the two-term clock polynomial whose coefficients were as determined from the group delay solution. The weights w_i used in (1) were calculated from the differences between the observation times according to

$$w_i^{-1} = (t_{i+1} - t_i)(t_i - t_{i-1}) \tag{5}$$

What are the reasons that governed these choices? The use of periodic trigonometric functions in (1) and (3) insures that the function f is insensitive to errors in ϕ_i^{obs} that are multiples of 2π. The μ_i were subtracted from the ρ_i so as to reduce the sensitivity of f to the effects of unmodeled variations in the relative behavior of the clocks at the two sites; by virtue of the interpolation used in (3) the μ_i are insensitive to any constant or linearly increasing errors that might corrupt $\phi^{\text{osc}}(t)$ between t_{i-1} and t_{i+1}. Because the μ_i are still sensitive to the next higher time derivative of the error in $\phi^{\text{osc}}(t)$, the weights w_i were

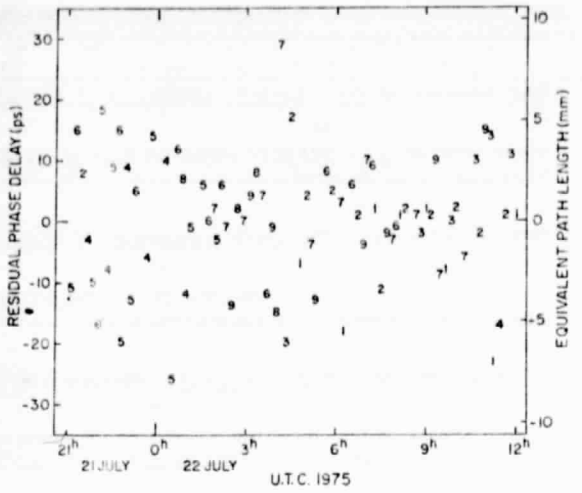

Fig. 2. Same as Figure 1 except that the analysis was of the (precise) phase delay measurements. Note the difference in scale.

chosen to vary inversely with the product of the time intervals between the neighboring observations. The effects of the uncertainties in the modulo-2π measurements of ϕ^{obs}, per se, were relatively small and hence were ignored in the choice of weights. Finally, we note that the maximization of (1) is equivalent to a minimization of the weighted sum of squares of the differences $\rho_i - \mu_i$ when these differences are small.

The maximum of f with respect to the components of B, expressed in an earth-fixed coordinate system, was actually found for each experiment through direct evaluation of f at the vertices of a three-dimensional rectangular grid. The grid spacing was approximately 3 mm (10 ps or about $\frac{1}{10}$ wavelength) in each coordinate, and the search region was centered at the base line solution obtained from the analysis of the group delays from one of the early experiments. The search extended ± 0.8 ns ($\simeq \pm 6$ wavelengths) in the direction of each of the two orthogonal equatorial components of the base line and ± 1.6 ns ($\simeq \pm 13$ wavelengths) in the direction of the polar component. The uncertainty of the group delay solution was of the order of 1 wavelength in each coordinate and thus corresponds to a small fraction of the region searched. The function f had a well-defined maximum within the search region for all experiments except the three shortest ones (two utilized independent standards, and one a common standard); in each of the latter three cases a local maximum was present in nearly the same location as it was for the other eight experiments and was taken as the 'correct' maximum to use for further analysis.

Given the value $\mathbf{B}_m$ that maximized f for a given experiment, the appropriate number of 2π to add to each measured phase was easily determined: ϕ_i^{obs} was incremented by the integer number of 2π that minimized $|\rho_i(\mathbf{B}_m)|$. The conversion of these values of phase to the equivalent values of phase delay was accomplished, as was indicated above, by division of the former by ω.

The phase delays, thus freed from ambiguity, were then utilized in the final stage of the analysis. The delays from each experiment separately were used in a uniformly weighted least squares analysis to estimate the three components of the base line vector and all the coefficients of polynomials representing the difference in behavior of the two clocks. The number and the degree of the polynomials used depended on the duration of the experiment, approximately 1 degree of freedom having been provided for each hour of observation. (For the longer experiments, up to three different polynomials were used to span the total duration of the experiment in a nonoverlapping manner so that the highest degree of any one polynomial used was equal to 5.) The theoretical values of the delays utilized (1) the source coordinates listed in Table 2, as mentioned above, (2) the smoothed values of UT1 and polar motion published in Circular D by the Bureau International de l'Heure, (3) standard models for precession, nutation, and tidal displacement, and (4) a simple model of the effects of the atmosphere that also accounted for the small ($\simeq 30$ m) difference in the altitude of the two antennas (see *Robertson* [1975] for details). The results were not changed significantly by the addition, to the set of parameters to be estimated, of the zenith electrical path length of the atmosphere over one of the sites. Our results are also insensitive to the uncertainties in the models used to represent the earth's motions because of the shortness of the base line. Figure 2 shows the postfit residuals from a typical experiment (see Figure 1 for contrast); the rms of these residuals, about 10 ps, is equivalent to about 3 mm in distance.

Before discussing in detail the base line results from this second stage of the analysis, we remark that they did not differ by more than 5 mm in any coordinate for any experiment from the results obtained in the preliminary analysis. The differences stem in part from the use of more terms in the polynomials representing the differences in clock behavior and in part from the use of a more sophisticated model to represent the theoretical values of the delays.

4. Results

In Table 3 we present the final results of our analysis. The estimates of the base line coordinates from the different experiments are scattered by more than one would expect on the basis of the formal standard errors, a demonstration that the uncertainties in our results are dominated by systematic errors. Nevertheless, in computing the means and the scatters about these means we used as relative weights for the individual results the inverse squares of the formal standard errors obtained from the individual solutions. This choice was made primarily so that the weights would reflect, at least qualitatively, the sometimes very important differences in the relative reliabilities of the results from the different experiments; these differences are due mostly to the large variations in the number of observations and in the durations of the experiments. Although the weighted means and those computed with uniform weightings do not differ substantially, the root weighted mean scatters about the weighted means (hereafter 'rms scatters') were smaller than the corresponding scatters computed with uniform weighting by an average of about 30%, a result thus tending to support our use of formal weights. With this weighting the rms scatters for the vertical, the east, and the north components of the base line were, in fact, 7, 5, and 3 mm, respectively.

In Table 3 we also give the weighted means and rms scatters separately for the experiments in which two frequency standards were used ('unstarred' experiments) and for those that employed a single standard ('starred' experiments). The coordinates of the Westford site, as well as the distance between Haystack and Westford inferred from each experiment, are displayed graphically in Figure 3. The scatters in the results from the unstarred experiments range from about $1\frac{1}{2}$ to 2 times as large as the corresponding scatters from the starred experiments, except for the scatters of the longitude estimates, for which the unstarred experiments yielded an anomalously small spread. That the ratios of the corresponding scatters from the unstarred to those from the starred experiments are far less

TABLE 3. Summary of Haystack-Westford VLBI Experiments

Date[a]	Experiment Duration, hours	Number of Observations[c]	Westford Geocentric Coordinates[b]			Distance From Haystack,[e] mm	Root-Mean-Square of Postfit Residuals,[f] ps	Axis Offset,[g] mm
			Radius, mm	Longitude,[d] 10^{-8} °	Latitude,[d] 10^{-8} °			
Oct. 23, 1974	10.5	53	73.1 ± 4.2	3.6 ± 1.8	73.6 ± 2.2	81.3 ± 2.3	18	332 ± 13
Nov. 6, 1974	19.3	70	63.2 ± 2.2	6.3 ± 1.0	64.0 ± 1.2	92.1 ± 1.3	11	312 ± 6
Jan. 14, 1975	12.3	40	78.8 ± 4.1	3.4 ± 1.9	66.9 ± 1.8	88.4 ± 2.1	12	296 ± 13
Jan. 19, 1975	6.6	32	86.6 ± 2.9	4.0 ± 1.4	68.8 ± 1.2	86.1 ± 1.3	8	300 ± 14
Jan. 30, 1975*	7.0	22	72.6 ± 2.7	2.1 ± 1.2	63.4 ± 2.0	91.2 ± 2.2	7	286 ± 21
June 14, 1975	4.9	28	85.4 ± 7.0	6.0 ± 2.9	63.1 ± 3.6	92.3 ± 4.0	18	336 ± 23
July 11, 1975*	14.0	59	88.5 ± 2.5	3.8 ± 0.9	62.2 ± 1.1	92.6 ± 1.1	9	269 ± 12
July 21, 1975*	15.0	80	87.0 ± 1.9	9.9 ± 0.9	61.7 ± 0.8	94.9 ± 0.8	10	312 ± 6
Oct. 4, 1975*	19.5	93	73.0 ± 2.0	14.6 ± 0.9	59.5 ± 0.9	99.2 ± 1.0	11	307 ± 6
Jan. 15, 1976*	8.0	44	70.7 ± 1.6	18.7 ± 0.6	65.0 ± 0.7	94.4 ± 0.7	6	308 ± 6
Jan. 16, 1976*	13.0	66	73.5 ± 1.1	17.7 ± 0.5	64.9 ± 0.5	94.7 ± 0.5	5	307 ± 3
Weighted mean ± rms (unstarred only)[h]			73.4 ± 10.1	5.0 ± 1.3	67.1 ± 3.1	88.2 ± 3.6		312 ± 11
Weighted mean ± rms (starred only)			75.9 ± 6.2	14.2 ± 5.7	63.5 ± 2.0	94.9 ± 1.7		306 ± 8
Weighted mean ± rms (all)			75.4 ± 7.1	12.7 ± 6.3	64.1 ± 2.6	93.9 ± 3.1		307 ± 9
Survey[i]—VLBI (all)			10 ± 30	−157 ± 170	42 ± 70	−8 ± 20		10 ± 9

The standard errors given are based on scaling the (dimensionless) root-mean-square of the postfit residuals to unity.

[a]The geocentric position assumed for the Haystack antenna was the following: radius, 6,368,488480 km; longitude, 71.488650300°; latitude, 42.429358300°. The base line vector extends from the intersection of the azimuth and elevation axes at Haystack to a reference point on the azimuth axis at Westford that is offset horizontally by 318 mm from the elevation axis (see text). Values of radius, longitude, and latitude given in these columns should be added to 6,368,462,400 mm, 71.49428300°, and 42.41901400°, respectively.

[b]On the starred dates the Westford local oscillator signal was derived from the same hydrogen maser frequency standard as was that of Haystack, by means of cables, such that the relative frequency stability between the local oscillators of the two sites was ~1 part in 10^{14}. On the remaining dates, independent frequency standards were used at the two sites, the resulting relative local oscillator stability being ~1 part in 10^{13} (see text).

[c]Each observation consisted of a 3-min tape recording of the signal received from one of the extragalactic radio sources listed in Table 2. The signals received at the two sites were recorded simultaneously on separate tapes which were then cross-correlated to determine the interferometric observables.

[d]For this base line, 10^{-8} ° in longitude corresponds to ~0.82 mm of westward displacement, and 10^{-8} ° in latitude to ~1.11 mm of northward displacement.

[e]Values in this column should be added to 1,239,300 mm.

[f]10 ps = 3 mm; c = 299,792.5 km/s.

[g]The Westford axis offsets were estimated in separate solutions from those for which the Westford coordinate estimates are shown. Adding this axis offset parameter yielded slightly reduced residuals, the relatively large formal standard errors shown being attributable to the high correlation (~0.96) between the estimate of the axis offset and that of the vertical component of the base line vector.

[h]The weights used in the computations of the means were inversely proportional to the squared formal standard errors of the individual results; the rms given in each case refers to the scatter of the individual results about the mean and does not represent the formal standard error of the mean.

[i]The survey was performed in 1967 by R. Pressey, Inc. (see text for discussion of the uncertainties).

than the ratio of the corresponding instabilities of the standards implies that frequency variations are not the predominant source of error, as is discussed in more detail in section 5.

For the ensemble, unstarred plus starred, we note that of the three coordinates of the Westford site, only the estimates of longitude seem to show a systematic trend with time. We deem it premature to attempt to attribute any physical significance to this apparent trend.

The above results indicate the repeatability of our base line determinations. We purposely sought in these experiments to vary as many parameters as possible to expose potential sources of error; thus from experiment to experiment we varied the sources observed, the pattern in which they were observed, the spanned bandwidth, and the times of the day and of the year in which the observations were made. Nonetheless, we do not and cannot claim that the level of repeatability signifies accuracy. To establish the accuracy of our mean base line results definitively requires, mostly by definition, an accepted (and of course more accurate) standard of comparison. In our case none exists. Nonetheless, some useful external checks can be made. As the first example we note that a conventional survey was carried out in 1967 by R. Pressey, Inc., of Lynn, Massachusetts. The original intent of the survey was to provide only the length of the base line; for this purpose a geodimeter was used, and the estimated uncertainty in the length so determined was 20 mm. The comparison with our mean result, given in Table 3, shows a difference of only 8 mm. The survey values for the two components of direction of the base line may have been far less reliable. R. Pressey (private communication, 1967) indicates that an error of almost 30 arc sec may have been made in azimuth, corresponding to an equivalent distance uncertainty of about 180 mm, again larger than the difference between our results and the 1967 survey. The uncertainty in the determination of the direction of the vertical in the survey was unavailable from Pressey and was estimated by us to be about 5 arc sec, leading to a 30-mm uncertainty in radius, which is threefold larger than the difference between the interferometer and the survey results. We investigated the possibility of having a more accurate survey undertaken such that the uncertainties in the resultant base line components would be at the millimeter level. Unfortunately, the estimated cost was prohibitive, nearly $40,000.

Another check on the interferometer results was possible because at Westford, as distinct from Haystack, the azimuth and elevation axes do not intersect. The elevation axis, accord-

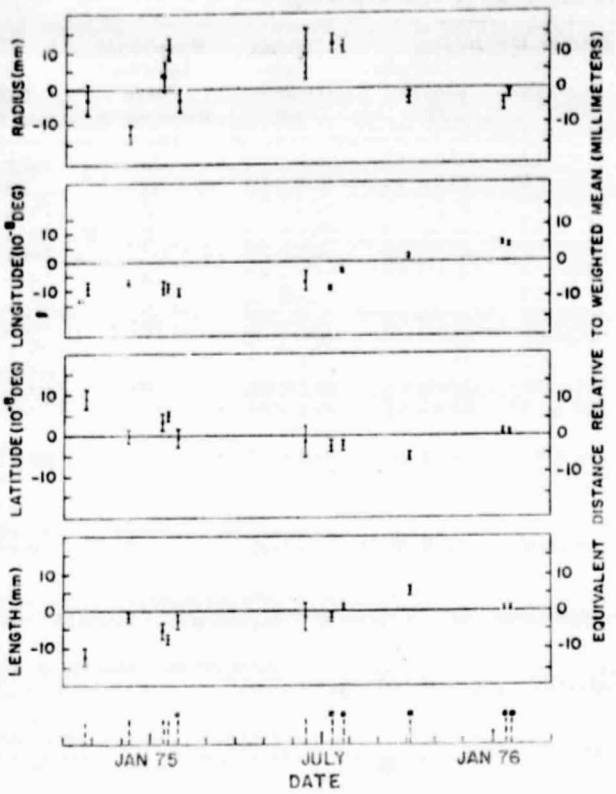

Fig. 3. Westford coordinates and base line lengths from 11 independent determinations by radio interferometry of the 1.24-km Haystack-Westford base line vector. The results are shown relative to their corresponding means as given in Table 3 for the ensemble of experiments. The error bars denote 1 (formal) standard deviation. The starred dates indicate that a single frequency standard was used; see text and Table 3 for more details.

ing to the construction blueprints for the antenna mount, is offset horizontally by 318 mm from the base line reference point on the azimuth axis. We therefore included in our theoretical model of the phase delay observable a parameter characterizing the length of this offset. The data for each experiment were reanalyzed with this length as an added unknown parameter; the results are shown in the last column of Table 3. The difference between the directly measured value and the weighted mean of the estimated values is 10 ± 9 mm, the relatively large uncertainty being due principally to the -0.96 correlation between our estimates of this offset and of the vertical component of the base line vector. The estimates of the base line components did not change significantly with the addition of the elevation axis offset parameter, although, of course, the uncertainties increased markedly.

5. Discussion of Errors

What are the important sources of error in our results and how might they be reduced? We devote this section to addressing this two-part question.

One potential source of error stems from the use of radio source coordinates (Table 2) obtained from long base line experiments. These positions are not necessarily appropriate for the short base lines employed here: many of the sources exhibit structure in their radio brightness on a variety of scales; our short base line interferometer is sensitive to the arc second structure, whereas the very long base line interferometers were sensitive mainly to the milli arc second structure. As Table 2 shows, we did not observe all of the same sources in each experiment; neither did we observe those common sources for the same fractions of their diurnal cycles in different experiments. Thus source structure effects could have contributed to the scatter of our base line results. By the same token, errors due to source structure would be reduced, by virtue of averaging, in our mean results. We sought evidence of sytematic source structure effects through comparison of the postfit phase delay residuals from several of these experiments, and also through possible correlations between the sources observed and the base line results, without success. We therefore doubt that our mean results were biased by more than 2 mm in any coordinate from this cause (see also section 6). In the future we can reduce this type of error further by extending the observations in an individual experiment over a longer period in order to (1) make accurate independent determinations of the appropriate short base line source positions simultaneously with the determination of the base line vector and (2) study the structure of the sources from analysis of the fringe amplitude data as we have done in experiments involving longer base lines. Unfortunately, antenna-scheduling constraints prevented us from utilizing these techniques in the present experiments. We also remark, in regard to source structure, that milli-arc-second-sized features in the brightness distribution can change noticeably in apparent position over time scales as short as weeks but that time scales for corresponding changes in arc-second-sized features are expected to be about 1000 times longer. Thus if repeatability, not accuracy, is the goal, observation of the same sources at the same (sidereal) times in the separate experiments will ensure that source position errors make no appreciable contribution to the scatter of the short base line results.

The propagation medium also contributes to the uncertainty in our results. However, as was expected (see section 3), this contribution seems to have been below the level of observability. The contributions of the ionosphere should be perhaps tenfold greater in the daytime, especially near dawn and dusk, than at night; yet no significant differences are seen in the behavior of the delay residuals for the corresponding parts of the diurnal cycle. Similarly, no seasonal pattern is discernible in the delay residuals, although variations in the water vapor contributions of the neutral atmosphere, the main atmospheric error source, are expected to be most pronounced in the summer (see, for example, *Moran and Penfield* [1976]). In addition, as we mentioned in section 3, our base line results are not changed significantly when the zenith electrical path length of the atmosphere is added to the set of parameters to be estimated. If it is desired in future experiments, the contributions of the ionosphere could be reduced further by simultaneous observations in two widely separated frequency bands, whereas the contributions of the neutral atmosphere may perhaps be reduced further through the use of water vapor radiometry. (See section 6.)

The possibility of systematic errors due to undesired wave reflections ('multipath') within the antennas and associated structures has been explored in several ways. On the basis of an analysis of other measurements made on the Haystack antenna, we estimate that multipath effects on our results are below the millimeter level. Further evidence that these effects are negligible in the present experiments is provided by the facts (1) that the base line vector estimates derived from the group delay data did not differ significantly from those derived from the phase delays and (2) that neither the group delay nor the phase delay results showed significant changes when the

local oscillator frequency switching range (see section 2) was changed from 78 to 112 MHz.

Changes in the physical dimensions of the antennas with changes in the thermal environments and with changes in pointing are potential sources of perhaps relatively large systematic errors in our results. Such dimensional changes are important only insofar as they change the electrical path length between the radio source and a fixed point at a site. We discuss thermal effects first. These would probably not have introduced errors that repeated from experiment to experiment, since our 11 experiments were distributed reasonably well throughout both diurnal and seasonal cycles. Any uniform heating effects probably could be modeled accurately, if it were necessary, for future experiments. Differential heating effects, by contrast, are difficult to model, but because both the Haystack and Westford antennas are enclosed in radomes, temperature differences over the antenna structures can be kept relatively small.

Changes in elevation angle introduce changes in the dimensions of an antenna because of the changes in the gravitational loading. Such dimensional changes are expected to be repeatable, at least down to the millimeter level. Hence the error in the estimate of a base line vector caused by such gravitational 'flexures' would to this extent be the same for different experiments if the schedule of observations were kept constant. If the schedule were varied, then this error could vary, depending both on the schedule and on the variation with elevation angle of the length of the electrical path through the antenna system. For example, if this variation were exactly proportional to the sine of the elevation angle, then the variation in the path length would mimic exactly the effect of a vertical displacement of the antenna.

What are the actual variations with elevation angle of the path lengths for the Haystack and the Westford antennas? The only information that we presently have is a set of direct measurements (D. Stuart, private communication, 1976) of the variation of the distance D between the vertices of the main reflector and the Cassegrain subreflector of the Haystack antenna as a function of elevation angle h at 10° intervals between 0° and 90°. Over this range the measured variation differs by less than the estimated peak measurement uncertainty of 0.05 mm from that given by the formula

$$D(h) - D(0) = -1.27 \sin h \quad \text{mm} \tag{6}$$

The radio signal traverses this distance twice, so that the corresponding length variation for a ray path along the axis of the antenna is given by $-2.54 \sin h$ mm. If, for illustrative purposes, (6) were assumed to describe the effective path length variation for the entire antenna, the resulting systematic error in our base line determinations would then be insensitive to the observation schedule and would correspond to an apparent shift in the position of the Haystack antenna vertically upward by 2.54 mm. We must emphasize that as yet we have insufficient data on the overall gravitational flexure of the Haystack antenna, and no data for the Westford antenna, so that we are unable at present to place stringent limits on the systematic base line determination error due to flexure. If it is desired in the future, gravitational flexure effects could probably be calculated accurately from an appropriate set of direct measurements on the antennas. In any event the consequences for geodynamic applications of VLBI are expected to be negligible. Such flexures, as we have stated, are expected to be repeatable at least down to the millimeter level and, whatever is the form of their elevation angle dependences, would not significantly affect attempts to measure changes in base line vectors so long as the same pattern of observations is used in each experiment.

What experimental bounds can we place on any nonrepeatable component of the error in the base line vector estimates caused by gravitational flexure? To seek such bounds, albeit indirectly, we varied the elevation angle distributions from experiment to experiment; a typical sample of elevation angle histograms is given in Figure 4. These distributions are not as varied as one would like, to have maximized the potential contribution of gravitational flexure effects to the scatter of the base line vector estimates from the different experiments. Yet, one might reasonably conclude that the nonrepeatable component of the antenna flexure error in our mean results is most likely smaller than the rms scatter of these results.

Two other major sources of nonrepeatable error in our present results are believed to be the unmodeled and unmeasured variations in the clocks and cable lengths, respectively. To assess these effects in a manner other than noting the scatter in the coordinates determined from the separate experiments, we also analyzed the phase delay data by the so-called difference technique [*Shapiro et al.*, 1974; *Robertson*, 1975]. In this difference technique, pairs of observations of phase delays, obtained at neighboring epochs, are differenced, and the differences are analyzed with the weighted least squares algorithm. These (independent) difference observables have the

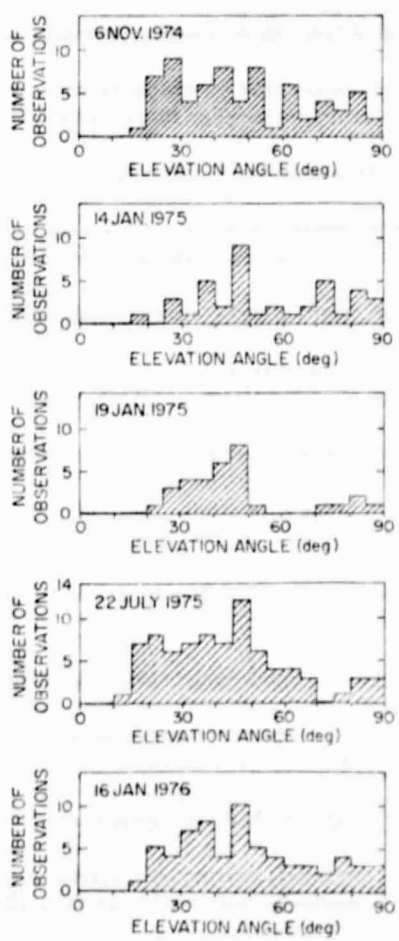

Fig. 4. Histograms of the elevation angles of the observations for several of the experiments.

advantage of being largely freed from the effects of long-term relative drifts in the frequency standards and in the cable lengths that in effect control the time-keeping at each site. As a result of using the difference observables and ignoring the corresponding sum observables, some information is lost, but we avoid the need for a large number of parameters to represent these long-term relative drifts in the effective time kept at the two sites. The base line coordinates obtained from the analysis of the differenced observables agreed with the results from the analysis of the undifferenced observables, on an experiment-by-experiment basis, to within 3 mm in all cases. We conclude from this agreement that our polynomial representation of the effective relative behavior of the clocks satisfactorily removed the long-term drifts and was virtually equivalent to the replacement of the original observables by differenced observables. By the same token, it follows that the long-term fluctuations of the standards used in the unstarred experiments (see Table 3) did not make a substantially larger contribution to the scatter of the base line determinations than did the corresponding fluctuations in the starred experiments. These conclusions are also supported by the lack of significant systematic trends in the postfit delay residuals. The short-term (between observations) fluctuations of the independent frequency standards, on the other hand, may well have contributed to the 'noise' apparent in the postfit residuals and to the fact that this noise is greater, on average, in the unstarred experiments than in the starred experiments. The uncertainties thus introduced in the base line estimates are not, however, likely to be highly correlated from experiment to experiment because of differences in observing schedule and in environmental conditions.

Although we consider it unlikely, there is a possibility that significant errors, other than those mentioned, could be introduced in the part of the system that follows the feed on the antenna. 'Zero base line' experiments can be performed to isolate any such errors by bringing the two interferometer receiving and recording systems together and feeding the same radio frequency noise into both. It is also possible to offset in delay and rate either the noise signal or the frequency standard input to one of the systems so as to simulate the major effects of the separation of the receivers in a real interferometer. Such zero base line experiments are being planned at Haystack with the instrumentation designed so that the results should enable us to uncover and to reduce to the millimeter level or below any remaining important sources of error contributed by the receiving, recording, and processing systems per se. (Some zero base line tests have already been performed at Haystack, but they did not allow for rate offsets.)

The resultant improved instrumentation and full calibration, in conjunction with hydrogen maser frequency standards that achieve fractional stabilities of ~1 part in 10^{14} over 10^3 s, should ultimately enable the combined contribution of all sources of error in the determination of short base line vectors via our interferometric technique to be reduced to the millimeter level. To place this goal in proper perspective, we note that *Elsmore and Ryle* [1976] state, albeit without provision of supporting details, that when the equatorial components of the base lines between the four fixed antennas of their 5-km linear array were determined by using conventional single-frequency-standard radio interferometry, they agreed in three separate sets of experiments to within 0.15 mm in each component. Here flexure effects were insignificant because the antennas involved were identical.

6. Other Applications

The elimination of 2π ambiguities in the phase delay observable, demonstrated here for the short Haystack-Westford base line and for an X band radio frequency (≃ 7.8 GHz), could also be accomplished in other situations. For short base lines, much lower radio frequencies could be used, provided only that ionospheric effects remained negligible; the elimination of the phase delay ambiguities would be correspondingly easier the lower the frequency. For long base lines, two types of complications arise: (1) the need to determine the contribution of the ionosphere when it affects group and phase delays by amounts not small in comparison to the delay equivalent of 1 wavelength for the radio frequency employed and (2) the need to estimate other parameters, such as those for source coordinates, in addition to those for the base line vector and for the clock behavior. To eliminate 2π ambiguities in the face of these difficulties, it is sufficient to make group delay measurements with uncertainties less than the delay equivalent of 1 wavelength and to make them simultaneously for each of two widely separated frequency bands. The next generation VLBI equipment currently being developed by our group—the Mark III system—will satisfy these criteria. This equipment will enable observations to be made with about tenfold higher signal-to-noise ratios at X band (~8 GHz) and at S band (~2 GHz) frequencies simultaneously. The major limit on accuracy for long base lines will then be due to the uncertainty in the determination of the effect of the neutral atmosphere on the delay observable. Recent studies [*Moran and Penfield*, 1976; *Winn et al.*, 1976] indicate that the use of radiometers and surface meteorological measurements to monitor the electrical path length of the water vapor in the atmosphere [*Schaper et al.*, 1970] should enable the uncertainty in the effect of the neutral atmosphere on the base line determinations to be reduced to the centimeter level.

The new VLBI equipment, in conjunction with our methods for ambiguity elimination, will also allow the measurement of any regional base lines to be made with subcentimeter accuracy. One approach is to employ, at opposite ends of a regional base line, two small transportable antennas (diameter approximately equal to 3 m) that observe sources simultaneously with a perhaps remote, but definitely large, fixed antenna (diameter greater than or approximately equal to 30 m). The large size of the fixed antenna is necessary to obtain an adequate signal-to-noise ratio (recall that this ratio is proportional to the product of the diameters of the two antennas forming each interferometer). The two base lines to the fixed antenna could be thousands of kilometers in length, and the determination of each from these observations could be uncertain at the several centimeter level. However, the short base line between the transportable antennas would be determined with much less uncertainty (~5 mm in 100 km) because, by analyzing only the differences between the simultaneous measurements made between each of them and the fixed antenna, most of the propagation medium and other undesired effects on the long base line measurements would be canceled. Differencing the interferometric phases obtained on the long base lines is equivalent to using the interferometric phase measured on the short base line, except for possible effects of source structure [see *Rogers et al.*, 1974]. As an illustration of the equivalence, we show, in Figure 5, a comparison between the phases measured directly with the Haystack-Westford baseline and those obtained from differencing the phases measured simultane-

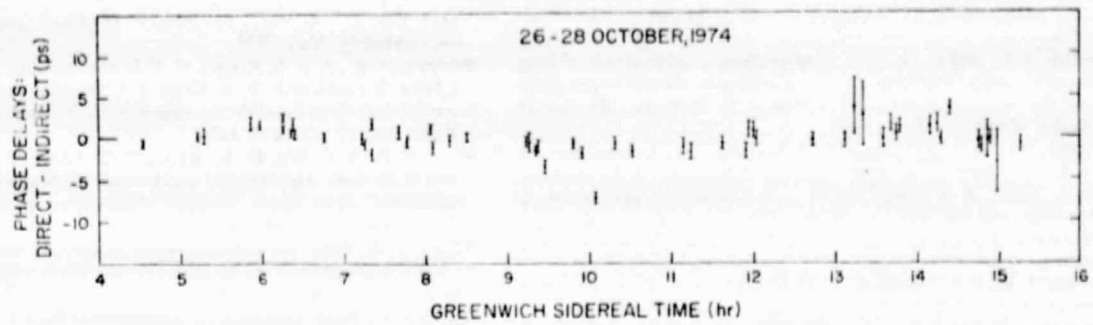

Fig. 5. Comparison of Haystack-Westford phase delays, measured directly, with those deduced from differencing the corresponding Haystack-NRAO and Westford-NRAO measurements. (See text for interpretation.)

ously with the two interferometers formed between Haystack and Westford, on the one hand, and the 845-km-distant, 43-m-diameter antenna of the National Radio Astronomy Observatory (NRAO), on the other. The source observed was 3C 84, which is well known to have a very complicated structure at the milli arc second level (see, e.g., *Rogers et al.* [1974] and *Pauliny-Toth et al.* [1976]). The comparison clearly shows that the effects of structure for this antenna configuration are very small and, if they were ignored, would cause differences of substantially less than a millimeter between the base line components determined from the short base line interferometric data and those determined from the differences of the corresponding data obtained from the two long base line interferometers. Should they ever prove important, such source structure effects could, however, be largely removed from the data through use of appropriate models of the radio brightness distribution of the sources and their variations with time. These models are being determined with ever increasing reliability from data obtained with VLBI arrays that are now being used to monitor these compact sources (see, for recent examples, *Wittels* [1975], *Cohen et al.* [1976], *Hutton* [1976], and *Wittels et al.* [1976]).

It is quite conceivable that use of this difference technique with small transportable VLBI systems could be economically as well as technically competitive with any other method available for measuring vector base lines with millimeter level accuracy, even for distances as small as a few kilometers.

Acknowledgments. We thank G. L. Epstein and L. Hazelton for their contributions to the data analysis; D. Kaufmann, H. Peters, and R. Coates of the Goddard Space Flight Center for their aid in securing the NP-3 Goddard hydrogen maser frequency standard for use at the Haystack Observatory for some of these experiments; and S. Henriksen, M. Ryle, and J. B. Thomas for their careful reading of the manuscript. Radio Astronomy programs at the Haystack Observatory are conducted with support from the National Science Foundation, grant GP-25865. The National Radio Astronomy Observatory is operated by Associated Universities, Inc., under contract with the National Science Foundation. The experiments reported here were supported in part by the United States Geological Survey, under contract 14-08-001-14148, and by the National Aeronautics and Space Administration, under contract NAS5-22843, both with the Northeast Radio Observatory Corporation. The Massachusetts Institute of Technology experimenters were also supported in part by the National Science Foundation, grant GA-32683, and in part by the National Aeronautics and Space Administration, grant NGR22-009-839.

REFERENCES

Clark, T. A., L. K. Hutton, G. E. Marandino, C. C. Counselman III, D. S. Robertson, I. I. Shapiro, J. J. Wittels, H. F. Hinteregger, C. A. Knight, A. E. E. Rogers, A. R. Whitney, A. E. Niell, B. O. Rönnäng, and O. E. H. Rydbeck, Radio source positions from very-long baseline interferometry observations, *Astron. J., 81*, 599–603, 1976.

Cohen, M. H., A. T. Moffet, J. D. Romney, R. T. Schilizzi, G. A. Seielstad, K. I. Kellermann, G. H. Purcell, D. B. Shaffer, T. I. K. Pauliny-Toth, E. Preuss, A. Witzel, and R. Rinehart, Rapid increase in the size of 3C 345, *Astrophys. J., 206*, L1–L3, 1976.

Elsmore, B., and M. Ryle, Further astrometric observations with the 5-km radio telescope, *Mon. Notic. Roy. Astron. Soc., 174*, 411–423, 1976.

Hinteregger, H. F., R. Ergas, C. A. Knight, D. S. Robertson, I. I. Shapiro, A. R. Whitney, A. E. E. Rogers, and T. A. Clark, Precision geodesy via radio interferometry: First results, *Bull. Amer. Astron. Soc., 3*, 467, 1971.

Hinteregger, H. F., I. I. Shapiro, D. S. Robertson, C. A. Knight, R. A. Ergas, A. R. Whitney, A. E. E. Rogers, J. M. Moran, T. A. Clark, and B. F. Burke, Precision geodesy via radio interferometry, *Science, 198*, 396–398, 1972.

Hutton, L. K., Fine structure in 3C 120 and 3C 84, Ph.D. thesis, Univ. of Md., College Park, 1976. (Also available as *Rep. X-693-76-268*, NASA Goddard Space Flight Center, Greenbelt, Md., 1976.)

Moran, J. M., and H. Penfield, Test and evaluation of water vapor radiometers and determination of their capability to measure tropospheric propagation path length, final report, contract NAS5-20975, NASA Goddard Space Flight Center, Greenbelt, Md., 1976.

Ong, K. M., P. F. MacDoran, J. B. Thomas, H. F. Fliegel, L. J. Skjerve, D. J. Spitzmesser, P. D. Batelaan, S. R. Paine, and M. G. Newsted, A demonstration of a transportable radio interferometric surveying system with 3-cm accuracy on a 307-m base line, *J. Geophys. Res., 81*, 3587–3593, 1976.

Pauliny-Toth, I. I. K., E. Preuss, A. Witzel, K. I. Kellermann, D. B. Shaffer, G. H. Purcell, G. W. Grove, D. L. Jones, M. H. Cohen, A. T. Moffet, J. Romney, R. T. Schilizzi, and R. Rinehart, High resolution observations of NGC1275 with a four-element intercontinental radio interferometer, *Nature, 259*, 17–20, 1976.

Reisz, A. C., I. I. Shapiro, J. M. Moran, G. D. Papadopoulos, B. F. Burke, K. Y. Lo, and P. R. Schwartz, W3(OH): Accurate relative positions of water-vapor emission features, *Astrophys. J., 186*, 537–544, 1973.

Robertson, D. S., Geodetic and astrometric measurements with very-long-baseline interferometry, Ph.D. thesis, Mass. Inst. of Technol., Cambridge, 1975.

Rogers, A. E. E., C. C. Counselman III, H. F. Hinteregger, C. A. Knight, D. S. Robertson, I. I. Shapiro, A. R. Whitney, and T. A. Clark, Extragalactic radio sources: Accurate positions from very-long-baseline observations, *Astrophys. J., 186*, 801–806, 1973.

Rogers, A. E. E., H. F. Hinteregger, A. R. Whitney, C. C. Counselman III, I. I. Shapiro, J. J. Wittels, W. K. Klemperer, W. W. Warnock, T. A. Clark, L. K. Hutton, G. E. Marandino, B. O. Rönnäng, O. E. H. Rydbeck, and A. E. Niell, The structure of radio sources 3C 273B and 3C 84 deduced from the 'closure' phases and visibility amplitudes observed with three-element interferometers, *Astrophys. J., 193*, 293–301, 1974.

Schaper, L. W., D. H. Staelin, and J. W. Waters, The estimation of tropospheric electrical path length by microwave radiometry, *Proc. IEEE, 58*, 272–274, 1970.

Shapiro, I. I., Estimation of astrometric and geometric parameters from VLBI observations, in *Methods of Experimental Physics*, vol.

12C, edited by M. L. Meeks, pp. 261–276, Academic, New York, 1976.

Shapiro, I. I., and C. A. Knight, Geophysical applications of long-baseline radio interferometry, in *Earthquake Displacement Fields and the Rotation of the Earth*, edited by A. Beck, pp. 284–301, D. Reidel, Hingham, Mass., 1970.

Shapiro, I. I., D. S. Robertson, C. A. Knight, C. C. Counselman III, A. E. E. Rogers, H. F. Hinteregger, S. Lippincott, A. R. Whitney, T. A. Clark, A. E. Niell, and D. J. Spitzmesser, Transcontinental baselines and the rotation of the earth measured by radio interferometry, *Science, 186*, 920–922, 1974. (Erratum, *Science, 191*, 451, 1976.)

Thomas, J. B., J. L. Fanselow, P. F. MacDoran, L. J. Skjerve, D. J. Spitzmesser, and H. F. Fliegel, A demonstration of an independent-station radio interferometry system with 4-cm precision on a 16-km base line, *J. Geophys. Res., 81*, 995–1005, 1976.

Whitney, A. R., Precision geodesy and astrometry via very-long-baseline interferometry, Ph.D. thesis, Mass. Inst. of Technol., Cambridge, 1974.

Whitney, A. R., A. E. E. Rogers, H. F. Hinteregger, L. B. Hanson, T. A. Clark, C. C. Counselman III, and I. I. Shapiro, Application of very-long-baseline interferometry to astrometry and geodesy: Effects on accuracy of frequency-standard instability, Proceedings of the 6th Annual Precise Time and Time Interval Planning Meeting, *Tech. Rep. X-814-75-117*, pp. 349–359, Goddard Space Flight Center, Greenbelt, Md., 1975.

Whitney, A. R., A. E. E. Rogers, H. F. Hinteregger, C. A. Knight, J. I. Levine, S. Lippincott, T. A. Clark, I. I. Shapiro, and D. S. Robertson, A very-long-baseline interferometer for geodetic applications, *Radio Sci., 11*, 421–432, 1976.

Winn, F. B., S. C. Wu, G. M. Resch, C. C. Chao, O. H. Van Roos, and E. H. Lau, Atmospheric water-vapor calibrations: Radiometer technique, *Deep Space Network Progr. Rep. 42-32*, Jet Propul. Lab., Pasadena, Calif., 1976.

Wittels, J. J., Positions and kinematics of quasars and related radio objects inferred from VLBI observations, Ph.D. thesis, Mass. Inst. of Technol., Cambridge, 1975.

Wittels, J. J., W. D. Cotton, C. C. Counselman III, I. I. Shapiro, H. F. Hinteregger, C. A. Knight, A. E. E. Rogers, A. R. Whitney, T. A. Clark, L. K. Hutton, B. O. Rönnäng, O. E. H. Rydbeck, and A. E. Niell, Apparent 'superrelativistic' expansion of the extragalactic radio source 3C 345, *Astrophys. J., 206*, L75–L78, 1976.

(Received November 9, 1976;
revised May 23, 1977;
accepted August 30, 1977.)

THE ASTRONOMICAL JOURNAL VOLUME 83, NUMBER 6 JUNE 1978

A HIGH DECLINATION SEARCH AT 8 GHz FOR COMPACT RADIO SOURCES

J. J. WITTELS, I. I. SHAPIRO, D. S. ROBERTSON[a], and C. C. COUNSELMAN
Massachusetts Institute of Technology, Cambridge, Massachusetts 02139

H. F. HINTEREGGER, C. A. KNIGHT, A. E. E. ROGERS, and A. R. WHITNEY
Haystack Observatory, Northeast Radio Observatory Corporation, Westford, Massachusetts 01886

T. A. CLARK, L. K. HUTTON, and C. MA
Goddard Space Flight Center, Greenbelt, Maryland 20771

A. E. NIELL and G. M. RESCH
Jet Propulsion Laboratory, Pasadena, California 91103

B. O. RÖNNÄNG and O. E. H. RYDBECK
Onsala Space Observatory and Chalmers University of Technology, Gothenberg, Sweden
Received 10 January 1978

ABSTRACT

With the Haystack-NRAO interferometer (baseline length of 20×10^6 λ at λ = 3.8 cm) we observed 37 sources whose declinations were above 50°. Seven of these sources have compact cores with diameters smaller than 5 milliarcsec and with correlated flux densities greater than about 0.5 Jy; the remaining sources have no cores with flux densities above about 0.3 Jy, the sensitivity limit of the interferometer. Two of the sources with detected compact cores, 4C 67.05 and 3C 418, were also observed with longer baseline interferometers; the diameter of the core of 4C 67.05 was estimated to be smaller than 1 milliarcsec and that of 3C 418 to be smaller than 0.4 milliarcsec. All diameter estimates were based on an assumed circular Gaussian distribution of radio brightness and refer to the contour with brightness density $e^{-1/2}$ that of the center. Positions for the detected sources were also obtained from the interferometric data, the uncertainty in these coordinate estimates ranging from 0.04 to 0.6 arcsec. The compact core detected in 3C 390.3 was found to lie near the center of this extended (approximately 4 arcmin in diameter) double radio source, and to be coincident to within 1 arcsec with an N galaxy previously identified with 3C 390.3.

I. INTRODUCTION

Applications of very-long-baseline interferometry (VLBI) to astrometry and geodesy benefit from the availability of compact radio sources spaced as widely as possible in declination. In the past, there were no known strong radio sources above about 50° declination for which compact components had been detected at X-band. Therefore, in October 1974, we used an interferometer with an 845-km baseline (20×10^6 λ at λ = 3.8 cm) to search for compact, high declination sources. Such sources also have a high probability of being interesting astrophysical objects since most sources observable with VLBI have variable flux densities and often variable compact structures as well.

II. OBSERVATIONS

We observed 37 radio sources with declinations above 50° using the Haystack Observatory's 37 m-diameter antenna in Westford, MA and the National Radio Astronomy Observatory's 43 m-diameter antenna in Green Bank, WV (HN interferometer). The observations, made with left circular polarization and centered at a frequency of 7850 MHz, utilized our band-width synthesis technique, and employed the Mark I recording system (Whitney 1974; Wittels *et al.* 1975; Whitney *et al.* 1976). For each source, one to four three-minute tapes were recorded. Results for the seven sources for which fringes were detected are given in Table I; the positions obtained are also shown [see Rogers *et al.* (1973) and Clark *et al.* (1976) for descriptions of the astrometric method used].

Our position for the compact core of 3C 390.3 is shown in Fig. 1 superposed on a radio-brightness map of this source obtained from observations at 1407 MHz with the Cambridge 1-mile interferometer (Macdonald *et al.* 1968). This position is coincident with that of the near-central radio component observed by Harris (1972) and with the location of an N-galaxy ($18^h45^m37^s.93 \pm .06$, $79°43'5''.5 \pm .9$; Lu and Frederick 1967) thus confirming the optical identification.

[a] Now at U.S. National Geodetic Survey, NOS, NOAA, Rockville, Maryland 20852.

 0004-6256/78/8306-0560$00.90

TABLE I. Sources with detected compact cores in October 1974

Source name	α^a (1950.0)	δ^a (1950.0)	Total flux density[b] (Jy)	Projected Baseline Length ($10^6\lambda$)	Projected Baseline Position angle (°)	Correlated flux density[c] (Jy)	Optical identification[d]
4C 67.05	02h24m41.14(2)	67°07'39.38(4)	1.93	19.8	268	1.95	
				19.9	267	1.97	
				22.1	193	1.46	
				22.1	192	1.50	
4C 55.16	08 31 04.34(2)	55 44 41.3(2)	3.49	21.9	199	1.39	Galaxy[a]
				21.9	197	≥1.03[e]	
				18.5	266	1.11	
				18.6	267	0.97	
3C 309.1	14 58 56.66(6)	71 52 11.4(5)	1.18	21.9	207	0.75	QSO ($z = 0.904$)[b,c]
				21.9	206	0.73	
3C 371	18 07 18.61(8)	69 48 57.1(4)	1.46	21.7	226	1.38	N Galaxy[c]
3C 390.3	18 45 37.7(2)	79 43 06.5(5)	1.26	21.1	225	0.46	N Galaxy ($z = 0.057$)[c,d,e]
				21.1	224	0.57	
OW 637	20 21 13.77(5)	61 27 20.1(1)	1.91	21.9	232	0.89	Galaxy[f]
				21.9	231	0.92	
3C 418	20 37 07.490(6)	51 08 35.66(3)	3.35	21.5	247	1.41	Candidate QSO[g]
				21.6	246	1.44	

[a] α and δ are the right ascension and declination, respectively, calculated from the delays and delay rates obtained in the 1974 October experiment, except for 3C 418 whose position is from Clark *et al.* 1976. The numbers in parentheses are the formal standard errors in the last significant figures shown. Elliptic aberration has been removed.

[b] The error in total flux density is about 0.08 Jy not including the effects of possible pointing errors, which were estimated to be no more than 10% of the half-beamwidth at half-power of either telescope.

[c] The uncertainty in each correlated flux density is about 5%, not including effects of possible pointing errors.

[d] The references are: (a) Veron (1971); (b) Burbidge and Burbidge (1969); (c) Wyndham (1966); (d) Sandage (1966); (e) Penston *et al.* (1971); (f) Radivich and Kraus (1971); and (g) Kristian *et al.* (1974).

[e] A large number of parity errors resulted in an unknown decrease in the magnitude of the correlation (see Wittels 1975 and Wittels *et al.* 1976).

All the sources listed in Table I, except perhaps 3C 371, are partially resolved by the HN interferometer. A summary of other successful VLBI observations of these sources is given in Table II. The remaining 30 sources, for which any correlated flux density was below the detection limit of about 0.3 Jy, are listed in Table III.

Two of the sources with detectable cores, 3C 418 and 4C 67.05, were also observed with higher resolution interferometers. The resulting correlated flux densities are presented in Figs. 2 and 3 and are discussed below; the observed closure phases were not significantly different from zero. Relevant auxiliary information is given in Table IV.

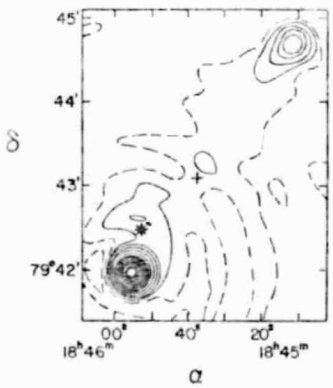

FIG. 1. A radio brightness map of 3C 390.3 obtained by the Cambridge 1 mile interferometer operating at a frequency of 1.4 GHz (courtesy of Macdonald *et al.* 1968). The cross marks the optical position of an N-galaxy (Sandage 1966; Lu and Frederick 1967), the radio position of the near-central component observed at 2.7 and 5.0 GHz (Harris 1972), and our position for the compact core observed at 8 GHz. The local brightness maximum in the map just to the northwest of the cross may be due to sidelobe structure in the Cambridge interferometer (Harris 1972). The asterisk marks the position given in an NRAO source list (1971, unpublished), which is offset from that of the compact core by almost 1 arcmin.

TABLE II. Summary of other VLBI observations of compact cores in radio sources at high declinations.

Source	λ(cm)	Total baseline length ($10^6\lambda$)	Correlated flux density (Jy)	Reference[a]
4C 67.05	13	100	>0.1	(a)
4C 55.16	13	25	1.4	(b)
	13	100	>0.1	(a)
3C 309.1	13	100	0.1	(c)
	18	4, 19	7.0, 1.2	(d)
3C 371	3.8	100	0.5	(e)
	13	25	0.5	(b)
	13	100	>0.1	(a)
3C 390.3	3.7	4	0.6	(f)
	6	6	0.6	(g)
	6	100	0.2	(h)
	13	100	>0.1	(c)
OW 637	13	100	>0.1	(a)
3C 418	13	100	>0.1	(c)

[a] References are: (a) Preston *et al.* (1975); (b) Broderick *et al.* (1972); (c) Preston (1977); (d) Kellermann *et al.* (1971); (e) Cohen *et al.* (1971); (f) Kellermann *et al.* (1975); (g) Schilizzi (1976); and (h) Preuss *et al.* (1977).

TABLE III. Sources with no detected compact cores in October 1974.

Source name	α[a] (1950.0)	δ[a] (1950.0)	Total flux density[b] (Jy)	Projected baseline: Length ($10^6\lambda$)	Projected baseline: Position angle (°)	Position reference[c]	Optical identification[d]
3C 11.1	00h02m54s.2	63°42'09"	0.39	21.9	228	FM	
3C 56.02	01 07 54.3	56 16 05	0.95	21.0	253	BDFL	
				21.8	238		
4C 72.02	01 22 17.0	72 31 06	0.18[e]	21.2	240	4CP	
4C 71.03	02 36 19.0	71 50 30	0.19[e]	20.7	253	4CP	
3C 91	03 34 03.7	50 36 04	0.95	21.3	250	FM	Obscure Field[a]
4C 67.09	03 41 52.5	67 56 44	<0.04[e]	20.8	254	BDFL	Galaxy[b]
4C 76.03	04 03 57.4	76 46 54	0.45	20.7	250	FM	
4C 74.08	04 07 05.0	74 43 23	2.10	19.0	294	4C	
				21.4	213		
4C 60.10	06 39 36.6	59 58 28	0.41	18.8	275	BDFL	
4C 69.10	06 55 56.4	69 56 33	0.36	19.8	270	BDFL	
4C 56.16	07 45 50.0	56 02 00	0.48	19.5	267	4C	Galaxy[b]
3C 231	09 51 43.0	69 54 59	1.82	22.0	203	BDFL	Galaxy[b]
				18.9	284		
4C 55.17	09 54 15.5	55 37 06	1.77	21.8	184	BDFL	Candidate QSO[c]
				18.6	274		
DA 302	11 25 41.3	58 50 22	0.14[e]	22.0	178	BDFL	
				17.0	289		
3C 263	11 37 10.8	66 04 28	0.53	22.1	178	BDFL	QSO ($z = 0.643$)[d]
				17.1	300		
4C 55.22	11 52 46.9	55 10 44	<0.04[e]	17.3	282	BDFL	Galaxy[c]
3C 268.1	11 57 48.5	73 17 40	0.51	21.9	192	PWH	
				18.6	293		
3C 282	13 06 31.3	66 00 10	0.26[e]	20.7	255	BDFL	Galaxy[e]
4C 62.22	13 58 57.8	62 25 03	0.87	21.3	246	BDFL	
				22.1	199		
3C 295	14 09 33.6	52 26 14	3.61	20.6	257	BDFL	Galaxy[f]
3C 343	16 34 01.4	62 51 43	0.67	21.7	237	BDFL	Candidate QSO[g]
				22.1	203		
3C 343.1	16 37 55.1	62 40 34	0.57	20.3	261	BDFL	Galaxy[g]
3C 363	17 47 32.1	59 44 16	0.31[e]	22.1	204	PWH	
4C 53.42	17 54 00.1	53 06 40	0.26[e]	21.8	203	PWH	
3C 383	18 33 32.2	63 19 13	0.40	22.1	202	BDFL	Galaxy[e]
4C 55.36	19 15 49.0	55 37 42	0.47	22.0	209	4C	
3C 402	19 40 22.7	50 29 40	0.56	21.8	212	BDFL	Galaxy[b]
3C 429	21 11 39.8	62 02 35	0.43	21.1	250	BDFL	
				21.6	239		
3C 440	22 01 50.4	62 25 57	0.65	21.9	231	BDFL	Galaxy[h]
3C 468.1	23 48 26.8	64 23 37	0.39	21.5	241	BDFL	

[a] α and δ are the right ascension and declination, respectively, used for pointing during the experiment.
[b] The error in the total flux density is about 0.08 Jy, not including effects of possible pointing errors. Values given as <0.04 indicate that no total power above the 0.04 Jy threshold of detectability was observed at that position.
[c] The references are: 4C—Gower *et al.* (1967); 4CP—Caswell and Crowther (1969); BDFL—Bridle *et al.* (1972); FM-Fomalont and Moffet (1971); and PWH—Pauliny-Toth *et al.* (1966).
[d] The references are: (a) Wyndham (1965); (b) Caswell and Wills (1967); (c) Veron (1971); (d) Hiltner *et al.* (1966); (e) Wills (1967); (f) Minkowski (1960); (g) Kristian and Sandage (1970); and (h) Veron and Veron (1975).
[e] These sources proved too weak for any core to have been detected.

III. DISCUSSION

The data from the October 1974 experiment allow us to estimate a maximum size for the core of each of the seven sources for which fringes were detected: assuming that the radio brightness distribution of each of these compact cores can be represented by a circular Gaussian function yields an upper limit of about 5 milliarcsec for the diameter of the contour of brightness density $e^{-1/2}$ times that of the center (hereafter "diameter"). The additional observations of 3C 418 and 4C 67.05 allow us to draw more detailed conclusions about the structure of these sources. The existence of another, lower resolution, study (Harris 1972) of 3C 390.3 also allows us to make certain comments on its structure.

The data for 3C 418, obtained from VLBI observations over transcontinental and intercontinental baselines spanning, at times, Goldstone, California to Onsala, Sweden, disclose a very compact core that contributes a correlated flux density of about 1.8 Jy and has a diameter smaller than 0.4 milliarcsec.

The maximum in the correlated flux density for 3C 418 observed with the HN interferometer at a resolution not corresponding to the maximum for that baseline is indicative of the presence of an asymmetric, extended component. Subtracting the core flux density obtained with the longer baselines from the correlated flux densities obtained with the HN interferometer during the same experiment, and matching the remaining 2.3 Jy of the total flux density to an elliptical Gaussian model of

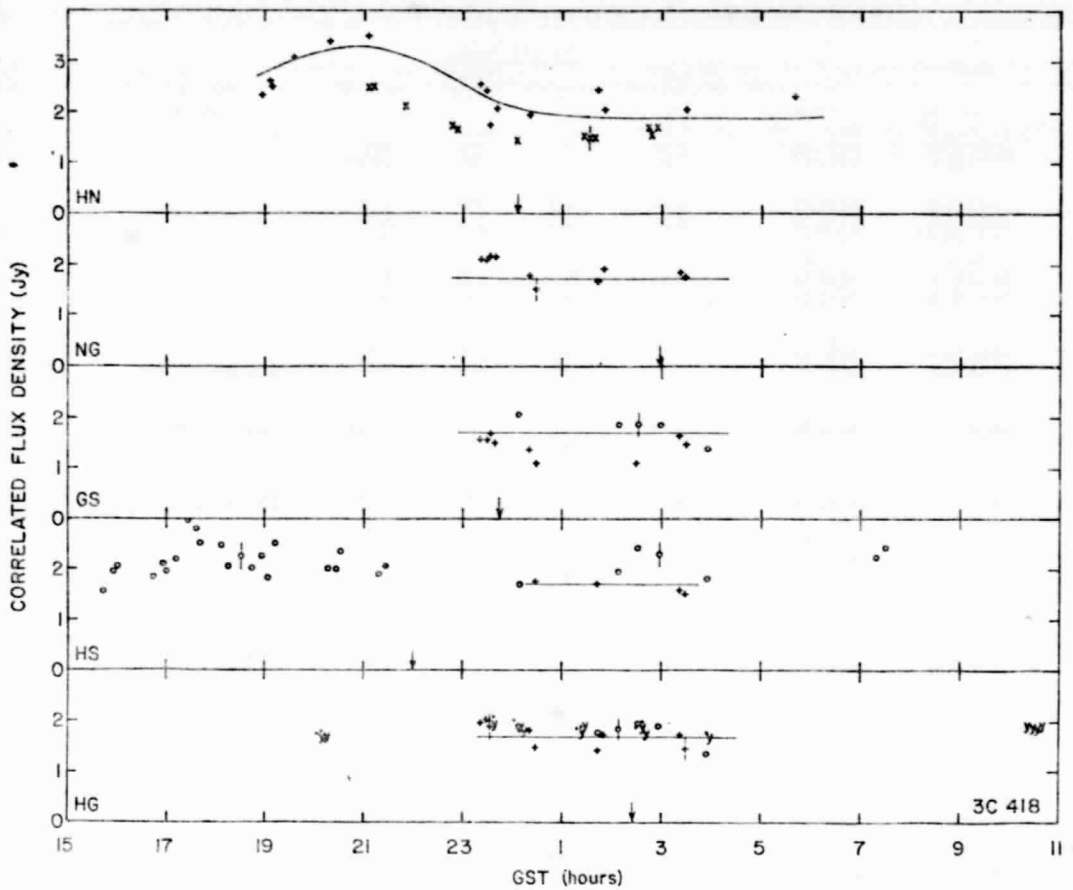

FIG. 2. Correlated flux density as a function of Greenwich sidereal time for 3C 418. Each symbol refers to a different experiment (see Table IV). Typical standard errors are shown. The arrows mark interferometer hour angle equal to zero for each baseline. The theoretical curves were based on the data from August 1973 and a point-core, elliptical-gaussian-halo model of the radio brightness distribution.

the radio brightness, gives a halo with diameters of about 10 ± 5 and 4 ± 2 milliarcsec, the major axis being along a position angle of 15 ± 4 deg. The decrease in the correlated flux density measured by the HN interferometer between August 1973 and October 1974 is matched, to within the uncertainties, by a decrease in the total flux density of the source (Table IV and Fig. 2) and may indicate variability of the compact core.

The correlated flux densities obtained from observations of 4C 67.05 (see Fig. 3) indicate that this source has

TABLE IV. Auxiliary information on experiments.

Experiment Date	Antennas[a]	Frequency (MHz)	Polarization[b]	Symbol[c]	Total Flux Density (Jy) 3C 418	4C 67.05
4–5 February 1973	GH	7850	L	∧	3.9 ± 0.2	
30–31 March 1973	GH	7850	L	y	3.8 ± 0.2	
17–23 May 1973	GHS	7850	L	○	3.7 ± 0.2	
10–14 August 1973	GHNS	7850	L	+	4.1 ± 0.2	
26–28 October 1974	HN	7850	L	×	3.4 ± 0.1	1.9 ± 0.1
24 August 1975	GH	8420	R	+		1.9 ± 0.2
15–16 October 1975	GHN	7850	R	○		2.1 ± 0.1

[a] Here G ≡ the 64 m diameter antenna in Goldstone, California; H ≡ the 37 m diameter antenna in Westford, Massachusetts; N ≡ the 43 m diameter antenna in Green Bank, West Virginia; S ≡ the 26 m diameter antenna in Onsala, Sweden.
[b] Here R ≡ right circular and L ≡ left circular polarization.
[c] The symbols appear in Figs. 2 and 3.

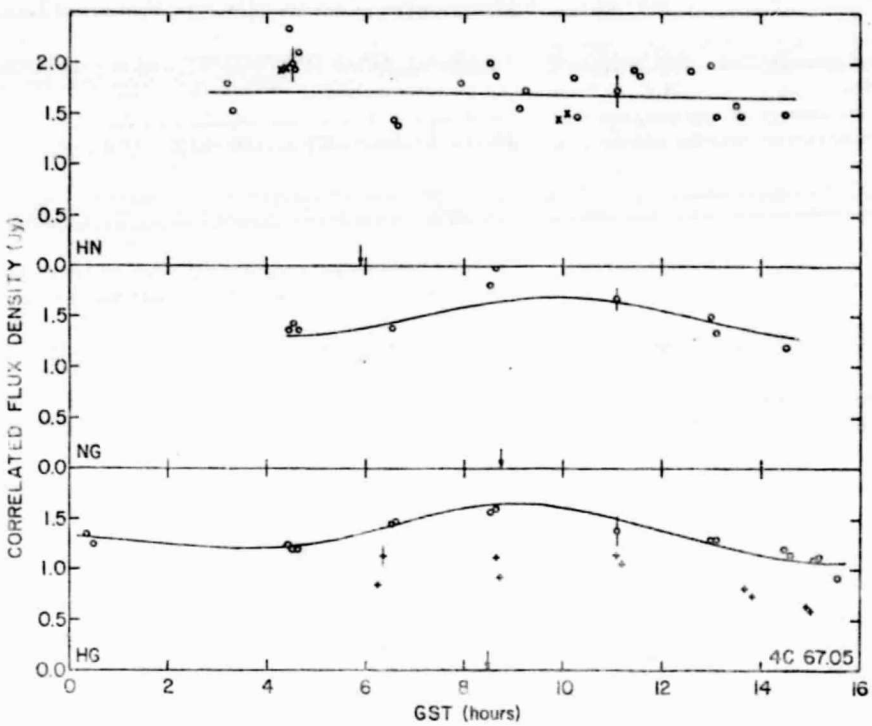

FIG. 3. As in Fig. 2, but for the source 4C 67.05. The [illegible] were based on the data from October 1975 and an elliptical Gaussian model of the ratio brightness distribution (see text).

a compact core which is partially resolved by the trans continental interferometers: the correlated flux densities on each of these two baselines (Table IV) exhibited a maximum near minimum resolution. A four-parameter elliptical Gaussian model of the source, when matched in a least-squares sense to the correlated flux densities and the closure phases from October 1975, shows that the core contributes 1.72 ± 0.05 Jy to the correlated flux density and has diameters of 0.6 ± 0.2 and 0.2 ± 0.2 milliarcsec with the major axis having a position angle of $-17° \pm 7°$. The correlated flux density predicted from this model is shown as the solid line in Fig. 3. Due to unexplained, and different, decreases in the correlated flux densities for the data from the different baselines involved in this experiment, these data were scaled based on the assumption that the compact structure of PKS 2134 + 004 is not time variable (see, for example, Wittels *et al.* 1975). If this scaling procedure is correct, the 60% increase in correlated flux density, found with the HG interferometer between August 1975 and October 1975, indicates that an outburst was in progress. Mitigating against the correctness of this procedure, however, is the fact that the total flux density probably increased by no more than 20% in this time interval (see Table IV).

Low-resolution observations of 3C 390.3 by Harris (1972), as mentioned in Sec. II, disclosed a component coincident with the compact core we observed. This component had a flux density of 0.35 ± 0.1 and 0.35 ± 0.05 Jy, respectively, at 2.7 and 5.0 GHz. In combination with our (average) measured value of 0.51 ± 0.05 Jy at 7.85 GHz, the flux densities suggest either that the spectrum of the core is inverted or that the flux density is variable in this frequency range. With the values used by Harris for the redshift of 3C 390.3 and for the Hubble constant, 0.057 and 100 km s^{-1} Mpc^{-1}, respectively, we can reduce the upper limit on the diameter of the core from 2 kpc to about 3.5 pc, still well above the 0.3 pc size assumed by Harris in his computation that yielded an energy within the core of $\sim 10^{52}$ erg.

IV. CONCLUSIONS

VLBI observations, over a baseline of length $20 \times 10^6\lambda$ at $\lambda = 3.8$ cm, disclose compact cores in seven out of 37 candidate sources with declinations above 50 deg. For these seven sources, the cores have diameters estimated to be smaller than about 5 milliarcsec and flux densities between about 0.5 and 2 Jy (see Table I). In one of these sources, 4C 67.05, the radio brightness of the core can be adequately represented by an elliptical Gaussian function with major diameter smaller than 1

milliarcsec. For another such source, 3C 418, the compact core has a diameter smaller than 0.4 milliarcsec and is accompanied by an asymmetric extended component. For the 30 other sources, an upper limit of about 0.3 Jy was placed on the flux density of any compact core. Caution should be exercised in drawing statistical inferences about the fraction of sources with compact cores whose accompanying flux densities exceed a given limit since the sample discussed here was incomplete and was selected with no consideration of possible bias.

We are indebted to the staffs of the participating observatories for their important aid. Some of the observations reported here were made as part of the Quasar Patrol sponsored by the National Aeronautics and Space Administration and the Jet Propulsion Laboratory. The experimenters at the Massachusetts Institute of Technology were supported in part by the National Science Foundation, Grant DES74-22712, and in part by the National Aeronautics and Space Administration, Grant NGR 22-009-836. Radio astronomy programs at the Haystack Observatory are conducted with support from the National Science Foundation, Grant MPS 71-02109 A07. This work also represents one phase of research carried out at the Jet Propulsion Laboratory, California Institute of Technology, under Contract NAS 7-100, sponsored by the National Aeronautics and Space Administration. The National Radio Astronomy Observatory is operated by Associated Universities, Inc., under contract with the National Science Foundation. The VLBI program at the Onsala Space Observatory is supported in part by the Swedish Natural Science Research Council and the Swedish Board for Technical Development.

REFERENCES

Bridle, A. H., Davis, M. M., Fomalont, E. B., and Lequeux, J. (1972). Astron. J. **77,** 405.

Broderick, J. J., Kellermann, K. I., Shaffer, D. B., and Jauncey, D. L. (1972), Astrophys. J. **172,** 299.

Burbidge, G., and Burbidge, M. (1969). Nature **222,** 735.

Caswell, J. J., and Crowther, J. H. (1969). Mon. Not. R. Astron. Soc. **145,** 181.

Caswell, J. J., and Wills, D. (1967). Mon. Not. R. Astron. Soc. **135,** 231.

Clark, T. A., Hutton, L. K., Marandino, G. E., Counselman, C. C. III, Robertson, B. S., Shapiro, I. I., Wittels, J. J., Hinteregger, H. S., Knight, C. A., Rogers, A. E. E., Whitney, A. R., Niell, A. E., Rönnäng, B. O., Rydbeck, O. E. H. Astron. J. (1976). **81,** 599.

Cohen, M. H., Cannon, W., Purcell, G. H., Shaffer, D. B., Broderick, J. J., Kellermann, K. I., and Jauncey, D. L. (1971). Astrophys. J. **170,** 207.

Fomalont, E. B., and Moffet, A. T. (1971). Astron. J. **76,** 5.

Gower, J. F. R., Scott, P. F., and Wills, D. (1967). Mem. R. Astron. Soc. **71,** 49.

Harris, A. (1972). Mon. Not. R. Astron. Soc. **158,** 1.

Hiltner, W., Crowley, A., and Schild, R. (1966). Publ. Astron. Soc. Pac. **78,** 464.

Kellermann, K. I., Clark, B. G., Niell, A. E., and Shaffer, D. B. (1975). Astrophys. J. **197,** L113.

Kellermann, K. I., Jauncey, D. L., Cohen, M. H., Shaffer, D. B., Clark, B. G., Broderick, J. J., Rönnäng, B., Rydbeck, O. E. H., Matveyenko, L., Moiseyev, I., Vitkevitch, V. V., Cooper, B. F. C., and Batchelor, R. (1971). Astrophys. J. **169,** 1.

Kristian, J., and Sandage, A. (1970). Astrophys. J. **162,** 391.

Kristian, J., Sandage, A., and Katem, B. (1974). Astrophys. J. **191,** 43.

Lu, P., and Frederick, L. J. (1967). Astrophys. J. **150,** L71.

Macdonald, G. H., Kenderdine, S., and Neville, A. C. (1968). Mon. Not. R. Astron. Soc. **138,** 259.

Minkowski, R. (1960). Astrophys. J. **132,** 908.

Pauliny-Toth, I. I. K., Wade, C. M., and Heeschen, D. S. (1966). Astrophys. J. Supp. 116.

Penston, M. J., Penston, M. V., and Sandage, A. (1971). Publ. Astron. Soc. Pac. **83,** 783.

Preston, R. A. (1977). Private communication.

Preston, R. A., Harris, A. W., Slade, M. A., Williams, J. G., Fanselow, J. L., Thomas, J. B., Morabito, D. D., Spitzmesser, D. J., Skjerve, L. J., Johnson, B., and Jauncey, D. (1975). Bull. Am. Astron. Soc. **7,** 517.

Preuss, E., Pauliny-Toth, I. I. K., Witzel, A., Kellermann, K. I., and Shaffer, D. B. (1977). Astron. Astrophys. 54, 297.

Radivich, M. M., and Kraus, J. D. (1971). Astron. J. 76, 683.

Rogers, A. E. E., Counselman, C. C. III, Hinteregger, H. S., Knight, C. A., Robertson, B. S., Shapiro, I. I., Whitney A. R., Clark, T. A. (1973). Astrophys. J. **183,** 801.

Sandage, A. R. (1966). Astrophys. J. **145,** 1.

Schilizzi, R. T. (1976). Astron. J. **81,** 946.

Veron, M. P. (1971). Astron. Astrophys. **11,** 1.

Veron, M. P., and Veron, P. (1975). Astron. Astrophys. **42,** 1.

Whitney, A. R. (1974). Ph.D. dissertation, Massachusetts Institute of Technology.

Whitney, A. R., Rogers, A. E. E., Hinteregger, H. F., Knight, C. A., Levine, J. I., Lippincott, S., Clark, T. A., Shapiro, I. I., and Robertson, D. S. (1976). Radio Sci. **11,** 421.

Wills, D. (1967). Mon. Not. R. Astron. Soc. **135,** 339.

Wittels, J. J. (1975). Ph.D. dissertation, Massachusetts Institute of Technology.

Wittels, J. J., Knight, C. A., Shapiro, I. I., Hinteregger, H. F., Rogers, A. E. E., Whitney, A. R., Clark, T. A., Hutton, L. K., Marandino, G. E., Niell, A. E., Rönnäng, B. O., Rydbeck, O. E. H., Klemperer, W. K., and Warnock, W. W. (1975). Astrophys. J. **196,** 13.

Wittels, J. J., Shapiro, I. I., Cotton, W. D., Counselman, C. C., Hinteregger, H. F., Knight, C. A., Rogers, A. E. E., Whitney, A. R., Clark, T. A., Hutton, L. K., Niell, A. E., Rönnäng, B. O., and Rydbeck, O. E. H. (1976). Astron. J. **81,** 933.

Wyndham, J. D. (1966). Astrophys. J. **144,** 221.

JOURNAL OF
THE SURVEYING
AND MAPPING DIVISION

PRECISION SURVEYING USING RADIO INTERFEROMETRY[a]

By James W. Ryan,[1] Thomas A. Clark,[2] Robert Coates,[3] Brian E. Corey,[4] William D. Cotton,[5] Charles C. Counselman III,[6] Hans F. Hinteregger,[7] Curtis A. Knight,[8] Chopo Ma,[9] Douglas S. Robertson,[10] Alan E. E. Rogers,[11] Irwin I. Shapiro,[12] Alan R. Whitney,[13] and Jill J. Wittels[14]

INTRODUCTION

Very long baseline interferometry (VLBI) is one of the most promising tools now under development for making global scale geodetic measurements. It was

Note—Discussion open until April 1, 1979. To extend the closing date one month, a written request must be filed with the Editor of Technical Publications, ASCE. This paper is part of the copyrighted Journal of the Surveying and Mapping Division, Proceedings of the American Society of Civil Engineers, Vol. 104, No. SU1, November, 1978. Manuscript was submitted for review for possible publication on November 22, 1977.

[a]Presented at the October 17-21, 1977, ASCE Annual Convention, Exposition and Continuing Education Program, held at San Francisco, Calif.

[1]Mathematician, Geophysics Branch, Goddard Space Flight Center, Greenbelt, Md.

[2]Staff Scientist, Lab. for Extraterrestrial Physics, Goddard Space Center, Greenbelt, Md.

[3]Sr. Scientist, Applications Directorate, Goddard Space Flight Center, Greenbelt, Md.

[4]Research Assoc., Dept. of Earth and Planetary Sci., Massachusetts Inst. of Tech., Cambridge, Mass.

[5]Research Assoc., Dept. of Earth and Planetary Sci., Massachusetts Inst. of Tech., Cambridge, Mass.

[6]Assoc. Prof., Dept. of Earth and Planetary Sci., Massachusetts Inst. of Tech., Cambridge, Mass.

[7]Member, VLBI Group, Haystack Observatory, Westford, Mass.

[8]Member, VLBI Group, Haystack Observatory, Westford, Mass.

[9]Research Assoc., Dept. of Physics and Astronomy, Univ. of Maryland, College Park, Md.

[10]Geodesist, Gravity, Astronomy, and Satellite Branch, National Geodetic Survey, Rockville, Md.

[11]Group Leader, VLBI Group, Haystack Observatory, Westford, Mass.

[12]Prof., Dept. of Earth and Planetary Sci. and Dept. of Physics, Massachusetts Inst. of Tech., Cambridge, Mass.

[13]Member, VLBI Group, Haystack Observatory, Westford, Mass.

[14]Research Assoc., Dept. of Earth and Planetary Sci., Massachusetts Inst. of Tech., Cambridge, Mass.

first utilized by radio astronomers whose desire was to investigate extraterrestrial radio sources with very high angular resolution. The predecessor of the Goddard Space Flight Center, Haystack Observatory, Massachusetts Institute of Technology (GSFC/HO/MIT) VLBI team performed its first VLBI experiment in 1969 using the Haystack Observatory 37-m diam radio telescope in Massachusetts, a 27-m diam antenna at the Owens Valley Radio Observatory in California, and the 43-m diam antenna of the National Radio Astronomy Observatory in West Virginia (2). In this experiment the baseline lengths between these antennas were measured with an accuracy of 1 m. Since that time the technology of VLBI has advanced so far that experiments have already been performed with 10-cm repeatability and experiments are in the final planning stages which will achieve a 5-cm level of accuracy (1).

VLBI Technique

Fig. 1, the geometry of a VLBI experiment, shows the basic principles of this technique. Two widely separated radio telescopes observe radiation from

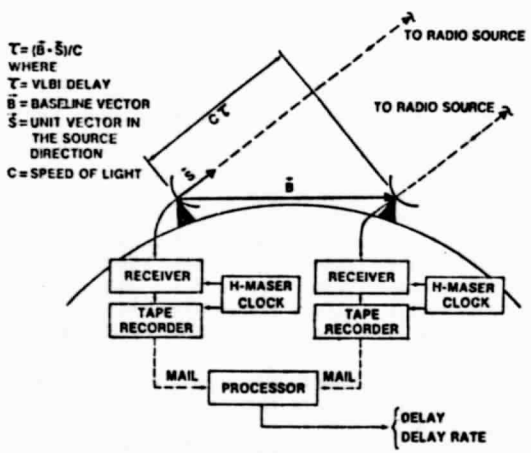

FIG. 1.—Very Long Baseline Interferometry (VLBI) Observation Geometry

some extragalactic radio source, typically a quasar. These extragalactic objects are selected because they are continuum sources, i.e., they radiate energy in a broad range of frequencies from a few megahertz to a many gigahertz, and because their small angular size and extreme distance from the earth—billions of light years—make them, for most purposes, fixed points in the sky. The angular diameter of the typical radio source used in a VLBI experiment is the same as that of a dime held over Washington, D.C. as seen from San Francisco. The receivers at each of the telescopes pass a broad band of the incident radiation; the frequency output of an atomic clock is used to convert the received radiation to a much lower frequency where it is digitized and recorded on tape. The radio sources can be thought of as raining on the earth a complicated random signal, and the VLBI observing scheme is simply a process

of observing this signal from various points on the surface of the earth, time-tagging its arrival with respect to a local clock at each site, and recording the time-tagged signals on tape. The tapes from the telescopes are sent to a central facility and cross-correlated in pairs. In an ideal case the two tapes would contain the identical random signal but time-tagged differently because the signal was received at different times. By delaying one tape relative to the other until they match, the time delay between the arrival of the signal at the two sites could be found. In the real case the signal recorded on the tapes is largely dominated by noise in the receiver systems at the telescopes; moreover, since the earth is rotating as the signals are accumulated the delay is continuously changing. Thus, the real processing is rather more complicated than the ideal case described here, but the underlying idea remains unchanged. Mathematical details of the processing are given in Ref. 8.

The measured delay (τ in Fig. 1) depends on vector Ŝ, a unit vector in the

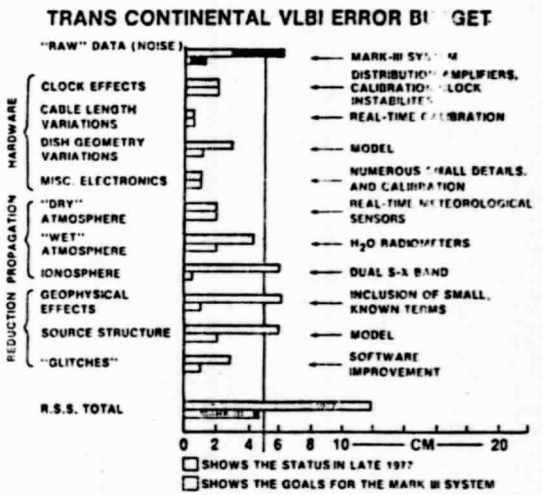

FIG. 2.—VLBI Error Budget (1 cm = 0.39 in.)

direction of the radio source, and vector B, the baseline vector. In an inertial coordinate system the components of S are constant for a given source, and the components of B vary because of the Earth's rotation, precession, nutation, etc., and because of relative motion of the sites due to solid earth tides and tectonic processes. The observations are also sensitive to various inadequacies of the VLBI hardware system and to environmental effects. In the final step of the VLBI process hundreds to thousands of observations are combined in a statistical adjustment of the baseline vectors, source coordinates, clock parameters, and parameters characterizing the environmental effects.

Status of Our VLBI System

Fig. 2 summarizes the magnitudes of the major error sources affecting the interpretation of VLBI data. For each effect the bar shows the extent to which

that effect limits the ability to recover baseline length accurately. In each case the upper bar shows our system as of late 1977 and the lower bar shows the planned state after our new system, the MARK III system, is fully implemented. In this context a VLBI system is the complete set of hardware and computer software used for the acquisition, processing, and analysis of VLBI data. The implementation of the MARK III system is the major current task of our group.

These error sources can be divided into systematic and random effects. The effects of random noise can be overcome by simply acquiring more data; the systematic effects are not so easily defeated.

VLBI Random Error Sources

Random effects are all covered in the first line of the bar chart—the line labeled "RAW" DATA. The effects of noise are specified almost exclusively by four parameters of the VLBI system: (1) The instantaneous recorded bandwidth; (2) the total spanned bandwidth; (3) the diameters of the antennas; and (4) the noise temperatures of the receivers. The total spanned bandwidth refers to the frequency window through which the source noise is received. The width of this window is limited by the passbands of the antenna feeds and parametric amplifiers employed in the telescopes. Experiments that have been carried out since September 1976 have employed new MARK III receivers that operate near 8.4 GHz and have a 400-MHz wide passband. With current technology it is impractical to record a 400-MHz wide signal, so the system samples the spectrum in discrete frequency windows. The width of these smaller windows, the instantaneous recorded bandwidth, is determined by the data rate of the tape recorders. It is in the area of tape recorders that the Mark III system will make its most significant improvement over all existing VLBI systems. Presently our team uses the MARK I tape recorder, which has a data rate of 720 kilobits/sec (360-kHz bandwidth) and which has remained virtually unchanged since it was first introduced in 1967. The MARK III tape recorder will have a record capability of 4 megabits/sec in each of 28 channels for a total record rate of 112 megabits per second (56-MHz bandwidth). To put this rate into perspective, a standard television channel could be recorded on each of the 28 MARK III channels. The third parameter that characterizes the effects of noise is the size of the telescopes- the smaller the antenna and the weaker the received signal, the lower the signal-to-noise ratio. Also, the accuracy of the antenna surface, i.e., how closely it conforms to a paraboloid, affects the efficiency with which the signals can be collected. The final parameter affecting overall noise is the receiver noise temperature. The new MARK III receivers are noncryogenic receivers; at present cryogenic receivers with considerably lower noise temperatures could be used but at considerably greater cost.

Various tradeoffs could be made among these error sources, but there is one that will be extensively exploited: increase in tape recorder data rate can offset decrease in antenna diameter. One of the principal rationales for developing the MARK III recorder was to provide for achieving centimeter level accuracy in baseline length determinations while using relatively small antennas. In Fig. 2 the upper bar in the line labeled "RAW" DATA, which terminates in a range from 3 cm–6 cm, characterizes a system using MARK I recorders and telescopes ranging in diameters upward from 30 m; the lower bar characterizes a system using MARK III recorders and antennas only a few meters in diameter.

VLBI Systematic Error Sources

The systematic error sources are tabulated in Fig. 2. "Clock effects" refer to the stabilities of the system clocks for periods ranging from a few minutes to a few days. Hydrogen maser clocks are currently in use and they are stable to a few parts in 10^{14} over all time intervals of major interest in our VLBI observations. They are the best clocks available and are likely to remain so for some time.

"Cable length variations" are inaccuracies in transfering clock signals from the hydrogen maser in telescope control facility to the MARK III receiver in the feed horn at the center of the antenna where the signals are used. The signals must travel a length of coaxial cable whose electrical path length may vary with time. In the MARK III system the electrical length of this cable will be continuously measured.

"Dish geometery variations" refer to the deformations of the antennas under the combined effects of wind and gravitational loading and differential heating. The effects of these variations on our results are of the order of 1 cm or less for the usual observing conditions.

"Miscellaneous electronics," which is a small error source, will not be reviewed here.

"Propagation media effects" are mainly caused by the earth's troposphere and ionosphere. The arrival of the radio source signal at the antennas is retarded by charged particles in the ionosphere and by the neutral atmosphere at lower altitudes. The total delay caused by the neutral atmosphere, which is about 7 nsec (2 m) in the zenith direction, scales approximately with the cosecant of the elevation angle so that it is approximately 80 nsec (24 m) at an elevation angle of 5°. The neutral atmosphere can be resolved into two parts: (1) A "dry component" caused by all components of the troposphere except water vapor; and (2) a "wet component" caused by the water vapor. The "dry component" can be estimated to a few percent by measuring the atmospheric pressure and temperature at each of the telescopes. The "wet component" can be estimated by measuring the temperature, pressure, and dew point at each telescope, but this is not fully satisfactory since the dew point at a telescope often is not well correlated with the water vapor along the ray path. To achieve a better calibration of the "wet component" each VLBI observing site will be instrumented with a water vapor radiometer that will measure the microwave brightness in the vicinity of the 23-GHz water vapor emission line. Tests have shown that this brightness is well correlated with total water vapor along the ray path. The ionosphere usually causes a much smaller effect than does neutral atmosphere, having a "worst case" effect of 30 cm in the zenith direction for X-band signals. The calibration of the ionosphere utilizes its dispersive nature: the delay of a signal of a given frequency is inversely proportional to the square of the frequency. The MARK III system will provide for acquiring simultaneous observations at X-band (8.4 GHz) and at S-band (2.3 GHz); since the ionospheric effect will be 13 times larger at S-band than at X-band a suitable comparison of the simultaneous observations will allow the effect of the ionosphere to be removed.

"Geophysical effects" include a host of small terms of which a principal one is the solid earth tide, the response of the solid earth to the same forces

that give rise to ocean tides. Its main effect is a semidiurnal change in the altitude of the telescope with a maximum amplitude of nearly 40 cm (4). These effects can be accounted for with a mathematical model parameterized with relevent Love numbers that can be estimated in the data analysis. Other geophysical effects include ocean loading, polar motion, and variations in the earth's rotations (UT1). Ocean loading is the subsidence of the solid earth in the vicinity of ocean basins as a result of the inflow of ocean tides. It has been observed with local-scale measurement systems such as tiltmeters and strain gages but never with any global-scale measurement system. Polar motion and UT1 will be examined in more detail in the following.

"Source structure" refers to the fact that while it is largely correct to think of the quasars as idealized points in the sky, they are in fact diffuse objects on some very small angular scale. As a result, the distribution of brightness must be taken into account by modeling the structure of each source. In fact, the source models that we obtain will be in themselves very interesting scientific results.

The final error source, "glitches," is a recognition that no hardware or software system developed by human beings is ever perfect. This entry is our estimate of the effects that have been overlooked and the software inadequacies remaining. The improvement from 3 cm–1 cm reflects the continual improvement of our computer programs.

In summary, the VLBI system currently in use by our team can determine baseline lengths with an uncertainty under 15 cm, and we should have a system capable of determining lengths with an uncertainty under 5 cm when the MARK III system is fully implemented.

The MARK III system will be able to determine other important geophysical parameters. The baseline vector between the telescopes can be determined by VLBI in a geocentric, crust-fixed coordinate system. With one 24-hr observing session the MARK III system will allow the equatorial components of the baseline to be determined to 5 cm. Polar motion, the movement of the rotation axis of the earth in the geocentric reference frame, should be determined to within 10 cm and UT1, the earth's angular position about its rotation axis relative to inertial space, should be determined to within 0.15 msec of time.

Actual VLBI System Performance

We have performed test experiments to determine how closely our VLBI system achieves the error estimates in Fig. 2. These tests have fallen into three catagories: (1) Tests designed to isolate specific elements in our system; (2) tests designed to determine the precision of our system, i.e., how well does it repeatedly recover some invariant parameter; and (3) tests that produce results that can be compared with other high accuracy systems.

Fig. 3 presents the results of a test performed on the 1.24-km baseline connecting two antennas, Haystack and Westford, near Boston (5). On this baseline the effects of errors caused by hardware can be largely separated from those caused by the environment. The latter, which include the effects of the troposphere, the ionosphere, and geophysical phenomena, almost entirely cancel because of the very short length of the baseline. Twelve VLBI experiments were carried out on this baseline between October 1976 and May 1977; the experiments

ranged in duration from 5 hr–20 hr. The rms scatter of the 12 length estimates about the mean estimated length was 3 mm; the corresponding scatter for the vector components, not shown on this figure, were 7 mm in the vertical components and 5 mm and 3 mm in the two horizontal components. To gain some idea of the accuracy of this result it was compared with the results from an existing conventional ground survey that had a length uncertainty of 20 mm. The difference between ground survey length and that from the VLBI experiments was 8 mm. The uncertainty in the ground survey orientation made the comparision of the baseline components meaningless. This comparison certainly supports the error budget in Fig. 2. In fact, the results are substantially better than would be predicted from the budget. The main reason is that we were able on this short baseline to resolve the so-called "phase delay ambiguity." This possibility is not taken into account in the error budget.

For the past year VLBI experiments have been performed between Haystack Observatory and the Owens Valley Radio Observatory near Big Pine, Calif.—a baseline of nearly 4,000 km. The hardware system employed was the one characterized by the upper bars on Fig. 2. It contained MARK III radio frequency

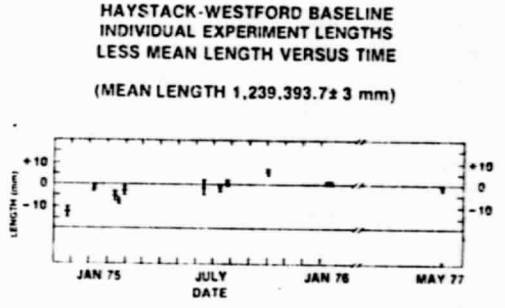

FIG. 3.—Haystack-Westford Baseline Length Results (1 mm = 0.04 mm)

equipment, i.e., parametric amplifiers and receivers, but used the MARK I data acquisition system. Based on the error budget this system should have been capable of yielding baseline length with 15-cm repeatability. Fig. 4 shows nine separate baseline length determinations spanning a period from September 1976–March 1977. The vertical lines for each point show the formal statistical uncertainty for that point. The actual root-mean-square scatter about the mean in 7 cm well within the error budget and in fact, all values fall within a 20-cm range.

This set of experiments has also been used to determine the changes in the x-component of polar motion since October 1976. The x component is the projection on the Greenwich meridian of the displacement at the earth's surface of the earth's spin axis relative to a defined geographic pole. Fig. 5 is a plot of the difference between the VLBI determinations of that displacement and those of the primary international services for polar motion, the Bureau International de l'Heure in Paris (BIH). This figure also shows a similiar plot for pole determinations made by the Defense Mapping Agency using the Doppler Satellite System. Without sufficiently good a priori knowledge of the baseline

orientation, VLBI measurements can not determine "absolute" pole position but only to its changes with time. Thus, pole position as defined by the BIH of October 4, 1978 is taken as exact. The plot shows a steady divergence between the VLBI results and those of the BIH with the difference reaching approximately 2 m in March 1977. This result is inconsistent with the claimed accuracies of both the BIH and the VLBI systems; however, the results from the Doppler Satellite System shows the same trend. In fact, had the Doppler value of the pole position on October 4 been adopted, the difference between the VLBI and the Doppler results would have remained near the uncertainty in the latter. Therefore, it appears that the discrepancy between the VLBI results and those of the BIH is due to an error in the BIH results, which are based primarily

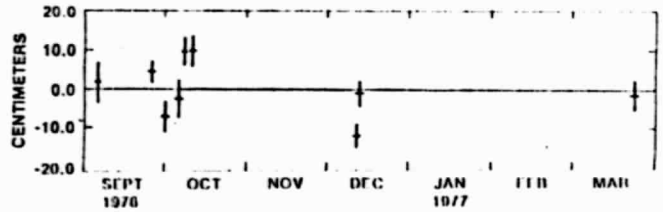

FIG. 4.—Haystack OVRO Baseline Length Residuals (Individual Experiment Results Less Mean Result; Mean = 392,888,162 cm) (1 cm = 0.39 in.)

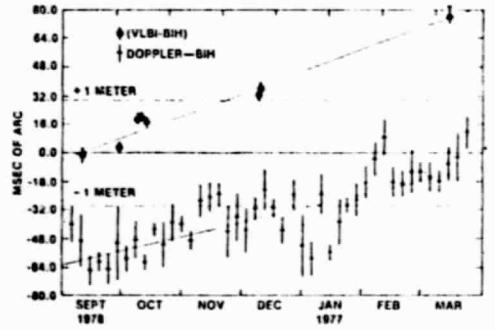

FIG. 5.—*X*-Component of Polar Motion—VLBI and Satellite Doppler Results

on optical data taken by observatories distributed around the world. It thus seems that VLBI systems, which can yield higher accuracy with far fewer observatories, may lead to a dramatic change in the way the earth's pole is tracked.

It is not possible to determine from an independent standard the accuracy of the VLBI transcontinental baseline lengths—there is simply no system with significantly better demonstrated accuracy. However, there are at least three systems now being developed which have claimed accuracies in the vicinity of those claimed for VLBI. These other systems are the satellite laser, the lunar laser, and the Doppler Satellite systems. Although there are plans to compare

all these systems, to date only comparisons between the VLBI system and the Doppler Satellite System have been made. Table 1 displays length comparisons for three baselines: Haystack to Goldstone, Calif.; Haystack to Owens Valley; and Haystack to Green Bank, V. Va. The lengths of the first two baselines are nearly 4,000 km and that of the third is more than 800 km. In order to make these comparisons the VLBI baseline determinations were transfered to the positions of the Doppler Satellite antennas using local survey information.

TABLE 1.—Intercomparisons Doppler Satellite with VLBI (Preliminary) (1 cm = 0.39 in.; 1 m = 3.28 ft)

Stations		Baseline Length		
From (1)	To (2)	Doppler, in meters (3)	VLBI, in meters (4)	Difference, in centimeters (5)
Haystack	Goldstone	3,899,798.61	3,899,798.84	−23
Haystack	Ovro	1,928,931.74	1,928,931.67	+7
Haystack	Greenbank	844,851.40	844,851.23	+17

The VLBI results for the Haystack-Goldstone and Haystack-Green Bank baselines were actually obtained about 5 yr ago with a system that was less accurate than that described in Fig. 2 (6,7); the Haystack-Owens Valley result was obtained in the nine recent experiments previously described. The claimed uncertainties in the Doppler satellite length determinations is 50 cm in all cases. The differences on all three baselines are well within the uncertainty of the Doppler Satellite results, and at least to the 1/2-m level these comparisons confirm the claims of the VLBI system.

Conclusions

Our group will soon implement a system expected to be capable of making transcontinental length measurements with 5-cm accuracies and of measuring polar motion and UT1 with comparable levels of accuracy. What then is the importance of this? To begin, the MARK III system will provide the technological basis for the establishment of a global grid of geodetic reference points of unprecedented accuracy. Beyond that the system will have the potential to measure a large number of scientifically interesting phenomena, including the following: UT1; long-term polar motion; diurnal polar motion; precession; nutation; solid earth tides; ocean loading; local crustal motions; and global plate motions. This last phenomenon has potential for profound results. Currently, geophysicists believe that the crust of the earth is made up of a small number of rigid plates, that these plates move relative to one another, and that motion at the plate boundaries causes the great earthquakes. This theory predicts that the plates are moving today with speeds of as much as 10 cm/yr, but the theory is based on data that average the plate motion over thousands and in some cases millions of years. With the possible exception of local measurements now being made in California along the San Andreas fault, there is no hard direct evidence that the plates are in motion now. Perhaps the global-scale

motion is episodic—no one knows. A few years of MARK III VLBI measurements should provide direct evidence on plate motion today. Geophysicists also speculate that variations in polar motion and UT1 are related to a variety of interesting phenomena including earthquakes, aseismic tectonic motion, core-mantle interactions, and meteorological phenomena. A detailed resolution of these effects will require a knowledge of UT1 and polar motion which VLBI has the potential to determine. With these objectives in mind the National Aeronautics and Space Administration (NASA) and the National Geodetic Survey (NGS) have under consideration a joint program to set up a polar motion and UT1 monitoring service based on MARK III technology to be operated by the NGS.

Appendix.—References

1. Coates, R. J., et al., "Very Long Baseline Interferometry for Centimeter Accuracy Geodetic Measurements," *Tectonophysics*, Vol. 29, Amsterdam, the Netherlands, 1975, pp. 9–18.
2. Hinteregger, H. F., et al., "Precision Geodesy via Radio Interferometry," *Science*, Vol. 178, Oct., 1972, pp. 386–398.
3. Holthem, L., Robertson, D. S., and Strange, W., "Orientation and Scale of Satellite Doppler Results Based on Combination and Comparison with Other Space Systems," presented at the April, 1978, 2nd International Symposium on Problems Related to the Redefinition of North American Geodetic Networks, held at, Washington, D.C.
4. Melchior, P., *Earth Tides*, Pergamon Press Ltd., Oxford, England, 1966, p. 21.
5. Rogers, A. E. E., et al., "Geodesy by Radio Interferometry: Determination of a 1.24-km Base Line Vector with 5-mm Repeatability," *Journal of Geophysical Research*, Vol. 83, No. B1, Jan., 1978, pp. 325–334.
6. Robertson, D. S., "Geodetic and Astrometric Measurements with Very-Long-Baseline Interferometry," thesis presented to the Massachusetts Institute of Technology, at Cambridge, Mass., in 1975, in partial fulfillment of the requirements for the degree of Doctor of Philosophy.
7. Shapiro, I. I., et al., "Transcontinental Baselines and the Rotation of the Earth Measured by Radio Interometry," *Science*, Vol. 186, Dec. 6, 1974, pp. 920–921.
8. Whitney, A. R., et al., "A Very-long baseline Interferometer System for Geodetic Applications," *Radio Science*, Vol. 11, No. 5, May, 1976, pp. 421–432.

Principles of Very-Long-Baseline Interferometry

Irwin I. Shapiro
Department of Earth and Planetary Sciences
Massachusetts Institute of Technology, Cambridge, Massachusetts 02139

Abstract. We present the basic principles of very-long-baseline interferometry as related to its use in the determination of vector baselines, polar motion, and earth rotation.

Introduction

Ten years ago, almost to the day, the first successful bandwidth-synthesis VLBI measurements were made. It is thus appropriate to now review the principles underlying the technique. The review will be restricted to aspects relevant to geodetic applications that involve observations of extragalactic radio sources. In such applications, arrays of two or more radio telescopes observe any given source simultaneously. From sets of observations of a suite of such sources, one can obtain the desired geodetic information: baseline-vector, polar-motion, and earth-rotation parameters.*

We shall first describe briefly the instrumentation used in these observations and then discuss the basic observables and their simplest interpretation. Finally, we consider some complications of the interpretation due to the various geophysical "signals" and non-geophysical "noise" that affect the observables.

Instrumentation

A VLBI system consists of an array of at least two antennas that observe the same radio source simultaneously. A direct electrical connection is not maintained between the antennas, thus allowing them to be separated by thousands of kilometers. The local-oscillator signals, used at each antenna to convert the radio-frequency signals from the source to the video (low-frequency) band, are derived from a frequency standard at the site. These standards are sufficiently stable that the relative phases of the signals from the source received at the two antennas are preserved.

The video signals are recorded on magnetic tape at each site, with the reference time for the recordings being derived from the same standard as is used to govern the local-oscillator signals. The tape recordings are then transported to a common center where those recorded simultaneously are cross-correlated to obtain the basic VLBI observables.

Observables

The basic observables in geodetic VLBI experiments are (i) the difference in the times of arrival at two antennas of a signal from a source; and (ii) the rate of change of this time difference. The measurement of the time-of-arrival difference can be of two types: the phase-delay difference or the group-delay difference. The phase-delay-difference observable (hereinafter "phase delay"), being based on measurements of phase, can be obtained very precisely, but usually ambiguously, due to the inability to resolve the "$2\pi n$" problem. The group-delay-difference observable (hereinafter "group delay") is usually determined with less precision than is the phase delay. But the group delay, being determined by the rate of change of phase delay with frequency, is usually unambiguous. To obtain reasonable accuracy in the measurement of group delay it is necessary to make phase-delay measurements over a wide band of frequencies simultaneously, or nearly simultaneously, since the uncertainty in the group-delay measurement is inversely proportional to this bandwidth. In practice, only a relatively narrow band of frequencies can be recorded. But this band can be split up into narrower bands which are spread over a very wide band. This technique is called bandwidth synthesis. In the newest, Mark III, system (see below), 28 narrow bands, each 2 MHz wide, are being distributed over a total band of up to 400 MHz. If the error in the measurement of phase for any one band is $\sigma(\phi)$, then the error $\sigma(\tau_g)$ in the measurement of the group delay will be given by $\sigma(\tau_g) \sim \sigma(\phi)/\Delta f$, where Δf is the rms spread of the center frequencies of the individual bands about their mean. Because these individual bands do not cover the entire spanned band, the estimate of the group delay, too, could be ambiguous. However, a proper choice of the spacing of the individual bands, as explained below, can insure that any inherent ambiguity can be eliminated reliably.

The difference of the phases of the

*Several groups are currently engaged in such geodetic applications of VLBI: (1) A group from the Goddard Space Flight Center, the Haystack Observatory, the Massachusetts Institute of Technology, and the National Geodetic Survey; (2) a Jet Propulsion Laboratory - National Geodetic Survey group; and (3) a Canadian-British collaboration. A European consortium is also being organized for similar purposes.

Proc. of the 9th GEOP Conference, *An International Symposium on the Applications of Geodesy to Geodynamics*, October 2-5, 1978, Dept. of Geodetic Science Rept. No. 280, The Ohio State Univ., Columbus, Ohio 43210.

signals that would be received at two antennas as a function of frequency exhibits curvature due primarily to the effects of the earth's ionosphere: the lower the frequency, the shorter the phase delay. The actual shape of the phase vs. frequency curve for VLBI observations will depend on the relative amounts of plasma between the source and the two sites. But with appropriate spacings of the narrow bands, one can "connect" unambiguously the phase at one band with those at all the other bands. For example, bands spaced in accord with a geometric series allows use of a bootstrap technique to connect phases first between the closest bands and then between the more widely separated bands through use of the characteristics of the curve established by the connection between the closest bands. Of course, the "absolute" phase would still be uncertain by multiples of 2π, but the relative phases between bands would be freed from any such ambiguity. Only the relative phases affect the group delay which is equal to the slope of the curve of phase delay vs. (angular) frequency.

Information Content

We now consider the information content of the observables under simplified assumptions. In particular, let us ignore the propagation medium and assume that the earth is rigid and rotates with a constant, known, angular velocity. We may then write the expression for the delay observable as a function of time as:

$$\tau(t) = \frac{1}{c}\vec{B}(t)\cdot\hat{s} + \tau_o^{cl} + \dot{\tau}_o^{cl}\,[t-t_o] \quad , \qquad (1)$$

where $\vec{B}$ is the baseline vector connecting a pair of antennas, $\hat{s}$ is a unit vector in the direction of the source, and τ_o^{cl} and $\dot{\tau}_o^{cl}$ are, respectively, the offsets in epoch and rate of the clock at one site with respect to those at the other site. This equation represents a diurnal sinusoid added to a straight line. The first term in the equation contributes the diurnal sinusoid due to the rotation of the baseline vector in inertial space. The slope of the straight line is due to the clock-rate offset and the intercept is due to a combination of the clock-epoch offset and the product of the polar components of $\vec{B}$ and $\hat{s}$. Clearly this curve can be specified by four parameters: the intercept and slope of the straight line, and the amplitude and phase of the sinusoid. (We do not consider the period of the sinusoid, since that is given by assumption.) Thus four measurements of the delay suffice, in principle, to determine $\tau(t)$; any additional measurements will be redundant. But how many unknown parameters are there for this situation? Naively, one would conclude that the baseline vector contributes three, the source two, and the clocks two, for a total of seven. However, the origin of right ascension of our system is arbitrary; only the origin of declination is fixed by the assumption of a known angular velocity for the earth. Since the right ascension of the source can be used to define this arbitrary origin, the number of unknown parameters is only six. Nonetheless, a unique solution cannot be obtained for these six parameters from observations of a single source. Observations of each additional source adds two unknowns: the coordinates of the source on the plane of the sky. But such observations also can be used to determine three additional parameters: the intercept of the straight line and the amplitude and phase of the sinusoid appropriate for the additional source. The slope of the straight line provides no new information since it is determined solely by the clock-rate offset. It is clear that with four observations of one source and three each of two more sources, a useful solution for all of the parameters of this simple model can in general be determined. (The measurements of delay rates simultaneously do not reduce the requirement for observations of three sources.) The accuracy of the determination of these ten parameters will depend, of course, not only on the accuracy of the measurements of delay (and delay rate), but also on the baseline, the distribution of the sources in the sky, and the distribution of the observations in time.

Complications

The situation actually encountered with VLBI is, of course, far more complicated than outlined in the previous section. We can conveniently divide these complications into two categories: signals and noise. Here signals refer to those effects on the observables which are of geophysical interest, and noise refers to those of no intrinsic interest. (This point of view, needless to say, is a rather parochial one since one person's noise is often another's livelihood.)

We shall consider precession, nutation, solid-earth tides, crustal motions, variations in UT1, and polar motion to be signals. On the other hand, clock instabilities and uncertainties in our knowledge of source characteristics and of the propagation medium shall be considered as noise. We discuss each set in turn.

Signals

Precession and Nutation. Changes in the direction in space of the spin axis of the earth with periods long compared

to a day are sensed with VLBI through the corresponding changes in the coordinates of the radio sources. These changes will, however, preserve the arclengths between sources. At present, estimates of the precession constant made from VLBI measurements have an uncertainty of a few tenths of an arcsecond per century, several-fold larger than the uncertainty associated with the presently accepted value based on optical observations. The VLBI estimate is consistent with the optical one to within twice the formal standard error of the former. No estimates of any of the nutation terms have yet been made.

Solid-Earth Tides. The semi-diurnal solid-earth tide imparts a distinctive signature to the VLBI observable, since almost all other effects introduce a diurnal signature. The maximum magnitude of this effect on the observable has been slightly greater than one nanosecond. Thus estimates of the local values of the vertical and horizontal Love numbers, ℓ and h, can be obtained from VLBI data. Current estimates agree, to within their uncertainty of about 0.05, with the "expected" values.

Crustal Motion. Changes in crustal configuration can be sensed by long-term changes in baseline lengths; in addition, significant changes in the corresponding baseline directions for an array of antennas would signify crustal motions provided that these changes were incompatible with a rigid rotation of the array. No measurements of crustal motions have yet been obtained from VLBI data, but there is every reason to believe that such motions will be detected within a few years.

UT1 and Polar Motion. Variations in the rate of rotation of the earth and in the position of the axis of figure with respect to the axis of rotation affect the directions of baseline vectors. As with the arclengths between sources with respect to precession and nutation, the lengths of baselines are unaffected by such variations in the rate of rotation of the earth and in the position of the pole.

We should stress that the VLBI observables, for an arbitrary baseline, have no sensitivity to the "initial" orientation of the earth and direction (in space) of its axis of figure. Only changes in these quantities can be detected. In addition, any "common-mode" errors in the epoch settings of the clocks at the antenna sites will be indistinguishable from corresponding changes in the orientation of the earth about its spin axis (UT1). Finally, note that VLBI data obtained for one baseline are sensitive to only two independent combinations of the three parameters needed to specify changes in the position (in space) of the axis of figure of the earth and in the orientation of the earth about this axis: Such changes affect only the direction of the baseline which is described by only two independent parameters. Consider, as an example, a wholly north-south baseline. With such a configuration, the VLBI data would have no sensitivity to a rotation of the earth about the pole. For an east-west baseline, on the other hand, polar motion in a direction along the meridian of the midpoint of the baseline would not affect the VLBI observables. In both these cases, the baselines would undergo parallel displacements which cannot be detected from observations of sources "at infinity." Two baselines, or at least three antennas, are needed in a VLBI array to detect all three components of the changes in UT1 and pole position. These baselines must, of course, not be parallel.

Estimates of UT1 and polar motion from VLBI data now have accuracies comparable to those of other techniques, such as the classical optical methods, the Doppler tracking of satellites (for polar motion), and the laser ranging to retroflectors on the moon (for UT1). It is expected that the accuracy of the VLBI estimates will improve nearly tenfold within the next five years due primarily to the introduction and use of the new, Mark III, VLBI system. A prototype of this system has already been tested successfully; five copies of the complete system are currently under construction for placement at suitably distributed antennas. It will be important to check the improved determinations of polar motion and UT1 through redundancy and through comparison with the results from other improved techniques in order to assess the accuracy of these determinations.

Noise

Clock Instabilities. The two parameters, for clock epoch and rate offsets, do not provide an adequate representation of the relative behavior of the clocks at any two antennas of an interferometric array over the period of many hours needed to determine the baseline vector, source positions, etc. This statement applies to the current field units of all atomic clocks, including the hydrogen-maser frequency standards.

A number of possibilities exists to minimize the impact of these clock instabilities on the accuracy with which geophysical information can be extracted from VLBI data. First, one can use higher-order polynomials to represent the relative clock behavior; here the point of "diminishing returns" sets in at about the sixth order. Second, the clock performance, especially of hydrogen-maser standards, can be improved to match that achieved in the laboratory. The sensiti-

vity of the maser standards to environmental effects can also be reduced to minimize the introduction of diurnal signatures into the VLBI data. Third, one can reduce the effects of long-term drifts in the relative clock behavior by using clock stars. Thus, one can make observations repeatedly, say every hour, of some suitable source and use these observations to correct for the relative clock drifts. To be suitable, this source should be visible from both sites for a large fraction of the diurnal cycle and should yield a reasonably large correlated flux density so that accurate delay observations are possible to make.

Source Characteristics. The radio sources affect the determination of geophysically interesting quantities through the strength of their radio emissions, their distribution on the sky, and the accuracy with which we can determine their positions. These positions, in turn, depend on the structure and internal kinematics of the regions of radio emission in each object.

At present, the entries in the catalog of known, and potentially-usable, extragalactic radio sources number in the hundreds. Positions of a few dozen of those with the strongest emissions are now being determined routinely with an estimated accuracy of about 0".02, except for the declinations of sources that lie near the equatorial plane. The accurate determination of the declination of those sources requires the use of interferometers with baselines that possess large components in the north-south direction. Few such baselines have so far been available for extensive sets of measurements.

Aside from the examination of the characteristics of the postfit residuals, the main method for assessment of the accuracy of source-position determinations is the comparison of results obtained with different equipment. Such comparisons, made several years ago and based on data obtained with somewhat less advanced VLBI systems, showed agreement to within about 0".05 rms. (Note that a 0".001 error in source position corresponds approximately to a two-centimeter error in length for a 4,000-km baseline.)

Most extragalactic radio sources are not "points" when viewed on the scale of milliarcseconds. Rather, they exhibit complicated structure. This structure in their brightness can be mapped and a suitable feature in the map, or the overall center of brightness, can be used as a reference point. There are, however, technical difficulties in the determination of unambiguous brightness maps. These difficulties are being overcome and reliable maps on the scale of tenths of a milliarcsecond are now being obtained for some of the radio sources.

There is yet a further difficulty in the use of extragalactic radio sources: most are not static. Dramatic changes have been observed in the brightness structure of some of these sources at the level of tenths of a milliarcsecond in angular resolution on a time scale of a few months. Thus, to enable positions of extragalactic radio sources to be used effectively as a reference system at the level of milliarcsecond accuracy for geophysical applications of VLBI, one must monitor the brightness distributions of these sources as a function of time and, perhaps, as a function of radio frequency as well.

Propagation Medium. In regard to any substantial effects on VLBI data, the propagation medium can be considered to be composed of two components: the ionosphere and the troposphere. The effects of the ionosphere can, and will, be virtually eliminated by observing simultaneously in two widely separated radio frequency bands (≃2GHz and ≃8GHz). The Mark III VLBI system is equipped for such dual-band observations. Moreover, enough suitable sources exist to allow effective use of the dual-band technique.

The troposphere is in effect non-dispersive at radio frequencies and is therefore a more troublesome contributor of noise. The troposphere can also be decomposed into two components: wet and dry. For the latter, the assumption of hydrostatic equilibrium is a very good one; measurements at each site of surface pressure combined with a good model of the atmosphere, then allows a good estimate to be made of the phase delay added in the zenith direction by the dry component: about 7.5 nanoseconds (equivalent to an increase in path length of about 2.3 m). It is widely thought that the error in this estimate can be kept at the 0.1% level or perhaps below. Mapping to other zenith angles, however, will increase the error somewhat since the "slant" atmospheric path length cannot be determined so accurately from the pressure measurement at the antenna site. The situation with the wet component is more difficult. The water-vapor in the atmosphere is not in hydrostatic equilibrium and is quite variable in amount. Although the total effect on the path length of radio waves is, on average, only about 7% of that of the dry component, the wet component cannot be modeled accurately. Various simple techniques have been used to try to ameliorate this problem. Such techniques involve various combinations of model atmospheres and mapping functions with or without dependence on surface measurements of temperature, pressure, and dew point, and with or without parameters that can be estimated for each site from short, ~8 hr, spans of data. Unfortunately, these techniques may well be defi-

cient, especially for long baselines, in removing the effects of the atmosphere on the estimates of the "vertical" component of the baseline with which they are highly correlated.

The technique which has elicited the greatest expectations for providing the solution to the wet-component problem is based on the use of radiometer measurements at each site of the brightness temperature of the atmosphere at and near the ≈23GHz line in the spectrum of water-vapor emission. Studies indicate that this brightness temperature can be related with reasonably high accuracy to the excess path length attributable to the water-vapor content of the atmosphere. However, to date, almost all VLBI results have been obtained without the benefit of water-vapor radiometer measurements.

Atmospheric effects thus loom as the limiting factor in the accuracy achievable with VLBI in the determination of geophysical quantities. What will that limit be? An assessment based on theory alone is unlikely to be accurate. Measurements are clearly called for. Series of VLBI experiments should be made with supplementary water-vapor radiometer measurements, under a variety of local weather conditions, and for various baseline lengths. For short baselines, up to several kilometers in length, independent determination of the baseline vector can usually be made, with some effort, at the millimeter level of accuracy by means of conventional survey techniques. For long baselines, up to several thousand kilometers in length, independent means of verification at the relevant level of accuracy seem to be limited to laser ranging to artificial satellites or to the moon; such verification, however, will not be easy nor inexpensive for a number of practical reasons. The repeatability and consistency of VLBI results themselves may well have to provide the main standards. Since suitably accurate, and independent, estimates of UT1 and polar motion may not be available, repeated checks on the individual components of the vector baseline will likely require multi-site experiments, say with four or more separated antennas, to reduce the confusion between UT1 and pole position changes on the one hand and changes in baseline direction on the other. The many antenna sites serve to over-determine UT1 and polar motion, with the redundancy providing the meaningful check on the consistency of the estimates of some of the baseline components. For some combination of the precision and the time spanned by the sets of measurements, one must be concerned also about the genuine changes in baselines expected from plate tectonics; of course, detection of such changes are a major purpose of the measurements.

At present, checks on the repeatability of baseline determinations have involved primarily two-element interferometers. For short baselines, of the order of one kilometer in length, repeatability has been obtained at the five millimeter level in all components, and verified later by the results of a conventional survey. For long baselines, of the order of several thousand kilometers in length, only repeatability in baseline length has been meaningful; here the spread about the mean in a recent series of a dozen sets of measurements was under five centimeters. The source positions used in the analysis of each of these experiments were fixed in accord with the results from the ensemble of experiments; errors in these positions tended therefore not to have a serious effect on the repeatability of the determinations of baseline length.

Conclusion

The future of VLBI as applied to geodetic and geophysical problems, especially to the determination of UT1 and polar motion, looks quite bright. Although the last ten years have been devoted almost exclusively to the development of VLBI, the next ten should yield significant results.

Acknowledgment

This work was supported in part by the National Science Foundation and in part by the National Aeronautics and Space Administration.

Bibliography

Cannon, W. H., et al., 1979, J. Geophys. Res., 84, in press.

Cohen, M. H., et al., 1977, Nature, 268, 405.

Clark, T. A., et al., 1976, Astron. J., 81, 599.

Ong, K. M., et al., 1976, J. Geophys. Res., 81, 3587.

Robertson, D. S., et al., 1979, Proc. of IAU Colloq. No. 82, in press.

Rogers, A. E. E., et al., 1978, J. Geophys. Res., 83, 325.

Shapiro, I. I., et al., 1974, Science, 186, 920.

Thomas, J. B., et al., 1976, J. Geophys. Res., 81, 995.

Synchronization of Clocks by Very-Long-Baseline Interferometry

THOMAS A. CLARK, CHARLES C. COUNSELMAN, III, MEMBER, IEEE, PETER G. FORD, LEONARD B. HANSON, HANS F. HINTEREGGER, WILLIAM J. KLEPCZYNSKI, CURTIS A. KNIGHT, DOUGLAS S. ROBERTSON, ALAN E. E. ROGERS, MEMBER, IEEE, JAMES W. RYAN, IRWIN I. SHAPIRO, AND ALAN R. WHITNEY, MEMBER, IEEE

Abstract—**Two hydrogen-maser clocks, one at the Haystack Observatory in Massachusetts and one at the National Radio Astronomy Observatory in West Virginia, were synchronized by means of very-long-baseline interferometry (VLBI) observations of several extragalactic radio sources on March 28, and again on September 23, 1977. Observations were made sequentially in eight 360-kHz bands distributed between about 8.4 and 8.5 GHz with spacings designed to enable the group-delay difference between the signals received at the two observatories from a given source to be estimated unambiguously, within an uncertainty of less than 1 ns set by receiver noise. The epoch and the rate differences between the observatories' clocks for each experiment were estimated by analysis of observations that spanned several hours. The application of corrections for the contributions to the delays of the antennas, feeds, receiver systems, and recorders, yielded absolute determinations of the clock epoch differences. During each experiment, portable cesium clocks were flown from the U.S. Naval Observatory in Washington, DC, to the observatories and back. The traveling-clock data, analyzed in each case after the VLBI synchronization had been completed, confirmed the VLBI results to within 18 and 14 ns for the first and second experiments, respectively.**

I. Introduction

IN PRINCIPLE, it has been possible for several years to synchronize clocks accurately by means of very-long-baseline interferometry (VLBI) observations of extragalactic radio sources [1], [2]. In fact, the atomic clocks utilized in many astrometric and geodetic VLBI experiments [3]–[5] have been synchronized with standard errors at the nanosecond level or below. But these impressively small uncertainties have represented only internal, statistical measures of precision. Externally verifiable, or "absolute" accuracies have usually been limited to the microsecond level or above, by uncertainties in instrumental delays, and by unresolved ambiguities in the determinations of the group-delay differences between the signals received at the two antennas [6]. Accurate absolute synchronization by VLBI was recently demonstrated for the first time for a short (~ 1 km) baseline [7]. In this experiment, care was taken to estimate or to measure all instrumental delays and to resolve all delay ambiguities. Here we report the first accurate synchronization results for a relatively long, 845-km baseline. Synchronization via a real-time satellite link between widely separated VLBI sites was accomplished slightly earlier [8], but the accuracy achieved was nearly an order of magnitude lower than in our experiments.

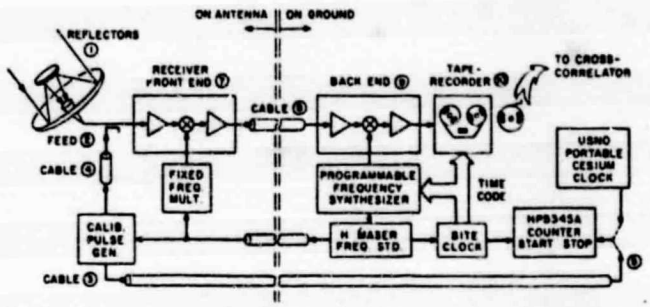

Fig. 1. Block diagram of VLBI Terminal. Numbers refer to corresponding entries in Table I.

II. Experiments

Our two synchronization experiments involved the hydrogen-maser clocks at the 37-m diameter radio telescope of the Haystack Observatory in Westford, MA, and the 43-m diameter radio telescope of the National Radio Astronomy Observatory (NRAO) in Green Bank, WV. The first experiment was conducted on March 28, and the second on September 23, 1977. Fig. 1 shows a block diagram of the interferometer terminals used.

The Massachusetts Institute of Technology experimenters were supported in part by the NSF under Grant EAR76-22615 and in part by the NASA under Grant NGR22-009839. The Haystack experimenters were supported by NASA contract NAS5-22843. All NASA support was obtained from the Office of Space and Terrestrial Applications. Radio astronomy programs at the Haystack Observatory are conducted with support from the NSF, Grant GP-25865. Lincoln Laboratory is operated with support from the U.S. Air Force. The National Radio Astronomy Observatory is operated by Associated Universities, Inc., under contract with the NSF.

Manuscript received March 19, 1979; revised June 12, 1979.

T. A. Clark and J. W. Ryan are with the Goddard Space Flight Center, Greenbelt, MD 20771.

C. C. Counselman, III, P. G. Ford, and I. I. Shapiro are with the Department of Earth and Planetary Sciences, Massachusetts Institute of Technology, Cambridge, MA 02139.

L. B. Hanson is with the M.I.T. Lincoln Laboratory, Lexington, MA 02173.

H. F. Hinteregger, C. A. Knight, A. E. E. Rogers, and A. R. Whitney are with the Haystack Observatory, Northeast Radio Observatory Corporation, Westford, MA 01886.

W. J. Klepczynski is with the U.S. Naval Observatory, Washington, DC 20390.

D. S. Robertson is with the National Geodetic Survey/National Ocean Survey, National Oceanic and Atmospheric Administration, Rockville, MD 20852.

0018-9456/79/0900-0184$00.75

TABLE I
DETERMINATION OF DIFFERENCES BETWEEN EPOCHS INDICATED BY HAYSTACK AND NRAO CLOCKS FROM VLBI EXPERIMENTS

Line Number (See Figure 1)	Description	Delay or Time Difference (μs) 28 March Haystack	28 March NRAO	23 September Haystack	23 September NRAO	Method of Determination
1	Antenna reflector geometry	0.070	0.052	0.070	0.052	Estimated from mechanical drawing
2	Antenna feed	0.009	0.002	0.009	0.002	Estimated from mechanical drawing
3	Cable	0.605	0.591	0.605	0.587	Measured with time-domain reflectometer. At NRAO, different cables were used on on the two dates.
4	Cable	0.008	0.009	0.008	0.009	Estimated from measured physical length.
5	Site clock epoch minus calibration pulse epoch	0.778	0.763	0.758	0.131	Measured with HP5345A counter. Differences due to different cables and clock settings used on different dates.
6	Delay of multi-band signal, referred to receiver input and corrected for delay of calibration pulse to receiver input	-0.102	-0.127	-0.082	0.501	Lines (1)+(2)-{(4)+[(5)-(3)]}
7	Receiver front end	0.01	0.01	0.01	0.01	Estimated from circuit parameters
8	Cable	0.61	0.63	0.61	0.63	Measured with time-domain reflectometer
9	Receiver back end	5.60	5.00	5.60	5.00	Estimated from measured impulse response
10	Tabe recording system	-21.01	-22.14	-21.01	-22.14	Measured by test signal injection
11	Net delay of single-band signal, referred to recorder output	-14.71	-16.45	-14.71	-16.45	Lines (1)+(2)+(7)+(8)+(9)+(10)
12	NRAO clock epoch minus Haystack clock epoch, from single-band VLBI data		20.21		15.53	Multi-parameter solution (epochs: 19:20 UTC, 28 March 1977 and 15:20 UTC, 23 September 1977)
13	Line 12 corrected for single-band net delay		21.95		17.27	Lines $(12)-[(11)_N-(11)_H]$
14	NRAO clock epoch minus Haystack clock epoch, from multi-band VLBI data (ambiguous)		xx.813		xx.820	Same as line (12), but based on multi-band VLBI data
15	Line 14 corrected for multi-band delay to receiver input		xx.838		xx.237	Lines $(14)-[(6)_N-(6)_H]$
16	NRAO clock epoch minus Haystack clock epoch		21.838		17.237	1 μs ambiguity resolved by line (13)

TABLE II
DETERMINATION OF DIFFERENCE BETWEEN EPOCHS INDICATED BY HAYSTACK AND NRAO CLOCKS FROM COMPARISON WITH USNO PORTABLE CS CLOCKS PC653 AND PC1255 ON 28 MARCH 1977

Line Number	Clocks Compared	Difference (μs)	Time and Place of Comparison
1	PC653 clock epoch-PC1255 clock epoch	1.813	13:10 UTC, 28 March 1977, in Washington, D.C., before departures for VLBI sites
2	PC653 clock epoch-PC1255 clock epoch	1.839	03:10 UTC, 29 March 1977, after return to Washington, D.C.
3	Haystack clock epoch-PC 1255 clock epoch	13.120	19:11 UTC, 28 March 1977, at Haystack
4	NRAO clock epoch-PC653 clock epoch	33.114	19:28 UTC, 28 March 1977, at NRAO
5	NRAO clock epoch-Haystack clock epoch	21.820	Lines (4)-(3)+[(1) + (2)]/2

In these experiments, the difference between the group delays of a signal traveling to the two sites from a distant quasi-stellar radio source was measured using a bandwidth synthesis technique [6], [9]. In particular, the signal in eight 360-kHz bands, spaced between 8391 and 8491 MHz, was sampled sequentially. Each such multiband delay measurement had a 1 μs ambiguity imposed by a 1-MHz common divisor of the spacings between the centers of the narrow, 360-kHz bands. However, the ambiguity was eliminated by using the less precise, but unambiguous, delay measurement obtained from the cross-correlation of the signals received at the two sites in a single 360-kHz band.

To utilize these delay measurements properly in the synchronization of the clocks at the two sites, it was necessary to determine a number of instrumental delays. The delays due to the antennas and feeds were estimated from drawings, whereas the delays due to the receiver systems, from preamplifier through recorder, were directly measured as a function of frequency across the 100 MHz synthesized band. For this latter purpose, a periodic train of pulses was injected into the receiver input. Each pulse was less than 30 ps wide with the interpulse interval being 1 μs [10].

The difference between the readings of the independent clocks at the two sites was derived for each experiment from the analysis of VLBI observations of several radio sources, by simultaneous estimation of baseline vectors and clock-difference parameters [11]. The positions of the radio sources had been determined previously [12]. In the first experiment, the clock synchronization via VLBI was checked by transporting two cesium clocks from the U.S. Naval Observatory (USNO) in Washington, DC, one to each of the telescopes, and both back to Washington. In the second experiment, two cesium clocks were transported together from the USNO to NRAO, then to Haystack, and finally back to the USNO. For each experiment, the round-trip travel times of the clocks were about half a day.

III. RESULTS

The result for the clock synchronization from the VLBI experiment performed on March 28, 1977 is given in Table I. The first six lines describe the determinations of the delays of the multiband signals through the Haystack and NRAO systems. Lines seven through thirteen refer to the single-band signal and serve only to remove the 1 μs ambiguity from the corresponding multiband epoch difference. The final value, in line 16, shows the estimated difference between the epochs of the hydrogen-maser clocks at the two radio telescopes, after corrections were applied both for the instrumental delays and for the resolution of the integral microsecond ambiguity. This result should be compared with line 5 of Table II, which shows the difference between these two clocks as estimated from the traveling clocks, after the readings of the latter were corrected via linear interpolation for relative drift, based on pre- and post-trip comparisons. The magnitude of the difference between the VLBI and the traveling-clock results was 18 ns.

Table I also shows the VLBI result from the experiment performed on September 23, 1977; Table III gives the corresponding result from the traveling clocks. For this experiment, since Haystack was visited by the traveling clocks approximately seven hours later than NRAO, it was necessary to account for the estimated drifts, over this interval, of the traveling clocks relative to Haystack's clock. (See line 8 of Table III.) The latter's rate was already known relative to that of the USNO Master Clock through long-term comparisons via Loran C. The rates of the traveling clocks were determined from direct comparisons with this Master Clock, before and after the trip. For this experiment, the magnitude of the difference between the VLBI and the traveling-clock synchronization results was 14 ns.

In both experiments, the VLBI results were obtained before those from the traveling clocks. In the first experiment, the VLBI result was in hand less than 24 hours after the observations had been completed, the magnetic tapes recorded at NRAO having been placed on the first available airplane flight to Boston.

The accuracies of the VLBI clock synchronizations were not limited by the uncertainties in the measurements of the delay differences of the signals received from the radio sources; these uncertainties were generally well under 1 ns. The limiting uncertainties were in the corrections for the various instrumental delays. The total error from these sources is estimated to be under 10 ns. The uncertainties of

TABLE III
DETERMINATION OF DIFFERENCE BETWEEN EPOCHS INDICATED BY HAYSTACK AND NRAO CLOCKS FROM COMPARISONS WITH USNO PORTABLE CS CLOCKS CS1117 AND CS1368 ON 23 SEPTEMBER 1977

Line Number	Clocks Compared	Difference (μs)	Time and Place of Comparison
1	Haystack clock epoch - Cs 1117 clock epoch	16.430	22:27 UTC, at Haystack
2	Haystack clock epoch - Cs 1368 clock epoch	17.184	22:27 UTC, at Haystack
3	Average of lines (1) & (2)	16.807	
4	NRAO clock epoch - Cs 1117 clock epoch	33.658	15:19 UTC, at NRAO
5	NRAO clock epoch - Cs 1368 clock epoch	34.426	15:19 UTC, at NRAO
6	Average of lines (4) & (5)	34.042	
7	NRAO clock epoch - Haystack clock epoch	17.235	Uncorrected for drifts
8	NRAO clock epoch - Haystack clock epoch	17.223	Referred to epoch of 15:20 UTC by use of Cs clock mean drift rate of 3.05 (±0.05) ns/hr and Haystack hydrogen-maser mean rate of 1.3 (±0.2) ns/hr, both measured relative to USNO Master Clock (short-term "jitter" in the clock rates have no significant effect on this correction).

the synchronizations via the traveling clocks were limited by unmodelled clock drifts, and are estimated to be under 20 ns. No corrections were made for the net relativistic effects on the readings of the traveling clocks since these effects were under 5 ns.

It should be emphasized that the accuracy in the absolute synchronization of clocks with VLBI is not limited to the 10 ns level achieved in the present experiments. Several different techniques have been proposed [7] for use with VLBI to obtain absolute clock synchronization at a subnanosecond level of accuracy over transcontinental and intercontinental distances.

ACKNOWLEDGMENT

We thank W. E. Carter for the suggestion that the traveling clocks be taken together to the two VLBI sites for the second experiment.

REFERENCES

[1] M. H. Cohen, "Introduction to very-long-baseline interferometry," *Proc. IEEE*, vol. 61, pp. 1192–1197, Sept. 1973.
[2] C. C. Counselman, III, "Very-long-baseline interferometry techniques applied to problems of geodesy, geophysics, planetary science, astronomy, and general relativity," *Proc. IEEE*, vol. 61, pp. 1225–1230, Sept. 1973.
[3] H. F. Hinteregger *et al.*, "Precision geodesy via radio interferometry," *Science*, vol. 178, pp. 396–398, Oct. 27, 1972.
[4] I. I. Shapiro *et al.*, "Transcontinental baselines and the rotation of the earth measured by radio interferometry," *Science*, vol. 186, pp. 920–922, Dec. 6, 1974.
[5] J. B. Thomas *et al.*, "A demonstration of an independent-station radio interferometry system with 4-cm precision on a 16-km base line," *J. Geophys. Res.*, vol. 81, pp. 995–1005, Feb. 10, 1976.
[6] A. E. E. Rogers, "Very long baseline interferometry with large effective bandwidth for phase-delay measurements," *Radio Sci.*, vol. 5, pp. 1239–1248, Oct. 1970.
[7] C. C. Counselman, III, *et al.*, "VLBI clock synchronization," *Proc. IEEE*, vol. 65, pp. 1622–1623, Nov. 1977.
[8] S. H. Knowles *et al.*, "Real-time accurate time transfer and frequency standards evaluation via satellite link long baseline interferometry," in *Proc. 9th PTTI Meeting* (Technical Memorandum 78-104, NASA Goddard Space Flight Center, Greenbelt, MD), 1978.
[9] A. R. Whitney *et al.*, "A very-long-baseline interferometer system for geodetic applications," *Radio Sci.*, vol. 11, pp. 421–432, May 1976.
[10] A. E. E. Rogers, "A receiver phase and group delay calibration system for use in very-long-baseline interferometry," NEROC Haystack Observatory, Westford, MA, Haystack Technical Note 1975-6, 1975.
[11] I. I. Shapiro, "Estimation of astrometric and geodetic parameters," in *Methods of Experimental Physics*, vol. 12, Part C, M. L. Meeks, Ed. New York: Academic Press, 1976, pp. 261–276.
[12] T. A. Clark *et al.*, "Radio source positions from very-long-baseline interferometry observations," *Astron. J.*, vol. 81, pp. 599–603, Aug. 1976.

Charles C. COUNSELMAN III and Irwin I. SHAPIRO
Department of Earth and Planetary Sciences
Massachusetts Institute of Technology
Cambridge, Massachusetts 02139

MINIATURE INTERFEROMETER TERMINALS FOR EARTH SURVEYING

Summary

A system of miniature radio interferometer terminals is proposed for the measurement of vector baselines with uncertainties ranging from the millimeter to the centimeter level for baseline lengths ranging, respectively, from a few to a few hundred kilometers. Each terminal would have no moving parts, could be packaged in a volume of less than 0.1 m^3, and could operate unattended. These units would receive radio signals from low-power (< 10 w) transmitters on Earth-orbiting satellites. The baselines between units could be determined virtually instantaneously and monitored continuously as long as at least four satellites were visible simultaneously. Acquisition of the satellite signals by each terminal would require about one minute, but less than a second of signal integration, and the collection of only a few kilobits of data from two receiving units would suffice to determine a baseline. Different baseline lengths, weather conditions, and desired accuracies would, in general, dictate different integration times.

1.0. Introduction

The technique of very-long-baseline interferometry (VLBI) is only a decade old and barely approaching adolescence. Nonetheless this radio interferometric method has seen broad application, especially in astronomy. In geodetic applications, the demonstrated level of repeatability of baseline-length determinations ranges from ~ 3 mm for ~ 1 km distances [1] to ~ 3 cm for transcontinental distances [2]. This combination of precision and range should make VLBI a very powerful technique for monitoring the time dependence of regional and continental baselines. Yet it is still not widely used for this purpose. Why? A principal reason has been cost. Applications of VLBI to geodesy have hitherto involved observations of the random, weak, radio signals received from distant, extragalactic, sources. The achievement of useful signal-to-noise ratios with these sources has dictated the use of large diameter antennas, expensive atomic frequency standards, and wideband tape-recording and correlating systems.

In contrast, only very small, simple, and inexpensive ground equipment is required to utilize the relatively strong, precisely controlled, radio signals that can be transmitted from Earth satellites. Nonetheless, although several methods have employed satellite signals to determine baselines, none of these methods has yet achieved the measurement precision demonstrated with VLBI. Why not? What is the "secret ingredient" of the interferometric technique? Basically it is the use of ***differencing***. Interferometry, ***per se***, involves the differencing of the phases of signals received at the two ends of a baseline. With properly designed equipment, the inherent "2π" ambiguity in these phases of radio signals from a given source can be eliminated, and

Bull. Geod. 53 (1979) pp. 139-163.

C.C. COUNSELMAN III and I.I. SHAPIRO

advantage taken of precise phase measurements of the signals from several sources, to determine a baseline with an uncertainty equal to a small fraction of the wavelength of the radio signals. Further, this baseline determination does not depend on the signals from any source having any particular temporal regularity.

The baseline vectors determined by radio interferometric techniques can be related to the best known approximation to an inertial frame -- the positions in the sky of compact, extragalactic, radio sources. Of course, when the baseline vector is determined from interferometric observations of radio signals from satellites, an extra step is required to relate the positions of the satellites to those of the distant radio sources. Again, the technique used is interferometric but, here, use of the full panoply of the conventional VLBI armamentarium is required.

A system that combines the advantages of VLBI with the benefits of strong satellite signals could open a new era in geodesy. We describe a relatively simple system here. It would employ compact ground equipment with no moving parts and low-power radio transmitters on a set of satellites. We dub this combination the Mighty MITES System, MITES being an acronym for Miniature Interferometer Terminals for Earth Surveying. Our system appears to be potentially more efficient than any other so far proposed for the three-dimensional monitoring of crustal strain accumulation and release over distances ranging from tens of meters to hundreds of kilometers. This system could also be applied to a variety of other surveying and navigation problems on land, sea, and air, and in space.

2.0. System Description

In this section we discuss, in turn, the basic concepts underlying our proposed system, our preliminary thoughts on the design of the relevant satellite and ground equipment, and some possible design modifications.

2.1. Basic Concepts

Here we outline briefly some of the concepts upon which our proposed system is based.

2.1.1. Observable

The basic quantity that would be measured with this system is the interferometric phase -- the difference between the phases of radio signals from a single satellite received at any two terminals. These phases would each be obtained simultaneously for a set of different radio frequencies ("tones") covering a wide, ~ 1 octave, band so that (i) the effect of the ionosphere could be virtually eliminated, and (ii) the inherent "2π" ambiguity of the phase observable could be resolved. Measurements of the frequencies of the received signals would be made concurrently to enable conversion of the phase differences to corresponding delay differences.

2.1.2. Baseline Determination

These delay differences could be interpreted in a standard manner to determine the components of the baseline vector. For observations of a given satellite at a given instant, the interferometric phase delay can be expressed approximately as

$$\tau = \frac{1}{c}\vec{B}\cdot\hat{s} + \tau^{cl} \quad , \qquad (1)$$

Errata Sheet

C.C. COUNSELMAN III and I.I. SHAPIRO
Miniature Interferometer Terminals for Earth Surveying
Bull. Géod. 53-2 (1979) pp. 139-164

p. 139 (Summary) line 2. In place of : "the millimeter to the centimeter level"
read : "a few millimeters to a few centimeters"

p. 139 line 5. In place of : " $\sim$3cm" *read* " $\sim$5cm"

p. 140 line 2. In place of : "equal to a small fraction", *read :* "as small as a fraction"

p. 141 line 6. In place of : "Section 3.1", *read :* "Section .0"

p. 141 line 33. In place of : "We define", *read :* "We defer"

p. 144 line 5. In place of : "dowlink", *read :* "downlink"

p. 144 Table 1. In place of : "Total DC Input $\leq$ 35 W"
read : "Total DC Input $\leq$ 36 W"
and in place of : "Gain $\lesssim$ 10 db"
read : "Gain $\sim$ 10 db"

" " " "

p. 156 line 9. In place of : "three centimeter", *read :* "four centimeter"

p. 157 line 6. In place of : "3.1", *read :* "3.0"

p. 157 formula (2). In place of : " $\tilde{\tau}_{10}$ ", *read :* " $\tilde{\tau}_{12}$ "

p. 162 line 24. In place of : "at both the ν 1.6 GHz", *read :*
"at both the ν 1.2 GHz and ν 1.6 GHz"

p. 162 line 31. In place of : "were viable .... could be achieved"
read : " is viable ..... can be achieved"

p. 163 line 4 and qq. In place of : "To cut this figure .... Section 2.3)"
read :

"Such obstacles could serve to complicate the elimination of the 2π phase ambiguities at least by the need to observe for long periods of time, perhaps up to several hours or more.

We conclude that the need to decode the GPS signals and to eliminate the 2π ambiguities in phase will require rather more expensive ground terminals and substantially longer observation times than would the Mighty MITES System to achieve comparable accuracies in baseline determination.

p. 163 References

2 : date is 1979

15 : contract NAS 5-20975

where $\vec{B}$ is the baseline vector, $\hat{s}$ is a unit vector in the direction of the satellite being observed, and τ^{cl} represents the difference between the epoch settings of the clocks at the two terminals (i.e., their departure from synchronism). For the purpose of this simplified explanation, we assume $B \ll r_s$, where r_s is the minimum distance of a satellite from a terminal, and we suppress the effect of the difference in rate of the clocks at the two terminals (see Section 3.1). Equation (1) shows that at any instant, the observed delay contains information on the projection of the baseline vector along the direction to the satellite, and on the clock–synchronization error. To determine all three components of the baseline vector simultaneously with the synchronization error at any instant, the signals from at least four satellites must be observed and the resultant four linear equations solved for the four unknowns. For a unique solution, the satellites cannot all appear to lie on the same circle in the sky. If they do, then the component of $\vec{B}$ in the direction of the center of this circle cannot be separated from τ^{cl}. (See, also, Section 3.0).

2.1.3. Reference System

We assume that the positions of the four (or more) satellites observed are known with respect to a well–defined coordinate system. Different coordinate systems could be utilized, depending on the application. We consider one example : a nearly inertial coordinate system with an orientation defined by the directions of extragalactic radio sources. Such a system could be used if three (or more) base stations made continual differential interferometric phase observations of the satellites with respect to those extragalactic radio sources that appear in the same part of the sky [3], [4]. Given that the vector positions of the base stations with respect to the directions of the extragalactic sources were already known, virtually instantaneous measurements of the differential interferometric phases between a satellite and an extragalactic source from observations from each of two independent baselines suffice to determine the satellite's direction in this nearly inertial frame. Thus, the vector baselines between our compact ground terminals could be related to this frame through their coordinates in the satellite frame. The base stations would of course require conventional VLBI instrumentation to observe the extragalactic radio sources. As long as the direction of the comparison extragalactic source is neither too far from that of the satellite nor too near that of the sun, the observations of the satellite need be made only of the highest transmitted tone.

We define until Section 4.0 discussion of the limits on achievable accuracy in the determination of the baseline vector with respect to a reference frame.

2.1.4. Global Positioning System

The satellites of the NAVSTAR Global Positioning System (GPS) [5], scheduled for launch during the next few years, will have orbits almost perfectly suited to our proposed VLBI system. In the planned steady–state configuration, there will be 24 such satellites, eight distributed in each of three orbital planes, spaced by $120°$ in nodal longitude. Within each plane the satellites will be approximately evenly distributed around a nearly circular orbit of $\sim 63°$ inclination, $\sim 20{,}000$–km altitude, and ~ 12–hour period. As a result, at any place on the surface of the Earth at least six satellites will always be visible, and of these at least four will be suitably distributed (i.e., not all on or near any single circle in the sky).

C.C. COUNSELMAN III and I.I. SHAPIRO

The expected useful lifetime of a GPS satellite is five years with a maximum of about seven set by the amount of stored gas for the attitude–control system. Thus, in principle at least, there will be continual opportunities to modify the payload to accommodate our proposed system.

2.2. Satellite Equipment

We now describe the equipment we propose to place on each satellite. First, we discuss the factors governing the choice of subsystems and then each of the subsystems. For definiteness, we consider the design in the context of the GPSsatellites.

2.2.1. Requirements

What special requirements must be satisfied by the equipment aboard the satellites for our proposed system to be operated successfully ? First of all, the satellite must transmit a sufficiently strong and stable signal. The signal must also be structured to allow the user to resolve the "2π" ambiguity in the interferometric phase. In effect, the same cycle of the signal must be identified on both ends of the baseline. The usual method of making such an identification in VLBI is to combine observations made simultaneously at several different frequencies, or tones, f_i $(i = 1, 2, ...)$. The respective ambiguity spacings in delay, equal to $1/f_i$, are different, and the overall delay ambiguity can be resolved if, within the range of possible delays allowed by *a priori* information, there is a unique delay that is consistent with the phase observations at all frequencies. The task of resolving the phase ambiguity is complicated, however, by the dispersion of the propagation medium and by possible interference from reflected signals (see Section 6.0). The set of frequencies used must be chosen with these complications in mind.

Since, for the range of frequencies of possible interest, the Earth's ionosphere introduces a delay proportional to the inverse square of the frequency of the signal, it would appear desirable to employ the highest possible frequencies with the proposed system. However, we must also consider our paramount desire for a simple system. This desire to avoid, for example, high–gain antennas and high transmitted power levels places an upper bound on the usable frequency. Since, for given antenna directivities and transmitted power, the received power is inversely proportional to the square of the frequency, sufficiently high signal–to–noise ratios can only be obtained simply at low frequencies. The optimum range of frequencies is approximately 1–2 GHz, limited on the low end by the ionosphere and on the high end by signal–to–noise ratio considerations. An approximately one octave spread in the frequencies of the tones is important for the elimination of 2π ambiguities in the face of both the ionosphere and the possible interference from reflected signals.

Within this one–octave range of frequencies there are several wide bands allocated under existing international regulations for purposes that would encompass those of the proposed system [6]. This system requires relatively little spectrum space – no more than ten narrow bands, each at most 100–200 kHz wide, within the ~1–to–2 GHz range. The precise placement of these bands within this range is quite flexible and could be adapted to existing constraints. Basically, we require one band near the low–frequency limit, one near the high–frequency limit, and the others distributed between these limits. The inter–band spacings would range from a minimum of ~1 MHz to a maximum of ~400 MHz. The spacings could be in approximately geometric progression but do not have to vary monotonically with frequency (see Section 6.0 for further discussion).

2.2.2. Transmitter

To satisfy these requirements, each satellite could be equipped to transmit an unmodulated circularly polarized continuous wave (CW) with ~ 1 watt of power in each of up to ten bands. To avoid having to contend with interference between signals received from different satellites, each of these bands could be subdivided into contiguous, nonoverlapping "channels". Since each GPS satellite could share a channel with that other satellite spaced 180 deg apart in longitude, the number of channels need only be 12. Setting the width of each channel equal to 8×10^{-6} of its center frequency would allow for a tolerance on transmitted frequency of ± 1 part in 10^6, as well as for the extremes of Doppler shift, of ± 3 parts in 10^6, which could be observed on Earth for signals from satellites in orbits of the GPS type. Thus the total width of the band of 12 channels at ~ 1 GHz would be $\lesssim 100$ kHz, and at ~ 2 GHz would be $\lesssim 200$ kHz. Should less of the spectrum be available, modifications are possible to compensate, as discussed in Section 2.4. Here we proceed on the assumption that no modifications will be required.

Transmitters are available commercially which yield 1 w of radio-frequency output for 3.6 w of d.c. input power. Such devices have dimensions and mass of about 5 cm x 5 cm x 10 cm and 0.9 kg, respectively. Thus, for a total of ten bands, 36 w of DC power and a volume of $0.0025\ m^3$ would be required. These transmitters have an adequate long-term frequency stability of 1 part in 10^9 and a more than adequate spectral purity of ~ 1 part in 10^{10}. The overall volume and mass could undoubtedly be lowered for use in space, especially if the ten transmitters were packaged together. The total DC power requirements could also be lowered by some combination of an insignificant sacrifice in spectral purity and a use of a single oscillator to generate multiple tones through modulation which, itself, requires little power. However, to maintain high reliability, one would prefer not to eliminate too much redundancy.

2.2.3. Power Combiner

The outputs of the separate transmitters would be combined before being fed to an antenna. Design of such a combiner would be straightforward, involving mainly a set of resonant, low loss circuits.

2.2.4. Antenna

We envision each satellite equipped with a circularly-polarized antenna of modest directivity ($30^\circ \lesssim$ beamwidth $\lesssim 60^\circ$), which illuminates the entire visible portion of the Earth approximately uniformly. Such an antenna would have at least 10 db gain, but would be physically small and would not require precise pointing. A suitable antenna would also have a bandwidth sufficiently broad to yield this gain over the span from 1 to 2 GHz. (Variations in the transmitting antenna's gain, as well as in the receiving antenna's effective aperture, at the frequencies of the various tone transmissions, could be compensated by suitable adjustments in the relative transmitted powers). Types of antennas that might satisfy these requirements include cavity-backed spirals and conical spirals. The sizes and masses of such antennas are quite modest. For example, a commercially available cavity-backed spiral for these frequencies has a gain of nearly 10 db and is about 12 cm in diameter and 10 cm deep, with a mass of about 1 kg.

These characteristics of the satellite equipment are summarized in *Table 1*, and

an overall block design is shown in ***Figure 1.*** This equipment would, of course, require integration into the GPS configuration. Questions of location, mass, volume, and heat generation and dissipation all must be addressed. The only positional requirement is that the antenna must face earth–ward ; the other major requirement is, of course, for the appropriate supply of direct current. Any requirement for uplink and dowlink telemetry would be very modest, because the system is so simple.

Table 1

Possible Characteristics of Satellite Equipment For Use With The Mighty Mites System

Equipment	*Description / Characteristics*
Transmitter	
Frequencies	$\leqslant$ 10 tones spaced between 1 and 2 GHz
Polarization	circular
Power	~ 1 w per tone
Total DC Input	$<$ 35 w
Total Volume	~ 0.0025 m^3
Total Mass	$\lesssim$ 10 kg
Antenna	
Type	cavity–backed spiral
Bandwidth	~ 1 to 2 GHz
Beamwidth	~ 30 to 60 deg
Gain	$\lesssim$ 10 db
Dimensions	12 cm dia x 10 cm deep
Mass	~ 1 kg

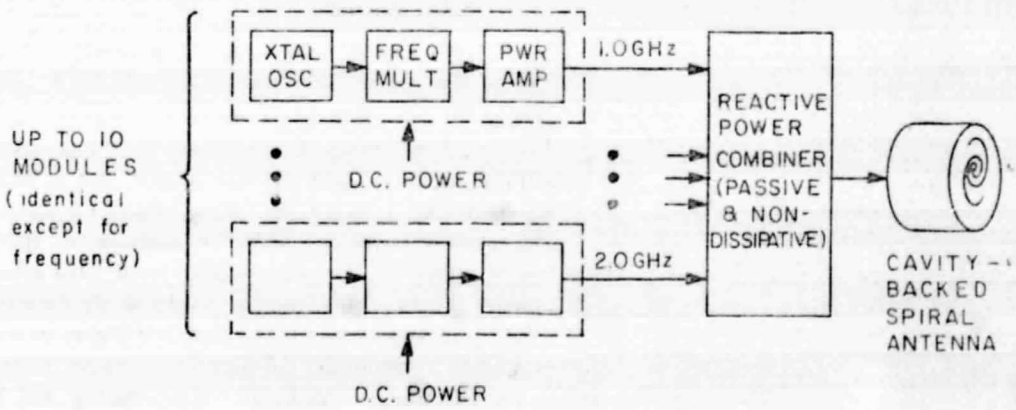

Fig. 1 – Block diagram of radio transmitting equipment to be placed on satellite, for use by Mighty MITES.

2.3. Ground Terminal

The most important feature of the satellite equipment just described is that it enables a relatively simple ground terminal to be used. Each such ground terminal would consist of an antenna, a receiver, a frequency and time standard, digital counting and timing circuitry, a calibration signal generator, atmospheric sensors, control logic, a system to store and/or telemeter data, and a power supply. We discuss these components, each in turn, after first describing some of the requirements that the ground terminal must meet.

2.3.1. Requirements

The ground terminal must have an antenna matched in circular polarization to the satellite antenna, but with little directivity.

We wish to avoid the complexity and expense of re-pointing the receiving antenna, by either mechanical or electrical means. Further, the antenna must receive signals *simultaneously* from widely separated directions in the sky, with elevation angles as low as 10°. The receiving antenna must also operate over an approximately 2-to-1 range of frequency, corresponding to a wavelength range of approximately 15 to 30 cm.

With any receiving-antenna design, it is also necessary to ensure that the phase of the signal received directly from a satellite is not altered significantly (see Section 6.0) and in an unknown way through interference that could arise from waves reflected or scattered to the antenna from the ground. The significance of such phase errors depends, of course, on the desired geodetic accuracy. In Section 4.3 we show that the errors in baseline determination would generally be comparable to the equivalent path-length errors in the measurements of the interferometric phase delays. Thus, for example, to achieve one centimeter baseline accuracy, would require phase errors under 24 deg for $f \approx 2$ GHz. Equivalently, the reflected signal would have to be at least 7 db weaker than the directly received signal. For one millimeter geodetic accuracy, the field strength of the reflected and scattered signals, and/or the antenna's sensitivity to such signals, would have to be attenuated tenfold (20 db in power) further. On the other hand, if geodetic precision, rather than accuracy, were the goal, as in some applications, one could tolerate a more cluttered and uneven environment for the receiving antenna because the distribution of azimuths and elevations of the GPS satellites as viewed from any given location repeats approximately with a period of 12 hours, so that the signal-reflection pattern and the consequent electrical phase variations would also be repeated periodically.

2.3.2. Antenna

The requirement that the phase of the signals received directly from the satellite not be altered significantly by signals reflected or scattered into the antenna could be satisfied by ensuring that the receiving antenna has an unobstructed view of the sky above 10° elevation, and that no large, elevated planar reflectors such as building walls or fences are situated so as to reflect satellite signals toward the antenna. The antenna would have to be placed above a $\sim$ 30 to 90 cm diameter metal "ground screen" of sheet metal or stiff wire mesh placed flush with the ground. The exact diameter needed and the restrictions on the local terrain would depend on the degree of suppression required for the signals reflected from the ground to achieve the desired accuracy. The screen would also serve to reduce pickup of thermal "noise" radiated from the ground. (This method

of siting an antenna is commonly used for high–accuracy measurements of microwave antenna radiation patterns).

The antenna would be mounted in the center of the ground screen and could have various forms. We describe one possible antenna design here. Mechanically somewhat complicated, but with apparently more than adequate electrical properties, this antenna would consist of a short stack of crossed pairs of horizontal, half–wavelength dipoles. They would be made of metal rod or tubing with each pair cut for one of the, at most, ten frequency bands. Of course, the closely–spaced bands could be served by a single pair of dipoles. Each dipole pair would be placed three–eighths of a wavelength above the ground screen. The two orthogonal dipoles comprising each pair would be fed in phase quadrature for circular polarization. Each pair could be connected to a separate, narrowband, receiver preamplifier if desired; more than one pair could also be connected efficiently to a single broadband preamplifier.

With a height of $3\lambda/8$ above a horizontal ground plane, the dipole pair has greater than unity gain relative to a circularly–polarized "isotropic" antenna at all elevation angles above about 20°, and its gain is about -5 db at 10° elevation, although the response approaches zero at the horizon. There would also be negligible ohmic loss with this antenna.

A crossed–dipole stack would have to be specially designed and tuned to the MITES system frequencies. However, this task is rather simple, and the cost of replicating the resultant dipole array in moderately large quantity would probably be under \$ 50 per unit.

Finally, we note that the phase–shift characteristics of the antenna itself, in conjunction with its ground screen, would be unimportant if identical antennas were used for all terminals; but, in any event, the antennas could be calibrated on a test range.

2.3.3. Receiver

The receiver could have a simple, uncooled, transistor radio–frequency (RF) front–end amplifier, or possibly two or more such amplifiers, each tuned to a different portion of the 1–to–2 GHz range spanned by the transmitted signals. In either case the total volume and mass of the front end would be under $100\ cm^3$ and 0.1 kg, respectively. A system noise temperature of 200° K could be easily achieved and would be sufficiently low, given the characteristics of the transmitted signals and the antennas described above. No difficult gain or phase stability demands would need to be met, because the output of the final amplifying stage of the receiver would be hard–limited or "clipped", and because delays of the signals through the receiver would be separately monitored, as discussed in Subsection 2.3.6.

After passage through the front–end amplifier, the signals received in each of the 100–to–200–kHz–wide bands would be mixed with a fixed–frequency local oscillator (LO) signal, derived by coherent multiplication from the master oscillator, to convert them to an intermediate–frequency (IF) band centered at ~ 200 kHz. The value of 200 kHz was chosen to minimize the requirements on time resolution in the subsequent measurement of the phase of the IF signals (see Subsection 2.3.5). A lower value could be chosen because of the desire to keep the ratio of the frequencies of the highest and the lowest IF signals below three in order to prevent interference from the odd harmonics generated by clipping. The down conversion to IF might be accomplished in a single stage with a quadrature–phasing, single–sideband mixer of the type described

by [7], or depending on considerations of dynamic range, stability, etc., two or more conversion stages might be used.

2.3.4. Time and Frequency Standard

Since observations would be made of a least four satellites simultaneously, the departure of the clock at each terminal from synchronism in epoch (and rate) with the clock at every other terminal can be determined from the observations as explained in Section 2.1.2. A high order of stability is therefore not required of the time and frequency standard at each terminal. The primary requirement is for sufficient short–term frequency stability, of ~ 1 part in 10^{10}, to maintain phase coherence during each, approximately one second, period of coherent integration. Long–term stability of ~ 1 part in 10^{6} is desired to facilitate acquisition of the satellite signals. The need for the ~ 1–sec observation periods of different terminals to overlap substantially implies that time must be kept at each terminal to an accuracy better than about 0.2 seconds, unless the observations are made continuously, in the latter case, interpolation between successive observations could be used to "match" time tags. Otherwise, drift in epoch error would have to be monitored and the clock in each terminal would have to be reset periodically, via telemetry if necessary. (See, also, Section 3.0).

These requirements on frequency and time are readily met by a compact, commercially–available, crystal oscillator. We shall henceforth refer to this as the "master" oscillator.

2.3.5. Digital Counting and Timing Circuitry

The digital counting and timing circuitry comprise the heart of the terminal and we describe them in some detail here. For convenience in description, assume that the received signals have been converted to the IF band, centered at ~ 200 kHz, as mentioned in Subsection 2.3.3. Each of these IF signals, one for each of the up to ten IF bands for the given satellite, would be bandpass filtered to approximately 100 to 300 kHz and symmetrically limited or "clipped" as mentioned earlier, to obtain a two–level signal which would be switched via "logic" circuits to selected inputs of a set of approximately 20 identical modules (see Subsection 2.3.8). Each such signal could be directable to the input of any module, according to the plan discussed below, although a more efficient arrangement is possible. The function of each module would be to measure the phase of the signal from one satellite in one band.

The IF input to a module would be fed to a second–order phase–locked loop whose bandwidth under the expected conditions of $+10$ db or greater signal–to–noise ratio (SNR) could be switched to values of either 7.5 Hz or 30 Hz, and whose tracking range in either case would span the IF band of from 100 to 300 kHz. (Note that the SNR is inversely proportional to the bandwidth of the loop and that the power received by the crossed–dipole antenna will be inversely proportional to the square of the radio frequency. Hence, under the assumption that the effective radiated power from each satellite is the same for all tones, the loop bandwidth for reception of the 2–GHz signals must be fourfold smaller than the loop bandwidth for the 1–GHz signals in order to maintain the same value of SNR). The loop would be locked to, and would track, the first suitable satellite signals encountered in this band. The loop SNR would be at least $+10$ db, and the corresponding root–mean–square (rms) random phase error in the loop output would be less than 13°, given (i) the effective transmitted power of

~ 10 w (1 w transmitted, coupled with 10 db of antenna gain); (ii) the worst–case satellite elevation angle of $10°$; (iii) the crossed–dipole receiving antenna; (iv) the receiving system noise temperature of $200°$ K (v) the 2–db clipping loss, and (vi) the 30–Hz and 7.5–Hz loop bandwidths for the 1–GHz and 2–GHz signals, respectively. The dynamic tracking error due to the time–rate–of–change of the input signal frequency would be well under $1°$, as would the static phase error, even with the use of the narrower loop bandwidth for the highest–frequency signals. The loop output would be fed to digital circuits which would perform two functions: (i) a continuously accumulating count of the integral cycles of the locked oscillator; and (ii) an accurate measurement modulo one cycle, of the oscillator phase, relative to that of the receiver clock. The instantaneous value of the accumulated cycle–count would be sampled nondestructively at selected times, according to the clock. The phase measurement would also be made at selected times, with ~ 100 ns time resolution, equivalent to ~ 0.02 cycle phase resolution at the ~ 200 kHz IF. This measurement could be made with a digital start–stop counter with a "clock" rate of 10 MHz. The count would be initiated by a command from the ground terminal controller at a selected time according to the terminal clock, and would be halted appropriately by the output of the locked oscillator, for example, by the next occurring positive–going transition. Averaging would be performed by timing a succession of such time intervals (i.e., by restarting and restopping the count) over a time span of approximately one second. By virtue of this averaging, the rms random noise of the equivalent phase measurement could be reduced to less than $5°$, the equivalent of 2 mm of electrical path length at a frequency of 2 GHz. (The equivalent noise bandwidth of the measurement would be ~ 2 Hz instead of ~ 1 Hz because of the image "fold over"; for the 2–GHz signals, the SNR in this bandwith would be > 18 db).

The phase–locked–loop portion of each module could be implemented with low–power, analog, integrated circuits and low–power Schottky transistor–transistor logic (TTL) circuits. All of this circuitry combined would consume less than 0.5 w. Continuous cycle–counting could be performed by a standard, low–power, "large–scale integrated" (LSI) circuit that also would consume about 0.5 w of power. The 100–ns resolution timing could be implemented with standard TTL circuits that would use approximately 2 w. However, power would have to be supplied to the latter circuitry only for the ~ 1 second interval during which the fractional–cycle phase measurement was being made. For many applications, these measurements might be repeated infrequently, at several–minute intervals, for example. In such cases, the average power consumed by each module would remain at the ~ 1 w level required to sustain the phase–locked–loop and cycle–accumulating circuits. Inasmuch as the complete receiver would require about 20 such modules, low power consumption per module is an important advantage.

The feasibility of building a module with the characteristics described has been demonstrated by the differential Doppler receiver developed by H.F. Hinteregger and one of us (C.C.C.) and applied to differential VLBI observations of the signals transmitted from the Apollo lunar–surface experiments packages [8], [3], [9]; see also *Figure 3* in [10].

2.3.6. Calibration Signal Generator

Signals from satellites would undergo delays in the RF amplifier(s), the mixers, and the IF amplifiers of the receiver. These delays could be calibrated by injecting a

suitable signal of low power directly into the RF input of the receiver. The calibration signal could consist of a periodic train of pulses, each $\lesssim 20$ ps in duration and all derived directly from the master crystal oscillator. A pulse repetition frequency of $\lesssim 100$ kHz would be chosen so that at least two of the harmonics of this calibration signal would appear within the passband of each IF amplifier. Two harmonics are required to monitor the group delay as well as the phase delay variations of the receiver. The group delay – the variation of phase with frequency – is important to monitor because the signals received from different satellites have different frequencies.

The phases of the calibration–signal harmonics would be measured in exactly the same way as would the phases of the satellite signals. This method has been used successfully in the calibration of other geodetic VLBI receiver systems, at the millimeter level of accuracy [11], [1]. When combined with the results from just one set of measurements of the phase–shift–vs.–frequency characteristics of the IF portions of the receiver, carried out when these are originally built, the information from the calibration signals should serve to account for all receiver phase variations to within an uncertainty of under 1 deg. The calibration signals would not have to be monitored continuously, but could be checked, for example, before and after each satellite tracking period as discussed below.

2.3.7. Atmospheric Sensors

The delay of the radio signals introduced by the neutral atmosphere must be modeled accurately, as discussed in Section 4.1. Thus we would include a suitably compact, electronically–readable barometer, thermometer, and hydrometer in each interferometer terminal. Such instruments are available commercially and are incorporated, for example, in some compact satellite Doppler–tracking receivers. If the data from a particular set of terminals are to be analyzed at a central location, it may be feasible and more economical to omit the sensors from the terminals and to interpolate from weather–station records to obtain the values of the atmospheric parameters (see Section 4.1).

2.3.8. Control Logic

All of the control functions to be carried out in the ground terminal could be automated straightforwardly through the use of an integrated–circuit microprocessor. Routine functions would include collection of data including the atmospheric information, the cycle–counts, the time–increments, and the received signal and noise levels. Less routine functions would include the determination of the proper phase calibration of the signals received in the different bands. The switching of the phase–locked loops to the appropriate frequency for acquisition of the satellite signals would also be automated. For signal acquisition, at least two alternative strategies could be followed, each based on the controller's ability to (i) monitor the frequency of the oscillator in each phase–locked loop through cycle–counting, (ii) slew each such oscillator upward or downward in frequency; and (iii) note the amplitude of the coherently–detected signal from each phase detector.

If the controller were in two–way communication with a central processing station, this station could instruct the controller regarding the times and frequencies at which new satellites could be acquired. But it would also be possible, and often preferable, for the controller to operate automatically. At preset intervals, each of the

12 frequency channels in the lowest–frequency (~ 1 GHz) band would be swept by a phase–locked loop searching for a signal. (Note that it is vastly more efficient to conduct the search at the lowest frequency because **(i)** the loop bandwidth is wider ; **(ii)** the loop time constant is shorter ; and **(iii)** the spectrum to be searched is smaller. Since the first two factors each vary with the square and the third with the first power of the radio frequency, we conclude that the search time depends on the fifth power of the radio frequency !). For the signal strengths and bandwidths given previously, approximately 10 seconds would be required for one loop to search completely one of these 8–kHz–wide channels. Of course, different loops would be programmed to search different channels simultaneously. Once a new satellite had thus been acquired, others of the ~ 20 loops could be assigned by the controller to lock onto the signals transmitted in the other bands by the same satellite. Less searching would be required in this step, since the Doppler shifts would be known.

Whenever a satellite is acquired, the phases of all of the sinusoidal signals that it transmits would have to be measured simultaneously at least once, to later enable the interferometric phase ambiguities of the signals to be properly resolved. This task would require the simultaneous commitment of up to ten phase–locked loops to that one satellite. However, once this task, which would take only a few seconds, has been accomplished, only two loops would be needed to track the highest and lowest frequency signals from the satellite. Thus, after elimination of the 2π ambiguities, it would be necessary to maintain a continuous count of the cycles received from these two signals only to remove ionospheric effects. In the steady state, simultaneous tracking of, say, six satellites would require twelve loops, and eight loops would remain for other tasks. These tasks would include the periodic monitoring of the phases and amplitudes of the calibration signals in all of the IF bands, and the searching for new satellites. To reach the steady–state condition after five of the six satellites have already been acquired will require up to 20 of the phase–locked loops – ten for the steady state tracking of the first five satellites and up to ten loops to enable the proper phase connection to be made for the signals from the sixth satellite. The total time to reach a steady state would, on average, be about one minute.

The control logic must also contain means to recognize any lock on a spurious signal and to reject this signal ; in such a scheme, advantage must be taken of the known relation between the frequencies of the various tones transmitted by each satellite.

2.3.9. Data Storage and Telemetry

We estimate that about 3500 bits of data would need to be stored at, or transmitted by, each terminal for the initial determination of a baseline. This total includes allowances of 33 bits for the integer–cycle count, 9 bits for the fractional–cycle phase measurement, 12 bits for the measured value of frequency, and at least 1 error–flag bit to indicate loss of lock for each of the up to 10 signals received from each of 6 satellites, plus a few hundred bits for time tags and other labels and for data on the atmospheric parameters. This quantity of data could be transmitted over an ordinary telephone line in 2–3 seconds. After the initial signal–acquisition and phase–ambiguity–resolution operations had been completed, and when only two phase–locked loops were tracking each satellite, a baseline redetermination could be performed with an additional 1 kilobit of data from each terminal. Data from a large number of observations could also be stored within the terminal in inexpensive solid–state memory devices, and could be collected later, for example by "data–mule" telemetry. With the

addition to the terminal of a 1 watt microwave transmitter, the data could be relayed from a remote to a central location through a satellite repeater. Alternatively, if a telephone line were available within ~ 50 km , a UHF or VHF radio link and a telephone "patch" could be used.

2.3.10. Power Supply

The complete terminal as described would require about 50 watts of power. Thus, it could not operate *continuously* and unattended for long periods without a steady power source. For applications in which observations every second were not required, the average power consumption could be kept to about 1 watt , since most of the electronics, save the master crystal oscillator and the clock, would not have to be powered except during observations. In these applications, power might be drawn from batteries charged by an array of solar cells.

The possible characteristics of the interferometer ground terminal are summarized in *Table 2* and *Figure 2*.

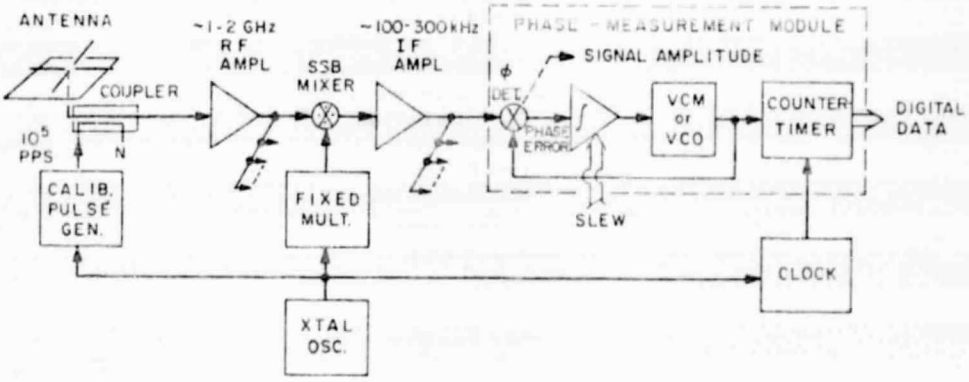

Fig. 2 – Block diagram of radio signal receiving and processing portions of Mighty MITES ground terminal. One RF–to–IF converter and one IF amplifier are required for each of the up to ten RF bands. Up to 20 phase–measurement modules are required as explained in the text.

Table 2

Possible Characteristics of Ground Equipment for the Mighty Mites System

Equipment	*Description / Characteristics*
Antenna	
Type	Crossed dipoles stacked $3\lambda/8$ above ~30 to 90 cm diameter ground screen
Polarization	Circular
Frequencies	Selected coverage from 1 to 2 GHz to match transmitted tones
Gain	>1 relative to circular "isotropic" antenna for elevation angles ≥ 20 deg; -5 db at elevation angle of 10 deg.
Receiver System	
Pre-amplifier(s)	Uncooled transistor(s)
Frequency range	1 to 2 GHz in one or a few bands
IF Amplifiers	Up to 10 identical units
Center Frequency	200 kHz
Bandwidth	200 kHz
Time & Frequency Standard	Crystal oscillator
Short-term Stability	~1 part in 10^{10}
Long-term Stability	~1 part in 10^{6}
Digital Counting and Timing Circuitry	~ 20 identical units
Phase-Locked Loop	
Bandwidths	7.5 and 30 Hz
Time Resolution	100 nsec
RMS Noise in Phase Measurement	$<5^{\circ}$ for one second integration in worst case
Calibration Signal Generator	
Pulse Duration	$\lesssim 20$ psec
Pulse Repetition Frequency	$\lesssim 100$ kHz
Atmospheric Sensors	Barometer, thermometer, hygrometer
Controller	Integrated-circuit microprocessor
Data Storage or Telemetry	
Capacity	1000 to 3500 bits per baseline determination
Medium	Solid-state memory, cassette recorder, radio link and / or telephone line
Total Power	
Peak	~ 50 w
Average	~ 1 w
Total Mass	~ 15 kg
Total Volume	~ 0.1 m^3

2.4. Possible Design Modifications

The particular design we described was motivated mostly by the desire for simplicity and reliability. However, many modifications of the design of the Mighty MITES system could be made to accommodate different requirements or constraints. For example, if necessary, the bandwidth required for the system could be reduced substantially with perhaps negligible degradation of performance. It is likely that a simple analysis, yet to be performed, would show that satellites separated by only 90° in orbital longitude could be assigned the same nominal transmitter frequencies without risk of mutual interference, because of the difference between the Doppler shifts of their signals as received on the Earth. If so, the number of channels, and the total bandwidth, could be halved. It might even be feasible to reduce the number of channels in each band to one; that is, all 24 satellites might have the same nominal transmitter frequencies. Typically, about eight satellites are simultaneously visible at a given ground location, but the Doppler-shift and random, transmitter-frequency, differences would cause the eight received frequencies to be scattered throughout the width of the band. Two received signals would have frequencies differing by less than, say, 5 Hz probably less than 5 % of the time. It should be possible to design a receiver to make accurate phase measurements on unmodulated signals which have similar strengths and frequencies that differ by as little as 5 Hz; the receiver could also give an indication of when valid measurements were not obtained due to insufficient frequency separation between two signals. However, this approach might introduce considerable complication into the receiver. A more efficient approach, if it were desired to have many or all satellites sharing a single channel, might be to modulate the signal transmitted by each satellite with a unique, but narrowband ($\ll 1$ kHz) "code" signal which could be detected in the receiver and used to discriminate between the transmissions from the different satellites. The latter approach is in fact used with the standard GPS navigational signals, except that the codes employed are rather complex and the modulation bandwidth is over 1 MHz. (The high GPS code complexity and bandwidth are required for purposes not essential for Mighty MITES).

3.0. System Operation

In this section, we recapitulate briefly the operation of the Mighty MITES system with some more detailed emphasis on the technique for elimination of the 2π ambiguity in the phase-delay measurements.

Each satellite would transmit a set of up to ten different tones. Each tone from each satellite would lie in a given radio-frequency (RF) band. These bands, up to ten in all with each 100 to 200 kHz wide, would be distributed suitable between ~ 1 GHz and 2 GHz. The ground terminal antenna, being approximately omni-directional for elevation angles above 10 deg and sensitive to signals in each of these bands, would pick up the tones from those satellites within view. The incoming signals in each band would then be amplified and converted to an intermediate frequency (IF) band, centered at ~ 200 kHz, by mixing the amplified signals with a local oscillator signal derived by coherent multiplication from the master crystal oscillator (Section 2.3.4.). The resultant IF signals would then be band-pass filtered, to select signals within a 100 to 300 kHz band, and clipped to obtain a two-level signal that could be handled easily by digital circuitry. A subset of the ~ 20 modules (Section 2.3.5.) that contain phase-locked loops would be automatically directed to search for signals originating in the 12 different channels in the lowest RF band (Section 2.2.2.), since the efficiency of the search would

be proportional to the inverse fifth power of the RF. (While the terminal is tracking signals from a given set of channels in this band, further search would be confined to the remaining channels). After acquisition of a signal in the lowest band, the terminal would seek to acquire the signals in each of the corresponding channels in the up to nine higher-frequency bands. The known separations between the frequencies in the various bands would enable this search to be conducted very efficiently. Should the search fail in a sufficiently large number of bands, the originally-acquired signal would be assumed to be spurious and a new search of the channel in the lowest RF band would be undertaken, picking up from the frequency of the spurious signal. Only ten seconds would be required for a module to completely search each ~ 8 kHz wide channel (Section 2.2.2.) in the lowest RF band as the loop bandwidth would be ~ 30 Hz (Section 2.3.5.), and its time constant ~ 0.03 s. Any module would also be able to track anywhere in the total 200 kHz-wide IF band. The signal-to-noise ratio for the satellite signals received would be sufficient for these operations to be carried out for elevation angles as low as ~ 10 deg.

The outputs from the set of loops, or modules, which had acquired signals from the up to ten tones transmitted by a satellite, would be analyzed by digital circuits to **(i)** accumulate a continuous count of the number of integral cycles made by the locked oscillator in the loop; and **(ii)** measure, modulo one cycle, the phase of this signal, relative to the clock in the terminal which is controlled by the master crystal oscillator. These two measurements, combined, would constitute the basic one made by each ground terminal, of the total phase of each of the up to ten tones received from each of the satellites being tracked. These phases would also be calibrated for the effects of delays within the receiver (Section 2.3.6.). The resultant total phases would be suitably averaged, say over one second, and time tagged according to the clock in the terminal. After initial acquisition, it might be sufficient for some applications to continue to monitor only the phases of the signals in the highest and lowest frequency channels for each satellite (see Section 2.3.8.).

In one mode of operation, these averaged data would be transmitted, along with auxiliary information including the measured values of the frequencies of the signals (Section 2.3.9.), from each terminal to some central location. At this central location, the data from any pair of terminals could be analyzed to **(i)** remove the 2π ambiguity and, simultaneously, the effect of the ionosphere; and **(ii)** estimate the components of the baseline vector between the locations of the two terminals. To perform this task additional information is needed, namely the positions of the satellites as functions of time. Crude or refined, ***a priori,*** information on terminal locations could also be used.

The radio frequencies of the tones would be distributed between ~ 1 and 2 GHz in a manner designed to facilitate removal of the 2π ambiguities in the interferometric phase delays. This distribution would involve spacings in frequency that are nearly in geometric progression, starting from a minimum spacing of about 1 MHz. (A strictly geometric progression would not be used primarily because of the legal constraints on frequency allocation, and because ***a priori*** knowledge, ***e.g.*** of the ionosphere, would be exploited).

The phase of each of the signals measured by each terminal could be converted to delay via use of the measured value of the radio frequency. The 2π ambiguity and the ionospheric effects could be eliminated from the resulting set of up to ten interferometric phase delays at each measurement epoch by a "bootstrap" algorithm in which the ambiguity is eliminated first between the delays that result from measurements

at the closely-spaced pairs of frequencies. These frequencies would be placed at the high, 2 GHz, end of the total band since the uncertainty in the ionospheric effects would be lowest there. Apart from the effects of noise, the *shape* of the ambiguity-free phase-delay vs, frequency curve is accurately known and, of course, taken into account in the algorithm. We omit the detailed presentation of this fairly straightforward algorithm to spare the reader the superficial complications engendered by symbols being festooned with the three sets of subscripts and superscripts necessary to distinguish the different satellites, ground terminals, and tones.

For continuing observations of the same satellites from the same terminals, the ambiguity and ionospheric elimination algorithms could be largely bypassed after the initial elimination. Only the interferometric phase delays for the highest and lowest tones need be followed continuously; these could be combined very simply to remove the ionospheric effect. Similarly, for terminals closely-enough spaced for ionospheric effects to be negligible, the ambiguity-removal algorithm could be simplified somewhat.

The corrected interferometric phase delays for the satellites tracked from a pair of terminals would be analyzed by, say, a standard least-squares algorithm for each epoch to determine the vector baseline, as outlined in Section 2.1.2. Variations in clock behavior at either terminal over the signal integration interval would not affect the baseline result since each satellite is observed at the same times from a given terminal. The effect of such variations would therefore cancel because of the linearity of Equation (1), which would cover the same time interval for the observations of each satellite. However, a "common-mode" error in the epochs of the clocks at the two terminals would affect the baseline result because the assumed positions used for the satellites would be incorrect. Time tags on the interferometric data accurate to a millisecond would reduce this error to a tolerable level. Such clock accuracy could easily be maintained for terminals in two-way communication with a central processor. Alternatively, with observations of at least five satellites simultaneously, one could solve for this common-mode epoch error. Another alternative, in principle, would be to obtain the time by decoding the standard GPS transmissions.

4.0. Limits on Attainable Accuracy

The accuracy attainable in baseline determinations will be limited primarily by errors in knowledge of (i) the propagation medium and (ii) the positions of the satellites. The effects of both of these sources of error increase, albeit differently, as the length of the baseline increases; we discuss each in turn. Finally, we discuss the less important limits due to the relative geometric configuration of terminals and satellites, and due to instrumental effects.

4.1. Propagation Medium

The propagation medium contains, in effect, two components: the ionosphere and the atmosphere. The influence of the former can be virtually eliminated, as described in Section 3.0., by utilizing its dispersive nature. The tropospheric effect on the electrical path length of the radio signals is harder to determine because the neutral atmosphere is nearly non-dispersive throughout the radio band of frequencies. This effect, typically about 8 ns at the zenith, is variable by about 1 ns, due mainly to variations in the amount of water vapor in the atmosphere. If ground-level measurements of atmospheric pressure, temperature, and dew point are used to calculate the atmospheric zenith delay, the rms error in the result may be reduced to approximately 2 to 3 cm [12].

However, for baselines of a few kilometers or less in length, and for sites at nearly equal elevations above sea level, the atmospheric delays introduced at the two ends of the baseline tend to cancel to a high degree. Our limited experience with such short baselines shows, for example, that tropospheric effects can be lowered to the millimeter level [1] and, in appropriate climates, to the tenth millimeter level [13] for baselines of length up to five kilometers. For long baselines, a series of interferometric measurements by our group [2] involving the Haystack and Owens Valley antennas, separated by nearly 4,000 km, demonstrated that a dozen baseline length determinations, distributed over a one and a half year period, show repeatability at the three centimeter level with the use of only surface measurements of atmospheric parameters. Higher accuracy results might be obtainable through use of water–vapor radiometers (see, for example, [14] and [15]) to monitor the water–vapor content above each terminal; perhaps the contribution of the troposphere to the uncertainty in baseline–vector determination could thereby be reduced to the centimeter level in all three components even for baselines of transcontinental dimensions. However, the efficacy of water–vapor radiometers for this purpose has yet to be established reliably in VLBI experiments under various climatic conditions. Moreover, at the present stage of technology, the water–vapor radiometers would be much larger, and more expensive, than our proposed ground terminals – the use of such radiometers would be similar to the tail wagging the dog.

One can also take advantage of averaging. Since a baseline determination can be made, on average, once per second, one can afford for most applications to average the results for many minutes or longer. Further, with more than four satellites observed simultaneously, another form of redundancy is possible. For both types, one can use the level of stability of the data and of the results as an indication of the accuracy of the baseline determination.

4.2. Satellite Positions

Errors in our knowledge of satellite positions are muted in their effects on baseline determination by the ratio of the baseline length to the satellite altitude. Thus for baseline lengths of a few hundred kilometers, the sensitivity to satellite position errors is reduced by a factor of nearly two hundred for satellites of the GPS type. For example, to achieve "instantaneous" accuracies of 2 cm over a 100–km baseline would require satellite position errors smaller than 4 m. (Note that for a baseline short compared to the satellite altitude, the interferometric delay is sensitive primarily to the direction of the satellite, not to its altitude). For transcontinental baselines, the immunity factor is under ten and satellite position errors become of correspondingly greater importance. But, as discussed earlier, effects of satellite position errors might be reducible to the level of the atmospheric errors if base stations were equipped to tie the satellite positions continuously over the required periods to those of extragalactic objects through differential VLBI observations. Averaging the baseline results over long periods of time, and, hence, over many satellites, would be acceptable for many applications and would tend to reduce the effects of satellite position errors.

4.3. Geometry

We now consider the effects on the accuracy of baseline determination of the geometric distribution of the satellites. Given the uncertainty in the measurement of interferometric phase delay, the determination of the corresponding uncertainty in the estimate of the baseline vector is non–trivial. The task is complicated largely because of

the unknown, systematic, effects introduced by the neutral atmosphere. However, one pertinent question can be answered by an elementary analysis : What is the purely geometrical multiplying factor in the conversion of phase–delay uncertainty to baseline–component uncertainty ? To obtain an answer, we use the following simplified expression for the interferometric phase delay obtained from observations of a satellite by two terminals (see, however, section 3.1)

$$\tau_{10} \simeq \frac{1}{c} \{ | \vec{s} - \vec{r}_2 | - | \vec{s} - \vec{r}_1 | \} + \tau^{cl}$$

$$\simeq \frac{1}{c} \{ (\vec{r}_2 - \vec{r}_1) \cdot \hat{s} + \frac{1}{4s} [2 (r_2^2 - r_1^2) - (\vec{r}_2 \cdot \hat{s})^2 + (\vec{r}_1 \cdot \hat{s})^2] \} + \tau^{cl} \quad (2)$$

$$r \ll s ,$$

where $\vec{r}_i (i = 1 , 2)$ and $\vec{s}$ are vectors, from the center of the Earth to the terminals and to the satellite, respectively. The analysis was based on the GPS configuration, with two satellites in each of the three orbital planes assumed to be crossing the equator at $t = 0$. Baseline with $| \vec{r}_2 - \vec{r}_1 | \ll s$ were considered as an illustration ; under these conditions, the term in brackets in Equation (2) can be ignored. However, the effects of parallax, due to the finite altitude of the satellites, must be considered and so $\hat{s}$ was calculated for the vector from the baseline midpoint to the satellite. Observations were assumed to be made of all satellites whose elevation angles, as viewed from the terminals, exceeded 10 deg .

From such observations, at each instant, the three components of the baseline vector and the epoch offset of the clock at one terminal with respect to that of the other, could be estimated and the standard errors in these estimates determined. The results from the analysis and related information on the geometry are presented in ***Figures 3*** and ***4***. ***Figure 3*** is based on the terminals being placed at a north latitude of 40 deg and zero longitude coincident at $t = 0$ with an ascending node of one of the orbital planes of the satellites. In ***Figure 3a,*** we show the elevation angles as functions of time for all satellites visible from the terminals. ***Figure 3b*** shows the results of the error analysis : the standard deviations in the estimates of the vertical and the two horizontal components of the baseline as functions of time. The standard deviations are given in units of the standard error in the determination of the interferometric phase delay. For either of the two horizontal components, the geometric multiplication factor is never more than 1.2 with its average value being about 0.8. The multiplication factor is larger for the vertical component whose uncertainty depends more importantly on the total spread of the elevation angles. Thus, as can be seen in the Figure, the multiplication factor is relatively large when the spread is small, and vice versa. For all three components, the standard errors as functions of time are discontinuous when a satellite passes either inside or outside the allowable elevation angle limit. We also note in the Figure that if the elevation angle cutoff at $t = 6$ hr were lowered by only 0.3 deg, the multiplication factor for the vertical component would drop nearly twofold, the total spread in the elevation angles then included being increased thereby from about 30 to 50 deg . ***Figure 4*** contains the corresponding results for observations from terminals placed at the same longitude, but on the equator.

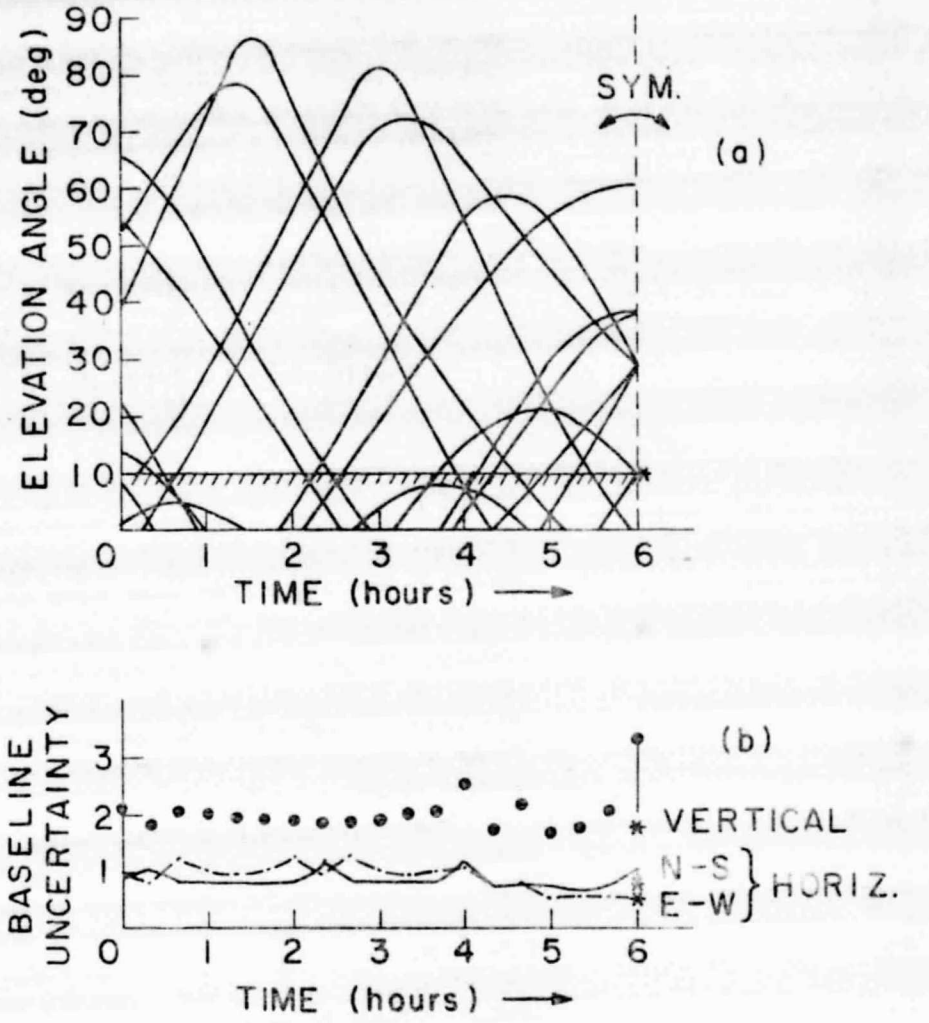

Fig. 3 — Error analysis for Mighty MITES system.

(a) — Elevation angles of satellites as seen from ground terminals at 40° N. latitude. Observations are made of all satellites visible above 10° elevation, except at t = 6 hours, when the two satellites with elevations of 9.7°, indicated by the asterisk (*), are also observed.

(b) — Standard errors of estimates of baseline vector components, computed at time intervals of 20 minutes. Points plotted at these intervals have been connected by continuous lines for clarity, although actual "curves" have discontinuities when satellites cross 10° elevation limit. Unit of baseline uncertainty is the standard error in measurement of interferometric phase delay, converted to equivalent path length. At time = 6 hours, results are shown both for 10° (regular symbols) and for 9.7° (asterisks) elevation-angle cut-offs.

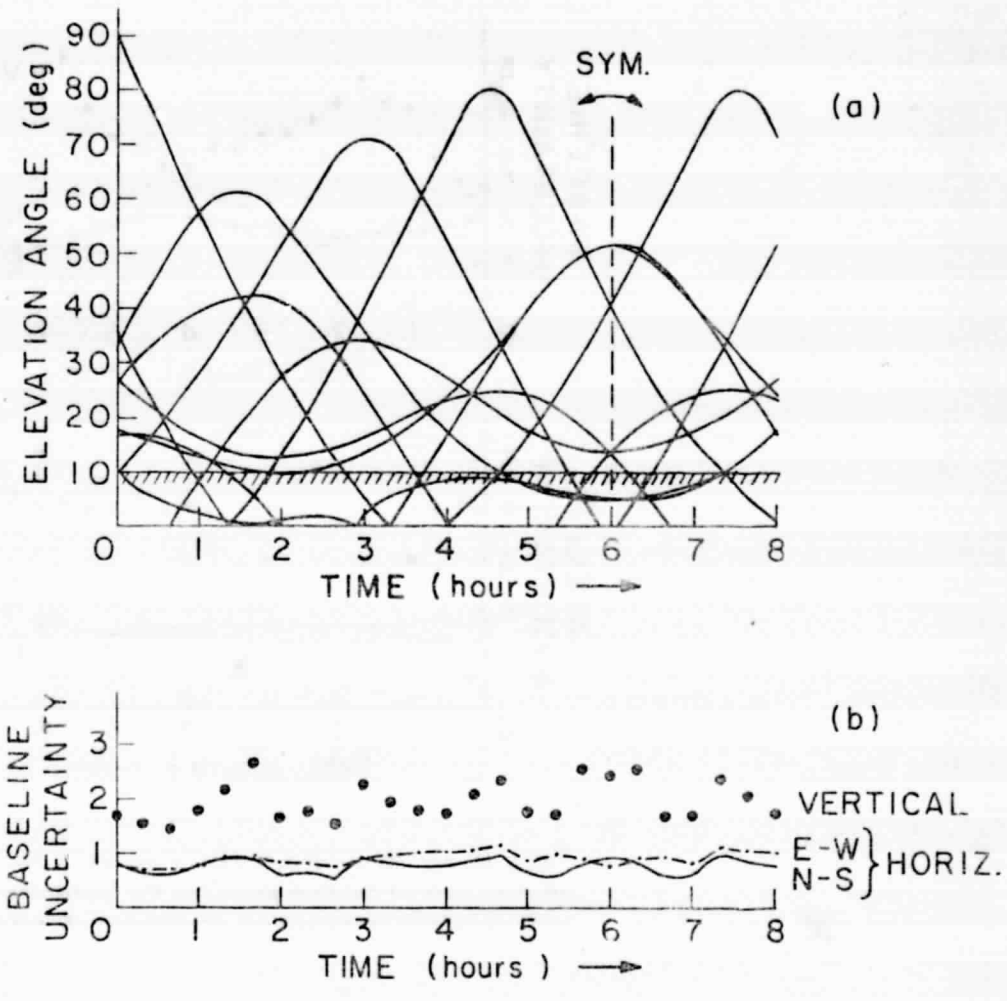

Fig. 4 (a) and (b) — Same as Fig. 3, except that terminals are at the equator.

The above error analysis, as mentioned, ignores the effects of the troposphere and of the uncertainties in the orbits of the satellites. To obtain an indication of the magnitude of the effects of the troposphere, we repeated the analysis, but with the standard error for each observation assumed equal to the cosecant of the elevation angle and with the elevation angle "cutoff" maintained at 10 deg. The results are summarized in ***Figure 5***. Here we see that the multiplication factors are larger, as expected, reaching up to 2.0 and 2.5, respectively, for the horizontal components for terminals at 40 deg and 0 deg latitude. The corresponding factors for the vertical component are both about 5.0, which serves to emphasize the importance of the observations being widely distributed in elevation angle, and, especially, being extended to high elevation angles.

In a further refinement, we could solve in addition for the common mode epoch error (see Section 3.0).

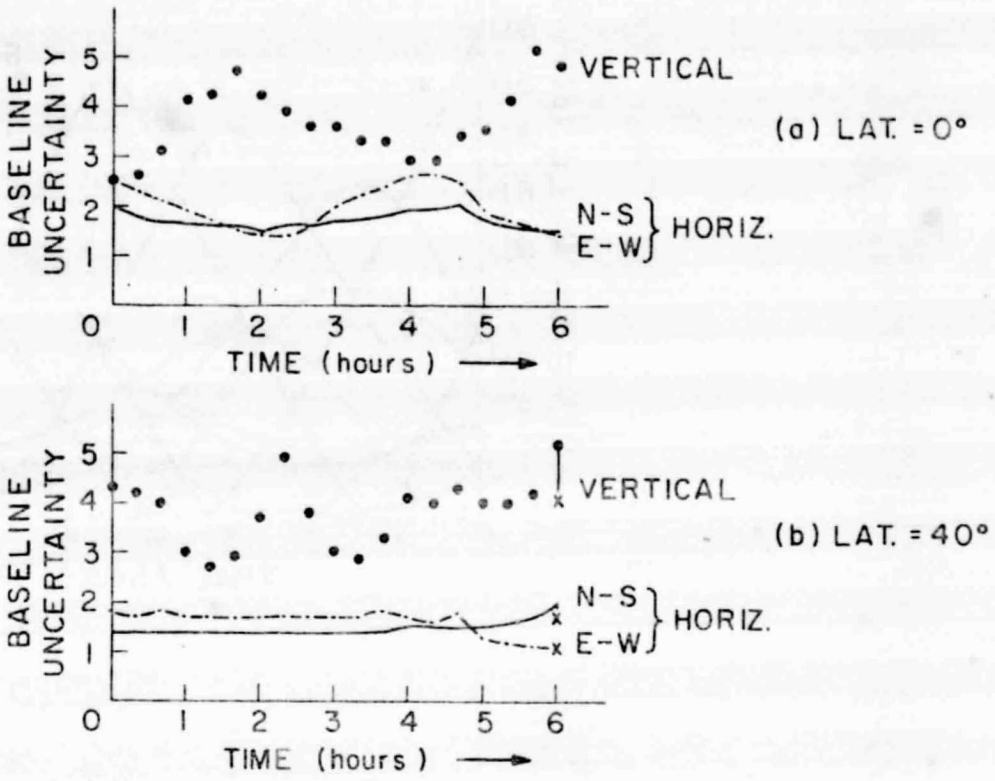

Fig. 5 (a) and (b) – Same as Figs. 4 (b) and 3 (b), respectively, except that here the standard error in the measurement of the interferometric phase delay, instead of being unity, is equal to the cosecant of the elevation angle of the satellite.

4.4. Instrument

For very closely spaced terminals the accuracy attainable in baseline determination could be limited by instrumental effects. For example, with a 100-meter spacing of terminals, of some interest for surveying and for monitoring the effects of earthquakes, the contribution to the error in baseline determination from the troposphere in good weather should be under 1 millimeter and from the satellite-position uncertainties under 0.05 millimeters. Any instrumental effects of order 1 millimeter could, under these circumstances, degrade the system performance. Thus, it would be especially important for such applications to minimize the effects of ground reflections, as discussed in Section 2.3. With proper design and calibration, other sources of systematic errors in the instrument could probably be kept to a level of about 0.3 psec, equivalent to 0.1 mm in distance. The random errors, due to signal-to-noise limitations (Section 2.3), could be reduced to this negligible level after less than ten minutes of integration. Should the ground reflections be the dominant contribution to the error, this fact would be disclosed in the slow variations with time of the estimate of the baseline.

caused by the changing directions of the signals. These variations would also tend to repeat with a 12–hour period, as indicated earlier.

A potential problem with current geodetic applications of VLBI concerns the determination of any changes with time of the length of the signal path through the antenna system. With the large structures now in use, one must account for deformations associated with changing winds, temperature, and gravity loads (see, for discussion, [1]). However, for a miniature terminal with a dipole–type antenna such changes are negligible at the millimeter level due to the small size and rigidity of the antennas.

5.0. Applications

There are a large number of potential applications of this interferometric system. We discuss two of these briefly.

5.1. Earthquake Monitoring

A primary use of the Mighty MITES would be to monitor the regional accumulation and release of strain. Their use would be most effective in regions around a fault such as the San Andreas where the terminals could be distributed widely, and yet densely, in the immediate vicinity of the fault and the data collected routinely. In effect, a seismic array could be set up, capable of measuring displacements with millimeter to centimeter precision in the 0 to 1 Hz part of the spectrum. The extraordinary time resolution of these measurements of baseline vectors and the high accuracy, especially for short baselines, should allow a very complete geometric characterization to be made of the crustal movements during actual earthquakes. Moreover, during earthquakes, any errors in our knowledge of satellite positions, which change slowly with time, would not significantly degrade the accuracy with which the *changes* in baseline vectors could be determined with the terminals * . These Mighty MITES should be sufficiently inexpensive to allow a dense net to be set up, and their ability to operate unattended should also cut down dramatically on the cost of the overall monitoring system.

5.2. Land Surveying

These terminals could also be used for more conventional surveying. For example, for local surveying, over distances of a few kilometers or less, two or more terminals could be employed. The surveyor would merely have to set the terminals down at the positions whose vector separations are desired and, after the minute or so required for signal acquisition, baseline results could be obtained once per second. The surveyor would also require satellite–position information, a small microprocessor, and either a radio or a line link to each terminal to be able to determine these baselines. The needed computations could easily be done in real time and would thus allow the surveyor to complete his tasks virtually as fast as he could place the terminals at the desired positions. Of course, observations could be continued by the surveyor as long as desired and the changes, or fluctuations, in the baseline vectors, as well as their running averages, could be monitored. Averaging largely removes the effects of short–term atmospheric fluctuations, caused, for example, by passing clouds.

Semi–permanent, self–contained, local arrays of terminals could also be used for a variety of purposes. As examples, we mention the monitoring of local crustal movements in the vicinity of nuclear plants, wells, pipelines, dams, mines, and rocket

* – Note, however, that during and immediately preceding and following earthquakes insufficient time would be available for averaging out short–term meteorological effects.

launching sites, and even the monitoring of oil rigs in the sea. In some cases, combination with gravity monitoring will yield a more powerful set of data for the [illegible] of both crustal motions and changes in the mass underlying the area.

For purposes of both two–way communication and supply of power, a direct electrical link to each terminal might be more suitable for fixed installations designed for long–term monitoring. If direct links are not convenient, small cassette recorders could be used to store data which could be collected intermittently.

6.0. Precision Geodesy With GPS – Other Interferometric Approaches

The various options originally considered for GPS ground terminals were not intended to yield accuracy in position determination better than about 1 meter. A crucial question is : can the already planned GPS signals be utilized in other ways to yield substantially higher accuracies in position determination ? Various possibilities can be envisioned. One possibility [16] would be to receive the GPS signals interferometrically as if they were random noise, as from extragalactic radio sources. Because of the strength of the GPS signals, even when treated as random noise, a 1–meter diameter, transportable, antenna can be used with conventional VLBI receiving and data processing techniques. The estimated precision in baseline determination [16] is 2 cm from 1.5 hours of data collection for baselines $\leqslant$ 300 km in length. This system promises comparable accuracy to that claimed for the Mighty MITES System, but at the sacrifice of cost, simplicity, and time resolution.

Another possibility is to utilize knowledge of the pseudo–random noise GPS codes so that the effective noise bandwidth at the receiver is of the order of, say, ten Hertz instead of the order of ten Megahertz. One may then consider rapid determination of the interferometric group delay, at both the ~ 1.6 GHz GPS bands, with accuracy sufficient to determine the ionospheric contribution and to eliminate the 2π ambiguities in interferometric phase delays. The two phase delays, one at each of the two frequency bands, could then be combined to refine further the knowledge of the ionospheric contribution and to yield an accurate vacuum–equivalent phase delay. (The requirements on group–delay accuracy are somewhat ameliorated for sites closely–enough situated for the ionospheric effects on the interferometric observable to be negligible). If this technique were viable, then the same accuracy in baseline determination could be achievable with the Mighty MITES System. However, one important caveat which bears on the cost must be considered : the achievement of sufficient group delay accuracy to eliminate the phase delay ambiguity may entail considerable complication with such a narrow ($\simeq 1\ \%$) fractional bandwidth available at each GPS band. Although signal–to–noise ratios may be sufficient, systematic effects on the frequency dependence of the phase delays could be serious. As an oversimplified illustration, consider ground reflections of the signal that introduce an (erroneous) contribution to the slope of the phase of the signal as a function of frequency across the band. A difference in phase of only 1°, in opposite directions, at both ends of a 10 MHz band, would introduce an error in group delay equivalent to a displacement of about 15 cm – a large fraction of the ~ 20 cm wavelength at 1.6 GHz. To be more quantitative about the possible sources of such reflected signals, we note that the root–mean–square (rms) phase error due to, say, isotropic, scattering by objects near the antenna is given approximately by

$$\langle \phi^2 \rangle^{1/2} \simeq 10 \frac{\sigma^{1/2}}{R} \text{ deg} , \qquad (3)$$

where σ is the cross section of the object, R is its distance from the antenna, and both are measured in compatible units. We assume here that the receiving antenna is isotropic. Thus, an object such as a tree with a $2\ m^2$ effective cross section, situated 15 m from the receiving antenna, would lead to a 1 deg rms phase error. To cut this figure to 0.1 deg would require the gain of the antenna to be 20 db less in the direction of the scattered radiation than in the direction of the directly received signals. A simple antenna with such high directivity could not receive signals from all satellites simultaneously; hence the effects of instabilities of the frequency standard could not be eliminated simply by subtraction, as in the Mighty MITES System. A more stable, and presumably more expensive, standard would be needed. We conclude that this problem of elimination of the 2π ambiguity in phase with the planned GPS signals may require a rather expensive system to insure sufficient suppression of the effects of ground reflections (see, also, Section 2.3).

o

o o

REFERENCES

1. A.E.E. ROGERS *et al.* : *J. Geophys. Res.*, 83, 325, 1978.
2. D.S. ROBERTSON, *et al.* : Recent Results of Radio Interferometric Determinations of a Transcontinental Baseline, Polar Motion, and Earth Rotation, in Proc. of IAU Symposium No. 82, (in press), 1978.
3. C.C. COUNSELMAN, *et al.* : *Science, 178,* 507, 1972.
4. R. PRESTON, *et al.* : *Science, 178,* 407, 1972.
5. B.W. PARKINSON : "NAVSTAR Global Positioning Systems (GPS)", presented at the 1976 National Telecommunications Conference in Dallas, Texas (I.E.E.E. Catalog Number 76 CH 1149–4 CSCB).
6. International Telecommunications Union, "Radio Regulations" (International Telecommunications Union, Geneva, 1968).
7. A.E.E. ROGERS : *Proc. I.E.E.E., 59,* 1617, 1971.
8. C.C. COUNSELMAN, and H. HINTEREGGER : *Proc. I.E.E.E., 61,* 478, 1973.
9. R.W. KING, *et al.* : *J. Geophys. Res., 81,* 6251, 1976.
10. C.C. COUNSELMAN : *Annual Review of Astronomy and Astrophysics, 14,* 197, 1976.
11. A.R. WHITNEY, *et al.* : *Radio Science, 11,* 421, 1976.
12. C.W. MURRAY, and J.W. MARINI : GSFC Technical Memorandum, 1976.
13. B. ELSMORE, and M. RYLE : *Mon. Not. Roy. Astron. Soc., 174,* 411, 1976.
14. L.W. SCHAPER, *et al.* : *Proc. I.E.E.E., 58,* 272, 1970.
15. J.M. MORAN, and H. PENFIELD : Final Report, Contract NAS8–20375, 1976.
16. P.F. MacDORAN : Presented at the International Symposium on the Use of Artificial Satellites for Geodesy and Geodynamics, Lagonissi, Greece, 29 May – 6 June 1978.

Received : 31.01.1979
Accepted : 16.02.1979

Reprinted from:

THE ASTRONOMICAL JOURNAL VOLUME 84, NUMBER 10 OCTOBER 1979

SUBMILLIARCSECOND ASTROMETRY VIA *VLBI*. I. RELATIVE POSITION OF THE RADIO SOURCES 3C 345 AND NRAO 512

I. I. SHAPIRO, J. J. WITTELS, C. C. COUNSELMAN III, and D. S. ROBERTSON[a]
Department of Earth and Planetary Sciences and Department of Physics, Massachusetts Institute of Technology, Cambridge, Massachusetts 02139

A. R. WHITNEY, H. F. HINTEREGGER, C. A. KNIGHT, and A. E. E. ROGERS
Haystack Observatory, Northeast Radio Observatory Corporation, Westford, Massachusetts 01886

T. A. CLARK and L. K. HUTTON[b]
Goddard Space Flight Center, Greenbelt, Maryland 20771

A. E. NIELL
Jet Propulsion Laboratory, Pasadena, California 91103

Received 27 April 1979

ABSTRACT

The relative position and relative proper motion of the radio sources 3C 345 and NRAO 512 were estimated from four sets of very-long-baseline interferometric observations, spaced between October 1971 and May 1974. Use of phase-connection techniques yielded the result
$\alpha(3C345-NRAO\ 512)=2^m\ 29^s.436\ 68\pm0^s.000\ 03$
$\delta(3C345-NRAO\ 512)=1'\ 40''.726\ 3\pm0''.000\ 3$
for the separation in 1950.0 coordinates of the centers of brightness of the compact components of the two sources, and an upper bound of $0''.000\ 5$ per year on their relative proper motion (70% estimated confidence limits).

I. INTRODUCTION

The establishment of a celestial reference frame and a cosmic distance ladder has been a major concern of astronomers throughout this century. The determination of a reference grid and the placement of the lower rungs of a distance ladder have been accomplished primarily with optical measurements of positions, parallaxes, and proper motions of stars in the Galaxy. These same problems can also be attacked effectively with the use of radio observations. The measurement with very-long-baseline interferometry (VLBI) of the differences in the fringe phases for pairs of distinct radio sources with small angular separation can, for example, yield the relative positions of the sources with errors of well under a milliarcsecond. Repetitions of such determinations over a period of years can also lead to values for their relative parallaxes and proper motions or to stringent bounds on them.

In this paper we describe the VLBI method in some detail and present results from four sets of observations, spread over two and a half years, of the pair of radio sources 3C 345 and NRAO 512 which have an angular separation of about 0°.5. The source 3C 345 has a redshift of $z = 0.595$, and hence a proper-motion distance of about 2 Gpc, if we assume $H_0 = 60\ \mathrm{km\,s^{-1}\,Mpc^{-1}}$ and $q_0 = 1$. The source NRAO 512 has also been identified with an optical counterpart for which a tentative value of $z = 1.67$ has been determined (Lynds 1975), leading to a proper-motion distance of 3 Gpc. If these distances are correct, the peculiar velocities would have to be very peculiar indeed in order for us to detect any relative parallax or proper motion. However, because of inferred "superluminal" velocities in 3C 345 (Wittels 1975, Cohen *et al.* 1976, Wittels *et al.* 1976a), we sought evidence for any related motion of its center of brightness with respect to NRAO 512.

In Sec. II, we discuss the basic theory underlying the VLBI method, in Sec. III the observations, and in Sec. IV the data-reduction procedures. The results are presented in Sec. V and discussed in Sec. VI. Auxiliary formulas are relegated to three appendices.

II. THEORY

We first discuss the difference fringe phase and then describe some of its properties. The fringe phase itself, for observations of a single point source, is given approximately by:

[a] Now at U. S. National Geodetic Survey, NOS, NOAA, Rockville, Maryland 20852.

[b] Now at Seismological Laboratory, California Institute of Technology, Pasadena, California 91125.

 0004-6256/79/101459-11$00.90

$$\phi(t) \simeq (\omega B/c)\,[\cos D \cos\delta \cos(A_0 + \Omega t - \alpha) + \sin D \sin\delta] + \phi^{pm}(t) + \phi^{in}(t), \quad (1)$$

where ω is the (angular) radio frequency of the observations; B, A_0, and D are the length, right ascension at epoch, and declination, respectively, of the baseline; c is the speed of light; Ω is the magnitude of the angular velocity vector of the earth; α and δ are the right ascension and declination, respectively, of the source; and ϕ^{pm} and ϕ^{in} are the respective contributions to the fringe phase from the propagation medium and the instrumentation, including frequency standards. The equivalent phase delay is obtained by division of Eq. (1) by ω.

If we consider that observations are made simultaneously of a second source whose right ascension and declination are $\alpha + \Delta\alpha$ and $\delta + \Delta\delta$, respectively, we can form the difference fringe phase (or the difference phase delay):

$$\begin{aligned}\Delta\phi(t) &\equiv \phi_2(t) - \phi_1(t)\\ &\simeq (\omega B/c)\,\{\Delta\alpha \cos D \cos\delta \sin(A_0 + \Omega t - \alpha)\\ &- [\Delta\delta \sin\delta + \tfrac{1}{2}(\Delta\alpha)^2 \cos\delta] \cos D \cos(A_0 + \Omega t - \alpha)\\ &+ \Delta\delta \sin D \cos\delta + O(\Delta\alpha\Delta\delta, \Delta\alpha^3)\} + \Delta\phi^c(t), \quad (2)\end{aligned}$$

where the subscript on ϕ is the source index, and where we carry the expansion to one power higher in $\Delta\alpha$ than in $\Delta\delta$ because, for the source pair being studied, $\Delta\delta = O(\Delta\alpha^2)$. The term $\Delta\phi^c$ represents primarily the contributions due to the intrinsic ambiguity of phase and to the propagation medium. The contribution of the instrumentation to the difference fringe phase is usually very small, if the observations of the two sources are made simultaneously; if not, the instrumentation can make an appreciable contribution (see Secs. IV and V).

Often, knowledge of the baseline vector, the source position, and the propagation medium is of sufficient accuracy to allow the "$2\pi n$" phase ambiguity to be eliminated. In such cases, the information on $\Delta\delta$ contained in the term $\Delta\delta \sin D \cos\delta$ is useful. Otherwise, estimates of $\Delta\alpha$ and $\Delta\delta$ are obtained solely from the coefficients of the sinusoidally varying terms in Eq. (2).

How sensitive are such estimates to errors in the values used for other relevant quantities? We distinguish two types of errors, those that are dependent on time and those that are independent of time. The former affect the determinations of both the relative position and the proper motion of the sources, for example, whereas the latter affect only the determination of the relative positions. The largest effects of the first kind, discussed in Appendix A, are those due to polar motion and to variations in the earth's rotation (UT1), whereas the largest of the second kind, also discussed in Appendix A, are those due to uncertainties in the baseline length and in the position of the reference source in the sky. (Although, in principle, these latter errors are also dependent on time, this dependence can be ignored in practice.)

We have so far assumed that both sources are unresolved by the interferometer or have sufficient symmetry that the fringe phases behave as for point sources. If the source is partially resolved, one has to define a suitable point of reference, such as the center of brightness of the overall source or of a distinguishable component within the source.

If the radio-brightness structure of each source were to remain constant, then there would be no effect on a determination of relative position or proper motion so long as all other aspects of the measurements, such as the hour-angle coverage in each set of observations, were also kept constant. However, we know that many, if not all, compact radio sources undergo perceptible changes in their brightness structure over time periods of several years (see, for examples, Wittels *et al.* 1975, Cohen *et al.* 1977). We must, therefore, determine the structure of each source and refer the observations of fringe phase to either the center of brightness, as described in Appendix B, or to some suitable feature within the source. If one is interested in the position or motion of the center of mass of a source, there is a potential difficulty in the use of the center of brightness or of any other reference point within the brightness distribution: There is no guarantee that this reference point coincides with, or remains at the same location relative to, the center of mass. However, one could argue that the outbursts of radio energy that emanate from compact radio sources originate close to the center of mass. Since in many of these sources outbursts seem to recur on time scales of a few months to a few years, a long-term average of the position of the center of brightness or of any other suitable reference point, ought to coincide closely with the center of mass. In any event, only an apparently uniform transverse motion of the reference point with respect to the center of mass could be confused with *bona fide* motion of the latter. Any "erratic" component of apparent relative proper motion between two sources could probably be attributed reliably to the relative motion of the reference points with respect to the two centers of mass.

III. OBSERVATIONS

Our observations were made at a radio frequency of approximately 7850 MHz ($\lambda \simeq 3.8$ cm) in our standard Mark I VLBI mode (Wittels *et al.* 1975) on the dates, and with the antennas, listed in Table I. The equipment is described in detail by Whitney (1974) and Whitney *et al.* (1976). For the first three experiments, which involved the Haystack Observatory and the Goldstone Tracking Station, the only unusual aspect (see also Knight *et al.* 1971) was the recording of data from both sources on each magnetic tape. Since the signals from 3C 345 were stronger than those from NRAO 512, we recorded on each tape 50 s of data from observations of 3C 345 and 110 s from observations of NRAO 512. An interval of 70 s was allowed after each observation to

TABLE I. Description of experiments.

Experiment number	Date	Duration of experiment	Baseline	Cycle time[1]	Bandwidth synthesis	Minimum elevation angle		
						H	*G*	*N*
1	10 October 1971	5 hr 22 min	HG[2]	5 min	No	50 deg	16 deg	—
2	9 May 1972	5 45	HG	5	Yes	13	39	—
3	4 July 1972	3 56	HG	5	No	62	27	—
4	2 May 1974	3 38	HG	4	Yes	46	59	51 deg
			HN	8	Yes			
			NG	8	Yes			

[1] See text for definition.
[2] H ≡ Haystack (430; 110), G ≡ Goldstone (1,600; 30), and N ≡ NRAO Green Bank (650; 100), with the numbers in parentheses denoting, respectively, the typical effective apertures (m^2) and system temperatures (K) of these three radio telescopes for these experiments.
Note: A hydrogen maser frequency standard and the Mark I recording system (360 kHz bandwidth) were used at each site for each experiment.

repoint the antennas, resulting in an overall cycle time of 5 min. For the fourth experiment, the signals from each source were recorded for 90 s on each tape, with an interval between observations of 30 s to allow the antennas to be repointed, yielding an overall cycle time of 4 min at Haystack and Goldstone. However, at the National Radio Astronomy Observatory (NRAO), which was involved only in the fourth experiment, only one tape recorder was available, and observations were, therefore, made only during every other four-min cycle, for an overall 8-min cycle time (see Table I).

IV. DATA REDUCTION

Here we outline briefly the major steps involved in the estimation of the relative position of the two sources from the tape recordings of their signals.

a) Cross Correlation

The fringe phases and rates for each source from each tape pair, except for those from the first experiment, were estimated with the aid of the "Mark I" digital correlator at the Haystack Observatory and the data-reduction programs described by Whitney *et al.* (1976). The data from the first experiment, obtained prior to the completion of the Haystack correlator, were processed on a general-purpose digital computer at the Goddard Space Flight Center, using the programs described by Hinteregger (1972) and Whitney (1974). In each case, the processing actually yielded the difference between the fringe phase (and fringe rate) and a model of that fringe phase (and fringe rate), based on the best available prior information and on preliminary estimates for the differences in the epoch settings and rates of the clocks used at the different sites. Thus, the fringe phases and rates obtained directly from the cross correlation were in the form of residuals.

b) Phase Connection

Before the fringe phases estimated from individual observations (tape pairs) were used to obtain accurate estimates of source positions, the number of 2π changes of phase between successive observations of the same source were determined to "connect" the observations. Proper phase connection can be accomplished provided the time interval between successive observations is sufficiently short and the estimate of fringe rate sufficiently accurate.

The method we used to connect the fringe phases can be outlined as follows [see Wittels (1975) for a detailed description]: A polynomial in time, up to degree five, was matched by weighted least squares to the ensemble of residual fringe rates for a given baseline, source, and experiment. The time integral of each of these "best-fitting" polynomials was then subtracted from the corresponding residual fringe phases, where the latter were evaluated from each second of data. The resultant residual fringe phases varied slowly enough with time so that those from one tape pair could be connected with those from the preceding or following tape pair with only a small probability that a spurious number of 2π's was introduced. The phase connection was actually carried out by means of a simple computer algorithm and was confirmed by visual inspection; the connection was checked again in the final processing of the data.

c) Difference Observables

After proper phase connection, the fringe phases for each source were transformed into equivalent phase delays. Difference observables were then formed by subtraction of the phase delay from an observation of one source from the delay from the following observation of the second source. Each difference observable had two time arguments since the observations of the two sources were made at different times. Except for "edge effects," each observation appeared in one, and only one, difference observable. This differencing technique produced observables largely freed from the main sources of error.

In addition to the phase delay, there is another observable, the group delay (see, for example, Whitney *et al.* 1976), that was obtained in the May 1972 and May 1974 experiments. The uncertainties in the group-delay measurements are about eightyfold larger than those in the phase delays, due mainly to the relatively small, $\simeq 25$

MHz, spanned bandwidth (Whitney *et al.* 1976). Despite this lower accuracy, the group delays have the virtue of providing the best available check on our estimates of relative source position (Clark *et al.* 1976). These measurements were also differenced, like the phase delays, to reduce the effects of errors.

d) Least-Squares Analysis

The phase delays and group delays for each experiment were analyzed separately with a weighted-least-squares algorithm to obtain the differences, $\Delta\alpha$ and $\Delta\delta$, in the positions of the two sources. (The fringe rates were used only for phase connection.) For these analyses, the total, not the residual, observables were used. Further, for the analyses of the phase delays, both the difference observables and the phase-delay observables themselves for one source were used. The latter were included because of their greater sensitivity to the "long-term" relative behavior of the clocks at the various sites. In fact, the sole practical effect of the use of these (undifferenced) observables was to improve the determination of the influence of the clock behavior on the difference observables. In principle, the sum observables could have served this purpose better; however, a program limitation prevented their use. Tests showed that this limitation had no significant effect on our results.

The parametrized theoretical model, which was matched to these observables, included the effects of the atmosphere and of all known, non-negligible contributions to the motions of the antenna sites (Robertson 1975). Aside from $\Delta\alpha$ and $\Delta\delta$, the parameters estimated in the analysis of the data from the two-site experiments were six in number: the five coefficients of a fourth-degree polynomial used to represent the relative behavior of the clocks at the two sites, and the single parameter needed to represent the $2\pi n\omega^{-1}$ ambiguity in the offset of the phase delays for one source from those for the other. This last parameter was estimated only in the analysis of the phase delays as the group delays are unambiguous; if the standard error in the estimate of this parameter is small compared to $2\pi\omega^{-1}$, and if the estimate itself is near $2\pi n\omega^{-1}$ for some value of n, then one can select the proper value of n with confidence. In such cases, the analysis is repeated, with n fixed at the selected value. For each of our experiments, the value of n was, in fact, determined reliably.

For the three-site, May 1974 experiment, additional "clock" and ambiguity parameters were also estimated. The values of the most important parameters that were not estimated in any of the analyses are given in Table II.

V. RESULTS

In this section we (i) present the estimates of the relative position of 3C 345 and NRAO 512; (ii) examine the sensitivity of these estimates to changes in the parameters of the theoretical model; (iii) discuss the postfit residuals; (iv) describe and interpret the error ellipses for the estimates of relative position from the individual experiments; and (v) discuss the bound on relative proper motion obtained from the ensemble of experiments.

a) Relative Source Position

The relative position of 3C 345 and NRAO 512 obtained from each of the four experiments is shown in Table III. The values of $\Delta\alpha$ and $\Delta\delta$ obtained from the two types of observables are in good agreement, as expected.

TABLE II. Fixed parameters.

Source coordinates (1950.0)[1]			
3C 345:	$\alpha = 16^h41^m17^s.634759$		$\delta = 39°54'10''.95838$
Station coordinates (earth centered)			
	Cylindrical radius	*West longitude*	*Polar component*
H:[2]	4700.64332 km	71°.4886503	4296.69616 km
G:	5204.14078	116.8885637	3676.86770
N:	5003.16905	79.8359600	3943.94526
Precession constant			
P = 5026".75/century			
UT1 and polar motion			
Smoothed values published in Circular D by the Bureau International de l'Heure.			
Earth tides			
Radial Love number, $h = 0.584$.			
Horizontal Love number, $l = 0.045$.			
Tidal lag angle, $\theta = 1$ deg.			
Electrical path length of atmosphere (zenith directions)			
H:		8.0 ns	
G:		6.7	
N:		7.4	

[1] Elliptic aberration removed.
[2] See Table I for definitions of abbreviations.

TABLE III. Estimates of relative position: 3C 345 Minus NRAO 512.

Experiment number	$\Delta\alpha^1 - 2^m29^s.436\,680$ Group delay[2] ($\times 10^5$ s)	$\Delta\alpha^1 - 2^m29^s.436\,680$ Phase delay[2] ($\times 10^5$ s)	$\Delta\delta^1 - 1'40''.726\,30$ Group delay[2] ($\times 10^4$ arcsec)	$\Delta\delta^1 - 1'40''.726\,30$ Phase delay[2] ($\times 10^4$ arcsec)	Root-mean-square of postfit residuals (phase delay only) Difference observables (ps)	Root-mean-square of postfit residuals (phase delay only) Single-source observables (ps)
1		0.5 ± 0.4		0.5 ± 1.1	12	15
2	-40 ± 80	-0.4 ± 0.8	50 ± 40	-0.7 ± 0.9	19	36
3		$+2.8 \pm 0.4$		-1.4 ± 1.9	13	18
4	150 ± 430	-4.5 ± 0.5	180 ± 260	1.2 ± 1.5	14	18

[1] $\Delta\alpha$ and $\Delta\delta$ represent the right ascension and declination, respectively, of the position of 3C 345 minus that of NRAO 512. The reference position is the weighted mean from all four experiments (see text).

[2] The uncertainty shown is the formal standard error, determined by scaling the measurement standard deviations uniformly such that the root-weighted-mean-square of the postfit residuals is unity. For the analyses of the phase delays, the standard deviations for the difference observables and the single-source observables (see text) were scaled separately so that, for each type, the root-weighted-mean-square of the postfit residuals is unity.

The root-weighted-mean-square scatters about the weighted mean for the estimates of right ascension and declination from the analysis of the phase-delay data for each experiment are $0^s.000\,03$ and $0''.000\,1$, respectively.

The scatter for the right ascension difference is considerably larger than would be anticipated based on the formal standard errors (see Table III). This anomaly may be due at least in part to an inadequate model for the brightness distribution of 3C 345 which is elongated mostly in the right ascension direction with an extent of the order of $0^s.000\,1$ (Wittels *et al.* 1976a). By contrast, the scatter in the estimates of declination is slightly under the value expected from the formal standard errors. Moreover, expected errors, for example, in the values used for UT1 (see below), would have produced a severalfold larger scatter. We thus conclude that the small scatter in the estimates of declination is fortuitous and that $0''.000\,3$ is an appropriate estimate of the uncertainty in our determination of $\Delta\delta$. Our results for $\Delta\alpha$ and $\Delta\delta$ in 1950.0 coordinates can therefore be summarized as:

$$\Delta\alpha(\text{3C 345} - \text{NRAO 512}) = 2^m\,29^s.436\,68 \pm 0^s.000\,03,$$

$$\Delta\delta(\text{3C 345} - \text{NRAO 512}) = 1'\,40''.726\,3 \pm 0''.000\,3, \quad (3)$$

where the values quoted represent the weighted means from the analysis of the phase-delay data for each experiment, and where the uncertainties quoted represent our estimates of 70 percent confidence limits that include consideration of the possibly dominant effects of systematic errors.

We also combined the estimates of $\Delta\alpha$ and $\Delta\delta$, and their correlations, from all experiments and solved for the relative position of the two sources under the assumption of zero relative proper motion. The results do not differ significantly from the values given in Eq. (3). The right ascension is virtually identical and the declination is about $0''.000\,2$ higher due to the effect of the correlations.

Finally, we reanalyzed the phase-delay data after interpolating the phase delays for 3C 345 to the epochs of the NRAO 512 observations and vice versa; in both cases, the result for the weighted means of the estimates of $\Delta\alpha$ and $\Delta\delta$ were consistent with the values given in Eq. (3).

b) Sensitivity Study

How sensitive are our estimates of $\Delta\alpha$ and $\Delta\delta$ to the fixed parameters (Table II) used in the analysis? To provide an answer, we carried out an extensive series of tests (see also Appendices A and B) to determine this sensitivity for the coordinates of the reference source, the baseline vector, the precession constant, and the pole position and orientation (UT1) of the earth, and for the models used for earth tides, the atmosphere, and source structure (Wittels 1975). For almost all of the parameters, plausible changes in value did not affect the estimates of $\Delta\alpha$ and $\Delta\delta$ significantly; such changes were smaller than the formal standard errors. However, changes in UT1 by 2 ms did produce changes of up to $0''.000\,7$ in the estimates of $\Delta\delta$, but insignificant changes in the estimates of $\Delta\alpha$, as expected (see Appendix A). Further details are given by Wittels (1975).

We also estimated the precession constant from the difference VLBI observables. The estimate we obtained agreed with the accepted value to (just) within the $2''$/century uncertainty of our estimate, thus confirming the insensitivity of our results for source position to a plausible error in the value used for this constant.

c) Postfit Residuals

The postfit residuals obtained from the analyses of the phase delay data are illustrated in Fig. 1(a) for the October 1971 experiment. Figure 1(b) displays the corresponding residuals from a solution based on these data, but for which a 2π error in phase connection was deliberately introduced at the boundary of the ~40-min gap in the data; the resultant systematic trends give dramatic evidence of the error. The difference in the two solutions

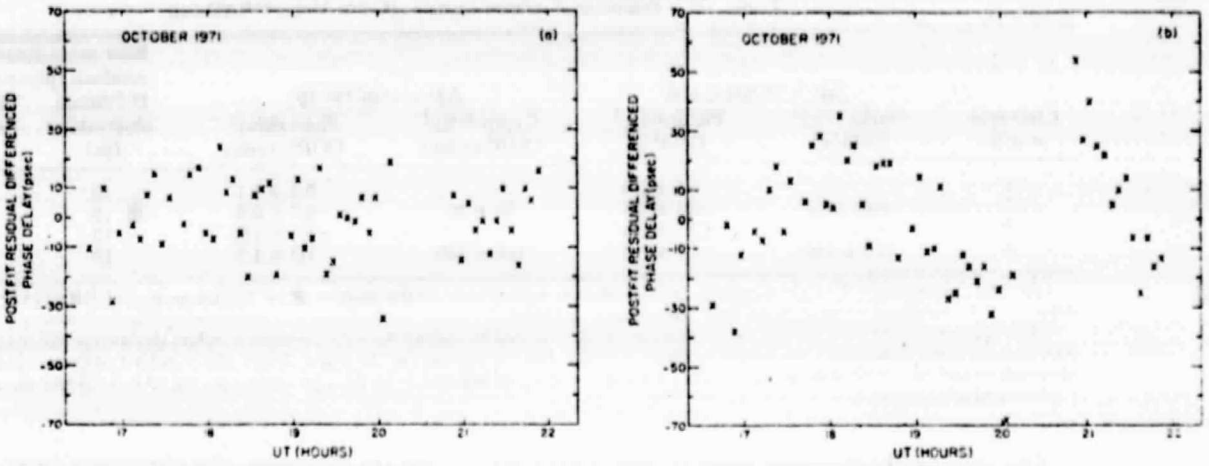

FIG. 1. The postfit residuals for the differenced phase delays for the 10 October 1971 experiment. In (a) the phases are properly "connected," whereas in (b) a 2π error was intentionally introduced in the connection across the gap in the data that occurred between about 20:10 and 20:50 UT.

is also dramatic quantitatively: The root-mean-square (rms) of the postfit residuals is 45% higher for the second than for the first solution.

The rms of the postfit residuals for the difference observables and for the single-source observables for each experiment are given in Table III. For three of the experiments, the latter are about one third higher than the former with the individual rms values being nearly independent of experiment. However, the rms values for the second experiment deviate noticeably from this pattern. This deviation is attributable to the very heavy rainfall at Haystack during this experiment. The rms of the difference observables was also relatively smaller than that for the single-source observables, indicating that the former were more immune to the ("long-term") trends in the weather pattern. The rms of the residuals is in each case severalfold larger than expected purely from signal-to-noise ratio considerations. The causes of these increases are not understood in detail; however, with the exception of the second experiment, we suspect that the receiver systems, especially the frequency standards, were more important contributors than were the uncancelled portions of the propagation medium. For time scales of the order of a few hours, the standards seemed to have been stable to about one part in 10^{13}. [This conclusion is very similar to that reached by Moran *et al.* (1973) from VLBI experiments involving a set of hydrogen-maser frequency standards partly overlapping with ours.]

In regard to the propagation mediu ~, we note that, for the fourth experiment only, for each pair of observations, 3C 345 and NRAO 512 were each observed at the same elevation angle at a given site. There was no noticeable effect of this equality on the postfit residuals; temporal variations in the atmosphere or other sources of variation were presumably more important contributors to the postfit residuals than were any inadequacies of our (static) model for the electrical path length of the atmosphere as a function of elevation angle.

d) Error Ellipses

The characteristics of the error ellipses for the estimates of $\Delta\alpha \cos\hat{\delta}$ and $\Delta\hat{\delta}$ from the individual experiments are given in Table IV. These ellipses are contours of constant probability density, centered on the estimates of $\Delta\alpha \cos\hat{\delta}$ and $\Delta\hat{\delta}$. Each principal semiaxis of each ellipse denotes one (formal) standard deviation for the estimate of that linear combination of $\Delta\alpha \cos\hat{\delta}$ and $\Delta\hat{\delta}$ that corresponds to the direction of the semiaxis. The directions of these axes depend importantly on the declination of the sources and on the part of the u-v plane covered by the observations in a particular experiment (see Wittels *et al.* 1976b). For a related reason, the ratio of the major to the minor axis is higher the shorter the experiment.

If there were no systematic errors affecting our esti-

TABLE IV. Error ellipses[1]

Experiment number	Semi-major axis ($\times 10^4$ arcsec)	Semi-minor axis ($\times 10^4$ arcsec)	Position angle of major axis (deg)
1	1.1	0.3	−10
2	1.2	0.5	42
3	1.9	0.4	−9
4	1.6	0.3	19

[1] Error ellipses are contours of constant probability density in the $\Delta\alpha \cos\hat{\delta} - \Delta\hat{\delta}$ plane, based on the separate analyses of the phase-delay data (see Table III). If there were no sources of systematic error unaccounted for, the true values of $\Delta\alpha \cos\hat{\delta}$ and $\Delta\hat{\delta}$ would lie inside the error ellipse centered on the estimated values with probability 0.4 (Shapiro 1958). The marked lack of overlap of the error ellipses in the $\Delta\alpha \cos\hat{\delta}$ coordinate is an indication of the importance of the systematic errors.

mates, we could conclude that the true values of $\Delta\alpha \cos\delta$ and $\Delta\delta$ lay inside such an error ellipse with probability 0.4 (see, for example, Shapiro 1958). The fact that some of the error ellipses fail to overlap by a substantial margin in the $\Delta\alpha \cos\delta$ coordinate, is an indication of the importance of systematic errors in our experiment.

e) Relative Proper Motion

We also combined the estimates of $\Delta\alpha$, $\Delta\delta$, and their correlation from each of the four experiments to determine the relative proper motion of the two sources. In particular, we estimated four parameters: the values of $\Delta\alpha$ and $\Delta\delta$, referred to 1973.0, and the direction and magnitude of the relative proper motion. The proper motion of 3C 345 minus that of NRAO 512 was found to be $0\overset{''}{.}000\ 25 \pm 0\overset{''}{.}000\ 20\ y^{-1}$ along a position angle of $220° \pm 60°$. The uncertainties represent formal standard errors obtained by scaling uniformly the errors accompanying the estimates of $\Delta\alpha$ and $\Delta\delta$ from the individual solutions such that a value of unity was obtained for the root-weighted-mean-square of the postfit residuals, adjusted for the number of degrees of freedom. This result for relative proper motion does not differ from zero significantly, especially when one considers the distribution of the individual results. More formally, we may conclude, with about 70% confidence, that any relative proper motion of the centers of brightness is no more than $0\overset{''}{.}000\ 5\ y^{-1}$. (Of course, the circular boundary enclosing this limit in the proper-motion plane is not strictly a contour of constant probability density because our formal estimate of relative proper motion is not zero.)

VI. DISCUSSION

Finally, we discuss the bounds that can be placed on the distances to 3C 345 and NRAO 512, the prospects for improvement in the determination of relative position and proper motion of these sources, and some other possible applications of the basic technique.

a) Bound on Distance

From an upper bound on relative proper motion, we can deduce nothing useful about the distances of two sources from the earth without making some additional assumptions (see Appendix C). If we assume that the transverse velocity of each source is at least 100 km/s, and that the directions of these two velocities form an angle greater than 60°, we may then conclude that each source is at a distance greater than ~40 kpc from the earth. (By contrast, the lower bound on distance that can be inferred from parallax considerations is about 5 kpc, if the two sources are assumed to be at sufficiently different distances from the earth.) Considering the directions to 3C 345 and NRAO 512 ($b^{II} \simeq 41°$; $l^{II} \simeq 65°$), we can further conclude that both sources are outside the Galaxy. This result is hardly a surprise. The assumed transverse velocities would have to be very superluminal indeed to obtain lower bounds that approached the accepted proper-motion distances of several gigaparsecs for these sources.

b) Prospects for Improvement

What are the prospects for the utilization of astrometric VLBI measurements to decrease both the uncertainty in relative position and the upper bound on the relative proper motion of these objects? Several avenues are open. First, the facts that the smaller of the semiminor axes of the error ellipses were smaller than $0\overset{''}{.}000\ 1$ and that those from several of the different experiments were appreciably inclined to one another, imply that observations over the entire period of mutual visibility of the participating antennas should lead to a standard deviation smaller than $0\overset{''}{.}000\ 1$ in both $\Delta\alpha \cos\delta$ and $\Delta\delta$. A covariance analysis for a simulated schedule of Haystack–Goldstone observations, with a cycle time of 5 min, an elevation angle cutoff of 15 deg at both sites, and a measurement error of 10 ps for each phase-delay difference, yielded results in agreement with this implication; we obtained $\sigma(\Delta\alpha \cos\delta) \sim \sigma(\Delta\delta) \sim 5 \times 10^{-5}$ arcsec, with a correlation between the two estimates of approximately 0.4.

Second, repetitions of the measurements would, of course, lead to a decrease in the uncertainty in the determination of both the relative position and the upper bound on proper motion, given that systematic errors do not dominate.

Third, if instrumental deficiencies were the major contributors to the postfit residuals, then use of more stable frequency standards, calibration of the instrumentation to the picosecond level or below, and increases in the signal-to-noise ratios through use of a wider-band recording system, will insure that the accuracy of the results will be limited only by the propagation medium. Frequency standards with a stability of about five parts in 10^{15} over periods from 200 s to 1 day are now available (Vessot 1976; see, also, Rogers *et al.* 1976) and would contribute only about a picosecond error to the phase-delay difference from neighboring observations of two sources. Equipment to calibrate receiver systems to the picosecond level, not available in 1971–74, is now available (Rogers 1975). Further, a 56-MHz-bandwidth VLBI recording and processing system is in an advanced stage of development and will have sufficient sensitivity to reduce the noise contribution to each phase measurement with the Goldstone–Haystack interferometer to the picosecond level, even if the correlated flux density for NRAO 512 drops to the 0.1 Jy level. The correlated flux density obtained from observations of this source has in fact declined steadily at an average rate of about 0.1 Jy/year from a level of about 1.5 Jy in 1971.

The limit on accuracy that will be set by the propagation medium after the implementation of these system

improvements is difficult to estimate reliably, but may be at the 2 pg level or below for high elevation angles in good weather for the small, half-degree separation between 3C 345 and NRAO 512.

To utilize such accuracy effectively, it will be necessary to improve appropriately the determination of the rotation of the earth and of the brightness distribution of 3C 345. The rotation of the earth can be obtained with the needed accuracy from contemporaneous VLBI observations of a suite of sources suitably distributed across the sky. The brightness distribution can be obtained reliably if the observations are made with a well-distributed array of antennas. With such a configuration, the observations of NRAO 512, which is, in effect, a point source, can also be used to good advantage as a phase reference for the observations of 3C 345 to enable both fringe amplitude and fringe phase to be used for the determination of the brightness distribution of the latter. (With observations from only two antennas, the phase-reference technique cannot be used very effectively for the mapping of a source.)

The resulting determinations of relative position will probably enable one to determine, for example, which parts of the brightness distribution are moving with respect to NRAO 512 and which, if any, are not. Certainly these distinctions should be possible to draw after a decade of data gathering, with each session extended over the full period of mutual visibility, provided only that the different parts of the brightness distribution can be followed unambiguously for such a period of time. Detection of such motion could be of fundamental importance in distinguishing between various theoretical models of superluminal motion.

c) *Other Applications*

We may also apply this VLBI technique to other source pairs such as 3C 273B and 3C 279, 3C 84 and Beta Persei (Algol), and VRO 42.22.01 (BL Lacertae) and 3C 418. Provided that source-structure changes in 3C 84 do not create too severe a problem and that sufficient sensitivity exists to obtain accurate fringe phases from observations of Algol, significant information should be obtainable on some of the orbital elements of the components of the Algol system in addition to an accurate measurement of the system's proper motion.

Similar observations of suitable pulsar-quasar pairs could yield very accurate proper-motion values and distances (parallaxes) for the pulsars, and, possibly, disclose whether or not they belong to multiple star systems. Pulsars could, in turn, be used as phase references for the improved determination of the brightness distributions of compact extragalactic radio sources that appear nearby in the sky.

Finally, we note that accurate determinations of the relative positions and proper motions of compact sources are of major importance as well for their use in the monitoring of the crustal motions of the earth.

We thank the Radio Astronomy Experiment Selection (RAES) Panel, successively chaired by J. Greenstein, M. Cohen, and G. Burbidge, and formed by the National Aeronautics and Space Administration (NASA) and the Jet Propulsion Laboratory, for establishment of the "Quasar Patrol" during which some of the observations reported here were made. We are indebted to the staffs of the Haystack Observatory, the Goldstone Tracking Station, and the National Radio Astronomy Observatory for their aid during the observations, and give special thanks to G. Catuna for aid in data processing. Participation of the MIT experimenters was supported in part by the National Science Foundation, Grant DES 74-22712, and in part by NASA, Grant NGR 22-009-839. Radio Astronomy programs at the Haystack Observatory are conducted with support from the National Science Foundation, Grant MPS 71-02109 A07. The portion of the research carried out at the Jet Propulsion Laboratory, California Institute of Technology, was under contract NAS7-100, sponsored by NASA. The National Radio Astronomy Observatory is operated by Associated Universities, Inc., under contract with the National Science Foundation.

APPENDIX A: SENSITIVITY ANALYSIS

Here we present a simplified analysis that illustrates the sensitivity of the estimates of $\Delta\alpha$ and $\Delta\delta$ to errors in the values used to represent the pole direction and orientation (UT1) of the earth, the baseline vector, and the coordinates of the reference source (see Sec. II and Table II). We assume, unrealistically, that the estimates of $\Delta\alpha$ and $\Delta\delta$ are based on the sinusoidal terms in Eq. (2) and on measurements of $\Delta\phi$, all equally accurate and closely and uniformly spaced throughout a diurnal period. Under these conditions, for example, the estimates of the coefficients of $\sin(A_0 + \Omega t - \alpha)$ and $\cos(A_0 + \Omega t - \alpha)$ in Eq. (2) will be uncorrelated.

Let $d\Gamma_\parallel$ and $d\Gamma_\perp$ denote, respectively, the errors in our knowledge of the components of the direction of the pole of the earth parallel and perpendicular to the equatorial projection of the baseline. In addition, let dUT denote the error in our knowledge of the orientation of the earth about its axis of rotation. We then find

$$dA = d\mathrm{UT} - d\Gamma_\perp \tan D, \qquad \text{(A1)}$$

and

$$dD = d\Gamma_\parallel, \qquad \text{(A2)}$$

where dA and dD are the corresponding induced errors in the right ascension and declination, respectively, of the baseline. [The signs, or directions, of the errors $d\Gamma_\parallel$, $d\Gamma_\perp$, and dUT are, in effect, defined by Eqs. (A1) and (A2).] From Eq. (2), we can infer that the consequent changes in the estimates of $\Delta\alpha$ and $\Delta\delta$ will be, approximately:

$$d\Delta\alpha \simeq (\Delta\alpha \tan D)dD - (\Delta\delta \tan\delta + \tfrac{1}{2}\Delta\alpha^2)dA, \qquad \text{(A3)}$$

and

$$d\Delta\delta \simeq (\Delta\delta \tan D)dD + (\Delta\delta \cot\delta)dA, \quad \text{(A4)}$$

with dA and dD given, in this case, by Eqs. (A1) and (A2).

For an east-west baseline ($D = 0$), the estimates of $\Delta\alpha$ and $\Delta\delta$ have no sensitivity to either $d\Gamma_\parallel$ or $d\Gamma_\perp$; for a baseline normal to the equatorial plane, the sensitivity becomes infinite. Since $\Delta\delta \sim O(\Delta\alpha^2)$, there is virtually no effect of $d\Gamma_\parallel$ on the estimate of $\Delta\delta$, except when $D \simeq \pi/2$. These equations also show, for an arbitrary source, that the estimate of $\Delta\alpha$ is insensitive to dUT and to $d\Gamma_\perp$, except for $\delta \simeq \pi/2$. The sensitivity of $\Delta\delta$, on the other hand, to dUT and to $d\Gamma_\perp$ vanishes for $\delta \simeq \pi/2$ and is greatest for $\delta \simeq 0$.

Changes in Ω, as opposed to those in A_0, or UT1, as defined here, have only a slightly different effect; we ignore this difference in this semi-quantitative analysis.

An error, dB, in the baseline length introduces the following errors in the determination of the separation of the two sources:

$$d\Delta\alpha = -\Delta\alpha(dB/B), \quad \text{(A5)}$$

and

$$d\Delta\delta = -[\Delta\delta + \tfrac{1}{2}(\Delta\alpha)^2 \cot\delta]\,(dB/B). \quad \text{(A6)}$$

Errors $d\alpha$ and $d\delta$ in the coordinates of the reference source introduce errors in $\Delta\alpha$ and $\Delta\delta$ given approximately by:

$$d\Delta\alpha \simeq (\Delta\alpha \tan\delta)d\delta - (\Delta\delta \tan\delta + \tfrac{1}{2}\Delta\alpha^2)d\alpha, \quad \text{(A7)}$$

and

$$d\Delta\delta \simeq (-\Delta\delta \cot\delta + \tfrac{1}{2}\Delta\alpha^2)d\delta + (\Delta\alpha + \cot\delta)d\alpha. \quad \text{(A8)}$$

These latter results show that, except in the obvious pathological cases, $\Delta\alpha$ is most strongly affected by an error in δ and $\Delta\delta$ by an error in α.

Required modifications of these formulas for the case $\Delta\alpha = O(\Delta\delta^2)$ can be obtained by straightforward computation.

APPENDIX B: REDUCTION TO CENTER OF BRIGHTNESS

We treat here the determination of the corrections to the phase- and group-delay measurements needed to refer them to the center of brightness of the source.

At present, due to incomplete sampling, it is not possible to determine the brightness distribution of radio sources uniquely from VLBI data; however, relatively simple, time-dependent models with two components have been developed which represent the data for NRAO 512 (Wittels *et al.* 1975) and for 3C 345 (Wittels 1975, Cohen *et al.* 1976, Wittels *et al.* 1976a, Readhead *et al.* 1978) quite well.

We illustrate the removal of the effects of the brightness distribution for a model with two point components. Defining the center of brightness as the origin, so that $r_1B_1 = r_2B_2$, where r_i and B_i are the distance from the origin and the flux density, respectively, of Component i, we obtain the following expression for the fringe phase relative to that for the center of brightness:

$$\phi^{\rm rel}(u,v) \equiv \phi^{\rm obs}(u,v) - \phi^{\rm cb}(u,v) = \tan^{-1}\left(\frac{-B_1\sin q_1 + B_2\sin q_2}{B_1\cos q_1 + B_2\cos q_2}\right), \quad \text{(B1)}$$

where

$$q_i \equiv 2\pi r_i\,(u\sin P + v\cos P), \quad i = 1,2, \quad \text{(B2)}$$

and where $\phi^{\rm obs}$ would be the observed fringe phase, in the absence of error, were the source to consist of two point components; $\phi^{\rm cb}$ is the corresponding fringe phase for the center of brightness; P is the position angle of the line connecting the two components; and u and v represent the resolution of the interferometer in the directions of increasing right ascension and declination, respectively. (Units may be chosen such that r_i and P are expressed in radians with u and v expressed in ~~radians~~/radian.)

If the two components are of nearly equal flux density ($B_2 \gtrsim B_1$), we find

$$\phi^{\rm rel} \simeq \beta(\tan q - q) - \beta^2 q\,(\tan q - q/2), \quad \text{(B3)}$$

with

$$0 < \beta \equiv \frac{B_2 - B_1}{B_2 + B_1} \ll 1; \quad q \equiv q_1 + q_2. \quad \text{(B4)}$$

For 3C 345, this model with two point components yields $\beta \simeq 0.1$; hence Eq. (B3) is a useful approximation.

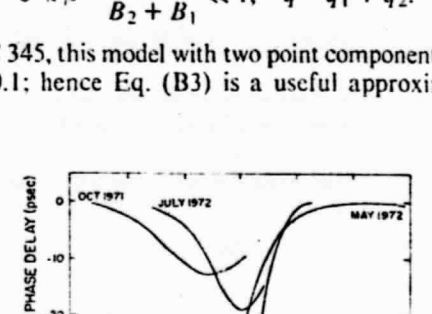

FIG. 2. Inferred contribution of the brightness structure of 3C 345 to the phase delay measurements for the Haystack–Goldstone baseline. Calculations were based on a model with two point components for the brightness of the source for the first three experiments, and on a model with two elliptical Gaussian components for the last experiment (see Wittels 1975). For each experiment, the contribution to the phase delay is shown only for the period encompassing the observations. Note that a 40 psec change corresponds to a change in position of a point source of about 0.0006 for the Haystack–Goldstone baseline.

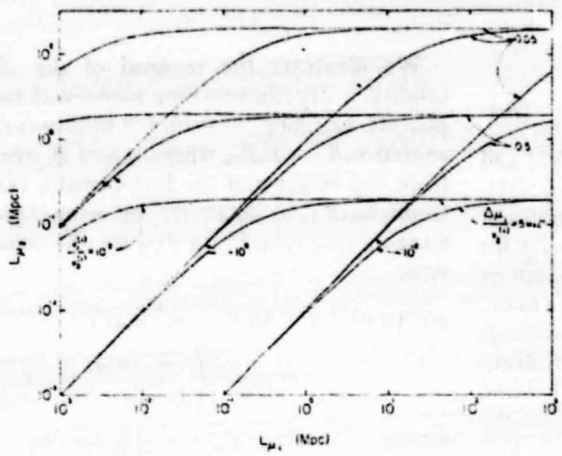

FIG. 3. The allowed distances for 3C 345 and NRAO 512 as a function of the parameters $v_1^{(i)}/v_2^{(i)}$ and $\Delta\mu_i/v_2^{(i)}$ (see text). A value of 5 Mpc^{-1} for $\Delta\mu_i/v_2^{(i)}$ corresponds, for example, to values of $\Delta\mu_i$ and $v_2^{(i)}$ of 10^{-4} arcsecy and 100 km/s, respectively. For $\Delta\mu_i < 0$, the sources appear to approach each other and the allowed distances can be obtained by changing the sign of $\Delta\mu_i/v_2^{(i)}$ and interchanging the labels on the axes [see Eq. (C2)].

When q is small, as is sometimes the case, we see that

$$\phi^{\rm rel} \simeq \frac{\beta q^3}{3} - \frac{\beta^2 q^2}{2}, \quad q \ll 1, \beta \ll 1. \qquad \text{(B5)}$$

and, therefore, that the correction phase $\phi^{\rm rel}$ tends to vanish as the combined fourth power of β and q under such conditions. Equation (B5), of course, represents a consistent approximation only if β and q are of the same order.

The correction phases for each experiment, obtained from the models of 3C 345 (Wittels 1975), are shown in Fig. 2.

Expressions for $\phi^{\rm rel}$ can be obtained as well for other reference points within the source or from other models for the brightness distribution.

The expression for the group delay, $\tau_g^{\rm rel}$, relative to that for the center of brightness, is given by:

$$\tau_g^{\rm rel}(u,v) = \frac{d\phi^{\rm rel}}{d\omega} = \frac{\beta(1-\beta^2)q(2-\cos q)}{4\omega[(1+\cos q)+\beta^2(1-\cos q)]} \underset{\beta \ll 1}{\simeq} \frac{\beta q}{4\omega}\left(\frac{2-\cos q}{1+\cos q}\right), \qquad \text{(B6)}$$

where ω is the center of the (angular) radio frequency band over which the observations are made, and where we assume that this band is small relative to the center frequency. For a radio frequency of 8 GHz, we see that $\tau_g^{\rm rel}$ will always be under about 0.25 ns for $q \lesssim \pi$ and $\beta \simeq 0.1$ since, under these conditions, $\tau_g^{\rm rel} < 3q(1-\beta)^2/8\beta\omega$.

APPENDIX C: RELATION BETWEEN PROPER MOTION AND DISTANCE

The general interpretation of a relative proper motion of two sources in terms of bounds on their distances involves cosmology. For the standard cosmology (see, for example, Weinberg 1972), it is easy to show that a source at proper-motion distance L_μ, and with peculiar velocity $\mathbf{v}$, will have components of apparent proper motion given by

$$\mu_i = \frac{dx_i}{dt} = \frac{v}{L_\mu}\frac{\sin\theta}{[1-\beta(L_p/L_\mu)\cos\theta]} \sin[P+(i-1)\mu/2], \qquad \text{(C1)}$$

where the x_i are angular distances along orthogonal directions on the plane of the sky measured from the position of the source; t is coordinate time; θ is the angle between $\mathbf{v}$ and the line from the source to the observer; v is the magnitude of $\mathbf{v}$; P is the position angle of $\mathbf{v}$ measured from the direction of increasing x_1 towards the direction of increasing x_2; β is v/c; and (L_p/L_μ) is the ratio of the parallax to the proper-motion distance (Weinberg 1972) and is always greater than unity for closed universes and less than unity for open universes.

The maximum with respect to θ of the factor $\sin\theta/[1-\beta(L_p/L_\mu)\cos\theta]$ is $[1-\beta^2(L_p^2/L_\mu^2)]^{-1/2}$ and is attained for $\cos\theta = \beta(L_p/L_\mu)$. Thus, for example, for a closed universe, even the detection of proper motion, along with the establishment (somehow!) that the center of brightness coincides with the center of mass, would *not* allow us to conclude unequivocally that a radio source is not at a "cosmological" distance, unless we have independent knowledge (somehow!) of its peculiar velocity. Because we are concerned here with *relative* proper motion only, a similar statement applies to the case of an open universe: regardless of the values of the peculiar velocities, any components of relative proper motion can be matched by a continuum of pairs of values of L_μ.

For two sources near the Galaxy, for example, a component, $\Delta\mu_i$, of their relative proper motion can be written in terms of their distances as

$$\Delta\mu_i \equiv \frac{d\Delta x_i}{dt} = \frac{v_1^{(i)}}{L_2} - \frac{v_2^{(i)}}{L_1} \qquad \text{(C2)}$$

where L_k and $v_k^{(i)}$, $k,i = 1,2$, represent, respectively, the "ordinary" distance to source k and the ith component of its transverse velocity. Figure 3 depicts the allowed distances for the two sources as functions of the two parameters $(v_1^{(i)}/v_2^{(i)})$ and $\Delta\mu_i/v_2^{(i)}$. It is also clear from this figure and Eq. (C2) that for any values of $v_1^{(i)}$ and $v_2^{(i)}$ one can always find arbitrarily small values of L_1 and L_2 which are consistent with an apparent proper motion smaller than any given upper bound. Nonetheless, it would probably be reasonable to assume that L_k will be comparable to, or exceed $|v_k^{(i)}/\Delta\mu_i|$, given an upper bound $|\Delta\mu_i|$ on a component of apparent proper motion.

REFERENCES

Clark, T. A., Hutton, L. K., Marandino, G. E., Counselman, C. C., Robertson, D. S., Shapiro, I. I., Wittels, J. J., Hinteregger, H. F., Knight, C. A., Rogers, A. E. E., Whitney, A. R., Niell, A. E., Rönnäng, B. O., and Rydbeck, O. E. H. (1976). Astron. J. **81**, 599.

Cohen, M. H., Kellermann, K. I., Shaffer, D. B., Linfield, R. P., Moffet, A. T., Romney, J. D., Seielstad, G. A., Pauliny-Toth, I. I. K., Preuss, E., Witzel, A., Schilizzi, R. T., and Geldzahler, B. J. (1977). Nature **268**, 405.

Cohen, M. H., Moffet, A. T., Romney, J. D., Schilizzi, R. T., Seielstad, G. A., Kellermann, K. I., Purcell, G. H., Shaffer, D. B., Pauliny-Toth, I. I. K., Preuss, E., Witzel, A., and Rinehart, R. (1976). Astrophys. J. Lett. **206**, L1.

Hinteregger, H. F. (1972). Ph.D. thesis, Massachusetts Institute of Technology.

Knight, C. A., Robertson, D. S., Rogers, A. E. E., Shapiro, I. I., Whitney, A. R., Clark, T. A., Goldstein, R. M., Marandino, G. E., and Vandenberg, N. R. (1971). Science **172**, 52.

Lynds, C. R. (1975). Private communication.

Moran, J. M., Papadopoulos, G. D., Burke, B. F., Lo, K. Y., Schwartz, P. R., Thacker, D. L., Johnston, K. J., Knowles, S. H., Reisz, A. C., and Shapiro, I. I. (1973). Astrophys. J. **185**, 535.

Readhead, A. C. S., Cohen, M. H., Pearson, T. J., and Wilkinson, P. N. (1978). Nature **276**, 768.

Robertson, D. S. (1975). Ph.D. thesis, Massachusetts Institute of Technology.

Rogers, A. E. E. (1975). Haystack Obs. Tech. Note, 1975-16.

Rogers, A. E. E., Whitney, A. R., and Hanson, L. B. (1976). Proceedings of the 8th Annual NASA and Department of Defense Precise Time and Time Interval Planning Meeting, Goddard Space Flight Center Technical Note X-184-77-149.

Shapiro, I. I. (1958). *Prediction of Ballistic Missile Trajectories from Radar Observations* (McGraw-Hill, New York), p. 87.

Shapiro, I. I., Robertson, D. S., Knight, C. A., Counselman, C. C., Rogers, A. E. E., Hinteregger, H. F., Lippincott, S., Whitney, A. R., Clark, T. A., Niell, A. E., and Spitzmesser, D. J. (1974). Science **186**, 920; (1976). Science **191**, 420.

Vessot, R. F. C. (1976). Private communication.

Weinberg, S. (1972). *Gravitation and Cosmology: Principles and Applications of the General Theory of Relativity* (Wiley and Sons, New York).

Whitney, A. R. (1974). Ph.D. thesis, Massachusetts Institute of Technology.

Whitney, A. R., Rogers, A. E. E., Hinteregger, H. F., Knight, C. A., Levine, J. I., Lippincott, S., Clark, T. A., Shapiro, I. I., and Robertson, D. S. (1976). Radio Sci. **11**, 421.

Wittels, J. J. (1975). Ph.D. thesis, Massachusetts Institute of Technology.

Wittels, J. J., Knight, C. A., Shapiro, I. I., Hinteregger, H. F., Rogers, A. E. E., Whitney, A. R., Clark, T. A., Hutton, L. K., Marandino, G. E., Niell, A. E., Rönnäng, B. O., Rydbeck, O. E. H., Klemperer, W. K., and Warnock, W. W. (1975). Astrophys. J. **196**, 13.

Wittels, J. J., Cotton, W. D., Counselman, C. C. III, Shapiro, I. I., Hinteregger, H. F., Knight, C. A., Rogers, A. E. E., Whitney, A. R., Clark, T. A., Hutton, L. K., Rönnäng, B. O., Rydbeck, O. E. H., and Niell, A. E. (1976a). Astrophys. J. Lett. **206**, L75.

Wittels, J. J., Shapiro, I. I., Cotton, W. D., Counselman, C. C. III, Hinteregger, H. F., Knight, C. A., Rogers, A. E. E., Whitney, A. R., Clark, T. A., Hutton, L. K., Niell, A. E., Rönnäng, B. O., and Rydbeck, O. E. H. (1976b). Astron. J. **81**, 933.

RECENT RESULTS OF RADIO INTERFEROMETRIC DETERMINATIONS OF A TRANSCONTINENTAL BASELINE, POLAR MOTION, AND EARTH ROTATION

D. S. Robertson, W. E. Carter
National Oceanic and Atmospheric Administration
National Ocean Survey/National Geodetic Survey

B. E. Corey, W. D. Cotton, C. C. Counselman, I. I. Shapiro, J. J. Wittels
Department of Earth and Planetary Sciences and Department of Physics
Massachusetts Institute of Technology

H. F. Hinteregger, C. A. Knight, A. E. E. Rogers, A. R. Whitney
Haystack Observatory

J. W. Ryan, T. A. Clark, R. J. Coates
National Aeronautics and Space Administration

C. Ma
University of Maryland

J. M. Moran
Smithsonian Astrophysical Observatory

ABSTRACT

Radio interferometric observations of extragalactic radio sources have been made with antennas at the Haystack Observatory in Massachusetts and the Owens Valley Radio Observatory in California during fourteen separate experiments distributed between September 1976 and May 1978. The components of the baseline vector and the coordinates of the sources were estimated from the data from each experiment separately. The root-weighted-mean-square scatter about the weighted mean ("repeatability") of the estimates of the length of the 3900 km baseline was approximately 7 cm, and of the source coordinates, approximately 0".015 or less, except for the declinations of low-declination sources. With the source coordinates all held fixed at the best available, a posteriori, values, and the analyses repeated for each experiment, the repeatability obtained for the estimate of baseline length was 4 cm. From analyses of the data from several experiments simultaneously, estimates were obtained of changes in the x component of pole position and in the Earth's rotation (UT1). Comparison with the corresponding results obtained by the Bureau

D. D. McCarthy and J. D. Pilkington (eds.), Time and the Earth's Rotation, 217–224.

International de l'Heure (BIH) discloses systematic differences. In particular, the trends in the radio interferometric determinations of the changes in pole position agree more closely with those from the International Polar Motion Service (IPMS) and from the Doppler observations of satellites than with those from the BIH.

For the past several years, our group has been involved in a major effort to improve the quality of data obtained by very-long-baseline interferometry (VLBI) through development of a third generation system referred to as the Mark III system. Portions of this system are presently in operation, and we expect the system to be in full operation by the end of 1979. The major improvements in the hardware and software already implemented can be cataloged as follows:

First: the use of wide-band parametric amplifiers which allow bandwidths of about 300 MHz to be synthesized, a tenfold increase over the previous limit. The significance of this increase in bandwidth lies in the fact that the uncertainty in the measurement of interferometric group delay is inversely proportional to the total bandwidth.

Second: the use of surface meteorological measurements with algorithms supplied by J. Marini of NASA's Goddard Space Flight Center. This combination has resulted in a significant decrease in the level of systematic errors caused by atmospheric effects.

Third: the use of equipment to calibrate instrumental effects, in particular the effect of the contribution to the measured delay of the path from the antenna feed horn to the recording apparatus. The uncertainty in such instrumental effects has thereby been reduced to the level of a few pico-seconds.

Fourth: the inclusion of several geophysical effects, resulting from the nonrigidity of the Earth, in the analysis programs (Woolard, 1959; Melchior, 1971; Guinot, 1970, 1974). These effects have an amplitude of a few hundredths of an arc second or less. Also we employed the value of the precession constant from the paper by Lieske et al. (1977).

Fifth: the use of rewritten analysis programs. The inter-comparison of the new programs with the old indicates that there are no coding errors in the parts that were in common with effects on the interpretation of the observations larger than 1 mm. (This test does not address possible errors in the physical models on which both programs were based or in the additions noted above. For example, the precession-nutation algorithms employed are unlikely to be accurate at the millimeter level.)

Utilizing the above mentioned improvements in hardware, we undertook a series of VLBI experiments, starting in September 1976. These experiments utilized the 37-meter-diameter antenna at the Haystack Observatory in Massachusetts, and the 40-meter-diameter antenna at the Owens Valley

Radio Observatory in California, to observe extragalactic radio sources. We have used the data from these experiments to estimate the components of the baseline vector, the coordinates of the radio sources, and the changes in the x component of the position of the Earth's pole and in the Earth's rotation (UT1). (This particular baseline is not sensitive to changes in the y component of the position of the pole because any change in that component causes a nearly parallel displacement of the baseline vector and, therefore, has little effect on observations of very distant sources. In any event, a single baseline can yield information on only two of the three angles required to specify the orientation of the Earth in inertial space.)

We discuss here the observations made with this interferometer in fourteen experiments, the last of these being in May 1978. Each experiment spanned from 15 to 48 hours in which from 120 to 240 separate, three-minute, observations were made. The data from each session were first analyzed separately, and the following parameters were estimated: the vector components of the baseline, the epoch and rate offsets of the clock at Owens Valley relative to those offsets of the clock at Haystack, the zenith electrical path length of the atmosphere at each site, and the right ascension and declination of each source, with one right ascension held fixed to define the origin of right ascension. To test the consistency of the results, the repeatability of the estimates of baseline length was examined. Baseline lengths were selected for examination because the values of the direction components of the baseline vector are affected by errors in the values used for the pole position and for UT1; similarly, the estimated values for the source coordinates are affected by errors in the formulas used for precession and nutation, although the arc lengths between sources are free from such errors.

The estimate of the baseline length from each experiment is shown in Figure 1. The error bars represent formal standard errors based on measurement errors modified so that the root-weighted-mean-square scatter about the weighted mean (hereinafter "RMS scatter" or "repeatability") of the postfit residuals is unity. The RMS scatter of these baseline length values is 7 cm, or, expressed as a fraction of the 3900 km baseline, about 2 parts in 10^8. The values of the source coordinates from these solutions have an RMS scatter of 0".015 or less, except for the declinations of the low-declination sources for which our observations have less sensitivity. The values for these coordinates appear to be somewhat more accurate than our previously published results (Clark et al., 1976) and will be discussed more fully in a separate paper.

To examine how the repeatability of the baseline results might have been affected by the prior availability of sufficiently accurate values of the source coordinates, we obtained new solutions with each source coordinate fixed at the weighted mean of its values from the 14 separate solutions, thereby reducing the number of parameters estimated in each solution from about 30 to about 10. We would expect the RMS

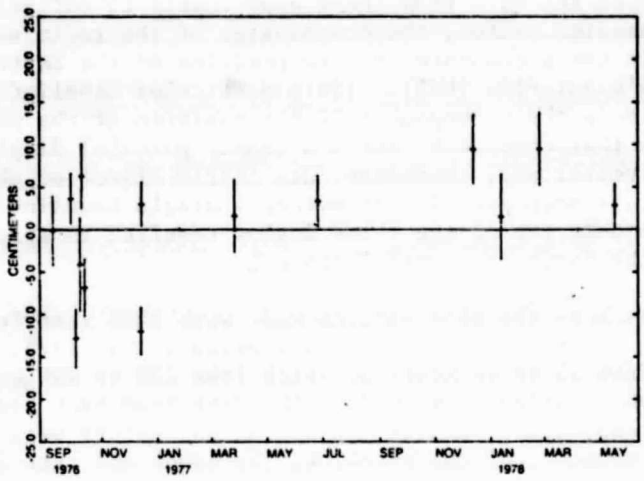

Figure 1. Differences between the estimates of baseline length and their weighted mean from 14 experiments with the Haystack-Owens Valley interferometer. The weighted mean of these estimates of baseline length was 392,888,164.4 cm. The value of the speed of light used to convert light travel time to centimeters was $2.99792458 \times 10^{10}$ cm/s. The source coordinates were also estimated in these analyses.

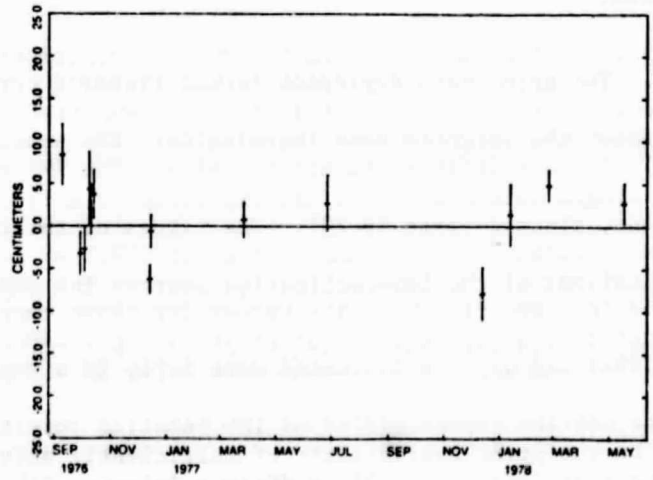

Figure 2. Same as Figure 1, but with each source coordinate kept fixed at the same value for all analyses (see text). The weighted mean of these length estimates was 392,888,162.6 cm.

scatter to be reduced, provided that any systematic errors affecting the data and the model are sufficiently benign. The estimates of baseline length from these solutions are shown in Figure 2; the RMS scatter is indeed reduced, to about 4 cm, and the mean itself, as one might expect, changed little, by only 1.8 cm. These results indicate that at present VLBI can be used to determine lengths of transcontinental baselines with a repeatability of about 4 cm.

It is not possible from VLBI data alone to determine the point at which the rotation pole of the Earth pierces its crust. It is possible, however, to measure changes in this position from the position at some arbitrary epoch, the position of the pole at that epoch being used to define the orientation of the baseline in the Earth-fixed frame. The ability to determine these changes is, therefore, related to the ability to determine the orientation of the baseline. An examination of the relevant error ellipsoids indicates that, for our interferometer, the inherent sensitivity of the VLBI data to baseline orientation is about a factor of four less than their sensitivity to baseline length. We would expect, therefore, that uncertainties in the determinations of changes in the position of the pole from these data would be no greater than about 30 cm, equivalent to about 0".01 uncertainty in the determination of the direction of the pole.

To determine changes in the position of the pole, we combined all of the data in a single analysis and estimated these changes and all other relevant parameters simultaneously. For one experiment, conducted on 4 October 1976, the position of the pole was fixed at the value determined by the BIH, as recorded in their Circular D publications, in order to define the orientation of the baseline. Our results for the position of the pole from the other 13 experiments are shown in Figure 3 in the form of the difference between the VLBI and the BIH values.

Also plotted in Figure 3 are the differences from the BIH values of the x component of the pole position determined by the IPMS from optical observations (tabulated at intervals of 0.05 years), and by the Polar Monitoring Service of the Defense Mapping Agency Topographic Center from satellite Doppler observations (tabulated at intervals of 5 days), both as recorded in the Series 7 publications of the U. S. Naval Observatory. The standard deviations for the IPMS data are typically about 50 cm or 0".015. The changes with time for all three sets have a common trend, systematically different from the BIH values. This common trend appears to have persisted at least through May 1978. Thus, the VLBI results seem to agree with both the IPMS results and the Doppler results better than any one of the three sets agrees with the BIH values. The RMS scatter of the differences between the VLBI and BIH determinations shown in Figure 3 is 0".030; the corresponding scatter for the Doppler results is 0".020; and for the IPMS results 0".027. This scatter in the VLBI results is about 30 percent less than that obtained previously (Shapiro et al., 1974; Robertson, 1975) from the analysis of VLBI observations made in 1972 and 1973.

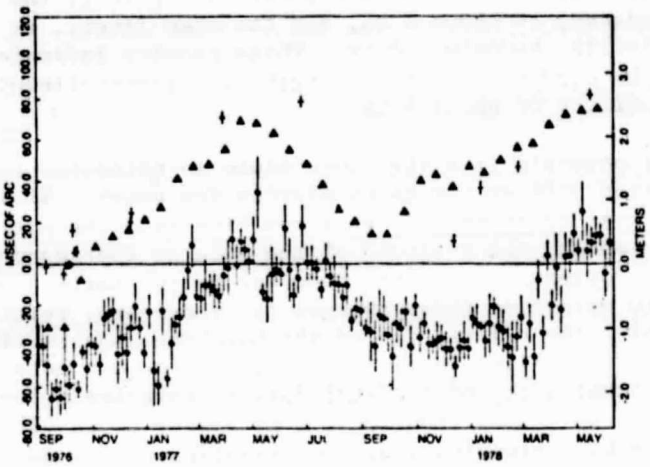

Figure 3. x-component of the pole position, from VLBI observations (+) of extragalactic radio sources, from Doppler observations (¢) of satellites, and from IPMS optical observations (▲) of Galactic stars, all relative to the values obtained by the BIH (see text). In the analysis of the VLBI data, the pole position was fixed at the BIH value for the experiment of 4 October 1976 (●).

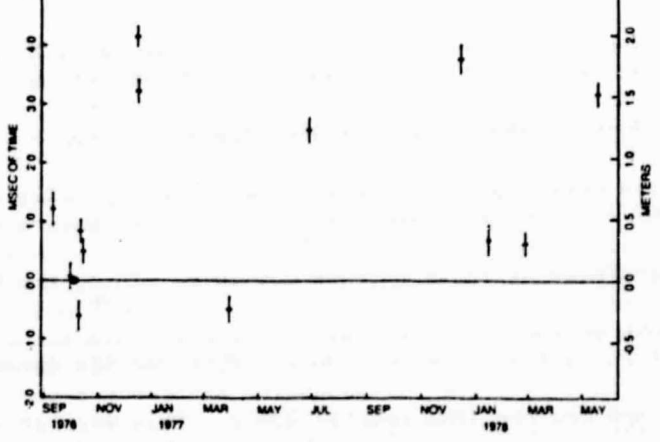

Figure 4. Comparison of the VLBI and BIH determinations of UT1. The VLBI value for UT1 for the experiment of 4 October 1976 was fixed at the BIH value (●).

Figure 4 shows the corresponding comparison of the VLBI and BIH results for UT1, obtained from the same analysis, with UT1 having been set at the BIH value for 4 October 1976. The RMS scatter here, about $0^s.002$, is again less than that obtained previously (Shapiro et al., 1974; Robertson, 1975) and is about the same as the scatter seen in the UT1 determinations from lunar laser ranging (King et al., 1978; see also Stolz et al., 1976).

In this paper we have summarized our current ability to determine baseline lengths, pole position, and Earth rotation with VLBI. Another paper presented at this conference (Carter et al., 1979) addresses plans we have for the improvement of both the quality and the quantity of such determinations.

REFERENCES

Carter, W. E., Robertson, D. S., and Abell, M. D.: 1979, this volume.
Clark, T. A., Hutton, L. K., Marandino, G. E., Counselman III, C. C., Robertson, D. S., Shapiro, I. I., Wittels, J. J., Hinteregger, H. F., Knight, C. A., Rogers, A. E. E., Whitney, A. R., Niell, A. E., Ronnang, B. O., and Rydbeck, O. E. H.: 1976, Astron. J. 81, pp. 599-603.
Guinot, B.: 1970, Astron. Astrophys. 8, pp. 26-28.
Guinot, B.: 1974, Astron. Astrophys. 36, pp. 1-4.
King, R. W., Counselman III, C. C., and Shapiro, I. I.: 1978, J. Geophys. Res. 83, pp. 3377-3381.
Lieske, J. H., Lederle, T., Fricke, W., and Morando, B.: 1977, Astron. Astrophys. 58, pp. 1-16.
Melchior, P.: 1971, Celes. Mech. 4, pp. 190-212.
Robertson, D. S.: 1975, PhD. Thesis, M.I.T.
Shapiro, I. I., Robertson, D. S., Knight, C. A., Counselman, C. C., Rogers, A. E. E., Hinteregger, H. F., Lippincott, S., Whitney, A. R., Clark, T. A., Niell, A. E., Spitzmesser, D. J.: 1974, Science 186, pp. 920-922.
Stolz, A., Bender, P. L., Faller, J. E., Silverberg, E. C., Mulholland, J. D., Shelus, P. J., Williams, J. G., Carter, W. E., Currie, D. G., and Kaula, W. M.: 1976, Science 193, pp. 997-999.
Woolard, E. W.: 1953, Astron. Papers of the Amer. Eph. 15, part 1.

DISCUSSION

J. D. Mulholland: The equations given by Johnston suggest that your claim to solve directly for UT1 assumes that the Z-component of the baseline is known without error.

W. E. Carter: The determination of UT1 is relatively insensitive to small errors in Z.

A. R. Robbins: I believe that tapes have to be played back in real time for cross-correlation, and that very few organizations can carry this out. Consequently it takes a very long time to get results from experiments. Can you comment on this?

W. E. Carter: The Mark III VLBI system, which will be utilized in project POLARIS, has been designed with a high degree of automation of the data handling and processing which will allow the solutions to be completed in a matter of days after receipt at the processing facility. In the future, communications satellites may be utilized, and the results could be determined nearly in real time.

K. Johnston: What form of atmospheric correction did you apply to the data? If H_2O radiometers had been used to measure the H_2O atmospheric content along the line of sight, how would this have improved the accuracy of your results?

W. E. Carter: Only surface meteorological measurements were used with a model derived by J. Marini at NASA. It appears that H_2O radiometers may reduce the uncertainty in the atmospheric corrections to the sub-centimeter level.

POLAR MOTION AND UT1: COMPARISON OF VLBI, LUNAR LASER, SATELLITE LASER, SATELLITE DOPPLER, AND CONVENTIONAL ASTROMETRIC DETERMINATIONS

D. S. Robertson
National Geodetic Survey, NOS, NOAA

T. A. Clark, R. J. Coates, C. Ma, J. W. Ryan
NASA, Goddard Space Flight Center

B. E. Corey, C. C. Counselman, R. W. King, I. I. Shapiro
Department of Earth and Planetary Sciences
and Department of Physics,
Massachusetts Institute of Technology

H. F. Hinteregger, C. A. Knight, A. E. E. Rogers, A. R. Whitney
Haystack Observatory

J. C. Pigg, B. R. Schupler
Computer Sciences Corporation

ABSTRACT

Very-long-baseline interferometry (VLBI) observations made with a 3900 km baseline interferometer (Haystack Observatory in Massachusetts to Owens Valley Observatory in California) have been used to estimate changes in the X-component of the position of the Earth's pole and in UT1. These estimates are compared with corresponding ones from lunar laser ranging, satellite laser ranging, satellite Doppler, and stellar observations.

INTRODUCTION

Significant progress is being made in the technology of measuring the motion of the Earth's pole and the irregularities in the Earth's rotation. Very-long-baseline interferometry (VLBI), lunar laser ranging, satellite laser ranging, and satellite Doppler observations all have the potential of measuring the Earth's orientation with a precision far better than than obtainable with classical techniques. In this paper we compare the VLBI determinations of polar motion and Earth rotation with the corresponding results from other techniques and attempt to assess the current state of the art of such measurements.

SENSITIVITY OF VLBI MEASUREMENTS TO POLAR MOTION AND UT1

VLBI delay observations of extra-galactic radio sources are insensitive to translations of the VLBI baseline, but are sensitive to some changes in the orientation of that baseline with respect to the (planar) radio wavefronts. To specify orientation in space, three angles are generally required; however, a baseline is one-dimensional and its orientation in space is specified by two angles. A rotation about an axis parallel to the baseline does not change the orientation of the baseline, but rather produces at most a translation of that baseline. VLBI observations are therefore insensitive to rotations about any axis parallel to the baseline. This result can be expressed analytically as follows: Define a cartesian coordinate system fixed to the rigid Earth, with the Z-axis in the direction of the reference pole, the X axis perpendicular to Z in the direction of the Greenwich meridian, and the Y axis completing a right-hand triad. The changes in the coordinates of the baseline vector caused by polar motion and variations in UT1 can be written as:

$$\Delta X = -\theta Y - xZ$$

$$\Delta Y = \theta X + yZ$$

$$\Delta Z = xX - yY$$

where θ is UT1-UTC in radians, and x and y are the coordinates of the instantaneous pole, also in radians. Non-zero values for ΔX and ΔY will introduce a sinusoidal signature in the delays observed for a non-polar source because of the rotation of the Earth. A non-zero value for ΔZ will introduce a time-independent change in the delays, whose magnitude will depend on the declination of the source being observed. For the case of a polar baseline ($X = 0$, $Y = 0$) the sensitivity to θ vanishes, and a change in pole position introduces a sinusoid in the delay observations whose amplitude and phase can be used to estimate the components of this change in pole position. For the case of an equatorial baseline oriented parallel to the plane of the Greenwich meridian ($Y = 0$, $Z = 0$) the sensitivity to the y component of the pole position vanishes. θ will introduce a sinusoidal variation in the observed delays, and x will introduce a constant offset in those delays. For $Y \neq 0$, the VLBI observations will be sensitive to a change in the component of the pole that is in the direction of the

meridian whose plane is parallel to the baseline, and insensitive to a change in the component perpendicular to that plane. Thus for an equatorial baseline, the effects of polar motion and UT1 are separable.

The VLBI measurements discussed in this paper were obtained in 14 separate experiments spread between September 1976 and May 1978. These experiments utilized the 37-meter-diameter antenna at the Haystack Observatory in Massachusetts, and the 40-meter-diameter antenna at the Owens Valley Radio Observatory in California. This baseline is nearly parallel to the Earth's equatorial plane, having a declination of less than 7°, and is even closer to parallel to the plane of the Greenwich meridian, making an angle of less than 0°.5 with that plane. The interferometric observations are therefore sensitive to changes in the X-component of the position of the pole and to changes in UT1 and are practically insensitive to changes in the Y-component of the pole.

POLAR MOTION

VLBI determinations of the X-component of the pole are shown in figure 1, displayed as differences from the corresponding values determined by the Bureau International de l'Heure (BIH). The VLBI values show peak-to-valley excursions from the BIH values of about 80 msec of arc, or a little more than two meters. The error bars shown are the formal standard errors, based on an adjustment of the measurement errors to yield an rms value of unity for the postfit residuals. Further analysis of these data, including detailed studies of effects of clock and atmosphere errors, as well as inclusion of some additional data from NRAO and Onsala (Sweden), may change these values by amounts up to a few times the formal standard errors.

VLBI measurements alone are sensitive only to changes in the pole position and therefore the zero point of figure 1 is necessarily arbitrary. It was set by fixing the value of the X-component of the pole position at the BIH value for the experiment of October 4-5, 1976.

Figure 2 shows the two-day average values of the X-component of the pole position determined from satellite Doppler observations by the Defense Mapping Agency Hydrographic and Topographic Control (DMAHTC). Again, the values are differenced from those of the BIH and are plotted on the same scale as before. A clear systematic trend is present which appears to have an annual period with an amplitude of about 30 msec of arc; the point-to-point (short-period) scatter has an RMS of about 25 msec. In order to better exhibit the systematic trend, we smoothed these data by convolution with a Gaussian function whose full-width at half-maximum was 10 days. The result is shown in figure 3.

Figure 4 shows the corresponding determinations of the X-component of the position of the pole from laser ranging observations of the LAGEOS satellite. These values were supplied to us by D. Smith of NASA's Goddard Space Flight Center. Figure 5 shows these values smoothed by the same filter used to produce figure 3. Again, an annual trend seems to be present.

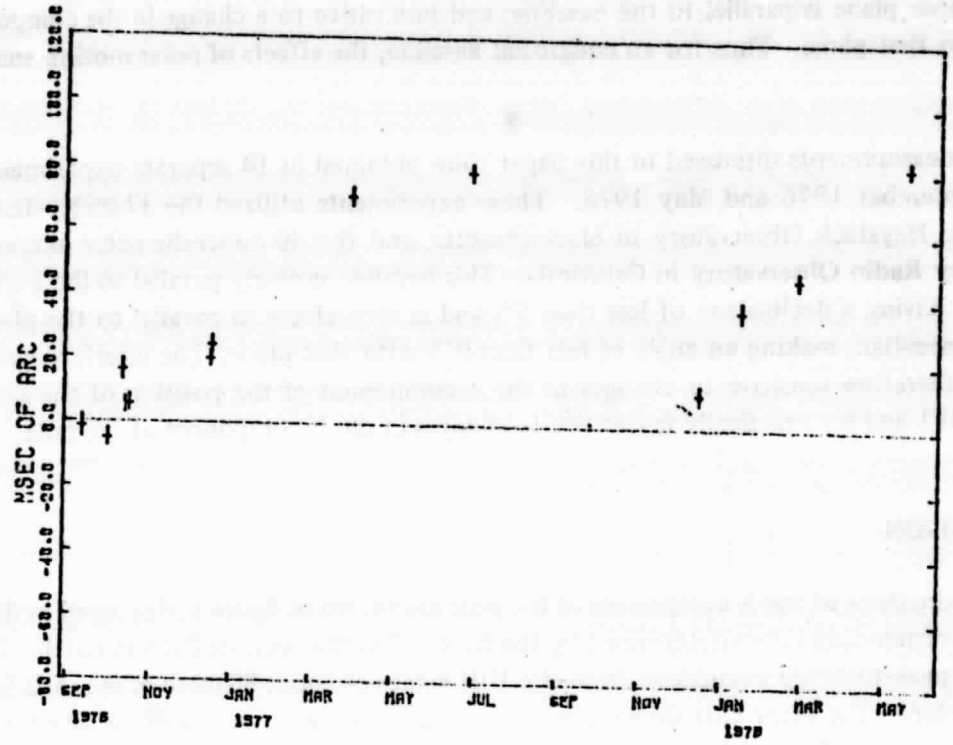

Figure 1.

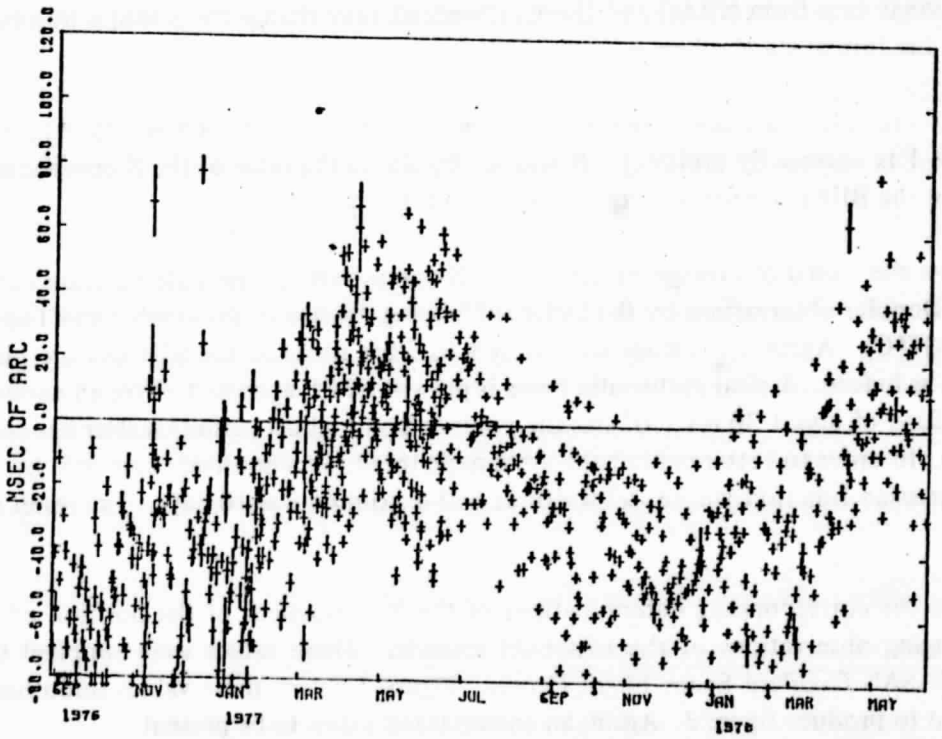

Figure 2.

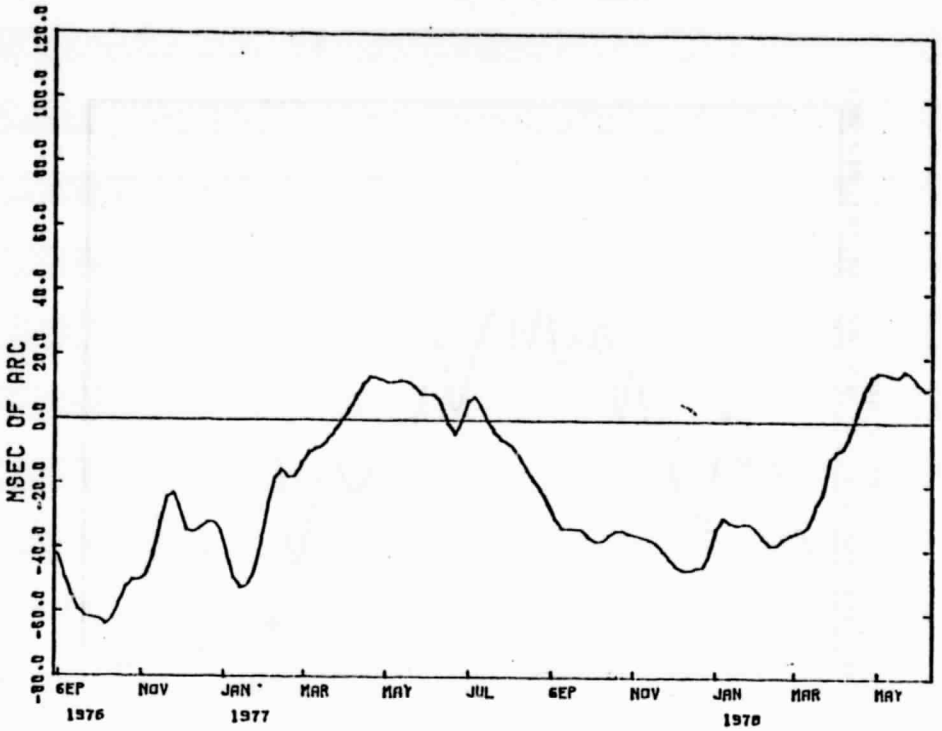

Figure 3.

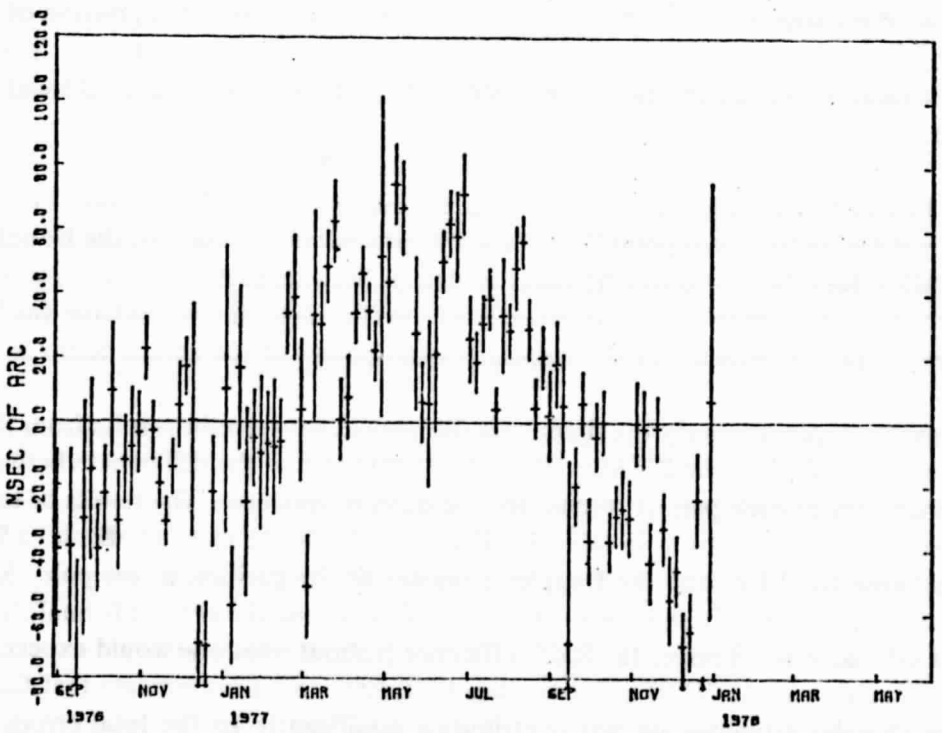

Figure 4.

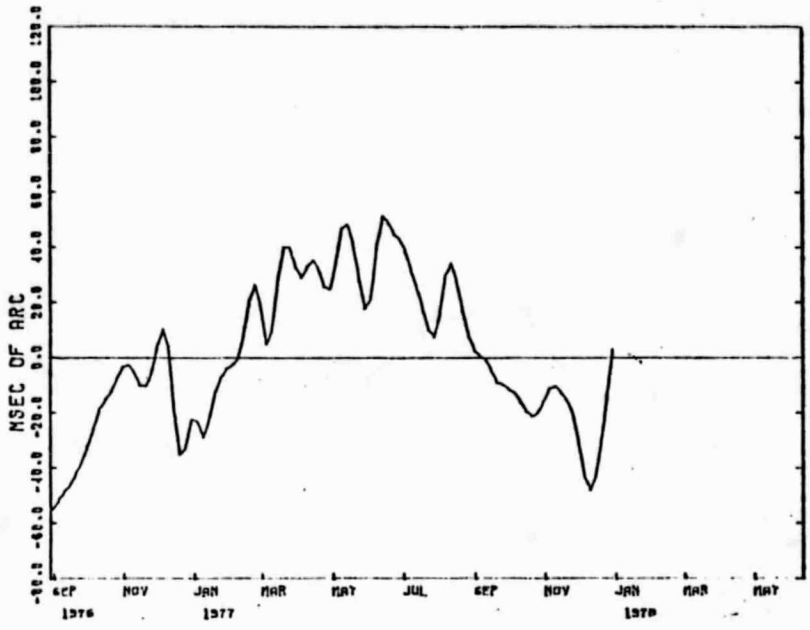

Figure 5.

Figure 6 shows the corresponding determination of the X-component of the position of the pole as determined by the International Polar Motion Service (IPMS) in Misuzawa, Japan. The IPMS employs only classical optical observations (PZT, VZT, etc.). Even here, the annual trend away from the BIH is clear.

Each of the figures of differences in estimates of pole position has a different bias. This bias can be removed by re-defining the "zero point." (In fact, this procedure was used for the Doppler, satellite laser, and IPMS values, but for different spans of data.) Shifting each set of differences shown in our figures by the mean value of its difference from the corresponding values from the Doppler set yields figure 7. The consistency of the amplitudes and phases of the annual terms is quite clear.

In order to evaluate quantitatively the short-term differences between the results from the different techniques, we can calculate the RMS deviation about the mean of the differences between the corresponding members of each pair of results, for the dates in common. The results of these calculations are tabulated in matrix form in table 1. The first value in the matrix indicates a 9 msec RMS difference between the VLBI and the Doppler estimates of the position of the pole. Since the expected standard error in the Doppler estimates of ~10 msec, and the average formal standard error of the VLBI estimates is ~3 msec, the RMS difference is about what one would expect. Although, admittedly, there are only 13 VLBI estimates, this RMS difference does indicate that the systematic errors in the Doppler estimates are not contributing significantly to the total errors. The other values in the table are consistent with the errors in the satellite laser ranging estimates of the pole position being ~12 msec, the corresponding IPMS errors ~15 msec, and the BIH errors ~25 msec.

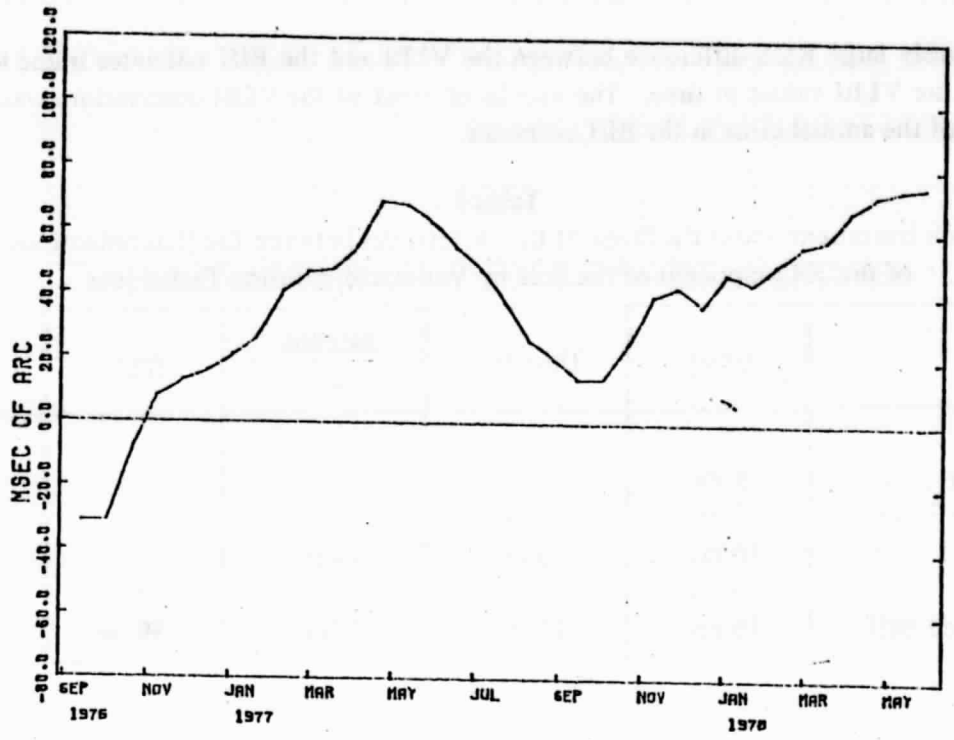

Figure 6.

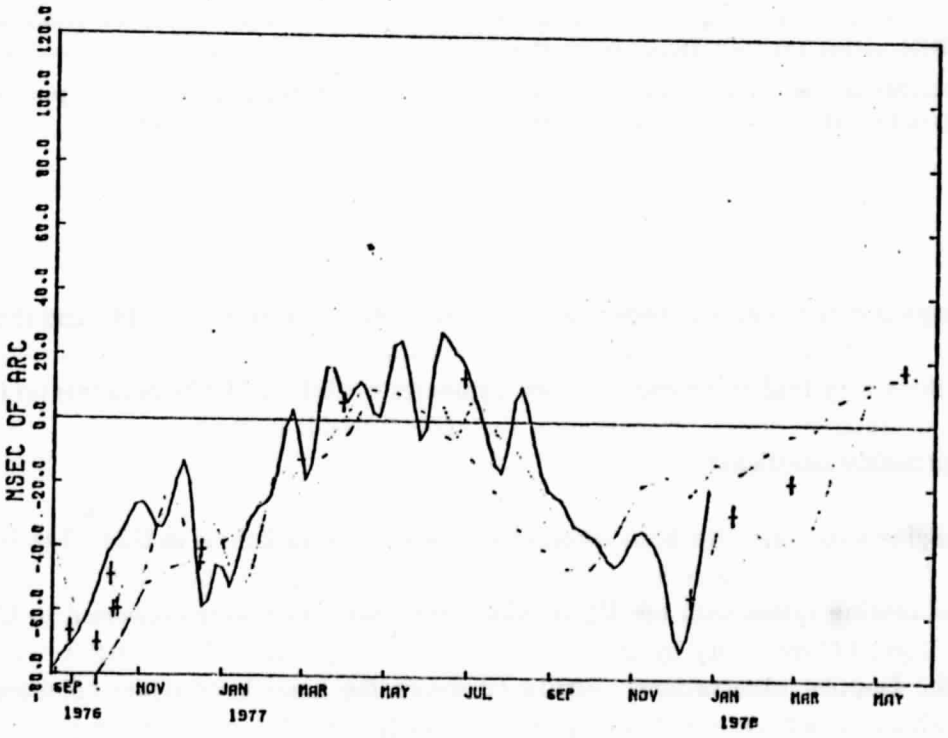

Figure 7.

The anomalously large RMS difference between the VLBI and the BIH estimates is due to the distribution of the VLBI values in time. The epochs of most of the VLBI observations were close to the extrema of the annual error in the BIH estimates.

Table 1
RMS Deviations about the Mean of the Differences between the Determinations of the X-Component of the Pole by Various Monitoring Techniques

	VLBI	Doppler	Satellite Laser	IPMS	BIH
VLBI	–				
Doppler	9 ms	–			
Satellite Laser	12 ms	14 ms	–		
IPMS	16 ms	15 ms	18 ms	–	
BIH	30 ms	23 ms	24 ms	27 ms	–
Corrected BIH	16 ms	11 ms	17ms	19 ms	15 ms

In May 1979, the BIH altered this picture by announcing that it would introduce an ad hoc correction to its X-component values in the form of an annual term and a semi-annual term. The form of the correction is displayed in figure 8. After application of this correction, the RMS difference between the BIH estimates and those from the other techniques are displayed in the last line of table 1. The errors in the BIH estimates of the X-component of the position of the pole appear to have been reduced by the correction to about the level of the errors in the IPMS values.

UT1

Figure 9 displays the differences between the VLBI determinations of (UT1-UTC) and the BIH determinations. As with the values of pole position, completion of a more detailed analysis of the VLBI observations may lead to changes in these estimates of (UT1-UTC) by amounts up to several times the formal standard errors. Nonetheless, the general trends in the differences from the BIH estimates are probably significant.

Lunar laser ranging data have also been employed to determine variations in UT1. The UT1 variations were modeled as a piece-wise linear function, as described by King et al. (1978). To compare the lunar laser ranging values with the VLBI values, the laser values were converted to UT1 from UT0 at the McDonald Observatory by using the estimate of the position of the Earth's pole as determined from the Doppler observations. Figure 10 shows the lunar laser values compared to the VLBI values which have been adjusted to allow for a different value used for the precession constant in the lunar laser program.

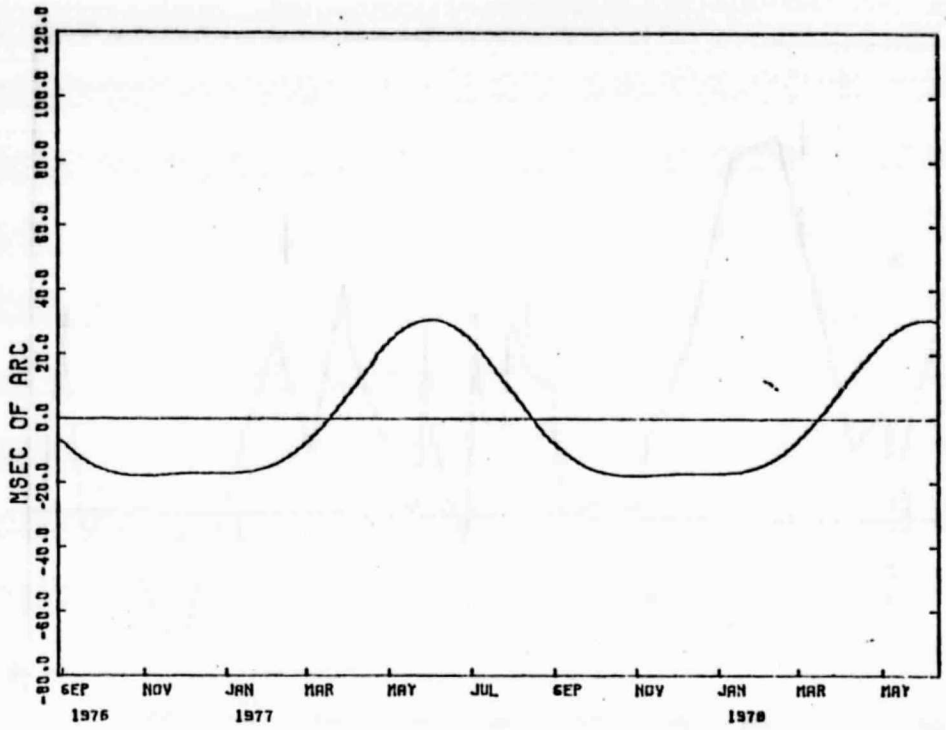

Figure 8.

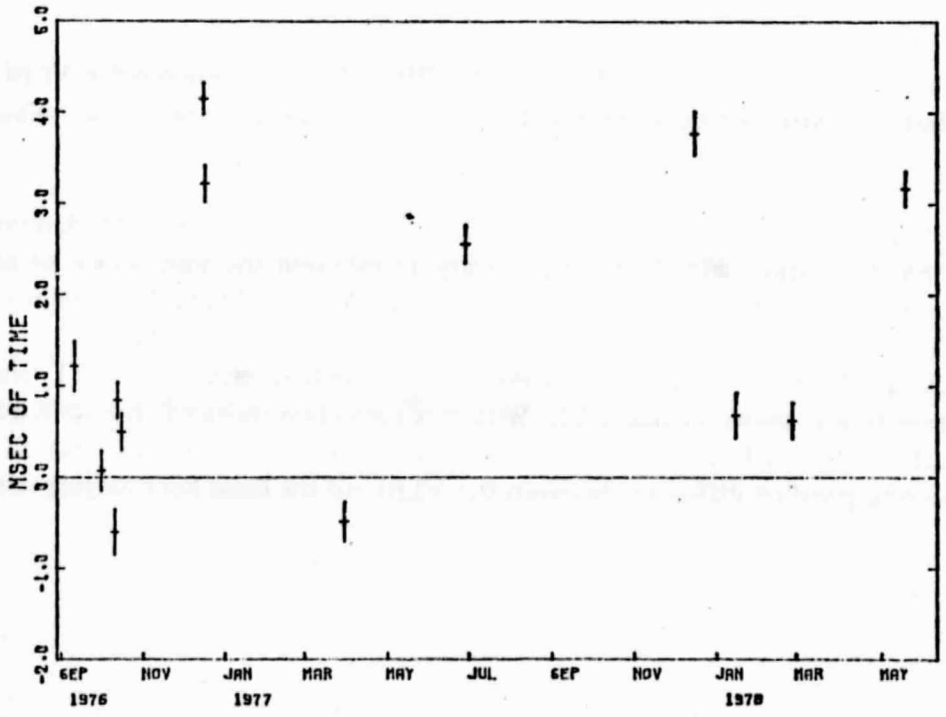

Figure 9.

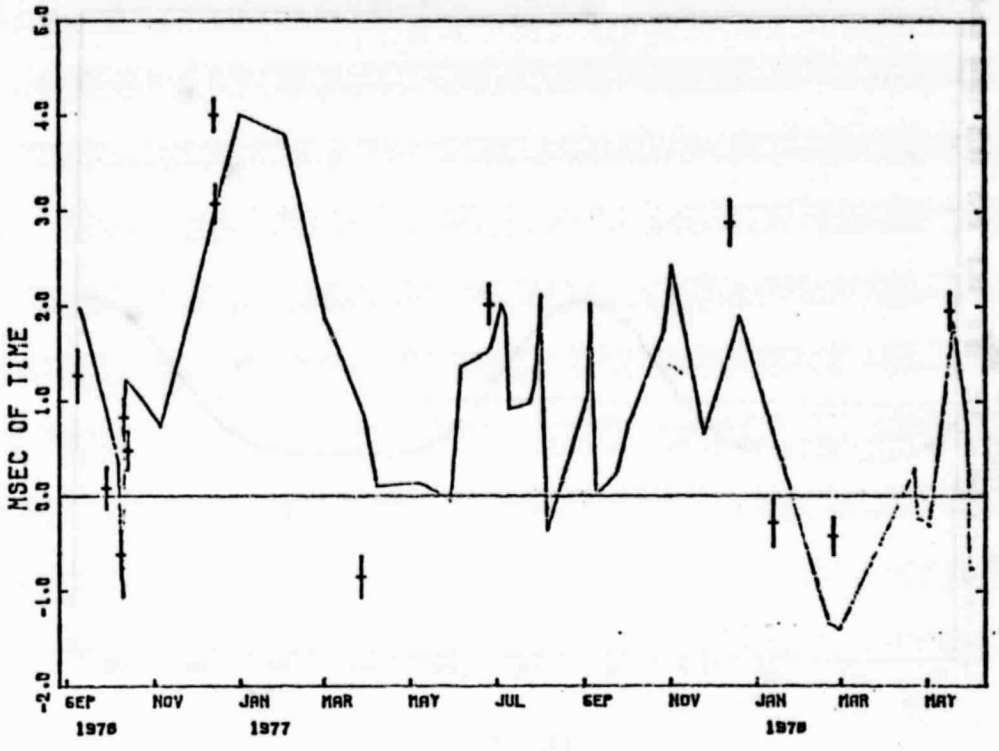

Figure 10.

The RMS differences between the lunar laser and the BIH values and between the VLBI and the BIH values are both 1.6 msec, but the difference between the VLBI and the lunar laser values is only 0.8 msec.

Although the general agreement between the VLBI and the lunar laser values is good, more regular monitoring of Earth rotation with VLBI is necessary to establish the significance of any small (>2 msec) differences between the BIH values and those from VLBI and lunar laser ranging.

The BIH has also published an annual and a semi-annual correction term for its UT1 values. The form of this correction is shown in figure 11. With this correction included, the RMS differences between the BIH and the VLBI and lunar laser results are 1.3 msec and 1.1 msec, respectively, still larger than the corresponding difference between the VLBI and the lunar laser ranging estimates of UT1.

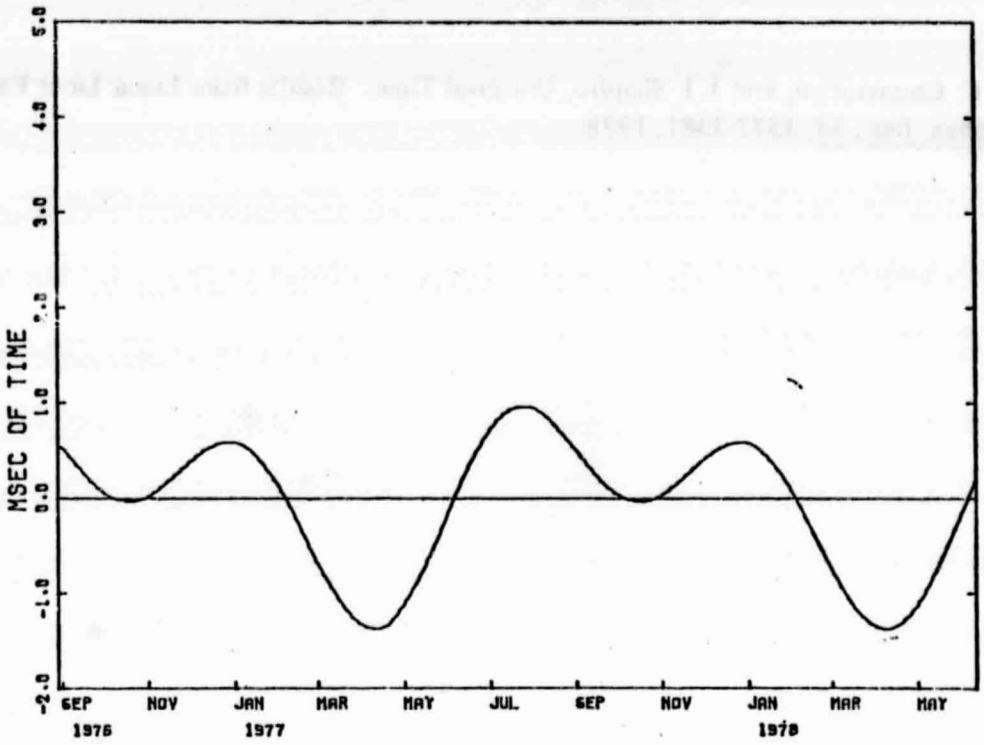

Figure 11.

CONCLUSIONS

The determination of the position of the Earth's pole from satellite Doppler and satellite laser ranging observations are approaching an accuracy of ~10 msec of arc (30 cm). The VLBI determinations may have better accuracy, although a determination of whether the VLBI accuracy is indeed better, and by how much, must await the collection and analysis of a far larger set of VLBI data.

The comparison of lunar laser ranging and VLBI determinations of UT1 suggests that the RMS of the uncertainties in each set are under 1 msec.

All of these comparisons have been hampered by the paucity of VLBI data. To rectify this problem, the National Geodetic Survey has undertaken Project POLARIS whose object is to obtain VLBI data at least several times per week, starting in 1982.

REFERENCE

King, R. W., C. C. Counselman, and I. I. Shapiro, Universal Time: Results from Lunar Laser Ranging, J. Geophys. Res., 83, 3377-3381, 1978.

BACKPACK VLBI TERMINAL WITH SUBCENTIMETER CAPABILITY

C. C. Counselman III and I. I. Shapiro
Massachusetts Institute of Technology

R. L. Greenspan and D. B. Cox, Jr.
Charles Stark Draper Laboratory Inc.

The measurement of short vector baselines with subcentimeter repeatability and accuracy using radio interferometric observations of quasars has already been demonstrated (reference 1). This paper describes our plans to achieve comparable performance using inexpensive, backpack portable equipment that processes less than one second of data per baseline redetermination. Figure 1 summarizes some of these objectives.

Our approach exploits the full measurement accuracy inherent in the precise radio signals that will be broadcast by each satellite in the NAVSTAR Global Positioning System (GPS) (reference 2). Figure 2 illustrates the measurement concept. The user equipment at each end of the unknown baseline receives signals from the same set of four or more GPS satellites. The equipment consists of a simple antenna, a GPS receiver, a microprocessor unit and a recording unit (reference 3). "Real-time" baseline determination can be accomplished by linking the microprocessor units with a communication channel that can transmit at the rate of about 1 kilobit per baseline redetermination.

Each GPS receiver measures its range to each satellite by means of the wide-band pseudo-noise P-Code modulation that is impressed on the GPS radio frequency carriers which are at 1.226 GHz and 1.57542 GHz (reference 4). These measurements will typically have a precision of about 0.5 meters, which is approximately 2.5 wavelengths at a frequency of 1.57542 GHz. The primary use of these relatively coarse measurements in the proposed program is to assist in resolving ambiguities of the more precise carrier-phase measurements that will also be made (see below).

- TO DEVELOP BACKPACK PORTABLE EQUIPMENT TO MEASURE VECTOR BASELINES FROM ~ 1 KM TO ~ 100 KM IN LENGTH WITH SUBCENTIMETER TO FEW CENTIMETER ACCURACY.

- TO DEVELOP EQUIPMENT THAT IS
  - SIMPLE IN CONCEPT AND IMPLEMENTATION
  - RELIABLE IN UNATTENDED OPERATION
  - INEXPENSIVE - LESS THAN $15,000 PER UNIT

Figure 1. Objectives.

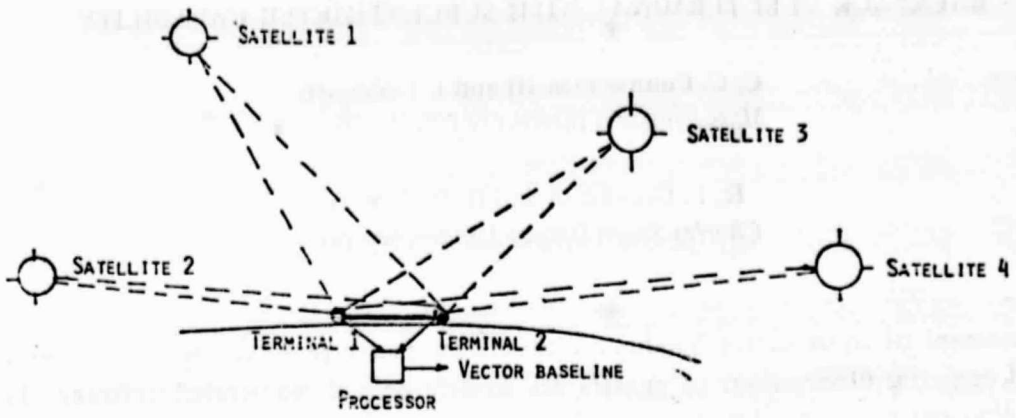

INSTRUMENTATION

- WIDEBAND OMNIDIRECTIONAL ANTENNA TO RECEIVE 1.6 GHz AND 1.2 GHz GPS TRANSMISSIONS
- SIMULTANEOUS RECEPTION FROM ALL SATELLITES
- MICROPROCESSOR-CONTROLLED SYSTEM FOR DATA COLLECTION AND FORMATTING
- DATA STORAGE AND/OR LOW-VOLUME DATA LINK TO MICROPROCESSOR-BASED DATA ANALYZER

Figure 2. GPS measurement concept.

The same knowledge of the pseudo-noise modulation on the transmitted GPS signal that enables the receiver to make coarse range measurements also enables that modulation to be stripped from the received signal, leaving a sinusoidal component that is modulated only by a low speed (50 bit/second) biphase encoded data signal. This data modulated carrier is tracked in current GPS receivers by a "Costas" phase detector, which uses a phase doubling nonlinearity to remove the effect of the biphase modulation (reference 5). The output of the loop is an unmodulated tone. The phase tracking error will be approximately 8° in typical noise environments; this value corresponds to approximately 4 mm at the GPS carrier frequencies (reference 6). The measurement is ambiguous by multiples of half the wavelength (approximately 10 cm) because the Costas loop output does not distinguish between input phases that differ by 180°. However, by using knowledge of the data signal format, one can regain the "lost" factor of two and obtain whole-wavelength (20 cm) spacing of the ambiguities.

The carrier phases obtained from the signals from four or more satellites (see figure 3) at each end of a baseline yield an extremely precise, albeit ambiguous, determination of the vector baseline (reference 3). One primary objective of the current plan is to assess the adequacy and flexibility of several alternatives for resolution of the ambiguities with simple equipment. Two leading approaches are:

1. Collect data from satellite observations over several hours during which the satellite geometry changes significantly. If the number of potential ambiguities from observations of each satellite is small, then the set of ambiguity values, one value for each satellite, that corresponds to the weighted least squares fit to the data will usually be the correct one.

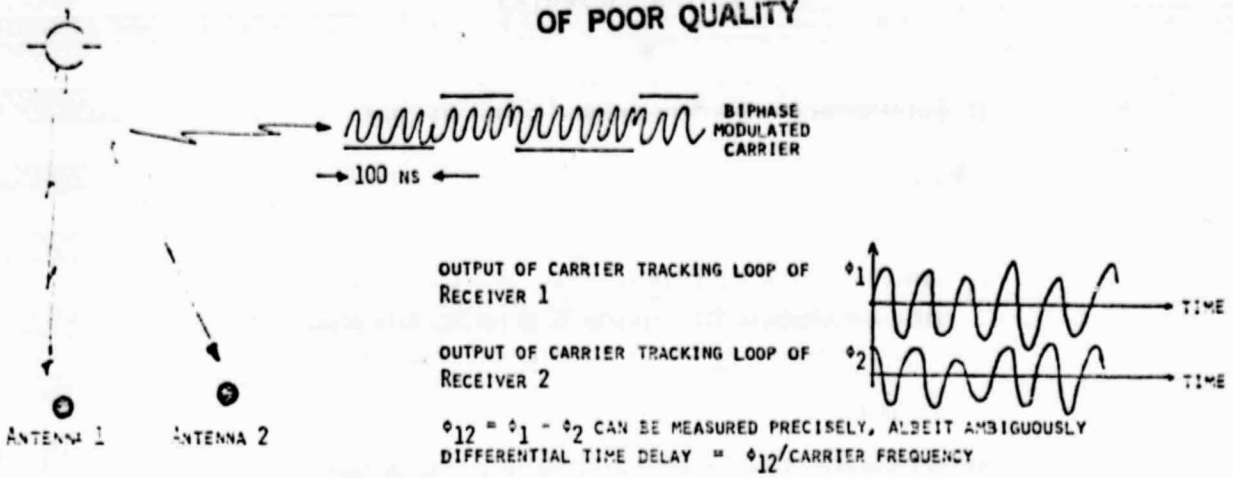

Figure 3. GPS signal processing concept ("reconstructed carrier").

This technique is described in reference 1. We note that all data used to resolve ambiguities are usable also for accurate determination of the baseline vector, after the ambiguities are resolved.

2. Measure the phase difference between the two GPS carriers received at each end of the baseline from each satellite to within a few degrees (note that both GPS carriers are synthesized coherently from the same oscillator). The corresponding phase-delay ambiguities will be light-time equivalents of integral multiples of the 0.43 m half-wavelength for the difference frequency (349 MHz). This approach is similar to the use of multiple tones in OMEGA to resolve "lane" ambiguities (reference 7). Used in conjunction with the coarse range measurement, the phase from both GPS carriers will allow a reduction in the initial ambiguities of the phase delay estimates. As the baseline length increases, the effectiveness of this technique will decrease because of ionospheric effects.

As the first phase in the development of the intended system, we plan to conduct an experimental program using commercially supplied GPS receivers. One or more standard baselines defined by receiving antennas will be established and surveyed. Each leg will be less than 100 meters in length. GPS signals received by the antennas will be processed to make a series of baseline determinations under a wide range of environmental conditions. The objectives of this experiment are:

1. to ascertain whether the accuracy of the baseline determination meets our goal (see figure 4);

2. to assess different techniques for ambiguity resolution; and

3. to determine whether the present GPS signal structure will allow the development of inexpensive and effective ground equipment.

1) EXPLOITATION OF KNOWN "PSEUDORANDOM" SIGNAL STRUCTURE [illegible] GAIN.

2) SATELLITE TRANSMITTED POWER AND SIGNAL PROCESSING GAIN YIELD A MEASUREMENT SNR EXCEEDING 35 dB PER Hz, EVEN USING A MODEST RECEIVER. T_N = 430°K (NOISE FIGURE = 4.0 dB).

3) GPS BROADCASTS ACCURATE EPHEMERIS DATA.

4) GPS SUPPORTS CLOCK SYNCHRONIZATION TO 10's OF NS SO THAT INHERENT EPHEMERIS ACCURACY CAN BE EASILY EXPLOITED.

Figure 4. Why size, weight and complexity objectives are feasible.

REFERENCES

Rogers, A. E. E. et al., Geodesy by Radio Interferometry: Determination of a 1.24 km Base Line Vector with ~5-mm Repeatability, Journal of Geophysical Research, Vol. 83, No. 1, 10 January 1978, pp. 325-334.

Milliken, R. J., and C. J. Zollar, Principles of Operation of NAVSTAR and System Characteristics, Navigation, Vol. 25, No. 2, Summer 1978, pp. 95-106.

Counselman, C. C. III, and I. I. Shapiro, Miniature Interferometer Terminals for Earth Surveying, Bulletin Géodésique, Vol. 53, No. 2, August 1979, pp. 139-163.

Borel, M. J. et al., Phase 1 GPS User Equipment, Navigation, Vol. 25, No. [illegible] 1978, pp. 179-194.

Viterbi, A. J., Principles of Coherent Communication, Section 10.4, pp. 286-293, McGraw-Hill, New York, 1966.

Martin, E.. H., GPS User Equipment Error Models, Navigation, Vol. 25, No. 2, Summer 1978, pp. 201-216.

Pierce, Omega, IEEE Transactions on Aerospace and Electronic Systems, Vol. AES-1, No. 3, December 1965, pp. 206-215.

ACTION	CONSEQUENCE
USE DETERMINISTIC PROPERTIES OF GPS SIGNALS	HIGH MEASUREMENT SNR
HIGH MEASUREMENT SNR	CAN USE OMNIDIRECTIONAL ANTENNA; INEXPENSIVE RECEIVER
OMNIDIRECTIONAL ANTENNA	NO BEAM STEERING SIMULTANEOUS OBSERVATION OF ALL SATELLITES
SIMULTANEOUS OBSERVATION AND PARALLEL CHANNEL RECEIVER AND HIGH MEASUREMENT SNR	CARRIER PHASE MEASUREMENTS IN ABOUT 1 SECOND AND BASELINE UPDATE EVERY SECOND IN STEADY STATE*
SHORT MEASUREMENT INTERVALS	QUARTZ CRYSTAL CLOCKS
DIRECT CARRIER PHASE MEASUREMENTS	SIMPLE NUMERICAL PROCESSING IN STEADY STATE, BASED ON SOLUTION OF LINEAR EQUATIONS

*STEADY STATE = AMBIGUITY REMOVED

Figure 5. Properties of GPS-based system.

- AMBIGUITY RESOLUTION REQUIRED AT START AND OCCASIONALLY THEREAFTER:
  - I.E., WHENEVER THERE IS A "LONG" ENOUGH INTERVAL BETWEEN BASELINE MEASUREMENTS THAT THE BASELINE MAY CHANGE SIGNIFICANTLY
- RESOLVE AMBIGUITIES BY APPLYING CONCEPTS TESTED IN HAYSTACK-WESTFORD EXPERIMENTS AND AUGMENTED BY USE OF TWO FREQUENCY BANDS FOR IONOSPHERE REDUCTION
  - USE CODE MODULATION (GROUP DELAY) FOR COARSE, BUT UNAMBIGUOUS BASELINE DETERMINATION

    TIME REQUIRED DEPENDS ON EXTENT OF GROUND CLUTTER (MULTIPATH)
  - USE CARRIER PHASES FOR REFINED BASELINE DETERMINATION

Figure 6. Ambiguity resolution.

OBJECTIVES

- ASSESS AMBIGUITY RESOLUTION TECHNIQUES.
- DEMONSTRATE ACCURACY OF BASELINE DETERMINATION.

Figure 7. Experimental program.

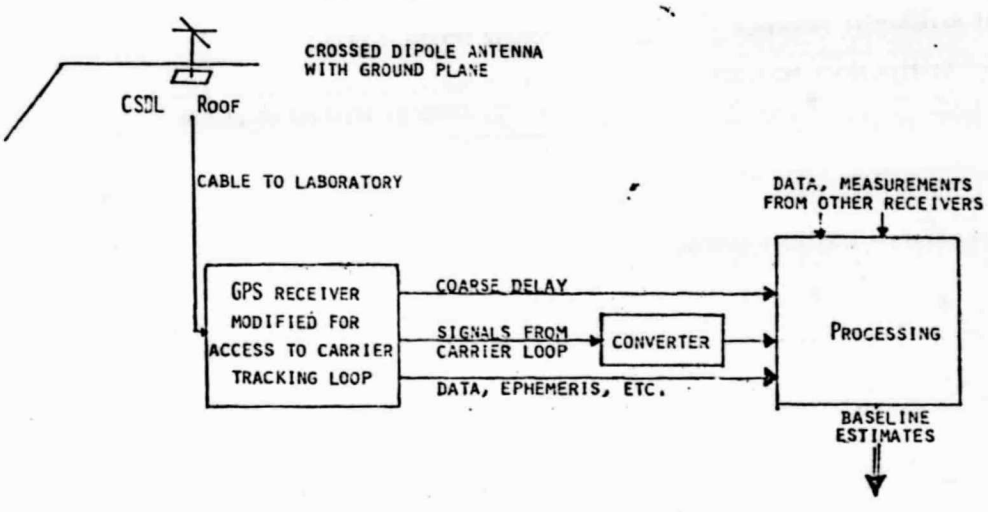

Figure 8. Experimental configuration.

FEATURES

- VERY SHORT BASELINE - < 100 METERS
  (RESULTS CAN BE ACCURATELY CHECKED BY INDEPENDENT TECHNIQUES. IONOSPHERIC REMOVAL NOT TESTED.)
- GPS 4-CHANNEL RECEIVERS
- CROSSED DIPOLE ANTENNAS WITH GROUNDPLANE
- PRECISE PHASE MEASUREMENTS ON RECONSTRUCTED CARRIER
- LOW DATA VOLUME FOR EACH BASELINE REDETERMINATION
  (LESS THAN 1 K BIT)

Figure 9. Experimental program.

JOURNAL OF GEOPHYSICAL RESEARCH, VOL. 85, NO. B5, PAGES 2685–2687, MAY 10, 1980

Comparison of Geodetic and Radio Interferometric Measurements of the Haystack-Westford Base Line Vector

WILLIAM E. CARTER

National Geodetic Survey, National Ocean Survey, NOAA
Rockville, Maryland 20852

ALAN E. E. ROGERS

Northeast Radio Observatory Corporation, Haystack Observatory
Westford, Massachusetts 01886

CHARLES C. COUNSELMAN III AND IRWIN I. SHAPIRO[1]

Department of Earth and Planetary Sciences, Massachusetts Institute of Technology
Cambridge, Massachusetts 02139

A three-dimensional geodetic measurement of the 1.24-km Haystack-Westford base line vector was performed to verify the accuracy of previously published radio interferometric measurements. The differences between the geodetic and the very long base line interferometry (VLBI) measurements of the base line length, the horizontal X and Y components, and the vertical Z component were −4, 2, 4, and −19 mm, respectively. After a correction was applied to the VLBI determination of the vertical component to account for a recently measured, repeatable gravitational flexure of the Haystack antenna, the discrepancy in this component was reduced to −6 mm. Other possible repeatable flexures in the two antennas, which have not yet been measured, could either further reduce or increase this discrepancy.

1. INTRODUCTION

Rogers et al. [1978] and *Robertson et al.* [1979] report results of very long base line interferometry (VLBI) experiments that demonstrate repeatability in base line length at the 3-mm level over short distances and at the 4-cm level over transcontinental distances, respectively. For most applications, repeatability alone is sufficient. However, if VLBI measurements are to be compared to, or combined with, measurements made by different methods, it is necessary that any significant biases be determined. The National Geodetic Survey (NGS) has therefore undertaken comparisons of the results of VLBI experiments with those of appropriately selected 'operational' geodetic methods [*Hothem*, 1979; *Hothem et al.*, 1979; *Niell et al.*, 1979; *Strange and Hothem*, 1980] (see also *Hinteregger et al.* [1972] and *Ong et al.* [1976]). Here we report the results of a comparison with the VLBI determination [*Rogers et al.*, 1978] of the 1.24-km base line vector from the Haystack to the Westford antennas in Massachusetts.

2. GEODETIC MEASUREMENTS

The Haystack and Westford antennas have elevation-azimuth mounts. The Haystack mount (Figure 1) has intersecting axes, and the point of intersection is defined to be the origin for the base line vector. The Westford mount is eccentric, and the termination of the base line vector is defined to be the point of intersection of the vertical axis and the horizontal plane that contains the horizontal axis (Figure 2). Neither reference point coincides with a physical monument, but both are accessible via measurements from nearby reference marks. We emphasize that this base line vector was not determined with respect to the center of mass of the earth, either by the geodetic survey or by VLBI.

The base line is obstructed by terrain, vegetation, and the radio telescope enclosures. Thus it was necessary to survey the network shown in Figure 3. NGS personnel designed and performed the survey as well as reduced and analyzed the data. Haystack Observatory personnel performed only support activities, such as making holes in the Haystack radome for lines of sight. (The Westford telescope was temporarily without its radome as a result of a freak storm in May 1977.) Extraordinary procedures were followed in the survey in order to reduce the uncertainty in determining each component of the base line vector. For example, a special NGS team, disjoint from the original, was used to remeasure the vertical component of the base line (see section 4). Detailed descriptions of the surveying methods, instrumentation, data reduction procedures, and analysis are given by *Carter et al* [1979]. The final results are shown in Table 1.

3. VLBI MEASUREMENTS

The Haystack-Westford base line vector was determined by *Rogers et al.* [1978] 11 times from separate sets of VLBI measurements during the period October 1974 to January 1976. The scatter between the results from the different experiments was significantly larger than would be expected from the formal standard errors for the determination of the base line components from the individual experiments, thus indicating the presence of significant systematic errors. One important contributing factor to the increased scatter was the incomplete calibration of the receiver systems. Subsequent completion and installation of a calibration system prompted a twelfth determination of the base line vector, which was carried out on May 8–9, 1977. The results are compared in Table 2 with the corresponding means from 11 prior VLBI experiments. The differences are sufficiently small that the overall means are

[1]Also affiliated with Department of Physics, Massachusetts Institute of Technology, Cambridge, Massachusetts 02139.

Paper number 8OB0076

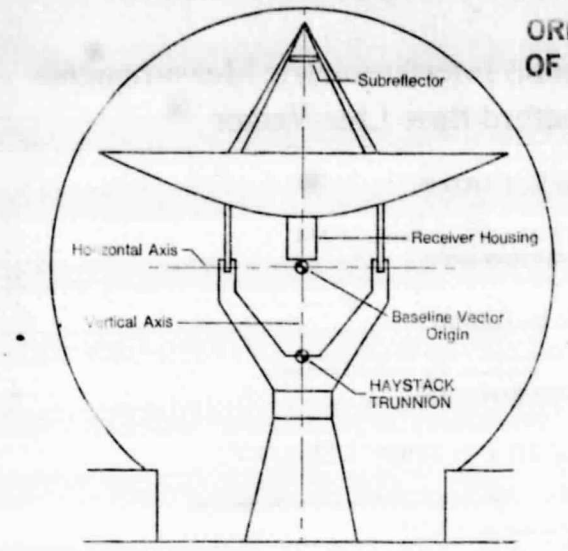

Fig. 1. The Haystack radio telescope, enclosed in a 46-m-diameter space-frame radome, is a 37-m-diameter Cassegrain-type instrument with intersecting elevation (horizontal) and azimuth (vertical) axes. The monument established during the geodetic survey, Haystack Trunnion, is indicated in the figure.

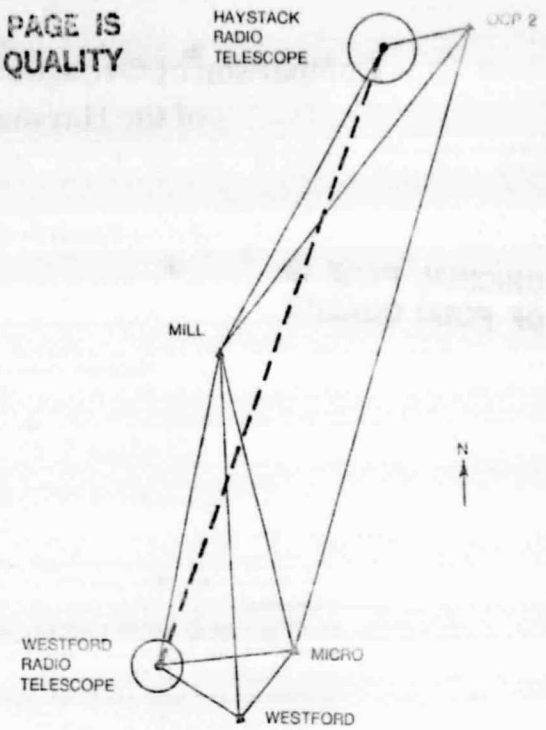

Fig. 3. Sketch of the geodetic network. The dashed line represents the 1.24-km Haystack-Westford base line vector.

not significantly changed by the inclusion of the results from the twelfth experiment.

4. COMPARISON OF GEODETIC AND VLBI RESULTS

Table 3 shows the differences between the geodetic and the mean of the VLBI determinations of the Haystack-Westford base line components. The only significant discrepancy is in the Z component, that is, along the local vertical. This result is not too surprising: Any gravitationally induced flexure of either telescope is expected to be primarily a function of elevation angle and to 'map' directly into the estimate of the local vertical component in the analysis of the VLBI measurements. The possible presence of such flexures and their likely effect were emphasized by *Rogers et al.* [1978].

Two actions were taken to try to identify directly the source of the discrepancy: (1) NGS employed a special team, as mentioned in section 2, to remeasure the base line. The resultant value of Z agreed with the original to within 3 mm. (2) Haystack Observatory personnel, with the aid of Lincoln Laboratory personnel, made a limited set of measurements (commensurate with available resources) of the flexural behavior of the two telescopes. A relatively large effect was discovered in the Haystack telescope: As the elevation angle E of the an-

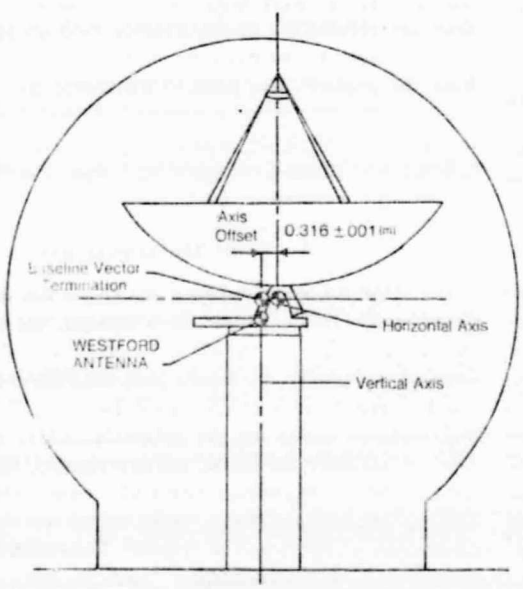

Fig. 2. The Westford radio telescope, enclosed in a 30-m-diameter inflated radome, is an 18-m-diameter Cassegrain-type instrument with (nonintersecting) elevation and azimuth axes. The monument established during the geodetic survey, Westford Antenna, is indicated in the figure.

TABLE 1. Results From Geodetic Measurements of Haystack-Westford Base Line Vector

Base Line Characteristic*	Value,† m
X component	−1149.592 ± 0.002
Y component	−462.196 ± 0.003
Z component	−30.024 ± 0.003
Length	1239.390 ± 0.001

*The origin of the standard (left-handed) Cartesian coordinate system is the reference point at Haystack (see Figure 1); the X direction is that of astronomic north, and the Z direction that of the local vertical, positive upward. The coordinate system was operationally determined in a manner consistent with the FK4 Fundamental Star Catalog and the Bureau International de l'Heure publications of pole position and universal time (UT1). The astronomic latitude and longitude determined for Haystack were 42°37'21.80" N and 71°29'19.07" W, respectively. The survey was performed in 1976.

†The uncertainties shown are the formal standard errors [*Carter et al.*, 1979].

TABLE 2. Results From VLBI Measurements of Haystack-Westford Base Line Vector

Base Line Characteristic*	Mean of 11 Determinations, † m [*Rogers et al.*, 1978]	Twelfth Determination, ‡ m (See Text)	Difference, §
X component	−1149.594 ± 0.003	−1149.597 ± 0.001	0.003
Y component	−462.200 ± 0.005	−462.196 ± 0.001	−0.004
Z component	−30.005 ± 0.007	−30.002 ± 0.003	−0.003
Length	1239.394 ± 0.003	1239.394 ± 0.001	0.000

*The origin of the coordinate system and the axis directions are the same as those for Table 1, except that here the VLBI catalog of positions of extragalactic radio sources [*Rogers et al.*, 1978] was used in place of the FK4 Fundamental Star Catalog. The two catalogs were intercompared for one member, a radio star in the FK4 list, and the difference in position was ~0.1" [*Clark et al.*, 1976], equivalent to a distance of ~0.6 mm for this base line.

†The uncertainties shown are the root-weighted-mean-square scatters of the individual results about their weighted means.

‡The uncertainties are the formal standard errors obtained for the root-mean-square of the postfit residuals set to unity by uniform scaling of the individual measurement errors by a factor of 0.9. (See *Rogers et al.* [1978] for a discussion.)

§Difference between the mean of 11 determinations and the twelfth determination (see text).

tenna increases, the distance between the receiver housing and the subreflector increases (see Figure 1). This increase is well approximated by 13 sin E, mm. The effect of this variation in the length of the optical path through the telescope exactly mimics the effect of lowering the reference point on the telescope. The resultant error introduced in the VLBI estimate of the vertical component of the base line vector was 13 mm. Other measurements of the dependence on elevation angle of distances between various parts of the telescope structures disclosed no changes more than 2 mm, and the net effect of these was under 1 mm.

These investigations thus identified the source of approximately 70% of the discrepancy between the geodetic and the VLBI determinations of Z (see Table 3). The existence of additional significant flexure effects, particularly of the primary reflectors of the two telescopes, has not been ruled out. Of course, an accounting for such effects could either further reduce or increase the discrepancy between the VLBI and the geodetic results.

Acknowledgments. We thank T. A. Clark of the Goddard Space Flight Center and the Haystack Observatory staff for their valuable assistance. We particularly thank C. A. Knight and A. R. Whitney of Haystack for their aid in the VLBI experiments and H. L. Sellers of Haystack and D. Stuart of Lincoln Laboratory, who measured the gravitational flexures of the telescopes.

TABLE 3. Comparison of the Geodetic and VLBI Measurements of the Haystack-Westford Base Line Vector

Base Line Characteristic*	Difference Between Geodetic Value and Mean VLBI Value, m	
	Uncorrected†	Partially Corrected‡
X component	0.002	0.002
Y component	0.004	0.004
Z component	−0.019	−0.006
Length	−0.004	−0.004

*See Tables 1 and 2 for definitions of cooordinate system.

†Uncorrected for gravitational flexure of telescopes (see text).

‡After partial correction for gravitational flexure of Haystack telescope (see text).

REFERENCES

Carter, W. E., C. J. Fronczek, and J. E. Pettey, Haystack-Westford survey, *NOAA Tech. Memo. NOS NGS 21*, Nat. Tech. Inform. Serv., Springfield, Va., 1979.

Clark, T. A., L. K. Hutton, C. Ma, I. I. Shapiro, J. J. Wittels, D. S. Robertson, H. F. Hinteregger, C. A. Knight, A. E. E. Rogers, A. R. Whitney, A. E. Niell, G. M. Resch, and W. J. Webster, Jr., An unusually strong radio outburst in Algol: VLBI observations, *Astrophys. J. Lett.*, *206*, L107–L111, 1976.

Hinteregger, H. F., I. I. Shapiro, D. S. Robertson, C. A. Knight, R. A. Ergas, A. R. Whitney, A. E. E. Rogers, J. M. Moran, T. A. Clark, and B. F. Burke, Precision geodesy via radio interferometry, *Science*, *178*, 396–398, 1972.

Hothem, L. D., Determination of accuracy, orientation and scale of satellite Doppler point-positioning coordinates, in *Proceedings of 2nd International Geodetic Symposium on Satellite Doppler Positioning, Austin, Texas, January 1979*, pp. 609–630, University of Texas Press, Austin, 1979.

Hothem, L. D., D. S. Robertson, and W. E. Strange, Orientation and scale of satellite Doppler results based on combination and comparison with other space systems, in *Proceedings of the 2nd International Symposium on Problems Related to the Redefinition of the North American Geodetic Networks*, pp. 167–180, U.S. Government Printing Office, Washington, D.C., 1979.

Niell, A. E., K. M. Ong, P. F. MacDoran, G. M. Resch, D. D. Morabito, E. S. Claflin, and J. F. Dracup, Comparison of a radio interferometric differential baseline measurement with conventional geodesy, *Tectonophysics*, *52*, 49–58, 1979.

Ong, K. M., P. F. MacDoran, J. B. Thomas, H. F. Fliegel, L. J. Skjerve, D. J. Spitzmesser, P. D. Batelaan, and S. R. Paine, A demonstration of a transportable radio interferometric surveying system with 3-cm accuracy on a 307-m base line, *J. Geophys. Res.*, *81*, 3587–3593, 1976.

Robertson, D. S., W. E. Carter, B. E. Corey, W. D. Cotton, C. C. Counselman, I. I. Shapiro, J. J. Wittels, H. F. Hinteregger, C. A. Knight, A. E. E. Rogers, A. R. Whitney, J. W. Ryan, T. A. Clark, R. J. Coates, C. Ma, and J. M. Moran, Recent results of radio interferometric determinations of a transcontinental baseline, polar motion and earth rotation, in *Proceedings of International Astronomical Union Symposium No. 82, Time and the Earth's Rotation, Cadiz, Spain, May 1978*, edited by D. D. McCarthy and J. D. H. Pilkington, pp. 217–224, D. Reidel, Hingham, Mass., 1979.

Rogers, A. E. E., C. A. Knight, H. F. Hinteregger, A. R. Whitney, C. C. Counselman, I. I. Shapiro, S. A. Gourevitch, and T. A. Clark, Geodesy by radio interferometry: Determination of a 1.24-km base line vector with ~5-mm repeatability, *J. Geophys. Res.*, *83*, 325–334, 1978.

Strange, W. E., and L. D. Hothem, Establishment of scale and orientation for satellite Doppler positions, *Phil. Trans. Roy. Soc. London, Ser. A*, *294*, 335–340, 1980.

(Received September 27, 1979;
accepted November 16, 1979.)

JOURNAL OF GEOPHYSICAL RESEARCH, VOL. 86, NO. B3, PAGES 1647-1651, MARCH 10, 1981

GEODESY BY RADIO INTERFEROMETRY: INTERCONTINENTAL DISTANCE DETERMINATIONS WITH SUBDECIMETER PRECISION

T. A. Herring,[1] B. E. Corey,[1] C. C. Counselman III,[1] I. I. Shapiro,[1,7]
B. O. Rönnäng,[2] O. E. H. Rydbeck,[2] T. A. Clark,[3] R. J. Coates,[3]
C. Ma,[3] J. W. Ryan,[3] N. R. Vandenberg,[3] H. F. Hinteregger,[4]
C. A. Knight,[4] A. E. E. Rogers,[4] A. R. Whitney,[4]
D. S. Robertson,[5] and B. R. Schupler[6]

Abstract. Analysis of very-long-baseline interferometer (VLBI) observations yielded estimates of the distances between three radio telescopes in the United States and one in Sweden, with formal standard errors of a few centimeters: Westford, Massachusetts-Onsala, Sweden: 5,599,714.66±0.03m; Green Bank, West Virginia-Onsala, Sweden: 6,319,317.75±0.03m; and Owens Valley, California-Onsala, Sweden: 7,914,131.19±0.04m, where the earth-fixed reference points are defined in each case with respect to the axes of the telescopes. The actual standard errors are difficult to estimate reliably but are probably not greater than twice the formal errors.

1. Introduction

Very long baseline interferometry (VLBI) has been used for the past decade to determine distances between radio telescopes and positions of radio sources. Improvement in the precision of baseline length determination in North America over this period has been substantial -- from a precision of about 1 m [Hinteregger et al., 1972] to a precision of under five centimeters [Robertson et al., 1979] for baselines from about 1000 km to just under 4000 km in length. Near the middle of the decade, distances between North America and Europe were determined with a precision of about half a meter [Robertson, 1975; see also Cannon et al., 1979]. In this paper we describe more recent VLBI determinations, with subdecimeter precision, of these intercontinental distances.

2. Data Analysis

The data analyzed consisted of interferometric group delays [Shapiro, 1976] which were obtained from three sessions of observations involving up to four antennas, as described in Table 1. All observations were made with the Mark I VLBI system with a center radio frequency of about 8 GHz. A multichannel bandwidth synthesis technique [Whitney et al., 1976] was used. Each recorded channel had the Mark I bandwidth of 360 kHz, whereas the synthesized bandwidth was ≈100 MHz in the first session of observations and ≈300 MHz in the last two sessions. A hydrogen maser frequency standard of modern, post-1970, design was used at each telescope for each session.

The Cartesian coordinate system used in the analysis was geocentric and earth-fixed with the Z axis parallel to the mean pole of rotation of 1900-1905, as defined by the International Latitude Service and maintained by the Bureau International de l'Heure (BIH). The X axis was defined to be perpendicular to the Z axis and in the direction of the Greenwich meridian. The Y axis completed the right-handed triad. Operationally, the origin of this system was defined by the coordinates for the intersection of the azimuth and elevation axes of the Haystack radio telescope, obtained from a combination of spacecraft-tracking and VLBI observations made at various sites. The orientation was defined by the BIH values for pole position and UT1 (1968 system), with the addition of fortnightly and monthly terms of small amplitude [Woolard, 1959], and by the models for diurnal polar motion [McClure, 1973] and earth tides (based on ephemeris positions of the moon and sun, on the Love numbers $h = 0.61$ and $\ell = 0.09$, and on the assumption of no dissipation). The small effects of antenna deformations [Carter et al., 1980], ocean loading, plate tectonics, and other errors in the model were ignored in view of the limited precision of the measurements being analyzed.

The orientation of this earth-fixed coordinate system in inertial space (with respect to the mean equinox and equator of 1950.0), was defined by the pole position, by UT1 and by the standard formulas for sidereal time, nutation, and precession, with certain small corrections: Woolard's [1953] theory as modified by Melchior [1971] was used for nutation; and 5,027".878 per tropical century at 1950.0 was taken for the precession constant. The origin of right ascension was defined by the value 12 hr 26 min

[1]Department of Earth and Planetary Sciences, Massachusetts Institute of Technology, Cambridge, Massachusetts 02139.

[2]Onsala Space Observatory, S-439 00 Onsala, Sweden.

[3]Goddard Space Flight Center, Greenbelt, Maryland 20771.

[4]Northeast Radio Observatory Corporation, Haystack Observatory, Westford, Massachusetts 01886.

[5]U.S. National Geodetic Survey, Rockville, Maryland 20852.

[6]Computer Science Corporation, Silver Spring, Maryland 20910.

[7]Also at Department of Physics, Massachusetts Institute of Technology, Cambridge, Massachusetts 02139.

Paper number 80B1609.
0148-0227/81/080B-1609$01.00

TABLE 1. Summary of VLBI Observations

Observation Session	Dates	Duration, hours	Antennas*	Number of Sources†	Declination Range of Sources, deg	Number of Group-Delay Observations**
1	Sept. 21-25, 1977	88††	H,N,O	10(6)	-5.5 to 50.8	529 (151)
2	Feb. 24-26, 1978	50	H,O,V	8(4)	0.5 to 50.8	291 (77)
3	May 17-19, 1978	45	H,O,N,V	10(10)	-5.5 to 50.8	830 (258)

* H ≡ 37-m diameter telescope of the Haystack Observatory, Westford, Massachusetts; N ≡ 43-m diameter telescope of the National Radio Astronomy Observatory (NRAO), Green Bank, West Virginia; O ≡ 20-m diameter telescope of the Onsala Space Observatory, Onsala, Sweden; and V ≡ 40-m diameter telescope of the Owens Valley Radio Observatory, Big Pine, California.

† The sources observed are listed in the caption to Figure 1. The numbers of sources observed at Onsala are given in parentheses.

** The numbers of observations involving Onsala are given in parentheses.

†† Onsala participated for the last 62 hours.

33.246 sec for the radio source 3C 273B (elliptic aberration removed).

Using this framework and a theoretical model for the group delays [Robertson, 1975; Ma, 1978], we estimated by weighted least squares the baseline vectors, the source positions, and the other relevant parameters. Included in the last category are parameters that allow for the estimation of changes in pole position and variations in UT1 when data from two or more sessions of observations are combined [Shapiro et al., 1974, 1976; Robertson et al., 1979]. In addition to these purely geometric parameters there are parameters in the model that represent the effects on the group delays of the propagation medium and of the behavior of the clocks at the various radio telescopes. The representation of the propagation medium includes the zenith tropospheric delay as a parameter. Since the signal delay through the troposphere varies with time and with location, a number of such parameters are utilized with this model. The effects of the ionosphere, always under ~1 ns in the zenith direction, but not separately modeled, are largely absorbed by these parameters because of the similarity in the signature in the group delays of the ionosphere and the troposphere. The representation of the behavior of the clock at one site relative to that at another consists of a polynomial in time of low order with the coefficients as parameters, the first two denoting the epoch and rate offsets. Since the clocks drift unpredictably with time, a number of such polynomials are usually employed.

The choice of the number of parameters to represent the combined effects of the troposphere and the ionosphere and the behavior of the clocks as well as the choice of the time interval of applicability of each parameter are to a certain extent subjective. We therefore investigated the effects on the results of a variety of such choices. As extremes for the representation of the troposphere and the ionosphere, we considered for each telescope the use of one parameter for the zenith delay for each session of observations and one such parameter for each 12-hour period of observations. For the clock behavior we chose the clock at Haystack as the reference and considered for each other telescope for each session the use of one parameter each for the relative offsets in epoch, rate, and (in several instances) rate of change of rate. The intervals of applicability of such 'clock polynomials' ranged from 7.5 to 24 hours; only for this latter case was a parameter included for the rate of change of rate. The variations in the estimates of baseline lengths resulting from these different parameterizations were up to 1.8 and 1.2 times the corresponding standard deviation obtained for the adopted parameterization for the data from each of the first two sessions and from the third session, respectively. In view of this stability, we deem it unlikely that either the propagation medium or the behavior of the clocks has introduced errors in baseline length much in excess of the formal standard deviations. The adopted choice of epochs and intervals of applicability for these parameters (see section 4) was based primarily on examination of the postfit residuals, especially those from observations at low elevation angles for the parameters representing the behavior of the propagation medium.

The inverse of the weight for each group delay was obtained from the sum of the variance found from a signal-to-noise analysis [Whitney, 1974] and an ad hoc term included to account for error sources that were not a function of signal strength. The inclusion of this term was motivated by the desire to (1) allow for the effects of systematic errors, and, relatedly, (2) weight the observations of the different sources more evenly, since for some strong sources the signal-to-noise analysis yielded uncertainties that were well below the suspected contributions of other errors. The magnitude of this ad hoc term was assumed constant for the data for a given baseline for a given session of observations. Its value was obtained from the constraint that chi-square per degree of freedom be unity, and its square root ranged from 0.10 to 0.25 ns. Omitting this ad hoc term from the variances changed the estimates of baseline length by up to 1.2 times the standard deviations obtained with this term included.

3. Results

Table 2 gives our estimates of the distances between the radio telescope in Sweden and the three in the United States. The reference point for each telescope is the intersection of the azimuth and elevation axes, except for the NRAO telescope where the reference is the point on the polar axis closest to the (nonintersecting) equatorial axis [Hinteregger et al., 1972].

Typical postfit residuals from the simultaneous analysis of the data from all sessions are shown in Figure 1. The root mean square of these residuals ranged from 0.13 ns for the Haystack-NRAO data from the last session to 0.49 ns for the Onsala-NRAO data from the first session, the ratio being approximately as expected in view of (1) the threefold smaller synthesized bandwidth used in the first session of observations, (2) the generally larger correlated flux densities obtained from observations involving the shorter baselines, and (3) the slightly higher sensitivity of the Haystack-NRAO system compared to the Onsala-NRAO system.

The repeatability of the estimates of the baseline lengths shown in Table 2 indicates that the formal standard errors may not be much smaller than the actual errors. However, one fact detracts from the importance of this indication: The uncertainties of the estimates of baseline lengths from the third session of observations were much smaller than those from the second which, in turn, were smaller than those from the first. The disparity between the uncertainties from the first and second sessions was due primarily to the contrast in synthesized bandwidths. The further discrepancy between the uncertainties from the first two sessions and those from the third was due mainly to geometry; the schedule of observations for the first two sessions was controlled by requirements of other experiments involving only the U.S. antennas and therefore did not properly provide for Onsala's participation.

The estimates for the propagation delay through the atmosphere and ionosphere in the zenith direction ranged from 6.7 ns (NRAO) to 8.2 ns (Onsala); the estimates for the clock parameters were also each in approximate accord with expectations, ranging up to 23 μs for epoch offsets and from $\sim 3 \times 10^{-14}$ to $\sim 2 \times 10^{-12}$ for rate offsets.

The estimates for the source positions, the distances between the radio telescopes in the United States, and the pole position and UT1 variations will be given elsewhere and discussed there along with a much larger collection of VLBI observations that involved only the telescopes in the United States.

4. Conclusions

Combination of data from three sessions of VLBI observations involving sites in Sweden and the United States yielded results of subdecimeter precision in the determination of the intercontinental distances. Since sufficiently accurate and well-distributed observations to determine baselines to Sweden with subdecimeter precision were available for only one session, the data are not useful for the establishment of

TABLE 2. Baseline Length Estimates

Observation Session(s)*	Haystack - Onsala			NRAO - Onsala			Owens Valley - Onsala		
	Length, m	Formal Standard Error, m	Difference,† m	Length, m	Formal Standard Error, m	Difference,† m	Length, m	Formal Standard Error, m	Difference,† m
1	5,599,714.948	0.301	0.288	6,319,318.156	0.354	0.404	---	---	---
2	4.516	0.120	-0.144	---	---	---	7,914,131.372	0.169	0.180
3	4.686	0.028	0.026	7.776	0.036	0.024	1.173	0.043	-0.019
1 + 2 + 3**	5,599,714.660	0.027	---	6,319,317.752	0.034	---	7,914,131.192	0.040	

* See Table 1 for definitions and text for discussion. The number of parameters estimated in each solution, in order of listing, was 47, 41, 56, and 102. The speed of light used to convert light seconds to meters was 299,792,458 m s^{-1}.

† Differences from adopted solution.

** Adopted solution.

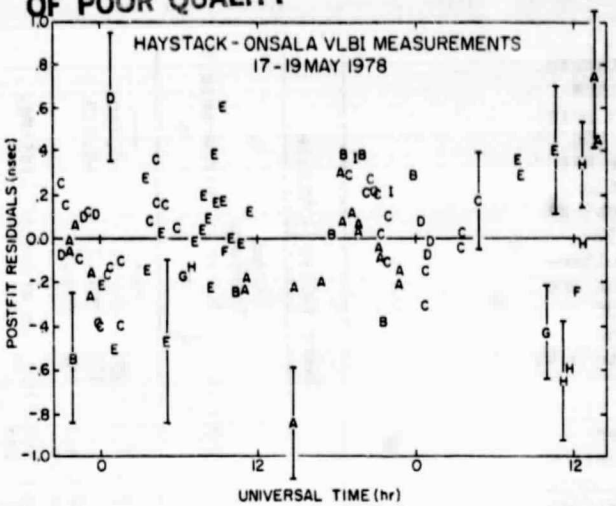

Fig. 1. Postfit residuals from the adopted solution (see Table 2) for the Haystack-Onsala group-delay measurements from session 3 (see Table 1). The root mean square of these residuals is 0.25 ns. The vertical bars represent ±1 standard deviation. Each letter in the figure denotes a different radio source: A ≡ NRAO 150; B ≡ 3C 84; C ≡ 4C 39.25; D ≡ 3C 273B; E ≡ 3C 345; F ≡ VRO 42.22.01; G ≡ 2134+00; H ≡ 3C 454.3; and I ≡ OJ 287. One other source, observed on some baselines in session 3, was 3C 279. See Clark et al. [1976] for approximate values of the coordinates for each source.

subdecimeter repeatability. Neither are the earlier VLBI determinations [Robertson, 1975] useful since they were less precise, and, in addition, involved a different telescope at Onsala which has yet to be located accurately with respect to the one we utilized (Table 1). Further, to assess inherent accuracy, comparisons would best be made with results from a more accurate technique. None now exists. The most accurate alternate technique currently available for the determination of these particular intercontinental baselines is based on observations of the Doppler shift of radio signals transmitted from satellites, plus standard ground surveys to tie the reference points for the Doppler measurements to those for the VLBI determinations. Such Doppler data exist (W. E. Carter, private communication, 1979), but the analysis and the ground surveys have not been completed and so no comparisons can yet be made.

Periodic repetitions of these intercontinental VLBI measurements are also planned with more radio telescopes in the interferometer array and with use of our new, more powerful, Mark III VLBI system. This system, among other attributes records data simultaneously from two well separated radio frequency bands, thus allowing ionospheric effects to be virtually eliminated as a source of error. The purpose of these further VLBI measurements will not only be to check on the repeatability of the present baseline determinations but, more importantly, to improve the precision to the level at which the expected [Minster and Jordan, 1978] ~1.7 cm/yr spreading rate between Europe and the United States could be detected reliably within a decade.

Acknowledgements. We thank Reuben Epstein and Lucien Froidevaux for their contribution to the early stages of the analysis of the data, the staffs of the participating observatories for their indispensable assistance during the observations, and Robert Cady for drafting the figure. The Haystack Observatory is operated with support from the National Science Foundation (NSF), grant GP 25865; the NRAO is operated by the Associated Universities, Inc. under contract with the NSF; the Onsala Space Observatory is supported by a grant from the Swedish Natural Science Research Council; and the Owens Valley Radio Observatory is sustained by a grant from the NSF. The MIT experimenters were supported in part by the U.S. Air Force, contract F19628-79-C-0064, the National Aeronautics and Space Administration, grant NGR22-009-839, and the NSF, grant EAR76-22615.

References

Carter, W. E., A. E. E. Rogers, C. C. Counselman, and I. I. Shapiro, Comparison of geodetic and radio interferometric measurements of the Haystack-Westford baseline vector, J. Geophys. Res., 85, 2685-2687, 1980.

Cannon, W. H., R. B. Langley, W. T. Petrachenko, and J. Kouba, Geodesy and astrometry by transatlantic long baseline interferometry, J. Geophys. Res., 84, 229-236, 1979.

Clark, T. A., L. K. Hutton, G. E. Marandino, C. C. Counselman, D. S. Roberston, I. I Shapiro, J. J. Wittels, H. F. Hinteregger, C. A. Knight, A. E. E. Rogers, A. R. Whitney, A. E. Niell, B. O. Rönnäng, and O. E. H. Rydbeck, Radio source positions from very-long-baseline interferometry observations, Astron. J., 81, 599-603, 1976.

Hinteregger, H. F., I. I. Shapiro, D. S. Robertson, C. A. Knight, R. A. Ergas, A. R. Whitney, A. E. E. Rogers, J. M. Moran, T. A. Clark, and B. F. Burke, Precision geodesy via radio interferometry, Science, 178, 396-398, 1972.

Ma, C., Very long baseline interferometry applied to polar motion, relativity and geodesy, Ph.D. thesis, Univ. of Md., College Park, 1978.

McClure, P., Diurnal polar motion, Rep. X-592--73-259, NASA/Goddard Space Flight Cent., Greenbelt, Md., 1973.

Melchior, P., Precession-nutations and tidal parameters, Celestial Mech., 4, 190-212, 1971.

Minster, J. B., and T. H. Jordan, Present-day plate motions, J. Geophys. Res., 83, 5331-5354, 1978.

Robertson, D. S., Geodetic and astrometric measurements with very-long-baseline interferometry, Ph.D. thesis, Mass. Inst. of Technol., Cambridge, 1975.

Robertson, D. S., W. E. Carter, B. E. Corey, W. D. Cotton, C. C. Counselman, I. I. Shapiro, J. J. Wittels, H. F. Hinteregger, C. A. Knight, A. E. E. Rogers, A. R. Whitney, J. W. Ryan, T. A. Clark, R. J. Coates, C. Ma, and J. M. Moran, Recent results of radio interferometric determinations of a transcontinental baseline,

polar motion, and Earth rotation, in Time and the Earth's Rotation, edited by D. D. McCarthy and J. D. Pilkington, pp. 217-224, D. Reidel, Dordrecht, Netherlands, 1979.

Shapiro, I. I., Estimation of astrometric and geodetic parameters from VLBI observations, in Methods of Experimental Physics, edited by M. L. Meeks, pp. 261-276, Academic, New York, 1976.

Shapiro, I. I., D. S. Robertson, C. A. Knight, C. C. Counselman III, A. E. E. Rogers, H. F. Hinteregger, S. Lippincott, A. R. Whitney, T. A. Clark, A. E. Niell, and D. J. Spitzmesser, Transcontinental baselines and the rotation of the earth measured by radio interferometry, Science, 186, 920-922, 1974.

Shapiro, I. I., D. S. Robertson, C. A. Knight, C. C. Counselman III, A. E. E. Rogers, H. F. Hinteregger, S. Lippincott, A. R. Whitney, T. A. Clark, A. E. Niell, and D. J. Spitzmesser, Transcontinental baselines and the rotation of the earth measured by radio interferometry, Science, 191, 451, 1976.

Whitney, A. R., Precision geodesy and astrometry via very long baseline interferometry, Ph.D. thesis, Mass. Inst. of Technol., Cambridge, 1974.

Whitney, A. R., A. E. E. Rogers, H. F. Hinteregger, C. A. Knight, J. I. Levine, S. Lippincott, T. A. Clark, I. I. Shapiro, and D. S. Robertson, A very-long-baseline interferometer system for geodetic applications, Radio Sci., 11, 421-432, 1976.

Woolard, E. W., Theory of the rotation of the earth around its center of mass, Astron. Pap. Am. Ephemeris Nautical Alm., XV (I), 1953.

Woolard, E. W., Inequalities in mean solar time from tidal variations in the rotation of the earth, Astron. J., 64, 140-142, 1959.

(Received July 10, 1980;
revised October 14, 1980;
accepted November 12, 1980.)

GEODESY BY RADIO INTERFEROMETRY: A CRITICAL REVIEW

Irwin I. Shapiro
Department of Earth and Planetary Sciences
and
Department of Physics
Massachusetts Institute of Technology
Cambridge, MA 02139

Introduction

Almost fifteen years ago, while plans for the first experiments in very-long-baseline radio interferometry (VLBI) were gestating within the minds of Canadian and United States radio astronomers [1], it occurred to me that this technique could be used to measure the motions of the earth's crust [2]. The potential accuracy in the determination of intercontinental baselines with VLBI -- one centimeter uncertainty from less than one day of observation -- was so dazzling that many people treated the idea like pie in the sky. Funding to develop VLBI for geophysical applications was thus initially very difficult to obtain. Nonetheless, by January 1969, the first baseline length was being determined with VLBI with the use of a bandwidth synthesis technique [3] and a rather considerable amount of borrowed equipment. The result [4] gave the distance between reference points on the Haystack radio telescope in Massachusetts and on a radio telescope of the National Radio Astronomy Observatory in West Virginia as 845.131±0.002 km. The most recent VLBI determinations of this length yield [5] 845.12990±0.00005 km. Still the potential centimeter accuracy has not been achieved. Nor have motions of the earth's crust been detected. The National Aeronautics and Space Administration has organized the Crustal Dynamics Project [6] to pursue these goals.

In the remainder of this paper, I will outline the basic principles underlying the determination of baselines by VLBI and discuss the major error sources along with the possible means for their reduction. Most of these topics have received considerable attention in the past [7], with one exception: the pitfalls of data analysis; I shall therefore place stress on this issue.

Instrumentation

A VLBI system consists of an array of at least two antennas that observe the same radio source simultaneously. A direct electrical connection is not maintained between the antennas, thus allowing them to be separated by thousands of kilometers. The local-oscillator signals, used at each antenna to convert the radio-frequency signals from the source to the video (low-frequency) band, are derived from a frequency standard at the site. These standards are sufficiently stable that the relative phases

of the signals from the source received at the two antennas are well preserved.

The video signals are recorded on magnetic tape at each site, with the time base for the recordings being derived from the same standard as is used to govern the local-oscillator signals. The tape recordings are then transported to a common center where those recorded simultaneously are cross-correlated to obtain the basic VLBI observables.

Observables

The basic observables in geodetic VLBI experiments are (i) the difference in the times of arrival at two antennas of a signal from a source; and (ii) the rate of change of this time difference. The measurement of the time-of-arrival difference can be of two types: the phase-delay-difference (hereinafter "phase delay"), an observable based on measurements of phase, can be obtained very precisely, but usually ambiguously, due to the inability to resolve the "2πn" problem. The group-delay-difference (hereinafter "group delay") observable is usually determined with less precision than is the phase delay. But the group delay, being proportional to the rate of change of phase with frequency, is usually unambiguous. To obtain reasonable accuracy in the measurement of group delay it is necessary to make phase-delay measurements over a wide band of frequencies simultaneously, or nearly simultaneously, since the uncertainty in the group-delay measurement is inversely proportional to this bandwidth. In practice, only a relatively narrow band of frequencies can be recorded. But this band can be split up into narrower bands which are spread over a very wide band. This technique is called bandwidth synthesis. In the newest, Mark III system, up to 28 narrow bands, each 2 MHz wide, are distributed over one or more wide bands, each of up to several hundred megaHertz. If the error in the measurement of phase for any one band is $\sigma(\phi)$, then the error $\sigma(d_g)$ in the measurement of the group delay will be given by $\sigma(d_g) \sim \sigma(\phi)/\Delta f$, where Δf is the rms spread of the center frequencies of the individual bands about their mean. Because these individual bands do not cover the entire spanned band, the estimate of the group delay, too, could be ambiguous. However, a proper choice of the spacing of the individual bands, as explained below, can insure that any inherent ambiguity can be eliminated reliably.

The difference of the phases of the signals that would be received at two antennas exhibits curvature as a function of frequency due primarily to the effects of the earth's ionosphere: the lower the frequency, the shorter the phase delay. The actual shape of the phase vs. frequency curve for VLBI observations will depend on the relative amounts of plasma between the source and the two sites. But with appropriate spacings of the narrow bands, one can "connect" unambiguously the phase at one band with those at all the other bands. For example, selecting bands spaced in accord with a geometric series allows use of a bootstrap technique to connect phases first between the closest bands and then between the more widely separated bands through use of the characteristics of the curve established by the connection between the closest bands. Of course, the "absolute" phase would still be uncertain by multiples of 2π, but the relative phases between bands would be freed from any such ambiguity. Only the relative phases affect the group delay which is equal to the slope of the curve of phase delay vs. (angular) frequency.

Information Content

We now consider the information content of the observables under simplified assumptions. In particular, let us ignore the propagation medium and assume that the earth is rigid and rotates with a constant, known, angular velocity. We may then write the expression for the delay observable as a function of time as:

$$d(t) = \frac{1}{c}\vec{B}(t)\cdot\hat{S} + \tau + \dot{\tau}t \ , \qquad (1)$$

where c is the speed of light, $\vec{B}$ is the baseline vector connecting a pair of antennas, $\hat{S}$ is a unit vector in the direction of the source, and τ and $\dot{\tau}$ are, respectively, the offsets in the epoch and rate of the clock at one site with respect to those at the other site. Let us assume that the radio source is extragalactic and defer discussion of the implications of the source being in an earth satellite. Under our assumption, then, $\hat{S}$ will be time independent and Equation (1) will represent a diurnal sinusoid added to a straight line. The first term in the equation contributes the diurnal sinusoid which is due to the rotation of the baseline vector in inertial space. The slope of the straight line is due to the clock-rate offset and the intercept is due to a combination of the clock-epoch offset and the product of the polar components of $\vec{B}$ and $\hat{S}$. Clearly, this curve can be specified by four parameters: the intercept and slope of the straight line, and the amplitude and phase of the sinusoid. (We do not consider the period of the sinusoid, since that is given by assumption.) Thus, four measurements of the delay suffice, in principle, to determine d(t); any additional measurements will be redundant. But how many unknown parameters are there for this situation? Naively, one would conclude that the baseline vector contributes three, the source two, and the clocks two, for a total of seven. However, the origin of right ascension of our system is arbitrary; only the origin of declination is fixed by assumption of a known angular velocity for the earth. Since, for example, the right ascension of the source can be used to define this arbitrary origin, the number of unknown parameters is only six. Nonetheless, a unique solution clearly cannot be obtained for these six parameters from observations of a single source. Observations of each additional source will add two unknowns: the coordinates of the source on the plane of the sky. But such observations also can be used to determine three additional parameters: the intercept of the straight line and the amplitude and

phase of the sinusoid appropriate for the additional source. The slope of the straight line provides no new information since it is determined solely by the clock-rate offset. It is clear that with four observations of one source and three each of two more sources, a useful solution for all of the parameters of this simple model can usually be determined. (The measurements of delay rates simultaneously do not reduce the requirement for observations of three sources.) The accuracy of the determination of these ten parameters will depend, of course, not only on the accuracy of the measurements of delay (and delay rate), but also on the baseline, the distribution of the sources in the sky, and the distribution of the observations in time.

The situation actually encountered with VLBI is, of course, far more complicated than outlined in the previous paragraph. For example, if the radio sources emanate from satellites, one must know their orbits. These can be determined from the VLBI observations, along with the baseline vectors between each pair of antennas, but the analysis is more complicated [8]. There is, however, one advantage in principle: measurements of delay rates alone suffice to determine all parameters if the orbits of the satellites are inclined to the earth's equator. From observations of extragalactic radio sources, it is not possible to determine the (constant) polar component of the baseline from delay-rate measurements. The biggest advantage in observing radio sources on satellites is, of course, the enormous strengths of the signals compared to those from extragalactic sources.

191

Aside from the complications introduced by the possibility of observing radio signals from satellites, there are others which we can conveniently divide into two categories: signals and noise. Here signals refer to those effects on the observables which are of geophysical interest, and noise refers to those of no intrinsic interest. We consider crustal motions, solid-earth tides, variations in UT1, polar motion, precession, and nutation to be signals. On the other hand, clock instabilities and uncertainties in our knowledge of source characteristics and of the propagation medium are considered as noise. We discuss each set in turn.

Signals

Crustal Motion. Changes in crustal configuration can be sensed most reliably by changes in baseline lengths; in addition, significant changes in the corresponding baseline directions for an array of antennas would signify crustal motions provided that these changes were incompatible with a rigid rotation of the array. No reliable determinations of crustal motions have yet been obtained from VLBI data, but there is good reason to believe that motions of the order of two centimeters per year or greater could be detected reliably within the next few years.

For very long baselines, of the order of thousands of kilometers, radio observations of extragalactic sources appear to offer the best near-term possibilities for measurement of such crustal motions. For short baselines, up to about one hundred kilometers, a more efficient and likely just as accurate method will be to observe the satellites of the NAVSTAR Global Positioning System (GPS) which orbit at an altitude of about 20,000 kilometers. This system, when completed, is projected to consist of as many as 24 satellites, eight uniformly distributed in each of three planes spaced 120 degrees apart in the longitudes of their ascending nodes and each with an inclination of about 63 degrees. At present six such satellites are in orbit, enough to be useful for crustal dynamics applications. Miniature interferometer terminals can be used to observe the radio signals from these satellites [9] to determine short baselines with high accuracy since the effect of uncertainties in knowledge of the satellite orbits on the baseline determinations is approximately proportional to the ratio of the baseline length to the satellite altitude. The radio signals from the GPS satellites are broadcast on two bands, centered at about 1.23 and 1.58 GHz; to determine the phase delay unambiguously requires observations extended over at least one hour [10]. However, once the baselines have been determined, re-measurement can be accomplished very quickly, with several minutes of observations or less, depending on the detailed circumstances. This attribute makes a GPS-based radio interferometric system for monitoring crustal motions near faults very attractive.

Solid-Earth Tides. The semi-diurnal, solid-earth tide imparts a distinctive signature to the VLBI observables, since almost all other effects introduce a diurnal signature. The maximum magnitude of this effect on the delay observable can be slightly greater than one nanosecond. Thus, estimates of the local values of the vertical and horizontal Love numbers, h and l, can be obtained from VLBI data. Current estimates agree, to within their uncertainty of about 0.05, with the "expected" values [5].

UT1 and Polar Motion. Variations in the rate of rotation of the earth (UT1) and in the position of the axis of figure with respect to the axis of rotation (polar motion) affect the directions of baseline vectors. The VLBI observables have no sensitivity to the orientation of the earth and the direction (in space) of its axis of figure with respect to conventional reference systems; only changes in these quantities can be detected. Further, any "common-mode" errors in the epoch settings of the clocks at the antenna sites will be indistinguishable from corresponding changes in the orientation of the earth about its spin axis (UT1). Finally, VLBI data obtained with only two antennas are sensitive to only two independent combinations of the three parameters needed to specify changes in the position (in space) of the axis of figure of the earth and in the orientation of the earth about this axis: Such changes affect only the direction of the baseline which is described by only two independent para-

meters. The lengths of baselines are unaffected by variations in the rate of rotation of the earth and in the position of the pole.

Estimates of UT1 and pole position from VLBI data now have accuracies comparable to those from other measurements [11]. However, it is expected that the accuracy of the VLBI estimates will improve nearly tenfold within the next five years due primarily to the introduction and use of the new, Mark III, VLBI system.

Precession and Nutation. Changes in the direction in space of the spin axis of the earth with periods long compared to a day are sensed with VLBI through the corresponding changes in the coordinates of the radio sources. These changes will, however, preserve the arclengths between sources. At present, estimates of the precession constant made from VLBI measurements have an uncertainty of a few tenths of an arcsecond per century [12], severalfold larger than the uncertainty associated with the presently accepted value based on optical observations. No estimates of any of the nutation terms have yet been made, although enough data will soon exist to make a useful estimate of at least the principal term of nutation.

Noise

192

Clock Instabilities. The two parameters, one each for clock epoch and rate offsets, do not provide an adequate representation of the relative behavior of the clocks at any two antennas of an interferometric array over the period of many hours needed to determine the baseline vector, source positions, etc. from observations of extragalactic radio sources. This statement applies to the current field units of all atomic clocks, including the hydrogen-maser frequency standards. Laboratory versions of hydrogen-maser standards have achieved stabilities of several parts in 10^{14} over many hours [13], a level quite sufficient for present crustal dynamics applications. However, performance of the older units in the field has often been two orders of magnitude or more worse.

A number of possibilities exists to minimize the current impact of these clock instabilities on the accuracy with which geophysical information can be extracted from VLBI data. One can use higher-order polynomials as well as parameterized functions with diurnal period to represent the relative clock behavior; here the point of "diminishing returns" sets in at about the sixth order for the polynomial. One can also reduce the effects of long-term drifts in the relative clock behavior by using "clock stars": Observations can be made repeatedly, say every hour, of some suitable source and these observations can be used to correct for the relative clock drifts. To be suitable, this source should be visible from both sites for a large fraction of the diurnal cycle and should yield a reasonably large correlated

flux density so that accurate delay observations are possible to make. (A similar approach would involve use of a second, small antenna at each site to monitor continuously a suitable strong Galactic source of water-vapor maser radiation.) Of course, for the future, hydrogen-maser standards that match present laboratory units in performance can be placed in the field, with the sensitivity of the standards to environmental effects reduced to benign levels to prevent effectively the introduction of diurnal signatures into the VLBI data.

For observations of GPS satellites the need for a highly stable frequency standard can be avoided. By the use of a very low gain, nearly omni-directional antenna radio signals can be received sumultaneously from all satellites above the horizon at each site. Thus, in effect, the (interferometric) signals from one satellite can act like a clock for the corresponding signals from the other satellites [9]. Only because the radio signals from the satellites are so strong [8] is this approach feasible.

Source Characteristics. The radio sources observed affect the determination of geophysically interesting quantities through the strength of their radio emissions, their distribution on the sky, and the accuracy with which we can determine their positions. These positions, in turn, depend on the structure and internal kinematics of the regions of radio emission in each object, if an extragalactic source, and on the orbit of each object, if a satellite.

At present, the entries in the catalog of known, and potentially-usable, extragalactic radio sources number in the hundreds. Positions of a few dozen of those with the strongest emisions are now being determined routinely with an estimated accuracy of a few milliarcseconds [12, 14], except for the declinations of sources that lie near the equatorial plane. (Note that a 0".001 error in source position corresponds approximately to a two-centimeter error in length for a 4,000-km baseline.) The accurate determination of the declination of a near-equatorial source requires the use of interferometers with baselines that possess large components in the north-south direction. Few such baselines have so far been available for extensive sets of measurements.

Most extragalactic radio sources are not "points" when viewed on the scale of milliarcseconds. Rather, they exhibit complicated structure. This structure in their brightness can be mapped and a suitable feature in the map, or the overall center of brightness, can be used as a reference point. There are, however, technical difficulties in the determination of unambiguous brightness maps. These difficulties are being overcome and reliable maps on the scale of tenths of a milliarcsecond are now being obtained for some of the radio sources.

There is yet a further difficulty in the use of extragalac-

tic radio sources: most are not static. Dramatic changes have been observed in the brightness structure of some of these sources at the level of tenths of a milliarcsecond in angular resolution on a time scale of a few months. Thus, to enable positions of extragalactic radio sources to be used effectively as a reference system at the level of milliarcsecond accuracy for geophysical applications of VLBI, one must monitor the brightness distributions of these sources as a function of time and, perhaps, as a function of radio frequency as well.

For signals from a satellite, the main concern is with the determination of the orbits of the satellite; the radio signals themselves appear for practical purposes as if from a true point source. The orbital uncertainties affect the determination of baselines more, the larger the baseline length, as mentioned above. For the GPS satellites, for observation over a short arc, the determination of the initial conditions of the orbit for an epoch within the time span corresponding to this orbital arc, poses the main problem; the model of the accelerations perturbing the orbit is well enough known not to be a concern. However, if the orbits of the satellites are needed for long arcs and for long baselines, then the uncertainties in the knowledge of the disturbing accelerations affecting the satellite become more important considerations.

193

Propagation Medium. In regard to any substantial effects on VLBI data, the propagation medium can be considered to be composed of two components: the ionosphere and the troposphere. The effects of the ionosphere can be virtually eliminated by observing simultaneously, and with proper calibration, in two widely separated radio frequency bands (≈2 GHz and ≈8 GHz). The Mark III VLBI system is equipped for such dual-band observations. Moreover, enough suitable sources exist to allow effective use of the dual-band technique.

The troposphere is nearly non-dispersive at radio frequencies and is, therefore, a more troublesome contributor of noise. The troposphere can also be decomposed into two components: wet and dry. For the latter, the assumption of hydrostatic equilibrium is a very good one; measurements at each site of surface pressure combined with a good model of the atmosphere allows a good estimate to be made of the phase delay added in the zenith direction by the dry component: about 7.5 nanoseconds (equivalent to an increase in path length of about 2.3 m). It is widely thought that the error in this estimate can be kept at the several tenths of one percent level, or perhaps below. Mapping to the zenith angle of the observation, however, will increase the percentage error somewhat since the "slant" atmospheric path length cannot be determined so accurately from the pressure measurement at the antenna site. The situation with the wet component is more difficult. The water-vapor in the atmosphere is not in hydrostatic equilibrium and is quite variable in amount. Although the total effect on the path length of radio

waves is, on average, only about ten percent of that of the dry component, the wet component cannot be modeled accurately. Various simple techniques have been used to try to ameliorate this problem. Such techniques involve various combinations of model atmospheres and mapping functions with or without dependence on surface measurements of temperature, pressure, and dew point, and with or without parameters that can be estimated for each site from short, ≈8 hr, spans of data. Unfortunately, these techniques may well be deficient, especially for long baselines, in removing the effects of the atmosphere on the estimates of the "vertical" component of the baseline with which they are highly correlated.

The technique which has elicited the greatest expectations for providing the solution to the wet-component problem is based on the use of radiometer measurements at each site of the brightness temperature of the atmosphere at and near the ≈23 GHz line in the spectrum of water-vapor emission [15]. Studies indicate that this brightness temperature can be related with reasonably high accuracy to the excess path length attributable to the water-vapor content of the atmosphere. However, to date, almost all VLBI results have been obtained without the benefit of water-vapor radiometer measurements.

Atmospheric effects thus loom as the limiting factor in the accuracy achievable with VLBI in the determination of geophysical quantities [1]. What will that limit be? An assessment based on theory alone is unlikely to be accurate. Measurements are clearly called for. Series of VLBI experiments must be made with supplementary water-vapor radiometer measurements, under a variety of local weather conditions, and for various baseline lengths, to properly assess the contribution of the radiometer measurements towards improvement of the accuracy of baseline determinations. For short baselines, up to several kilometers in length, independent determination of the baseline vector can usually be made, with some effort, at the subcentimeter level of accuracy by means of conventional survey techniques. For long baselines, up to several thousand kilometers in length, independent means of verification at a relevant level of accuracy seem to be limited to laser ranging to artificial satellites or to the moon; such verification, however, will not be easy nor inexpensive for a number of practical reasons. The repeatability and consistency of VLBI results themselves may well have to provide the main standards. Since suitably accurate, and independent, estimates of UT1 and pole position may not always be available, repeated checks on the individual components of the vector baseline will likely require multi-site experiments, say with five or more separated antennas, to reduce the confusion between UT1 and pole position changes on the one hand and changes in baseline direction on the other. The many antenna sites serve to overdetermine UT1 and pole position, with the redundancy providing the meaningful check on the consistency of the estimates of some of the baseline components. For some combination of the preci-

sion and the time spanned by the sets of measurements, one must be concerned also about the genuine changes in baselines from crustal motions; of course, detection of such changes is the major purpose of the measurements.

Data Analysis

In current practice, the analysis of VLBI data involves a number of subjective elements. The choice of a parameterized function to represent clock behavior and the choice of the number of parameters to be estimated, as well as their epochs and intervals of applicability, are, at present, all made at the discretion of the analyst. The parameterizaton of functions to represent the effects of the propagation medium are similarly discretionary. Finally, the analysis is usually repeated several, often many, times to eliminate "bad" data and to change the parameterization and the weighting of the data. At each stage the analyst examines his or her solution, including the estimate of the baseline(s) involved. These procedures are clearly a cause for concern; the possibility of subjective bias affecting the reported result should not be ignored. Consider an oversimplified example: a conservative analyst may be subjectively biased towards stasis; hence, if a preliminary result from a new experiment yields a value for a baseline that seems to differ significantly from past results, he or she may look very hard for errors and may repeat the analysis (with changes) a number of times--until the new result "falls into line". Similarly, an analyst with a subjective bias toward change, may not look so hard for errors if he or she obtains a baseline estimate from a new experiment that differs from previous ones.

194

I emphasize that the variations of concern here are not arbitrarily large. There is little danger, for example, for subjective bias to cause a change in baseline length of the order of one hundred times the formal (statistical) standard error. However, changes of five times this standard error are to me easily conceivable.

There are many possible ways to guard against subjective bias, none foolproof. Certainly, for geophysical applications, we should strive to automate the analysis as fully as feasible to remove the opportunities for subjective bias as well as possible. Further, until full automation is achieved, the analysis should be conducted and completed without the analyst having any knowledge of the baseline. This knowledge can be withheld by a variety of techniques such as suppression of the printout of the differential corrections: only the postfit residuals would be available for examination. Another procedure [16] would involve a disinterested party changing in a random manner the a priori, or initial, values for all baseline components and entering these values into the computer without the analyst's knowledge. (All stages of the data analysis are carried out with computers.) Finally, any intercomparison between estimates of baselines obtained by different groups using VLBI or different techniques,

for external verification, should be carried out in a truly blind manner. Each group should have no contact with the others and should present its results to a disinterested party who performs the intercomparison. Such safeguards are necessary to enable the scientific community to have confidence in the baseline estimates and their accompanying uncertainties.

Crustal dynamics studies are of prime importance for geophysics and many have serious implications for society; we must, therefore, use no less than the most rigorous methods feasible to insure the integrity of our measurements and their interpretation.

Acknowledgement

This work was supported by the Air Force Geophysical Laboratory, the National Aeronautics and Space Administration, the National Science Foundation, and the United States Geological Survey.

References

1. Broten, N.W. et al., Science, 156, 1592 (1967); Bare, C.C. et al., Science, 157, 189 (1967).

2. Shapiro, I.I., Science, 157, 806 (1967); Shapiro, I.I., NEREM Record, 10, 70 (1968).

3. Hinteregger, H.F., NEREM Record, 10, 66 (1968); Rogers, A.E.E., Radio Science, 5, 1239 (1970); Shapiro, I.I., and C.A. Knight, in Earthquake Displacement Fields and the Rotation of the Earth, L. Mansinha, D.E. Smylie, and A.E. Beck, Eds. (D. Reidel, Dordrecht, 1970), p. 284.

4. Hinteregger, H.F. et al., Bulletin of American Astronomical Society, 3, 467 (1971); Hinteregger, H.F. et al., Science, 178, 396 (1972); for other results for different baselines, see Shapiro, I.I. et al., Science, 186, 920 (1974); ibid. 191, 451 (1976); Thomas, J.B. et al., J. Geophys. Res., 81, 995 (1976); Ong, K.M. et al., J. Geophys. Res., 81, 3587 (1976); Rogers, A.E.E. et al., J. Geophys. Res., 83, 325 (1978); Robertson, D.S. et al., in Time and the Earth's Rotation, D.D. McCarthy, and J.D. Pilkington, Eds. (D. Reidel, Dordrecht, 1979), p. 217; Cannon, W. H., R.B. Langley, W.T. Petrachenko, and J. Kouba, J. Geophys. Res., 84, 229 (1979); Niell, A.E. et al., Tectonophysics, 52, 49 (1979); Carter, W.E., A.E.E. Rogers, C.C. Counselman III, and I.I. Shapiro, J. Geophys. Res., 85, 2685 (1980); Niell, A.E. et al. (NASA Conference Publication 2115, 1980), p.3; Herring, T.A. et al., J. Geophys. Res. (1981), in press.

5. Ryan, J.W. et al., in preparation.

6. This Project was organized in 1979 with T.L. Fischetti, E.A. Flinn, and R.J. Coates as Program Manager, Program Scientist, and Project Manager, respectively; see also NASA Technical Paper, TP-1464 (1979).

7. See, for example, Shapiro, I.I. [in Applications of Geodesy to Geodynamics, I. Mueller, Ed.(Ohio State, Columbus, 1979), p.29], where most of the material in the present paper can also be found.

8. Preston, R.A. et al., Science, 178, 407 (1972).

9. Counselman, C.C., and I.I. Shapiro, Bull. Géodesique, 53, 139 (1979); in Applications of Geodesy to Geodynamics, I. Mueller, Ed.(Ohio State, Columbus, 1979), p. 65; see also P.F. MacDoran, Bull. Géodesique, 53, 117(1979).

10. Counselman, C.C., I.I. Shapiro, R.L. Greenspan, and D.B. Cox, Jr. (NASA Conference Publication 2115, 1980), p. 414; Counselman, C.C., and S.A. Gourevitch, IEEE Trans. Geosci. Rem. Sens. (1981), in press; Counselman, C.C. et al., submitted for presentation at the AGU 1981 Spring Meeting; and C.C. Counselman, these Proceedings; see, also, P.F. MacDoran (NASA Conference Publication 2115, 1980), p. 403; and P.F. MacDoran, these Proceedings.

11. Robertson, D.S. et al., in Time and the Earth's Rotation, D.D. McCarthy, and J.D. Pilkington, Eds. (D. Reidel, Dordrecht, 1979), p. 217. See, also, Thomas, J.B. et al. (NASA Conference Publication 2115, 1980), p. 27.

12. Ma, C. et al., in preparation. See, also, Shapiro, I.I. et al., Astron. J., 84, 1459 (1979).

13. Vessot, R.F.C., private communication, 1980.

14. For earlier, less accurate determinations of source positions, see, for examples, Rogers, A.E.E. et al., Astrophys. J., 186, 801 (1973); Clark, T.A. et al., Astron. J., 81, 599 (1976); and Purcell, G.H. et al. (NASA Conference Publication 2115, 1980), p. 165.

15. See, for example, Moran, J.M., and B.R. Rosen, Radio Science, 16, 235 (1981), and references cited therein.

16. This procedure was suggested by T.A. Herring.